Neurodegenerative disease mechanisms induced by tau fragmentation in a novel model of human tauopathy

Iankova, Natalia

Awarding institution:
King's College London

Neurodegenerative disease mechanisms induced by tau fragmentation in a novel model of human tauopathy

Natalia Yankova

Thesis submitted in fulfilment of the degree of Doctor of Philosophy

Department of Basic and Clinical Neuroscience
King's College London
Institute of Psychiatry, Psychology & Neuroscience

April 2018

Declaration

I hereby declare that all the work presented in this thesis is my own. The astrocytic work (Chapter 3, Section 3.2.6) was undertaken in conjunction with Ms Sarah Freckleton (MSc Neuroscience student) and the neuronal morphology work (Chapter 4, Figure 4.2.3) with Ms Bianca Cronan (MSc Neuroscience student).

Publications arising from this thesis

Giacomini, C, Koo, CY, Yankova, N, Tavares, IAF, Wray, S, Noble, WJ, Hanger, DP & Morris, JDH 2018, 'A new TAO kinase inhibitor reduces tau phosphorylation at sites associated with neurodegeneration in human tauopathies' *Acta Neuropathologica Communications*, vol. 6, no. 37, Acta Neuropathologica Communications 2018 6:37, pp. 1-16. DOI: 10.1186/s40478-018-0539-8

Bondulich, MK, Guo, T, Meehan, C, Manion, J, Rodriguez-Martin, T, Mitchell, JC, Hortobágyi, T, Yankova, N, Stygelbout, V, Brion, J-P, Noble, WJ & Hanger, DP 2016, 'Tauopathy induced by low level expression of a human brain-derived tau fragment in mice is rescued by phenylbutyrate' *Brain*, vol. 139, no. 8, pp. 2290-2306. DOI: 10.1093/brain/aww137

Natalia Yankova

April 2018

Abstract

The tauopathies comprise a broad group of neurodegenerative diseases that are characterised by pathological alterations of tau in the brain that lead to synaptic dysfunction, changes in neuronal bioenergetics and loss of neuronal connectivity. There is growing evidence that tau fragmentation may be at least in part responsible for the clinical presentation in these disorders. In particular, diseases in which four microtubule-binding repeat tau isoforms are overrepresented, such as progressive supranuclear palsy, exhibit a truncated form of wild-type tau (termed Tau35) that is absent from age-matched control brain. However, whether this tau fragment is involved in disease pathogenesis is not yet clear.

In the work presented here, potentially pathogenic processes were studied in a new mouse model of tauopathy in which Tau35 is expressed under the control of the human tau promoter. Unlike most existing tau transgenic mice, expression of Tau35 comprises less than 10% of that of endogenous mouse tau and thus is more representative of human tauopathies. Tau35 mice demonstrate key features of human tauopathy, including progressive cognitive and motor deficits and reduced life-span. The work in this thesis has revealed that Tau35 mouse brain exhibits astrocytic activation, autophagosomal accumulation, and a reduction in the number of mitochondria. Investigation of changes in the peripheral nervous system revealed degenerative changes at the neuromuscular junction in aged Tau35 mice.

Primary cortical neurons cultured from Tau35 mice demonstrated elevated tau phosphorylation, morphological changes and a significant decrease in the density of dendritic spines. Further analysis of mitochondria in mature Tau35 cortical neurons showed a deficit in mitochondria that was comparable with that found in Tau35 mouse brain, including a reduction in the number of axonal mitochondria. Live-imaging of

Tau35 neurons demonstrated altered mitochondrial mobility with a preference towards mitochondrial retrograde movement and reduced anterograde mitochondrial flux.

In summary, these findings enhance our understanding of the effects of a particular disease-associated tau fragment on disease progression in the tauopathies. This work provides new insights into potential mechanisms that could represent early events that are adversely affected in the course of human tauopathy. This emulation of disease progression in a novel and highly relevant mouse model of disease will aid discovery of the critical molecular pathways that are affected and may also identify potential therapeutic strategies for human tauopathies.

Acknowledgements

I am lucky enough to have a lot of people to thank for helping and supporting me over the past few years on this remarkable yet challenging journey.

First of all, I want to thank my family, who unconditionally and generously gave me their love and support. My incredible mother, who has always been my role model, an example of strength, compassion and grace. My father for teaching me that only discipline, hard-work and persistence will allow me to reach my goals. And, of course, my brother, for encouraging me to always aim high and showing me that the sky is the limit. I would also like to thank my soon-to-be sister in law for being there for me when I need it. It happens, that more often than not, there are hundreds of miles between my family and I, but it's their continuous encouragement and faith in me that makes me feel that I can do anything I put my mind to.

I would like to thank my first supervisor, Diane Hanger, for giving me this tremendous opportunity to work in her laboratory. It's her guidance, scientific input, and enormous amount of patience that shaped me into the independent researcher that I have become. I would also like to thank my second supervisor, Wendy Noble, for her contributions during lab meetings, continuous support and very much needed pep talks. And, of course, I couldn't have done this without present and past members of the lab. Thank you! I want to particularly thank, Rebecca Gresham, for being an amazing and supportive lab parent.

I would also like to thank our incredible fellows: Beatriz Gomez Perez-Nievas, Maria Jimenez Sanchez, Elizabeth Glennon, Caterina Giacomini, Gabor Morotz and Patricia Gomez Suaga. Your guidance and scientific expertise were fundamental for my PhD

project. I want to say a big thank you to Bea for all that you taught me, in the lab and in life. I could not have done it without you!

I was also very lucky to have two great MSc students, Sarah Freckleton and Bianca Cronan. I was honoured to work with you and thank you for making my first time as a supervisor such an enjoyable and valuable experience.

Last but not the least, I want to thank my most wonderful, smart and talented colleagues and friends. Dina Dakkak, Anshua Ghosh, and Chun Hao Wong, thank you for all our 'meetings' in the meeting room, for making late nights in the lab more fun and for your tremendous support. It was my great honour to work alongside with you these years. Sarah Freckleton, thank you so much for all your help and support. I am grateful for you keeping me company on our endless trips to the BSU and for proof-reading pretty much everything I have written in the past couple of years. I wish you all the best in your PhD journey! I also want to massively thank Elena Turek, Ekaterina Shevchenko and Sergej Khon for being there for me no matter what, for continuous support and for always believing in me. My dearest friend, soon-to-be Dr Elena Turek, thank you for putting up with me over all these years, for opening your home to me and for including me in your family.

I am eternally grateful to have all of you in my life!

Natalia Yankova

April 2018

Abbreviations

ACh	Acetylcholine
AChR	Acetylcholine receptor
AD	Alzheimer's disease
ADP	Adenosine diphosphate
Aldh1L1	Aldehyde dehydrogenase 1 family member L1
ALS	Amyotrophic lateral sclerosis
Aβ	Amyloid beta
AMPAR	Alpha-amino-3-hydroxy-5-methyl-4-isoxazolepropionic acid
AMPK	AMP-Activated protein kinase
ANOVA	Analysis of variation
APP	Amyloid precursor protein
APS	Ammonium persulfate
ATG4	Autophagy-regulating protease 4
ATG7	Autophagy-related protein 7
ATP	Adenosine triphosphate
BACE1	Beta-secretase 1
BCA	Bicinchoninic Acid
Bcl2	B-cell lymphoma 2
BME	Beta-mercapto ethanol
BSA	Bovine serum albumin
BTX	Botulinum toxin
CA	Cornu ammonis
cAMP	Cyclic adenosine monophosphate
Casp6	Caspase 6
CBD	Corticobasal degeneration

CCCP	Carbonyl cyanide m-chlorophenylhydrazone
CD38	Cluster of differentiation 38
Cdk5	Cyclin-dependent kinase-5
cDNA	Complementary deoxyribonucleic acid
CHO	Chinese hamster ovary
CNS	Central nervous system
CREB	cAMP-response element-binding
CRH	Corticotropin-releasing hormone
CSF	Cerebrospinal fluid
DAB	Diaminobenzidine
DAPI	4',6-diamidino-2-phenylindole
DIV	Days in vitro
DMEM	Dulbecco's modified eagle medium
DMSO	Dimethyl sulfoxide
DNA	Deoxyribonucleic acid
dNTPs	Deoxynucleotide
DRP1	Dynamin-related protein 1
DTT	Dithiothreitol
ECM	Extracellular matrix
EDTA	Ethylenediaminetetraacetic acid
eGFP	Enhanced green fluorescent protein
EGTA	Ethylene glycol-bis (β-aminoethyl ether)-N,N,N',N'-tetraacetic acid
ER	Endoplasmic reticulum
ERRα	Estrogen-related receptor α
ESLB	Extra strong lysis buffer
FCCP	Carbonyl cyanide 4-trifluoromethoxyphenylhydrazone
FDB	Flexor digitorum brevis

FDL	Flexor digitorum longus
Fis1	Mitochondrial fission 1 protein
FOXO	Forkhead box O
FTD	Frontotemporal dementia
GAPDH	Glyceraldehyde 3-phosphate dehydrogenase
GFAP	Glial fibrillary acidic protein
GFP	Green fluorescent protein
GSK-3β	Glycogen synthase kinase-3 beta
HA	Human influenza hemagglutinin
HBSS	Hanks' balanced salt solution
HD	Huntington's disease
HDAC	Histone deacetylase
HDR	High dynamic range
HEPES	N-2-hydroxyethylpiperazine-N'-2-ethanesulfonic acid
HET	Heterozygous
HOM	Homozygous
HPRT	Hypoxanthine phosphoribosyltransferase
HSP60	Heat shock protein 60
ICC	Immunocytochemistry
IF	Immunofluorescence
IgG	Immunoglobulin G
IHC	Immunohistochemistry
LC3	Microtubule-associated protein 1A/1B-light chain 3
L-DOPA	L-3,4-dihydroxyphenylalanine
LIR	LC3-interacting region
Lrp4	Low density lipoprotein receptor-related protein 4

LTD	Long-term depression
LTP	Long-term potentiation
MAP	Microtubule associated protein
MAPK	Mitogen-activated protein kinase
MAPT	Microtubule-associated protein tau
MBR	Microtubule binding region
MES	2-(N-Morpholino) ethanesulfonic acid
MFN1	Mitofusin 1
MFN2	Mitofusin 2
MRC	Medical Research Council
MRI	Magnetic resonance imaging
mRNA	Messenger RNA
MTBD	Microtubule binding domain
mtDNA	Mitochondrial deoxyribonucleic acid
m-TOR	Mammalian target of rapamycin
MuSK	Muscle-specific kinase
Myo19	Myosin 19
Myo2	Myosin 2
N/A	Not applicable
NAD	Nicotinamide adenine dinucleotide
NF-M	Neurofilament medium chain
NFT	Neurofibrillary tangle
NGS	Normal goat serum
NMJ	Neuromuscular junction
NRF	Nuclear respiratory factor
NTFs	Neurofibrillary tangles
OCR	Oxygen consumption rate

OCT	Optimal cutting temperature
OPA	Optic atrophy protein 1
OXPHOS	Oxidative phosphorylation
PB	Pick body
PCR	Polymerase chain reaction
PD	Parkinson's disease
PDL	Poly-D-lysine
PE	Phosphatidylethanolamine
PFA	Paraformaldehyde
PGC-1α	Peroxisome proliferator-activated receptor gamma coactivator 1-alpha
PHFs	Paired helical filaments
PI	Propidium iodide
PI3K	Phosphatidylinositol 3-Kinase
PiD	Pick's disease
PINK1	Protein phosphatase and tensin homolog (PTEN)-induced kinase 1
PP2A	Protein phosphatase 2A
PRD	Proline rich domain
PS1	Presenilin 1
PSA	Puromycin-sensitive aminopeptidase
PSD95	Postsynaptic density protein 95
PSP	Progressive supranuclear palsy
PTEN	Phosphatase and tensin homolog
Rab7	Ras-related protein
ROS	Reactive oxygen species
SDS	Sodium dodecyl sulfate
SEM	Standard error of the mean

SH3	Src homology 3
SIRT1	Sirtuin 1
SOD1	Superoxide dismutase 1
SV2	Synaptic vesicle glycoprotein 2A
SQSTM1	Sequestosome 1
TAE	Tris-acetate-EDTA
TBS	Tris-buffered saline
TDP-43	Transactive response DNA-binding protein 43
TEMED	N,N,N',N'tetramethylethylendiamine
TFAM	Transcription factor A mitochondrial
TIFF	Tagged image file format
TOM20	Translocase of outer membrane receptor 20
VDAC	Voltage-dependent anion channel
WB	Western blot
WT	Wild-type

List of Figures

List of Tables

Chapter 1: Introduction

1.1 Tau Protein

Tau is a microtubule-associated protein that is encoded by the microtubule associated protein tau (*MAPT)* gene located on chromosome 17q21 (Weingarten et al., 1975; Neve et al., 1986; Andreadis, 2006). Tau is overall an unfolded and hydrophilic protein (Jeganathan et al., 2008; Mukrasch et al., 2009). The structure of tau is crucial for its normal function. It comprises of 4 components. Firstly, the N-terminus with an acidic region is followed by the proline-rich domain (PRD). Next is the microtubule binding region (MBR), that is essential for tau function and contains either three or four carboxyl terminal repeat domains (R) that facilitate tau binding to microtubules. The final section of tau protein is the C-terminus (Mandelkow et al., 1996). The microtubules binding domain consists of repeated motifs that allow tau to perform its main function i.e. binding and stabilising microtubules. Tau is found predominantly in neurons but is also present at low levels in glia and in interstitial fluid (Goedert et al., 1989; LoPresti et al., 1995; Goedert et al., 1996; Wang and Mandelkow, 2016; Yamada, 2017) The subcellular localisation of tau changes depending on the stage of neuronal development (Drubin et al., 1984). In developing neurons, tau is present throughout the neuron, including the cell body and neurites. As neurons mature, they become more polarised and tau is predominantly detected in axons, with much less tau apparent in dendrites and the nucleus (Black et al., 1996; Papasozomenos and Binder, 1987; Kempf et al., 1996; Mandell and Banker, 1996; Sultan et al., 2011).

Tau is a multi-functional protein, which in addition to its role as a microtubule stabiliser, is also involved in adult neurogenesis, modulation of several signaling pathways, synaptic function and DNA damage protection through nuclear organisation (Sjöberg et al., 2006; Reynolds et al., 2008; Gómez-Ramos et al., 2009; Ittner and Götz, 2011;

Sultan et al., 2011; Spillantini and Goedert, 2013). Some tau isoforms, particularly 1N4R, are present in the nucleus (Liu et al., 2013). Tau phosphorylation affects its function in the nucleus, especially tau being localised in the nucleus (Maina et al., 2015). Nuclear tau can bind to DNA, possibly protecting DNA integrity upon exposure to heat stress (Sultan et al., 2011).

1.1.1 Alternative splicing of *MAPT*

In the human central nervous system (CNS), the tau mRNA transcript expresses six tau isoforms of molecular weights between 37-48 kDa, due to alternative splicing of exons 2, 3 and 10 (Goedert and Jakes, 1990). In total, alternative splicing yields six tau isoforms that can be differentiated by the presence of zero, one or two N-terminal inserts (0N, 1N, or 2N, respectively) and the presence of either three (3R) or four (4R) MBR (Fig. 1.1). The 3R and 4R isoforms are present in approximately equal amounts in the brain of a healthy adult and the 2N (~9%) isoform is under represented in comparison with the 0N (~37%) and 1N (~54%) isoforms (Goedert and Jakes, 1990). There are certain specific patterns that the splicing of tau protein follows. For example, exons 2 and 3 each encode 29 amino acids in the amino terminal region of tau, and exon 3 is not transcribed in the absence of exon 2 (Fig. 1.1). Exons 4A, 6 and 8 are transcribed exclusively in the peripheral nervous system, generating a series of larger tau proteins of 110-120 kDa. Interestingly, during development, foetal brain expresses exclusively the shortest tau isoform (0N3R) (Fig. 1.1) (Goedert et al., 1988; Guo et al., 2017).

Mouse and human tau proteins are highly homogenous, sharing 92% sequence similarity, but they differ considerably in the N-terminal region, where there is only 57% sequence similarity (Goedert et al., 1988). However, it is important to note that rodent tau isoforms are represented in different proportions as adult mouse brain

expresses almost exclusively 4R tau isoforms (Takuma et al., 2003). In contrast, 3R tau is present only in foetal and new-born mice (Llorens-Martin et al., 2012).

Fig. 1.1 Six tau isoforms in the human CNS

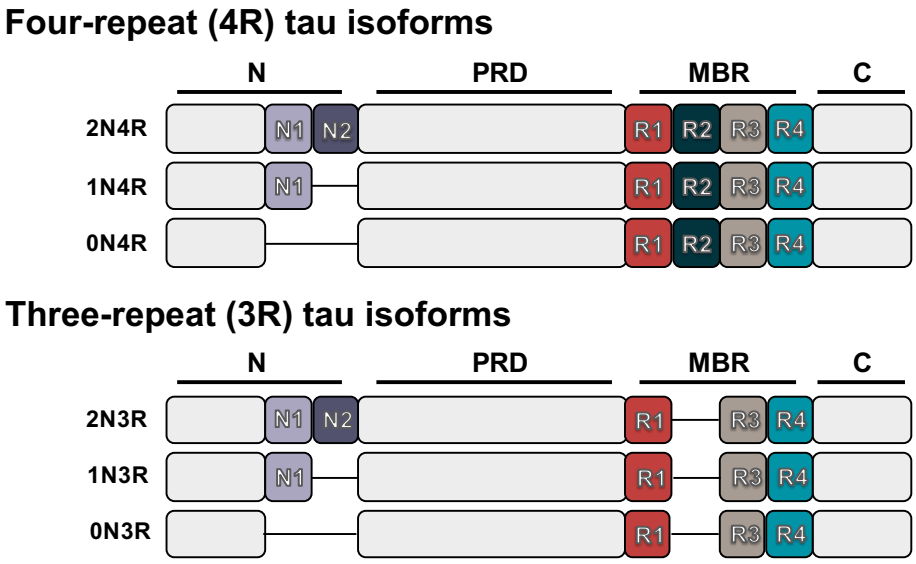

Six isoforms of tau are generated in the human CNS by alternative splicing. Distinct amino acid sequences encoded by exons 2 and 3 in the N-terminal region of tau are either excluded (0N), or differentially included, giving rise to 1N (exon 2) or 2N (exons 2 and 3) tau isoforms. It is followed by a proline rich domain (PRD). Alternative splicing of exon 10 in the microtubule binding repeats (MBR), results in 3R or 4R tau isoforms. The C-terminal region is common to all six human CNS tau isoforms (image adapted from Guo et al., 2017).

1.1.2 Tau protein structure and function

The 2N4R tau isoform comprises 441 amino acids, including 80 serine (S) and threonine (T) residues, 56 aspartate (D) and glutamate (E) residues, 58 lysine (K) and arginine (R) residues, 5 tyrosine (Y), and 3 phenylalanine (F) residues. Overall, tau is a basic protein, however, the ~120 N-terminal residues are predominantly acidic, and the ~40-residue C-terminus is approximately neutral (Wang and Mandelkow, 2016). It has been proposed that when tau is free in the cytoplasm it adopts a 'paperclip' conformation (Jeganathan et al., 2008; Mukrasch et al., 2009). The 'paperclip' is suggested to be formed when the C-terminus folds over the microtubules binding domain and the N-terminus folds over the C-terminus. However, upon binding to the microtubules, a more open tau conformation is adopted. In addition, tau conformation is readily disrupted by phosphorylation of tau on the proline residue that manipulates loosening or tightening of the 'paperclip' structure (Jeganathan et al., 2008; Mukrasch et al., 2009).

Fig. 1.2 Paperclip confirmation of Tau

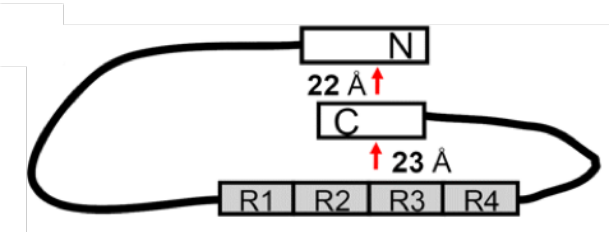

Full-length 2N4R tau adopts a paperclip conformation by folding of the C-terminal domain onto the microtubule-binding repeat (R1-R4) domain, with the N-terminal domain folding over the C-terminus (adapted from Jeganathan et al., 2008).

Tau participates in signalling cascades and regulates axonal transport in neurons (Chen et al., 1992; Kanaan et al., 2011). In addition, the two N-terminal inserts might affect the subcellular distribution of tau in neurons because, in mice, the 0N, 1N and 2N tau isoforms show distinct subcellular distributions (Liu and Götz, 2013; Liu et al., 2016). Moreover, distinct binding partners of tau display preferences towards different tau isoforms, as revealed by co-immunoprecipitation with tau isoform-specific antibodies. For example, in C57BL/6 mice compared to tau knockout mice, apolipoprotein A1 (ApoA1) displays a five-fold preference for interaction with 2N tau isoforms, whereas β-synuclein showed a preference for binding to 0N tau isoforms (Liu et al., 2016). ApoA1 is a major component of high density lipoprotein (HDL) and is involved in lipid metabolism (Saczynski et al., 2007). It has been also observed that ApoA1 has neuroprotective properties and its low concentration in plasma is associated with AD. (Slot RE et al., 2017) The other protein, β-synuclein, is an abundant presynaptic protein, similar to its homolog, α-synuclein. Both proteins are important for neuronal plasticity and synaptic vesicle regulation. (Sriwimol et al., 2018) However, β-synuclein has a much lower tendency to aggregate in comparison to α-synuclein. Furthermore, it has been found to inhibit α-synuclein aggregation. (James W.P. Brown., 2016)

Although tau plays a crucial role in brain development and function, tau knock out (TauKO) mice do not show a severe phenotype (Dawson et al., 2001; Harada et al., 1994). Neurons generated from TauKO mice appear to maintain their morphology and cytoskeletal organisation (Harada et al., 1994). However, TauKO mice show a selective deficit in long term depression (LTD) in the cornu ammonis 1 (CA1) region of the hippocampus in tau-knockout mice *in vivo* and *ex vivo* (Kimura et al., 2014a). In addition, changes observed in neurons in TauKO mice imply that tau may play an important role in neuronal activity and synaptic plasticity (Kimura et al., 2014b). However, knocking out tau led to a decrease in migration of new-born neurons from

the subgranular zone of the hippocampal formation to the granular layer, instead of a reduction in neurogenesis (Fuster-Matanzo et al., 2012).

1.2 Tau interactions

In addition to interacting with microtubules, tau has many other binding partners, such as α-synuclein, apolipoprotein E and presenilin 1 (Jensen et al., 2008). Tau protein binding to actin filaments allows control of cytoskeletal structure. Furthermore, tau can act as a signalling scaffold. In mouse brain, tau interacts with both the tyrosine kinase Fyn and the scaffolding protein postsynaptic density protein 95 (PSD95). Knocking out tau in mice abolishes the translocation of Fyn into postsynaptic sites in dendrites (Ittner et al., 2010).

The N-terminus of tau projects away from microtubules, allowing tau to bind to other components of the cell. The N-terminus of tau interacts with the microtubule motor protein dynein, through the p150 subunit of the C-terminus of dynactin complex that, in turn, allows interaction and transport of membranous cargoes, such as cellular organelles (Magnani et al., 2007). The different domains of tau bind many different types of molecules, suggesting a central role in signaling pathways and cytoskeletal organization (Kotani et al., 1985; Fulga et al., 2007; He, 2009).

1.3 Tauopathies

Neurodegenerative tauopathies are a heterogeneous group of dementias and movement disorders that are neuropathologically characterised by prominent intracellular accumulations of abnormal filaments that form neurofibrillary tangles (NFTs), formed of tau, as well as other tau inclusions in neurons and glia. Tauopathies include but are not limited to, Alzheimer's disease (AD), frontotemporal lobar degeneration (FTLD-tau), Pick's disease (PiD), and progressive supranuclear palsy

(PSP). These diseases can have both sporadic and familial origin. A key neuropathological characteristic of the tauopathies is the presence in the brain of tau deposits which may be apparent many years before the onset of clinical symptoms (Fig. 1.3) (Gauthier-Kemper et al., 2011). Extensive studies of tau have shown that the presence of a tau mutation alone is sufficient to cause neurodegenerative disease (Hutton et al., 1998).

Fig. 1.3 Different types of tau pathology in human tauopathies

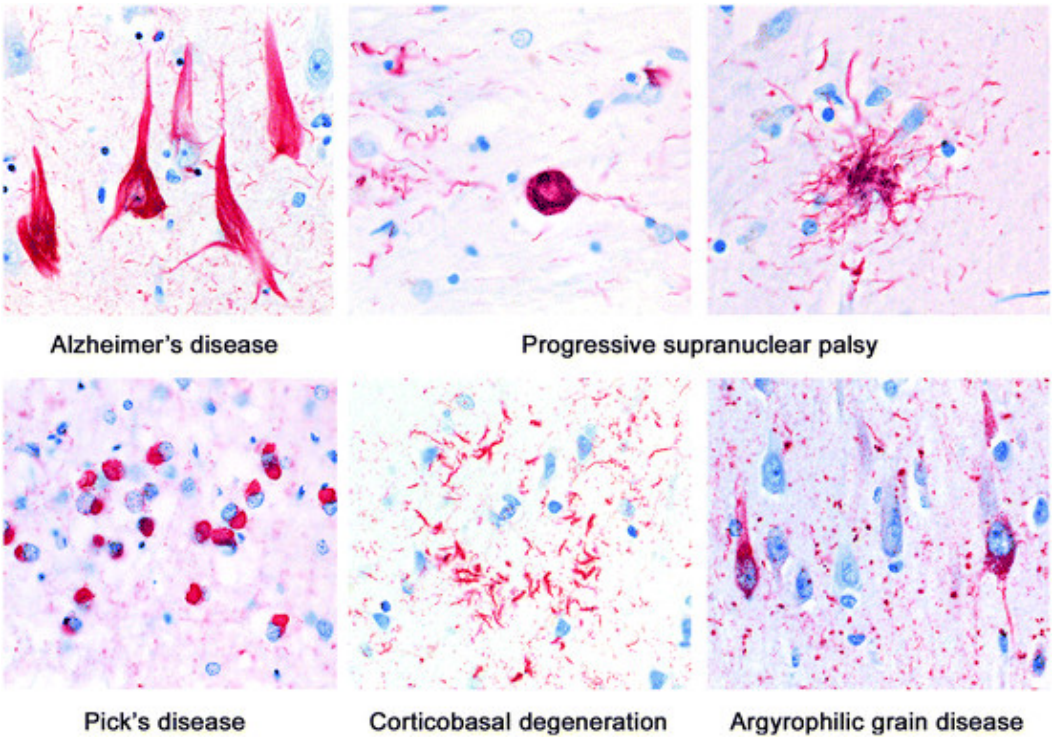

Immunohistochemistry with phosphorylation-dependent anti-tau antibody AT8. From left to right, upper panel: typical flame-shaped neurofibrillary tangles in AD; globose-type neurofibrillary tangles and tufted astrocytes in PSP. Lower panel: Pick bodies in PiD; astrocytic plaques in CBD; argyrophilic grains and pre-tangle neurons in argyrophilic grain disease (AGD) (Clavaguera et al., 2013).

1.3.1 Alzheimer's disease

AD is by far the most common form of dementia with 850,000 people in the UK alone living with the disease and this number is set to rise to 1 million by 2025 (Prince et al. 2014). Current predictions are that AD will affect 152 million people globally by 2050, making it a global epidemic (Brookmeyer et al., 2007). Age is the biggest risk factor for AD (Lindsay et al., 2002). Because of great improvement in healthcare and increase in longevity of the human population, AD is predicted to have a huge impact on the economy (Wimo et al., 2013).

In AD, the CNS contains tau which is abnormally phosphorylated and forms NFTs in the brain (Tortosa et al., 2011). NFTs are primarily localised to the soma, but when neuronal death occurs, they are released into the extracellular space and may become associated with microglia and astrocytes (Ikeda et al., 1992). The Braak classification system categorises neuropathological disease progression as six different stages (Braak and Braak, 1991). This staging is based on the evidence that NFTs spread throughout the brain in a consistent pattern (Braak and Braak, 1991). At first, NFTs appear in the transentorhinal cortex (Braak Stage I), followed by the cornu ammonis (CA) 1 region of the hippocampus (Braak Stage II), followed by accumulation in limbic structures, such as the subiculum of the hippocampus (Braak Stage III), then amygdala, thalamus and claustrum (Braak Stage IV). In later stages, NFTs appear in the isocortical areas, with associative areas affected first (Braak Stage V), followed by primary sensory, motor and visual areas (Braak Stage VI) (Fig. 1.4) (Hyman et al., 1984; Arnold et al., 1991; Braak and Braak, 1991). This hierarchical pattern of NFTs and degeneration in affected brain regions is very consistent and is in use as a post-mortem diagnostic tool (Montine et al., 2012; Alafuzoff et al., 2008).

Fig. 1.4 Braak staging of Alzheimer's disease brain

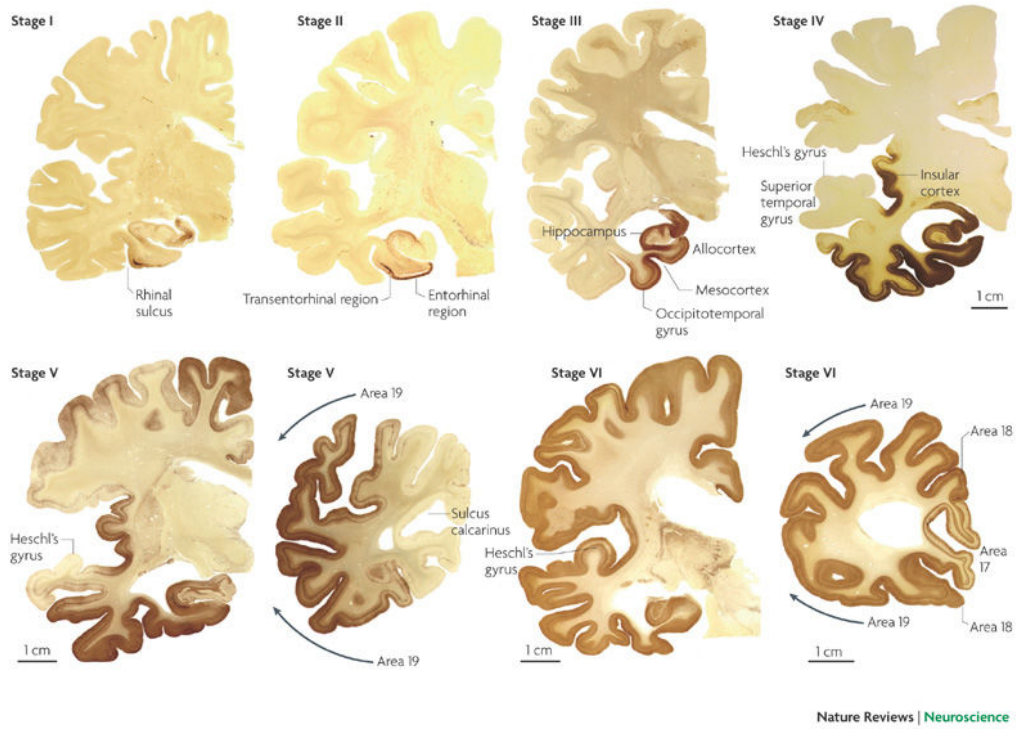

Braak classification of Alzheimer's disease by the progression of neurofibrillary tangles as shown (immunohistochemistry with an antibody against phosphorylated tau). NFT accumulation begins in the transentorhinal cortex in Braak Stages I and II, progression into limbic areas by Braak Stages III and IV, and its culmination in neocortical and primary sensory areas in Braak Stages V and VI (Kretzschmar, 2009).

1.3.2 Progressive supranuclear palsy

PSP is a form of tauopathy that is clinically identified as a primary motor disorder, although it can also present with symptoms of cognitive decline (Conrad et al., 1997; Baker et al., 1999). The UK PSP Association reports that there are 4,000 people living with PSP, which is characterised clinically by progressive gait disturbance with poor balance, early falls and a supranuclear gaze palsy (downward gaze) (Gold et al., 2012). However, due its clinical symptoms, PSP is often misdiagnosed as PD (Schrag et al., 1999). Neuropathologically, PSP is associated with the deposition of phosphorylated tau as globose NFT, neuropil threads, and fibrillary gliosis in the pallidum, subthalamic nucleus, red nucleus, striatum, substantia nigra, pontine tegmentum, oculomotor nucleus, medulla, and dentate nucleus (Tawana and Ramsden, 2001; Williams and Lees, 2009). In PSP, the gross structural appearance of tau-containing globose tangles is most commonly found in the basal ganglia, the midbrain, which is involved in supranuclear eye movements, cerebral cortex and spinal cord. Tau in PSP brain contains highly phosphorylated aggregates of predominantly 4R tau isoforms, indicating an abnormality in the balance of 3R/4R tau isoform expression.

1.3.3 Corticobasal degeneration

Corticobasal degeneration (CBD) is a neurodegenerative disease characterised by progressive asymmetrical rigidity and apraxia (Boeve et al., 1999; Mahapatra et al., 2004; Armstrong et al., 2013). The incidence of CBD is 7 in 100,000 people worldwide (Mahapatra et al., 2004). The symptoms and clinical presentation of CBD are very varied, including motor symptoms such as dystonia, myoclonus, tremor, alien limb phenomenon, motor speech disorders, eye movement disturbance, cortical dementia, and cortical sensory loss (Litvan et al., 1997; Houlden et al., 2001; Ludolph et al., 2009; Armstrong et al., 2013). Neuropathologically, CBD is characterised by asymmetric parietal and frontal cortical degeneration, with neurofilament protein-

positive ballooned neurons and tau-positive astrocytic plaques and coiled bodies in oligodendrocytes (Boeve et al., 1999). CBD brain features tau inclusions that are both intraneuronal and extraneuronal, containing mainly 4R tau (Mahapatra et al., 2004). CBD predominantly demonstrates damage to the basal ganglia and loss of myelination in the substantia nigra (Scaravilli et al., 2005), However, CBD is increasingly reported with other underlying pathologies, such as AD, PSP, and dementia with Lewy bodies (Hassan et al., 2014).

The diagnoses of PSP and CBD can be difficult due to the lack of specific biomarkers. In the absence of approved pharmacological treatments for PSP and CBD, management is based on relieving symptoms and assistance with activities of daily living (Mahapatra et al., 2004; Armstrong et al., 2013). At the moment, most people presenting clinically with these disorders are treated with L-3,4-dihydroxyphenylalanine (L-DOPA), the precursor of dopamine, or amantadine, an anti-parkinsonian medication, although there is limited evidence for benefit, some people experience modest improvement in their parkinsonian symptoms (Parkes et al., 1972; Lang et al., 2005; Wadia and Lang, 2007). Botulinum toxin has also proved to be helpful for both disorders in reducing dystonia and is particularly useful for eyelid dysmotility (Doble, 1996; Kompoliti et al., 1998; Shehata et al., 2015).

1.3.4 Frontotemporal lobar degeneration-tau and Pick's disease

FTLD-tau is a non-AD degenerative dementia with focal cortical neuronal loss, gliosis and tau inclusions (McKhann et al., 2001; Irwin et al., 2015; Bodea et al., 2016). FTLD-tau is characterised neuropathologically by frontotemporal atrophy with neuronal loss, gliosis, and cortical spongiform changes in frontal and temporal lobes. FTLD-tau is the consequence of mutations in the tau gene and it can present with an extensive variety of clinical symptoms (Avila et al., 2004b; Ludolph et al., 2009; Dickson et al., 2011). For example, one of the most common *MAPT* mutations, a proline to leucine substitution at codon 301 in tau (P301L tau) (Mirra, 1999), results in tau dysfunction and neuronal death (Hutton et al., 1998). Generally, tau mutations in FTLD-tau lead to language and memory impairment, motor deficits and behavioural abnormalities (Irwin et al., 2015; Bodea et al., 2016). FTLD-tau exhibits a preferential accumulation of 4R tau and sometimes 3R tau isoforms, providing a sub-classification of the tauopathies (Table 1). Furthermore, the ratio between 3R and 4R tau is thought to be the key to tau-related neurodegeneration. For instance, in AD this ratio is altered due to either increase of 4R tau or decrease or 3R leading to almost twice as much 4R than 3R tau (Ginsberg et al., 2006; Conrad et al., 2007; Dickson et al., 2011).

Table 1 Classification of the most common subtypes of tauopathies

Disorder	Major brain areas affected	Major clinical features
4R TAUOPATHIES		
CBD	Cortex and basal ganglia	Focal cortical syndrome and parkinsonism
PSP	Basal ganglia, brainstem and cerebellum	Atypical parkinsonism
FTDP-17T	Cortex, basal ganglia & brainstem	Focal cortical syndrome and parkinsonism
3R TAUOPATHIES		
PiD	Cortex and limbic lobe	Dementia and focal cortical syndrome
FTDP-17T	Cortex, basal ganglia & brainstem	Dementia and focal cortical syndrome
3R+4R TAUOPATHIES		
AD	Cortex and limbic lobe	Dementia and focal cortical syndrome
FTDP-17T	Cortex and limbic lobe	Dementia and psychosis

4R tauopathies: corticobasal degeneration (CBD), progressive supranuclear palsy (PSP), frontotemporal dementia with parkinsonism-17 tau (FTDP-17T); 3R tauopathies: Pick's disease (PiD), FTDP-17T; 3R:4R tauopathies: Alzheimer's disease (AD), FTDP-17T (adapted from (Dickson et al., 2011)).

PiD is also a form of frontotemporal dementia that results in disturbances in language and behaviour and is associated with frontal lobe atrophy (Dickson, 2001). Neuropathologically, there is progressive cortical atrophy mainly in anterior and frontal temporal lobes, white matter degeneration, achromatic neurons and intraneuronal lesions of cytoplasmic highly phosphorylated 3R isoforms, known as Pick bodies (PBs) in the hippocampus, selective brainstem nuclei and cerebral cortex (Hauw et al., 1994; Feany and Dickson, 1996; Takeda et al., 2013; Avila et al., 2004a; Robert and Mathuranath, 2007).

1.4 Tau phosphorylation

Phosphorylation is the most commonly described post-translational modification of tau, which harbours 85 potential phosphorylation sites (S, T, Y residues) (Hanger et al., 2009). Under pathological conditions, tau phosphorylation is increased, and this reduces its affinity for microtubules, resulting in destabilisation of the neuronal cytoskeleton (Drewes et al., 1995).

Fig. 1.5 illustrates the phosphorylation sites on tau that are involved in its normal function (blue) and those that are phosphorylated during disease (red). There are also amino acids that are phosphorylated in both healthy brain and in tauopathies (green). Specific antibodies have been generated that allow identification of a variety of different phosphorylation sites present on tau protein. These antibodies are designed to target different regions of tau protein.

Tau phosphorylation is regulated by both kinases that add phosphate, and by phosphatases that remove phosphate, from tau protein (Hanger et al., 2007; 2009). It appears that both the amount of tau and the activities of phosphatases and kinases contribute to tau phosphorylation (Pei et al., 1997; Hanger et al., 2009). Moreover, the higher the activity of the kinases, the greater the NFT formation in disease (Braithwaite et al., 2012). Many tau phosphorylation sites are targeted by the proline-directed serine/threonine-protein kinases, glycogen synthase kinase (GSK)-3α and GSK-3β (Hanger et al., 1992, Hanger et.al, 2009). For example, phosphorylation of tau on Thr231 by GSK3β induces tau aggregation (Rankin et al., 2007), whereas inhibition of GSK3β reduces tau phosphorylation (Lovestone et al., 1994; Serenó et al., 2009). This finding was further taken to clinical trial, however, inhibition of GSK3 using lithium did not result in an effective therapy for either AD or PSP (Leclair-Visonneau et al., 2016).

In addition, it was shown that abnormal sorting of human tau (htau) into the somatodendritic compartment of neurons, where hyperphosphorylated htau aggregates, is one of the early pathological hallmarks of tauopathies (Gotz et al., 1995; Avila et al., 2004a; Gendron and Petrucelli, 2009). However, the physiological effect of this missorting is unknown. It is thought that tau mis-sorting causes early synaptic dysfunction by suppressing α-amino-3-hydroxy-5-methyl-4-isoxazolepropionic acid (AMPAR) - mediated synaptic responses, probably through a global disruption of postsynaptic targeting or anchoring of glutamate receptors (Hoover et al., 2010). Furthermore, tau mislocalisation into dendritic spines is phosphorylation-dependent and is associated with suppression of synaptic function. This suppression was mediated, through a postsynaptic mechanism involving loss of cell surface AMPARs (Hoover et al., 2010). Furthermore, long-term potentiation (LTP), responsible for synaptic plasticity responsible for learning and memory, is also inhibited in rTgP301L and WT htau mice (Yoshiyama et al., 2007; Hoover et al., 2010; Polydoro et al., 2013).

Fig. 1.5 Tau phosphorylation in health and disease

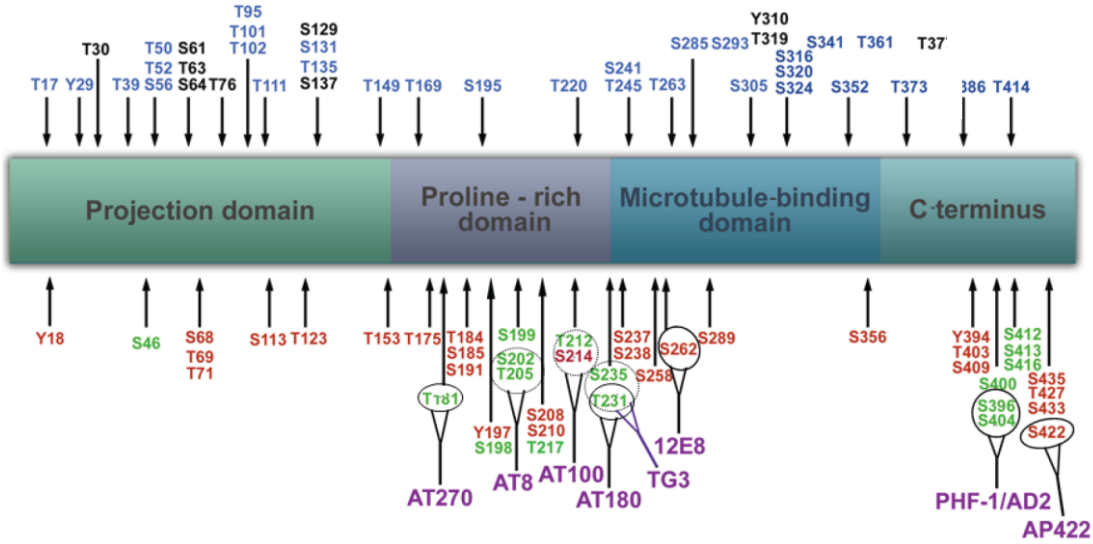

Phosphorylation sites on tau protein and epitopes specific for major tau antibodies. Amino acids phosphorylated in AD brain (red), both AD and control human brain (green), control human brain (blue), while those in black indicates phosphorylation sites that have not yet been well characterised. Tau antibodies specific for phospho-tau epitopes are shown in purple (adapted from (Šimić et al., 2017).

1.5 Tau aggregation

There are links between abnormal phosphorylation and aggregation of tau (Liu et al., 2007), as phosphorylation decreases the affinity of tau for microtubules and reduces microtubule stability. When tau becomes detached from microtubules, it forms both low order oligomers and higher order tau aggregates (Liu et al., 2007). Tau phosphorylation in the proline rich domain (PRD) (residues 172-251), disrupts tau binding to microtubules, leading to tau aggregation. In addition, phosphorylation in the C-terminal region of tau (residues 368-441), further promotes tau aggregation (Eidenmüller et al., 2001; Liu et al., 2007).

In the microtubule binding repeats (MBR) of tau, there are two segments that tend to form β-sheets and drive abnormal self-assembly of tau (Mukrasch et al., 2007; 2009). Structurally these segments contain six residues: VQIINK and VQIVKY (Pérez et al., 1996). These segments are located at the start of R2 and R3 of the MBR, respectively (Bulic et al., 2010). Oligomerisation of tau occurs when monomers and dimers are recruited, forming a nucleation center and clusters (Barghorn and Mandelkow, 2002). The P301L tau mutation is located within R2 of the MBR, and therefore it affects only 4R tau isoforms (Lewis et al., 2001). However, introducing a proline residue into the VQIVKY segment can lead to disruption the β-sheet structure in this region and therefore prevents tau aggregation (Bulic et al., 2010).

The overall charge of tau can dramatically impact its folding (Jeganathan et al., 2006). Addition of phosphate adds negative charge and tau acetylation on lysine residues cancels out their positive charge, both modifications impacting the overall charge on tau (Jeganathan et al., 2006). To further demonstrate the effect of altered charge on tau protein structure, negatively charged agents, such as heparin, have been shown to act as aggregation inducers. (Schafer et al., 2013).

However, the toxicity of aggregated tau is not yet clear. Multiple cell and animal models have been used to study the impact of aggregated and highly phosphorylated tau on disease progression (Wischik et al., 2014; Wagner et al., 2015; Bhaskar et al., 2010; Noble et al., 2013; Šimić et al., 2017). For example, in primary hippocampal neurons exposed to formaldehyde, tau significantly misfolds and polymerises (Nie et al., 2007). Expression of a fragment of mutant K18ΔK280 tau (comprising residues S258–I360, lacking K280) either alone, or together with full-length tau harbouring the ΔK280 mutation, caused cytotoxicity in N2a cells, which became positive for thioflavin S staining (Wang et al., 2007), indicating formation of β-sheet and implicating an association of aggregated tau with cytotoxicity. In contrast, findings from a transgenic tau mouse expressing P301L tau in an inducible manner, in which NFT develop from four months of age, demonstrated that memory is improved and neuronal loss is halted when the mutant tau gene is switched off, without affecting NFT accumulation (Santacruz et al., 2005). Previous studies suggest that pathological changes in tau such as mislocalisation to the somatodendritic compartment, increased phosphorylation and structural changes may be more damaging than NFT deposition (Wittmann et al., 2001; Spires et al., 2006). Therefore, it remains debatable whether NFTs are actually toxic, however, it is likely that tau species that are generated during the formation of NFTs are damaging to cells. There is accumulating evidence that soluble oligomeric forms of tau, that may be generated during NFT formation and tau overexpression, are more damaging to neurons and to synaptic function (Lasagna-Reeves and Kayed, 2011).

1.6 Tau acetylation

Tau acetylation is important for tau function. However, depending on which tau residue is acetylated, it may be either protective or pathological (Šimić et al., 2017; Trzeciakiewicz et al., 2017). Acetylation occurs on lysine residues and the effects of

acetylation are summarised in Table 2. Tau acetylation is regulated by acetylases including P300 acetyltransferase and cAMP-response element binding protein (CREB)-binding protein, which acetylate tau at several lysine residues within the MBR (Min et al., 2010; Kamah et al., 2014). Sirtuin 1 (SIRT1) and histone deacetylase (HDAC) 6 are responsible for tau deacetylation (Cook et al., 2014; Min et al., 2015). Notably, tau also has an intrinsic acetyltransferase activity and so it can also catalyse auto-acetylation at certain residues including K280 (Cohen et al., 2013). In summary, acetylation of several different lysine residues in tau, including K163, K280, K281 and K369, facilitates accumulation of phosphorylated tau and inhibits tau degradation (Min et al., 2010; 2015).

Table 2 Tau acetylation

Lysine residue	Effects of acetylation on tau function	References
K163	Inhibition of tau degradation Accumulation of hyperphosphorylated tau	Min et al., 2010
K174	Delays tau turnover Promotes tau toxicity Associated with human AD brain	Min et al., 2015
K259	Protects tau from phosphorylation Prevents tau aggregation Reduced acetylation in tauopathies	Cook et al., 2014
K280	Inhibition of tau degradation Accumulation of hyperphosphorylated tau Associated with many tauopathies	Min et al., 2010 Irwin et al., 2013
K281	Inhibition of tau degradation Accumulation of hyperphosphorylated tau	Min et al., 2010
K290	Protects tau from phosphorylation Prevents tau aggregation	Cook et al., 2014
K321	Protects tau from phosphorylation Prevents tau aggregation	Cook et al., 2014
K353	Protects tau from phosphorylation Prevents tau aggregation	Cook et al., 2014
K369	Inhibition of tau degradation Accumulation of hyperphosphorylated tau	Min et al., 2010

1.7 Tau propagation

Tau protein aggregates have been shown to spread from one area of the brain to another (Fig. 1.6) This method of tau propagation is referred to as ‘prion-like’ distribution. Therefore, tau aggregates, can be released into the intracellular space and uptake by neighbouring cell, i.e. intercellular and inter-organismal transmission. Tau inclusions originate in brainstem pons distributing to hippocampus and neocortex at later stages. This spreading of aggregates is important for disease progression and discovering potential therapeutic targets. (Goedert et al., 2015)

Fig. 1.6 Spread of tau inclusions in human brain

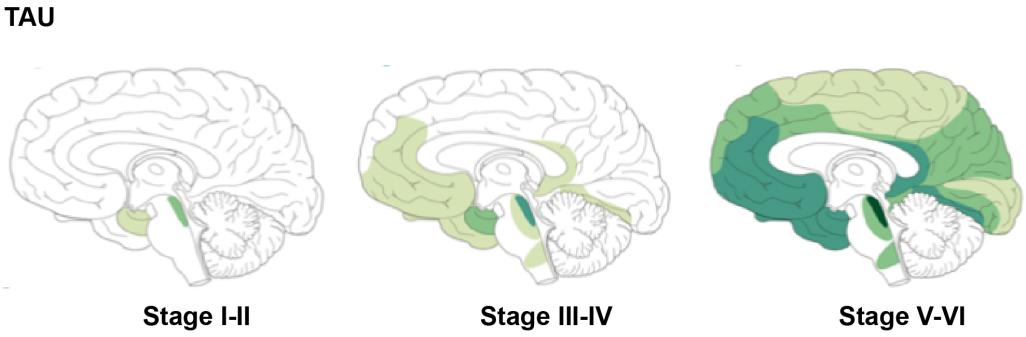

Tau inclusions distribution thoughout the human brain starting locus coeruleus, transentorhinal and entorhinal regions (Stages I and II). Followed by spreading to the hippocampal formation and some parts of the neocortex (Stages III and IV), and finally to large parts of the neocortex (Stages V and VI) (adapted from Goedert et al., 2015).

1.8 Tau degradation

Tau can be degraded by both autophagy and proteasomal pathways (Wang and Mandelkow, 2012). There are three major forms of autophagy: microautophagy, macroautophagy and chaperone mediated-autophagy (Cuervo, 2004). The most common of these sub-types of autophagy is macroautophagy, which involves lysosomal degradation of cytoplasmic material. Whereas proteasomal degradation is primarily responsible for short lived proteins, autophagy degrades many long-lived proteins, as well as damaged organelles, such as mitochondria and peroxisomes (Johansen and Lamark, 2011). Autophagic degradation occurs through the formation of a double-membraned autophagophore that increases in size to engulf cytoplasmic substrates, including tau and damaged organelles, for degradation. Further, an autophagosome is formed that moves towards the lysosome to fuse and form the autolysosome (Fig. 1.7). Lysosomal cathepsins play an important role in degradation of the content of the autolysosome (Chesser et al., 2013).

Fig. 1.7 Schematic representation of autophagy

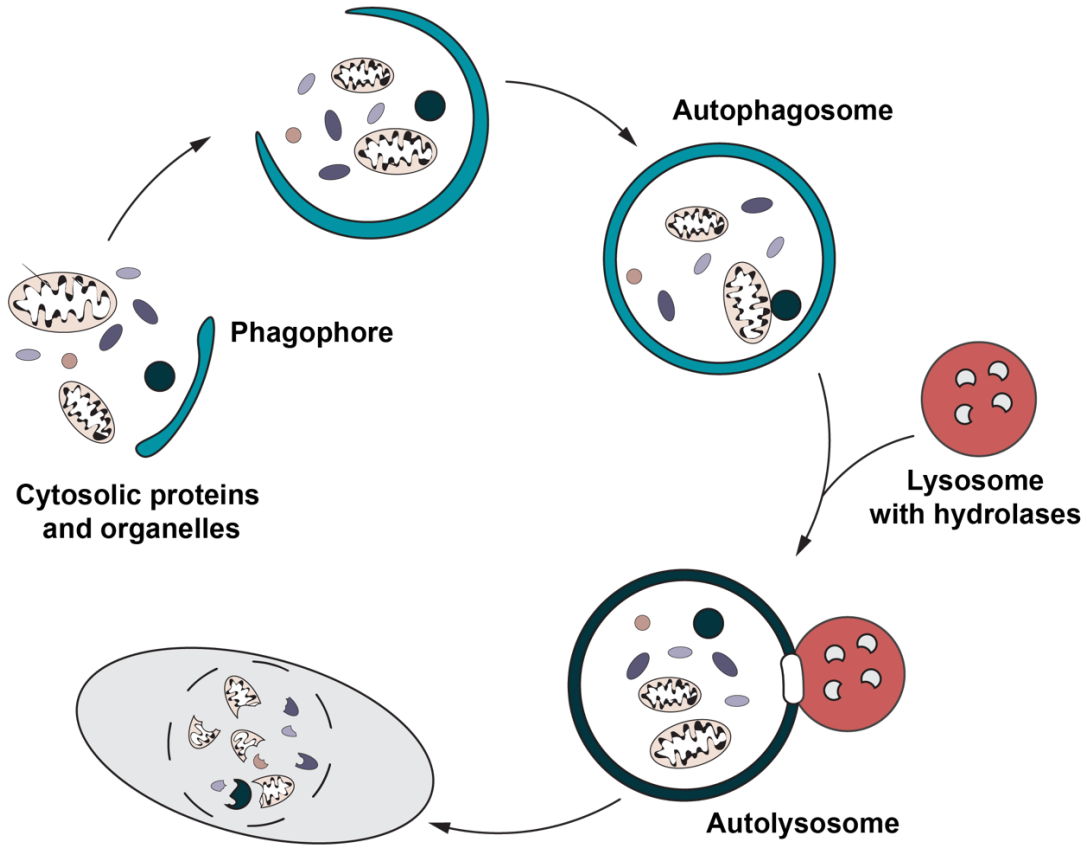

A membrane is formed around cytosolic material that needs to be degraded a double-membrane. Autophagosome is formed and then the outer membrane of the autophagosome fuses with a lysosome and the contents are degraded by lysosomal hydrolases (adapted from (Xie and Klionsky, 2007).

In AD brain, autophagic vacuoles appear to accumulate without degradation of their contents by lysosomes (Yu et al., 2004; Nixon et al., 2005). Furthermore, on the membrane of an autophagosome microtubule-associated protein 1A/1B light chain 3 (LC3) is localised (He and Klionsky, 2009). LC3 is essential for the fusion of the autophagosome and lysosome (Fig. 1.8). LC3-I is recruited from the cytosol and is modified by addition of phosphatidylethanolamine (PE) to form LC3-II, which associates with membranes (Kabeya et al., 2000). As intra-autophagosomal LC3-II is degraded by lysosomes, it is frequently used as a marker for autophagosome formation and for monitoring autophagic flux (Tanida et al., 2005). Another important component of the autophagy process is p62/sequestosome 1 (p62/SQSTM1), which facilitates the removal of damaged proteins and organelles by lysosomes (Fig. 1.8) (Bjørkøy et al., 2006; Ichimura et al., 2008; Zaffagnini et al., 2018). Indeed, CBD and PSP brains show abnormal accumulation of p62, as well as LC3 and colocalisation with phosphorylated tau (Piras et al., 2016). It has previously been shown that both LC3-I and LC3-II interact with microtubule-associated proteins and this facilitates their association with microtubules (Mann and Hammarback, 1994; Wang et al., 2006).

Microtubules are constantly modified after assembly to enhance their function. One such modification is acetylation, which results in an increased flux of vesicles along acetylated microtubules (Bulinski, 2007; Dompierre et al., 2007). These acetylated microtubules are required for fusion of autophagosomes with lysosomes to form autolysosomes (Xie et al., 2010), providing an important link between acetylation and autophagic degradation of substrate proteins. It is hypothesised that elevated autophagy may be beneficial for neurons affected by tauopathy by preventing accumulation of tau aggregates (Schaeffer et al., 2012).

Fig. 1.8 Schematic representation of LC3-II effects on the autophagosome

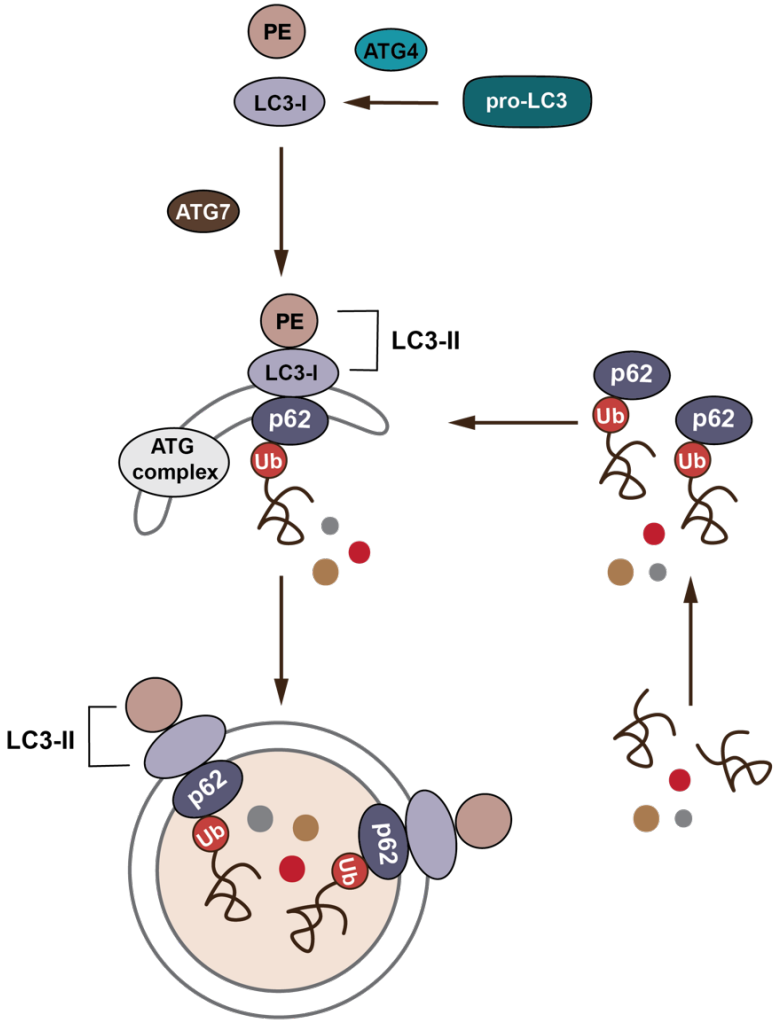

ATG4 cleaves pro-LC3 to form LC3-I which is then conjugated to phosphatidylethanolamine (PE) by ATG7 to generate LC3-II. ATG7 also mediates ATG complex formation and the latter along with LC3-II is highly critical for autophagosome formation. The adaptor protein p62/SQSTM1 binds to ubiquitinated proteins and LC3-II for mediating autophagy via localising into autophagic compartments, transporting ubiquitinated proteins and organelles for degradation (Novus Biologicals).

1.9 Tau truncation in the tauopathies

Proteolytic cleavage of disease-modifying proteins is found in a wide variety of human neurodegenerative diseases, including AD (Novák et al., 1993; Gamblin et al., 2003; Guo et al., 2004; Horowitz et al., 2004; Rissman et al., 2004), PiD (Guillozet-Bongaarts et al., 2007), CBD and PSP (Arai et al., 2005), Transactive response DNA-binding protein 43 (TDP-43) related FTLD (Igaz et al., 2009), and PD (Anderson et al., 2006), as well as polyglutamine diseases, such as Huntington's disease (HD) (Gafni and Ellerby, 2002; Gafni et al., 2004).

Initial evidence that cleaved tau is actively involved in tau aggregation and the formation of aggregated tau paired helical filaments (PHFs) was generated by using an antibody against the highly purified core of NFT (Goedert et al., 1988). This antibody recognised only tau protein that was C-terminally truncated at Glu391 (Novák et al., 1993). These findings revealed that the NFT core consists of tau fragments of 12 and 9.5 kDa (Novák et al., 1993). This finding was further supported by the discovery a 33 kDa N-terminally truncated form of tau from human AD brain (Nieto et al., 1991). This provided the first *in situ* evidence to suggest that tau truncation is a part of the pathological process of tau protein misfolding in AD. Similar results were also gained from immunohistochemical analysis of brain tissues from AD patients (Bondareff et al., 1990). There are a number of different tau fragments that have been identified to date in aged and diseased human brain and also in animal models of tauopathy (Table 3).

Table 3 Tau fragments detected in human brain

Tau fragment (residues)	Tauopathies	Pathological phenotype	References
C-terminally cleaved tau (40-53 kDa)	AD	Synaptic dysfunction	Sokolow et al., 2015
Delta tau (A15-D421)	AD	Tangles Amyloid plaques Synaptic dysfunction	Mocanu et al., 2008
NH_2-tau (E45-R230)	AD, ALS, aged brain	Neurodegeneration	Garg et al., 2011
NH_2-tau (Q124-L441)	aged brain	Increased tubulin acetylation Detyrosination of tubulin	Derisbourg et al., 2015
NH_2-tau (A125-R230)	AD aged brain	Increased tau phosphorylation Increased tau aggregation	Garg et al., 2011
NH_2-tau (I151-A391)	AD	Tangle formation Muscle weakness	Zilka et al., 2006
Tau35 (E187-441)	PSP, CBD	Tau pathology Cognitive dysfunction Motor dysfunction Increased tubulin acetylation Synapse loss	Wray et al., 2008; Bondulich et al., 2016
Tau-CTF_{24} (L243-L441)	AD, PSP, CBD, FTLD-tau	Increased tau phosphorylation Synapse loss	Matsumoto et al., 2015

Tau cleavage could generate fragments with either a toxic gain-of-function, thereby switching on a cell death cascade, or alternatively, could induce and drive aggregation of tau, together with any associated disease-modifying proteins. Supporting the latter scenario, is the fact that truncated protein fragments are upstream in the proteopathic cascade in neurodegenerative diseases and these can form the initial seeds required for aggregation (Zilka et al., 2006; Igaz et al., 2009; Levin et al., 2009; de Calignon et al., 2010; Filipcik et al., 2012). Alongside the tau fragments present in cell and animal models of disease, increasing numbers of proteases responsible for tau truncation have also been identified (Wang et al., 2010). Amongst these enzymes, caspases and calpain have been investigated most intensively and are described in more detail below. Additionally, recent studies have also proposed many other proteases that may play a role in tau cleavage, including thrombin, cathepsins, asparagine endopeptidase, puromycin-sensitive aminopeptidase and the proteasome (Fig. 1.9) (Hanger and Wray, 2010; Wang et al., 2010).

Fig. 1.9 Proteolytic processing of tau

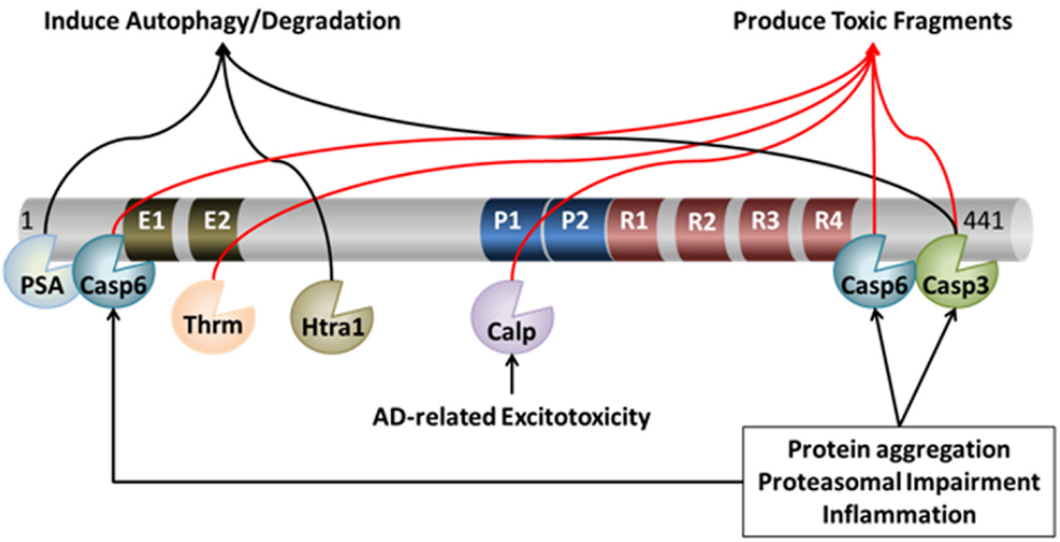

The figure demonstrates proteolytic processing of tau. For example, cleavage of tau by caspase (Casp) 3, Casp6, calpain (Calp), and thrombin (Thrm) leads to the production of toxic fragments of tau that exacerbate pathology. On the other hand, cleavage of tau by puromycin-sensitive aminopeptidase (PSA), high temperature requirement A (Htra1), and in some circumstances caspase-3, may facilitate its degradation (Chesser et al., 2013).

1.10 Astrogliosis in tauopathies

Astrocytes are exceedingly specialised and multi-functional glial cells found throughout the CNS (Sofroniew and Vinters, 2010; Osborn et al., 2016). The highly branched morphology and intimate contact of astrocytes with neurons, allows them to perform a diverse range of essential and complex roles that promote proper neuronal function. These roles include modulation of synaptic communication through uptake of neurotransmitters, maintaining ion homeostasis, regulating blood flow and maintaining the blood brain barrier, as well as roles in the immune response of the brain and neuroprotection (Ridet et al., 1997; Sofroniew and Vinters, 2010; Colangelo et al., 2014; Osborn et al., 2016). In reaction to any kind of insult to the CNS, astrocytes leave their quiescent state and become activated (Buffo et al., 2010). In a process known as reactive astrogliosis, these activated astrocytes undergo many morphological and functional changes, including cell hypertrophy, cell proliferation and migration towards affected areas, and the increased production of intermediate filament proteins such as glial fibrillary acidic protein (GFAP) (Buffo et al., 2010; Pekny and Pekna, 2014). The cellular and molecular mechanisms leading to reactive astrogliosis are not completely understood, however reactive astrocytes are a prominent histopathological feature of many neurodegenerative diseases, including AD (Hostenbach et al., 2014; Pekny and Pekna, 2014).

In their reactive state, astrocytes continue to multiply, migrate locally towards the injured area to form a glial scar, and release factors to facilitate tissue repair and replacement (Buffo et al., 2010; Burda and Sofroniew, 2014). As such, reactive astrogliosis may be a neuroprotective process in neurodegenerative disease (Osborn et al., 2016). However, the contributions of reactive astrocytes to neurodegenerative conditions are complex and not well understood, such that persistent astrocytic activation may also contribute to the progression of the disease (Burda and

Sofroniew, 2014). For example, it has been observed in AD that increased astrogliosis contributes to amyloid-β clearance, yet also results in cognitive decline (Serrano-Pozo et al., 2011; Osborn et al., 2016). Consequently, the role of activated astrocytes in neurodegenerative disease is currently a topic of great research interest (Osborn et al., 2016).

Research investigating reactive astrogliosis in neurodegeneration has primarily been conducted in AD and in amyotrophic lateral sclerosis (ALS), a motor disorder in which tau aggregation does not appear to play a role (Burda and Sofroniew, 2014). In AD, the presence of aggregated amyloid-β activates the process of astrogliosis (Osborn et al., 2016). However, astrogliosis has also been observed in tauopathies such as PSP and CBD, that do not have amyloid plaque pathology, suggesting a potential interaction between astrocytes and tau (Togo and Dickson, 2002). Importantly, significant differences in the reactivity of astrocytes have been found in different neurodegenerative diseases (Song et al., 2009). Even within the tauopathies, one study found that approximately 40% of subcortical astrocytes in PSP brain accumulate phosphorylated tau, whereas subcortical astrocytes in CBD did not accumulate tau (Song et al., 2009). Overall, there is currently very limited data available on the interaction between tau and astrocytes and, combined with the fact that reactive astrogliosis appears to be triggered in different and selective ways in neurodegenerative disease, further study on astrogliosis in tauopathies is warranted.

1.11 Dendritic spines and synaptic dysfunction in tauopathies

Dendritic spines mediate the majority of the excitatory connections in neuronal networks (Yuste and Bonhoeffer, 2001; Chklovskii et al., 2002). Spiny neurons are rarely found in lower organisms, suggesting that spines are evolved to accommodate a more sophisticated nervous system that is required to perform more advanced functions. Dendritic spines are classified morphologically as being either stubby, thin or mushroom. Stubby spines, that have no clear neck, are more common during early development of the neuron. In contrast, mushroom spines with fully formed necks and heads, are more abundant in the adult. However, it is not uncommon to observe stubby spines in adult neurons (Miller, 1981; Yuste and Bonhoeffer, 2004). Typically, a mature spine has a single synapse located on its head, indicating a tight relationship between spine formation and synaptic function (Miller, 1981; Yuste and Bonhoeffer, 2001). Dendritic filopodia are formed by a membrane folding of the dendrite that acts as a precursor of a dendritic spine (Fig. 1.10) (Miller, 1981; Yuste and Bonhoeffer, 2004).

Fig. 1.10 Schematic representation of dendritic spine morphology

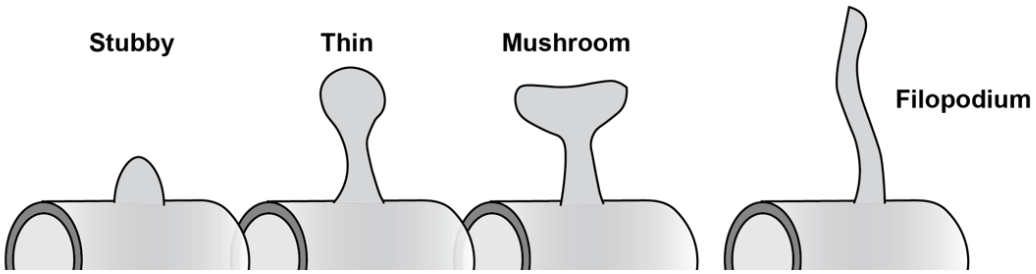

The figure shows a schematic representation of spine morphology. Spines are classified into stubby, thin and mushroom. In addition, the precursor to dendritic spine structure, termed a filopodium, is shown on the right (adapted from Yuste and Bonhoeffer, 2004).

Rodent models that recapitulate features of neurodegeneration have been very valuable in understanding possible changes in neuronal morphology. Some animal models of neurodegeneration, such as mice over- expressing human wild-type (WT) tau and rTg4510 mouse model (tau mutation P301L), have suggested changes in the dendritic architecture of neurons, alongside significant spine loss and the reorganisation of spine morphology (Halpain et al., 2005; Dickstein et al., 2010). Gaining a further appreciation of these modifications in spines is of vital importance to improve understanding of the processes that can adversely impact neuronal communication and ultimately cognitive function.

In a transgenic mouse model expressing the mutant human tau variant (P301L) associated with FTLD-tau, neocortical dendritic spines and synapse density were decreased in mice aged 9-10 months (Rocher et al., 2010; Crimins et al., 2011; Kopeikina et al., 2013). Moreover, a study using a transgenic mouse expressing human mutant P301S tau, demonstrated a continuous decrease in spine density and a significant restructuring of spine morphology over time (Hoffmann et al., 2013). Primary neuronal cultures derived from transgenic rodent models also exhibit significant modifications to dendritic structure. Hippocampal neuronal cultures from TauKO mice showed a delay in dendritic and axonal growth, while cultures from double knock-out tau/MAP1B (*Mapt*$^{-/-}$; *MAP1B*$^{-/-}$) mice demonstrated inhibited axonal elongation (Takei et al., 2000; Dawson et al., 2001). In mouse neurons overexpressing WT human tau, spine density decreased, while dendritic arborisation was increased at 12 months of age (Dickstein et al., 2010). In addition to changes induced by aberrant tau expression, neurons cultured from transgenic mice (Tg2576) overexpressing mutant amyloid precursor protein (APP, 695 residues) presented with a significant increase in dendritic length and a decrease in spine density (Rocher et al., 2010).

Synaptic plasticity is essential for learning and memory. In AD, synaptic loss is the leading cause of the early cognitive and behavioural deficit (Bondolfi et al., 2002; Ashe and Zahs, 2010; Rupp et al., 2012). Widespread synapse loss has long been identified using the presynaptic terminal marker synaptophysin, in AD brain (Soininen et al., 1995; Arendt et al., 2010). The number of spine-associated synapses and the amount of synaptophysin labelling is also reduced in the hippocampus of mice expressing “pro-aggregate” tau species (Decker et al., 2015). In addition, synaptic properties are altered in AD mice, Tg2576, from 3 weeks of age and they progressively decline, developing a deficiency in LTP at 8 months of age (Chapman et al., 1999; Gureviciene et al., 2004; Malenka and Bear, 2004). Tau mutation or tau overexpression both cause tau to mislocalise into the somatodendritic compartment (Kins et al., 2001; Brandt et al., 2005; Gendron and Petrucelli, 2009). Notably, neurons that demonstrate tau mislocalisation display decreased spine density (Thies and Mandelkow, 2007; Zempel et al., 2010). Tau has been shown to be present at the synapse (Harris et al., 2012; Pooler et al., 2014). Tau burden in the brain appears to correlate with cognitive impairment, which also closely matches with loss of synaptic density, with AD brains exhibiting extensive synaptic loss throughout disease progression (Masliah et al., 1989; DeKosky and Scheff, 1990; Serrano-Pozo et al., 2011). Synaptic dysfunction is believed to be an early event in tauopathies (de Calignon et al., 2010) with changes in the synaptic proteome often associated with the dysfunction of synapses in neurodegenerative diseases (Fig. 1.11) (Marttinen et al., 2015).

Previous research identified another synaptic protein, synapsin-1, as a tau-interacting protein (Kang et al., 2013). Tau was found to interact with several synaptic proteins involved in pre-synaptic signaling transduction such as synapsin-1, synaptotagmin and synaptophysin (Liu et al., 2016). Interestingly, it has been found that tau and synapsin-1 co-immunoprecipitate, both with each other and with actin. This leads to

the proposition that tau and synaptic proteins interact with actin in WT C57Bl/6 mice, altering actin dynamics, and possibly presynaptic vesicle transport, which could result in synaptic failure in neurodegeneration (Liu et al., 2016). This suggests that investigating the role of tau at the synapse may be important for developing new therapeutic strategies for protecting synapses in dementia.

Fig. 1.11 Key pre-synaptic and post-synaptic proteins

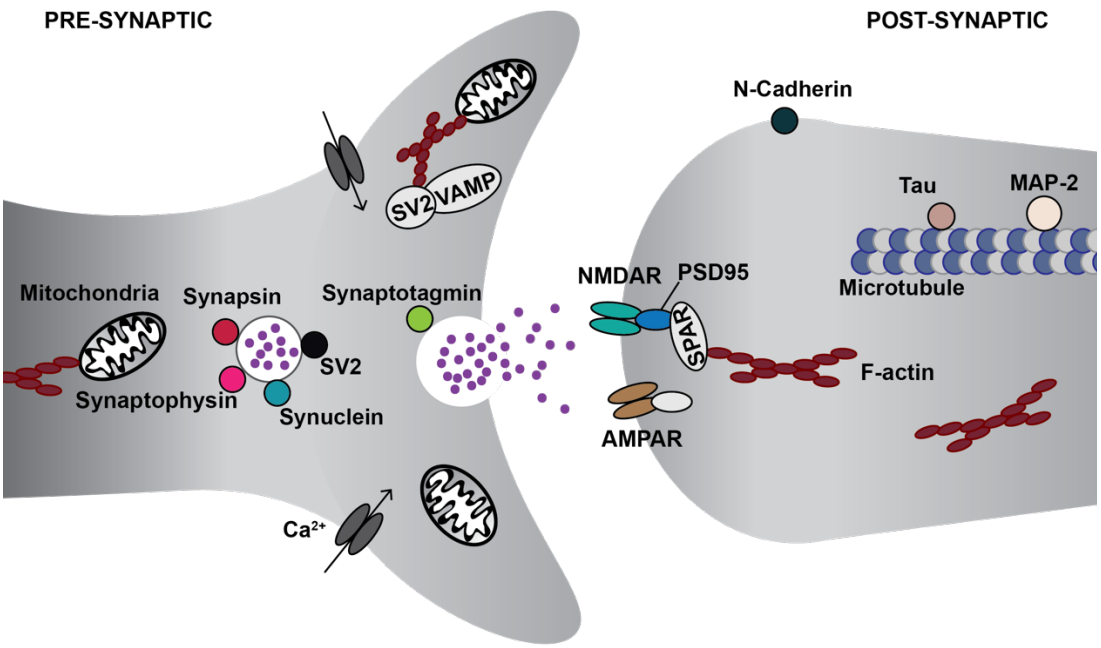

Pre-synaptic vesicle proteins synaptophysin, synapsin, synaptic vesicle glycoprotein 2A (SV2) and synaptotagmin are located on the synaptic vesicle membrane. The post-synaptic density marker 95 (PSD95) is located on the post synaptic membrane. (adapted from R&D Systems https://www.rndsystems.com/resources/articles/synaptic-proteins-and-receptors-schematic-rd-systems).

1.12 Axonal transport and tau

Axonal transport is a multi-factorial event that requires intact microtubules, functional motor proteins, correct cargo attachment to motors, and sufficient ATP, supplied by mitochondria (De Vos et al., 2008). As described before, the N-terminus of tau projects away from the microtubule and has the ability to bind motor proteins, both kinesin and dynein. Dynein transport cargoes towards the minus ends of microtubules, directing them to the cell body, the majority of kinesins transport cargoes towards the plus ends of microtubules in the direction of the axon terminus (De Vos et al., 2008). Tau can dynamically regulate the function of the axonal transport machinery through multiple mechanisms (Ebneth et al., 1998; Dixit et al., 2008), including reducing the binding frequency of both proteins and slowing both retrograde and anterograde axonal transport (Seitz et al., 2002). Tau interferes with kinesin, inhibiting its mobility by reducing single protein run length and velocity (Cuchillo-Ibáñez et al., 2008; Dixit et al., 2008; Ebneth et al., 1998; Stamer et al., 2002). It is also known that protein levels of both the kinesin motor-mediated axonal transport machinery and of the dynein-mediated retrograde transport machinery are reduced in AD (Morel et al., 2012). In addition to interfering with motor protein mobility, amino acids 2-18 of tau can regulate the release of cargo vesicles bound to kinesin (Kanaan et al., 2011). This occurs through activation of various kinases, such as protein phosphatase 1 and GSK-3β (Kanaan et al., 2011). Increased activation of GSK-3β can also contribute to the transport deficit by aberrant phosphorylation of light chain of kinesin, resulting in premature release of kinesin from its cargoes (Cuchillo-Ibáñez et al., 2008).

In neurodegenerative diseases in which axonal transport is impacted, neurons accumulate organelles and proteins that can form swellings in axons and cell bodies (Ballatore et al., 2007; Millecamps and Julien, 2013). Abnormal modification of tau, such as increased phosphorylation, truncation and acetylation, impairs the interaction

of tau with microtubules and the ability of tau to stabilise microtubules (Morris et al., 2015). In addition, tau overexpression leads to a high level of soluble tau that may be toxic for neurons and can affect axonal transport (Spires-Jones et al., 2011). In cultured neurons transfected with 3R or 4R tau isoforms, altered axonal transport results in perinuclear clumping of organelles such as mitochondria (Stoothoff et al., 2009).

In summary, there are several theories put forward to describe how tau overexpression contributes to a deficit in axonal transport. Firstly, studies of tau overexpression have demonstrated negative consequences to anterograde cellular transport by inhibiting the movement of kinesin-1 when excessively bound tau physically prevents transport along the microtubule (Dubey et al., 2008). Secondly, hyperphosphorylated tau could lose its affinity for microtubules, destabilising it and resulting in impaired trafficking. (Ballatore et al., 2007; Bretteville and Planel, 2008). However, studies in TauKO mice have shown that microtubules remain intact even in the absence of tau protein (Morris et al., 2011). Thirdly, other studies suggest that tau involvement in cell signalling can affect axonal transport. For example, tau may interfere with enzymes such as GSK-3β, demonstrating a more indirect involvement in regulation of transport processes (Tackenberg and Brandt, 2009).

1.13 Transgenic mouse models of tauopathy

Considerable advances in transgenic technology have enabled the generation of rodent models that recreate, to varying extents, characteristics of human tauopathies. Existing transgenic rodent models of human tauopathy invariably involve the overexpression of WT tau, mutant tau linked to FTDP-17, or structurally modified tau derived from AD brain, under the control of several different promoters (Zilka et al., 2009; Noble et al., 2010; Bondulich et al., 2016). Notably, only a few transgenic

models have successfully recreated features seen in human tauopathies, and these may develop substantial overexpression artefacts, as elevated tau leads to neuronal dysfunction (Ebneth et al., 1998; Zilka et al., 2009). Further, these transgenic models have been developed to model either AD or FTDP-17 pathology, which is unlike the pathology seen in other tauopathies, such as PSP, CBD, and PiD, each of which may have altered ratios of 3R to 4R tau (Denk and Wade-Martins, 2009). Transgenic rat models expressing human truncated tau have shown that tau fragments associated with either 3R or 4R tau isoforms develop NFTs in different distributions, which demonstrates a selective vulnerability of brain areas to NFT formation (Zilka et al., 2006; Filipcik et al., 2012). This is in line with previous findings that tau fragment patterns are closely associated with pathological processes and are able to act as potential biochemical markers that can distinguish between tauopathies (Arai et al., 2004). Thus, transgenic rodent models expressing different tau fragments may prove valuable for modelling other tauopathies with or without altered 3R to 4R tau isoform ratios.

1.14 The Tau35 fragment and Tau35 mouse model

A highly phosphorylated C-terminal tau fragment in the brains of people affected by PSP and other disorders in which 4R tau isoforms were over expressed, was previously identified in this laboratory (Wray et al., 2008). Furthermore, a new transgenic mouse model (Tau35) expressing this disease-associated tau fragment was generated (Bondulich et al., 2016). Mice expressing Tau35 were generated from Tau35 cDNA fused to a haemagglutinin (HA) tag to distinguish the transgene from endogenous mouse tau. The human tau promoter facilitated normal expression patterns of human tau. Transgene expression in Tau35 mice is only 7% of the total amount of tau (Bondulich et al., 2016). Tau35 mice exhibit age-related limb clasping, kyphosis and a reduced life span (Bondulich et al., 2016). This is consistent with some

other mouse models of tauopathies (Lewis et al., 2000; Laws and Hoey, 2004; Lalonde and Strazielle, 2011; Wu et al., 2012). Tau35 mice exhibit a progressive clasping of either their hindlimbs or all four limbs, and loss of hindlimb grip strength. In addition, abnormal spine curvature is apparent in Tau35 mice and the kyphotic index is reduced, demonstrating progressive, age-related kyphosis (Bondulich et al., 2016). Also, Tau35 mice demonstrated a reduced median survival of 717 days, compared to 788 days in WT mice, in the absence of any reduction in body mass in Tau35 mice (Bondulich et al., 2016). Experiments of motor coordination showed that Tau35 mice have a reduced latency to fall from the rotarod, which decreases with age, possibly caused by reduced muscle strength and motor ability. In addition, Tau35 mice have substantial changes in muscle fibres, such as multiple internalised nuclei and numerous degenerative/regenerative muscle fibres (Bondulich et al., 2016). Furthermore, Tau35 mice exhibit spatial learning and hippocampal-dependent memory deficits. These changes in learning and memory were apparent in the Morris water maze as the Tau35 mice showed an increased latency to find a hidden platform, whilst maintaining their swimming ability. No differences were found in non-associative short-term memory, olfaction or anxiety (Bondulich et al., 2016).

Fig. 1.12 Tau pathology in the hippocampus of Tau35 mice

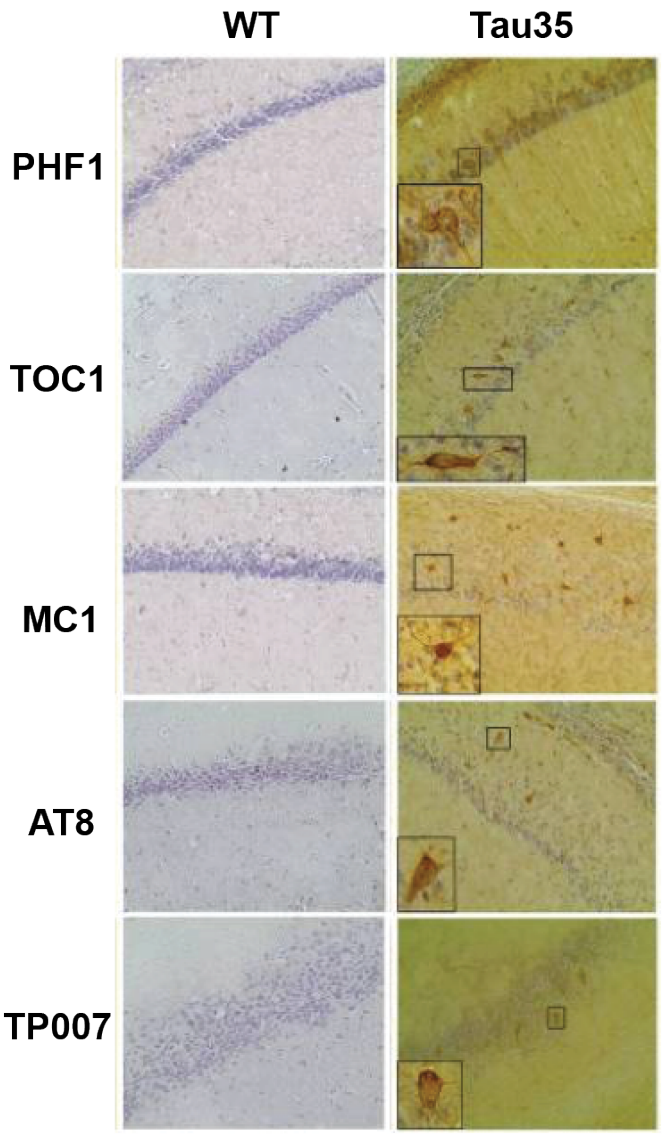

Tau-positive labelling of inclusions in Tau35 brain stained with PHF1, TOC1, MC1, AT8 and TP007 at 14-16 months (right), compared to 16 months WT control brain (left). n=3 mice for each genotype, scale bar = 200 μm.

Neurophysiological studies were performed on the CA1 area of the hippocampus of Tau35 mice that is involved in spatial memory encoding. The findings indicate that that Tau35 mice exhibit a significant increase in short-term facilitation of the synaptic response without changing long-term synaptic plasticity (Tamagnini et al., 2017). Tau35 expression also alters the intrinsic excitability of CA1 pyramidal neurons in mice, leading to an induction of higher cell capacitance and rise of action potential rate (Tamagnini et al., 2017). Tau35 accumulation results in hyperexcitability and hypoexcitability at polarised and depolarised potentials, respectively (Tamagnini et al., 2017). Taken together, these findings indicate multiple disease-associated changes in Tau35 mice that faithfully recapitulate some of those that are found in neurodegenerative tauopathies.

1.15 Mitochondria in health and disease

Mitochondria are required for a wide range of cellular processes (Detmer and Chan, 2007; Suen et al., 2008) such as ATP production (Benard et al., 2008), Calcium homeostasis (Frieden et al., 2004; Szabadkai et al., 2004), cell death (Sugioka et al., 2004), and production of reactive oxygen species (Yu et al., 2006). Maintaining the correct morphological structure of mitochondria is essential for their proper function. Mitochondria are bounded by two membranes: an inner mitochondrial membrane, that fold inwards to form structures, cristae, and an outer mitochondrial membrane. The mitochondrial matrix contains mitochondrial deoxyribonucleic acid (mtDNA) of approximately 16 kb (Anderson et al., 1981). The mtDNA encodes two rRNAs, 22 tRNAs, and 13 proteins which serve as subunits of the respiratory chain of the oxidative phosphorylation (OXPHOS) complex that generates ATP (Anderson et al., 1981). However, most mitochondrial proteins are encoded by nuclear DNA.

Neurons are energetically very demanding (Kann and Kovács, 2007) as they have a complex cellular organisation that requires a timely and appropriate transport and distribution of mitochondria for their correct function. Mitochondria in neurons serve as an energy power hub and an internal calcium storage pool for localised neuronal activities such as synaptic transmission, axonal and dendritic transport, and synaptic vesicle recycling (Li et al., 2004). Many studies suggest that reduced brain metabolism or mitochondrial dysfunction are amongst the prominent early features in brains of all major neurodegenerative diseases (Lin and Beal, 2006). ATP production in mitochondria is coupled to an electron transport chain in which the passage of electrons down the various electron carriers is associated with the transport of protons from the matrix into the intermembrane space. The majority of these protons enter the matrix via ATP synthase and therefore generate ATP. However, about 20% of mitochondrial oxygen consumption is not coupled to ATP production and protons enter the matrix through the phospholipid bilayer and through uncoupling proteins, generating heat (Rolfe and Brown, 1997). Mitochondrial metabolism also leads to the majority of reactive oxygen species (ROS) production in cells, which occurs when unpaired electrons escape the electron transport chain and react with oxygen to produce a superoxide. This superoxide plays an important role in intracellular signalling and can react with DNA and proteins. ROS are also associated with both neurodegeneration and with aging (Angelova and Abramov, 2018). Studies have shown that aged brain has reduced complex I and IV activity and increased production of ROS (Navarro et al., 2007).

Mitochondria are also altered in brains of people with neurodegenerative disorders such as AD. In particular, AD is characterised by reduced cerebral cortical glucose metabolism at pre-diagnostic stage and demonstrates reduced cortical oxygen uptake leading to reduced mitochondrial respiration at later stages of disease (Mosconi et al., 2009; Gibson et al., 2010). Studies of post-mortem human brain demonstrate

impaired bioenergetic metabolism in AD, that may play a role in the degenerative loss of hippocampal and cortical neurons (Mosconi et al., 2009). AD brain demonstrates evidence of reduced mitochondrial mass and respiration and expression of mitochondrial biogenesis genes in post-mortem AD brain tissue. There is evidence that impaired mitochondrial function in AD brain could be due to impaired glucose transport, impairment of glycolysis, reduced activities of mitochondrial oxidative decarboxylation in the tricarboxylic acid cycle, impaired mitochondrial respiration or combination of these processes (Mosconi et al., 2009). In post-mortem AD brain, mtDNA gene copy numbers were significantly reduced in hippocampus (Sheng et al., 2012) and cortex (Coskun et al., 2010). Therefore, growing evidence has demonstrated mitochondrial pathology in neurodegenerative diseases.

1.15.1 Mitochondrial dynamics: fusion, fission and trafficking

Mitochondria are highly dynamic organelles that undergo continual fusion and fission events which are regulated by several large GTPase proteins (Fig. 1.13). In fusion events, motile mitochondria make contact with stationary mitochondria, forming extensive tubular mitochondrial networks (Chan, 2006a; Cagalinec et al., 2013). Following fusion, mitochondrial fission events result in segmentation and the generation of two daughter mitochondria (Cagalinec et al., 2013). One of the mitochondria undergoes fusion with another mitochondrion, while the other one becomes depolarised and undergoes mitophagy (Chan, 2006b; Twig et al., 2008; Westrate et al., 2014).

The key regulator in the mitochondria fission process is cytosolic dynamin-related protein1 (DRP1) (Smirnova et al., 2001). During fission, DRP1 is recruited to the mitochondrial outer membrane by several receptor proteins such as Fis1, followed by forming a ring-like structure to sever the mitochondrial membrane (Fig. 1.13A) (Otera et al., 2010; Palmer et al., 2011; Losón et al., 2013). The molecular mechanisms

responsible for the initiation of mitochondrial fission remain largely unknown. Most recent studies imply that the endoplasmic reticulum (ER), together with actin filaments, plays a critical role in mitochondrial DRP1 recruitment (Friedman et al., 2011; Korobova et al., 2013). After the fission process is completed, the DRP1 complex remains on one of the daughter mitochondria (Chan, 2006a). Recent studies indicated that the DRP1 oligomeric complex on mitochondria could drive mitochondrial fragmentation leading to its inactivity (Lackner and Nunnari, 2009; Zunino et al., 2009).

Fig. 1.13 Schematic representation of mitochondrial dynamics in neurons

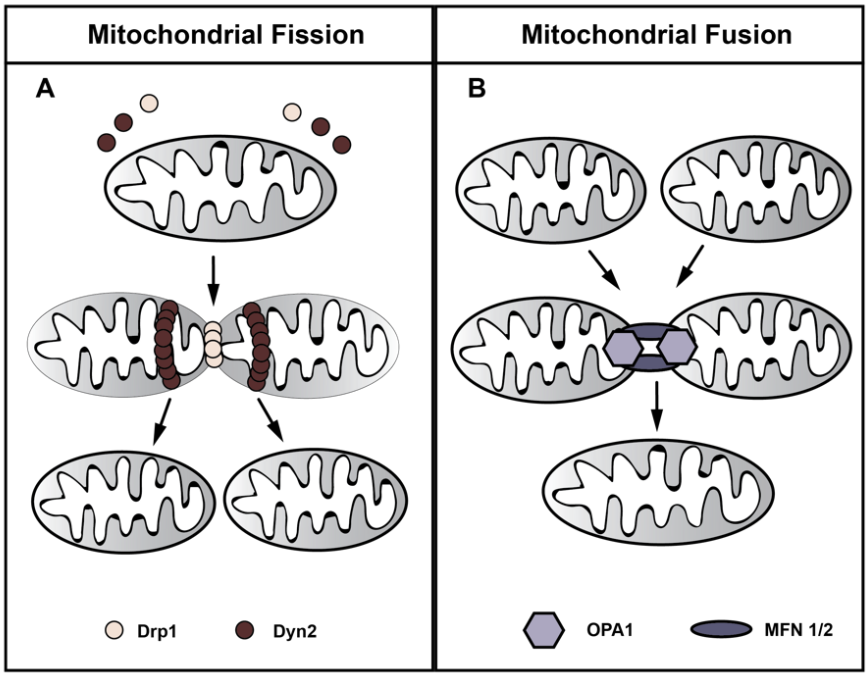

A Cytosolic dynamin-related protein (DRP) 1 attaches to the mitochondrial outer membrane by several receptor proteins. Then, another dynamin-like protein, dynamin 2 (DYN2), binds and allows lipid fusion and organelle division. **B** During fusion process there is outer membrane fusion and inner membrane fusion. Outer membrane fusion is facilitated by mitofusin (MFN) 1 and MFN2 to tether membranes together. Optic atrophy protein 1 (OPA) 1 allows the inner membrane fusion (Gao et al., 2017).

Mitochondrial fusion, Fig. 1.13B, involves both the outer and inner mitochondrial membranes and this process is regulated by at least three other large GTPase proteins, i.e., Mitofusin 1 (MFN1) and Mitofusin 2 (MFN2) for mitochondrial outer membrane fusion, and optic atrophy protein 1 (OPA1) for mitochondrial inner membrane fusion (Santel and Fuller, 2001). Similar to DRP1, MFN1, MFN2, and OPA1 controlled mitochondrial fusion also depends on their self-assembly and GTPase activity. It has been proposed that mitochondrial outer membrane fusion is mediated through interactions of the coiled-coil domains of MFN1 and MFN2 to form either homo-oligomeric or hetero-oligomeric complexes to tether membranes together (Ishihara et al., 2004; Züchner et al., 2004). The outer and inner mitochondrial membranes contain differing phospholipids, and the proper phospholipid composition is important for the regulation of mitochondrial fusion (Frohman, 2015). Nevertheless, determining the molecular mechanism of mitochondrial fusion has proven to be elusive due to the involvement of both the outer and inner membrane and the likely very complicated processes involved.

Mitochondria are highly mobile organelles that move bi-directionally along axons and act as ‘energy hubs’ in cells, delivering an energy supply where it is most needed. Particular regions of neurons, including synapses (Rowland et al., 2000) and active growth cones (Hollenbeck, 1993), require more mitochondrial ATP production due to their high rates of energy consumption. Mitochondria move along microtubules for fast movement and along actin filaments for slow movement and these processes are facilitated by different motor-adaptor complexes (Boland et al., 2008). The motor-adaptor complex consists of kinesin-1 and dynein that directly interacts with Miro1 and 2 (also known as RhoT1 and RhoT2), and Milton1 and 2 (also known as TRAK1 and TRAK2) to drive their movement along the microtubules (Fig. 1.14) (Glater et al., 2006; Hatch et al., 2014; Sheng, 2014). In addition, actin motors, such as Myo2 and

Myo19, are associated with mitochondria to facilitate the short-distance movement along actin filaments (Boldogh et al., 2001; Altmann et al., 2008).

Fig. 1.14 Mitochondrial trafficking in neurons

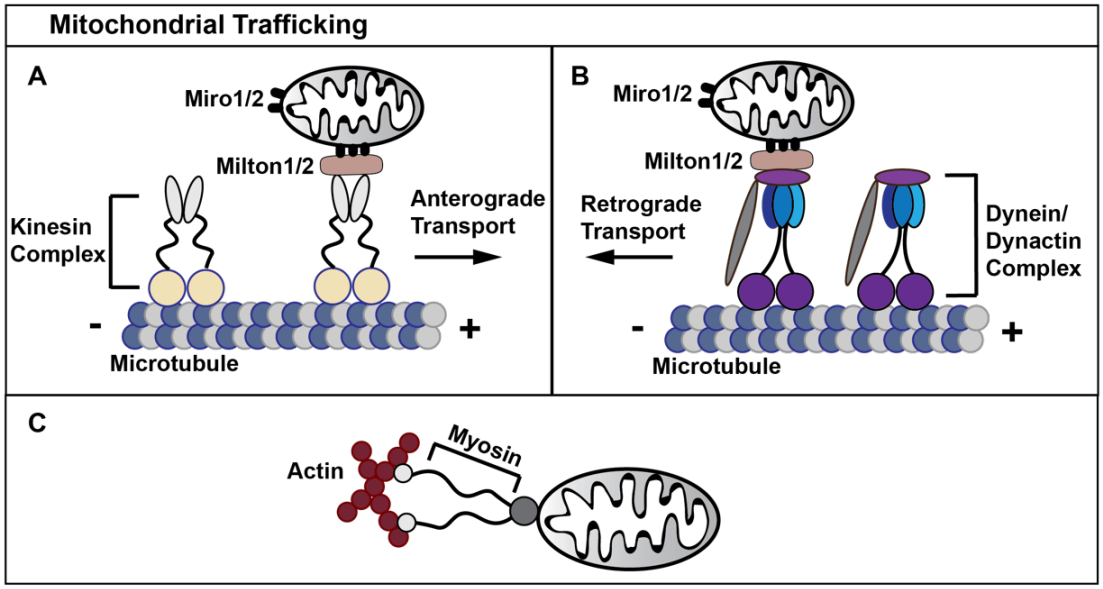

A,B The anterograde motor kinesin-1 and the retrograde motor dynein/dynactin complex directly interact with Milton1/2 and Miro1/2 on mitochondria to drive their movement along the microtubules. **C** Actin motors are associated with mitochondria to facilitate the short-distant movement along the filament (adapted from (Gao et al., 2017).

It is also worth noting that in addition to trafficking within the cell, mitochondria can be transported between different cell types. Neurons can release damaged mitochondria and transfer them to astrocytes for degradation (Hayakawa et al., 2016). Through a calcium-dependent mechanism involving CD38 and cyclic ADP ribose signalling, astrocytes can also release functional mitochondria to be taken up by neurons (Hayakawa et al., 2016).

Studies have shown that mitochondrial fragmentation, abnormal mitochondrial fusion, fission, and trafficking dynamics and altered distribution can contribute to pathological events in neurodegenerative disorders (Itoh et al., 2013; Burté et al., 2015). In 2004 Swerdlow and Khan proposed a 'mitochondrial cascade hypothesis' which stated that mitochondrial function, influenced by genetics and environment, is a primary event leading to late-onset AD pathology (Swerdlow and Khan, 2004).

1.15.2 Mitophagy

Impaired mitochondrial function may lead to detrimental cellular events such as reduced cellular energy, formation of ROS, that in turn can damage proteins, membranes and DNA (Wallace et al., 1999). Maintaining a healthy mitochondrial pool is essential for neuronal development and function. There are multiple mitochondria quality control pathways and one of these mechanisms is the engulfment and degradation of damaged mitochondria, which is termed mitophagy (Fig. 1.15) (Menzies et al., 2015).

As described in Section 1.6 above, autophagy is a process in which cytoplasmic substrates are engulfed in autophagic vesicles, fused to lysosomes and degraded. Mitophagy is the mechanism of clearing out the damaged mitochondria and is an example of macroautophagy. Recent studies have been investigating the hypothesis that the accumulation of dysfunctional mitochondria in neurodegenerative disease in

context of impaired mitophagy (Kerr et al., 2017). When mitochondria become damaged, the inner mitochondrial membrane becomes depolarised and this stabilises the protein phosphatase and tensin homolog (PTEN)-induced kinase 1 (PINK1) at the outer mitochondrial membrane. In turn, PINK1 phosphorylates MFN2 and ubiquitin, which recruit Parkin to the outer mitochondrial membrane. Parkin ubiquitylates several proteins that are recognised by ubiquitin-binding proteins optineurin (OPTN) and p62/SQSTM1 that recruit to the autophagy pathway (Lazarou et al., 2015). PINK1 can also induce low level mitophagy in a Parkin-independent manner (Lazarou et al., 2015). Multiple outer membrane proteins can regulate mitochondrial fusion-fission proteins (DRP1 and OPA1) to induce mitophagy in both Parkin-dependent and Parkin-independent manners (Sandoval et al., 2014; Chen et al., 2016). These mitophagy receptors bind to proteins associated with immature autophagosomes (LC3) via LC3-interacting region (LIR) motifs. The formation of protein bridges between the outer mitochondrial and phagophore membranes results in elongation and closure of the phagophore membrane, thereby engulfing the mitochondrion. The final stage of mitophagy is the fusion of the autophagosome with a lysosome, mediated by the phagophore LC3-binding proteins and the lysosome membrane-associated protein, Rab7. Finally, lysosomal hydrolases degrade the mitochondrion (Gao et al., 2015). Accumulating evidence suggests that correct regulation of mitophagy throughout life is important for prevention of age-related disorders, including neurodegenerative diseases (Fig. 1.15).

Fig. 1.15 Mitochondrial dysfunction and compromised mitophagy in neurodegenerative disease

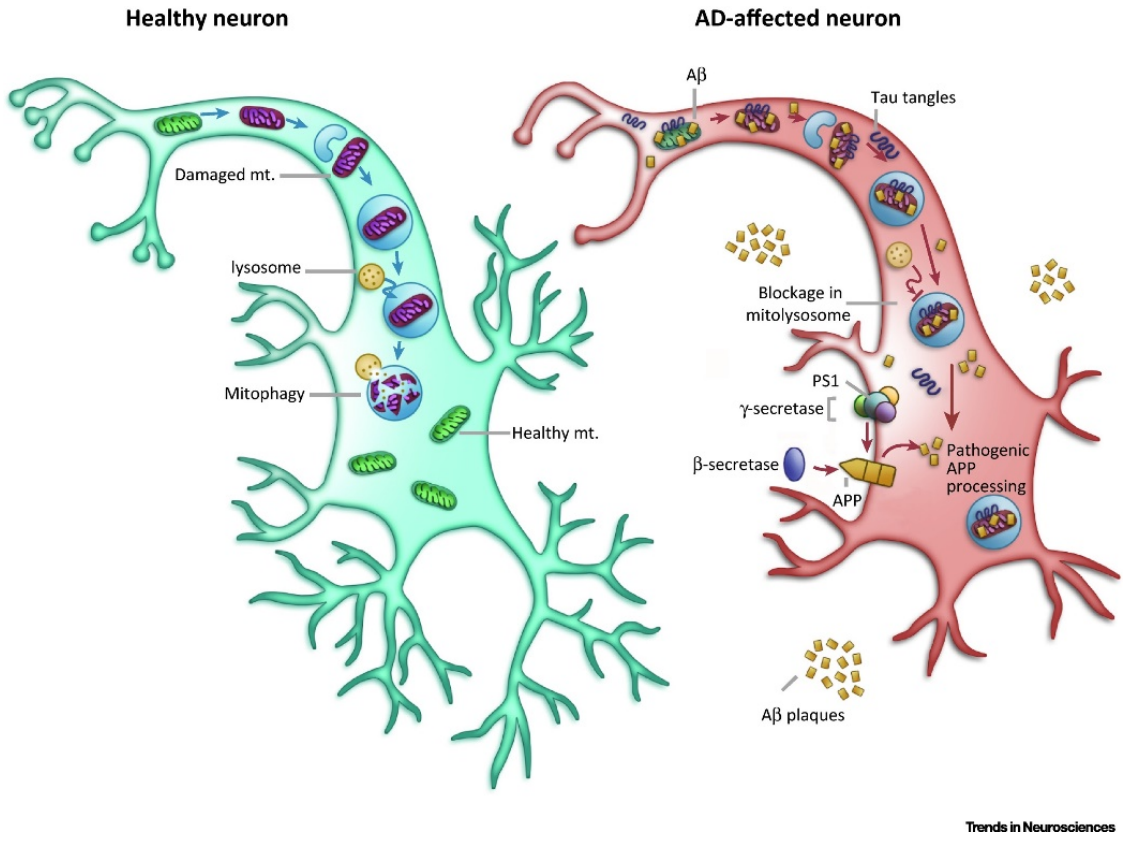

Dysfunctional mitochondria (purple) are packaged into autophagosomes and trafficked to lysosomes to be degraded. In AD-affected neurons, mitophagy is compromised leading to decreased energy production and increased oxidative stress. This causes amyloidogenic processing of amyloid precursor protein (APP) by β-secretase and γ-secretase/presenilin 1 (PS1) to increase and to accumulate phosphorylated Tau (pTau) aggregates. Pathogenic amyloid-β (Aβ) and pTau can impair mitophagy, leading to an increase in damaged mitochondria (Kerr et al., 2017).

1.15.3 Mitochondrial biogenesis

Mitochondrial function involves many proteins encoded both from nuclear and from mitochondrial DNA. Therefore, the biogenesis of mitochondria in general and its respiratory chain in particular, is dependent on the cross talk between mitochondrial and nuclear genomes. Both genomes are coordinated by a complex regulatory system. Mitochondrial transcription requires a single DNA polymerase (POLRMT), initiation (TFB2M) and stimulation transcription factor A mitochondrial (TFAM) transcription factor (Ramachandran et al., 2017). In addition, a complex machinery allows mitochondrial and nuclear gene products to be directed to the correct mitochondrial compartments, including assembly of the respiratory complexes. Defective mitochondrial biogenesis has been thought to be associated with neurodegenerative disorders (Li et al., 2017). However, the status of mitochondrial biogenesis in AD is unclear as various studies demonstrate alternative results. Some contradictory evidence has been presented suggesting the possibility that neurons in different stages of disease might exhibit different patterns of mitochondrial biogenesis (Liang et al., 2008). Beyond AD, little is known about mitochondrial biogenesis pathway activation and deactivation in tauopathies.

The mechanism that underlies mitochondrial biogenesis differs between tissues. However, it is generally considered that peroxisome proliferator-activated receptor gamma coactivator-1α (PGC-1α) is the master regulator that co-activates multiple metabolically important nuclear and non-nuclear receptor transcription factors (Fig. 1.16) (Houten and Auwerx, 2004; Handschin and Spiegelman, 2006; Fink et al., 2014). PGC-1α is highly expressed in brown adipose tissue, skeletal muscle and brain. PGC-1α is controlled through post-translational modification and increased expression to turn on mitochondrial biogenesis when it is required. For example, acetylation supresses PGC-1α activity, whereas phosphorylation by kinases such as

p38 mitogen-activated protein (MAP) kinase enhances PGC-1α activity (Knutti and Kralli, 2001; Puigserver et al., 2001; Fan et al., 2004; Fink et al., 2014).

Fig. 1.16 PGC-1α as a key regulator of mitochondrial biogenesis

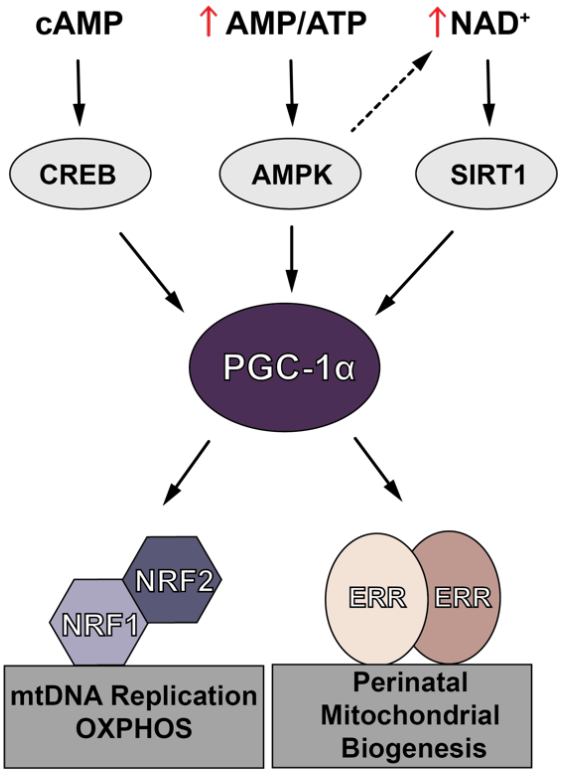

The transcriptional coactivator peroxisome proliferator-activated receptor gamma coactivator 1-alpha (PGC-1α) directly activates multiple transcription factors to control mitochondrial biogenesis and function. The control of PGC-1α expression responds to multiple intracellular second messengers and signaling molecules including nuclear respiratory factor (NRF) 1, NRF2 and estrogen-related receptor (ERR). Upstream PGC-1α is regulated through cAMP response element-binding protein (CREB), AMP-activated protein kinase (AMPK) and sirtuin (SIRT) 1. (adapted from Vega et al., 2015).

Downstream of PGC-1α are the nuclear respiratory factors (NRF) 1 and 2, which are transcription factors controlled by PGC-1α. PGC-1α plays a role in the activation of NRF2 and together they co-activate NRF1 (Scarpulla, 2008). NRF1 binds to the cytochrome c promoter and is associated with the expression of many genes needed for respiratory chain assembly and function (Scarpulla, 2002). Similarly, NRF2 also activates expression of cytochrome c oxidase. NRF1 and NRF2 often work together with many nuclear genes, particularly nuclear-encoded cytochrome oxidase subunits. NRF1/2 also activates transcription of nuclear-encoded respiratory genes and TFAM. TFAM initiates transcription of nuclear-encoded respiratory genes that are required for maintaining mtDNA copy number and stabilising mtDNA (Parisi and Clayton, 1991). It has also been shown that endogenous PGC-1α regulates neuronal estrogen-related receptor α (ERRα) transcription and effect electron transport chain expression (Bakshi et al., 2016). Furthermore, it has been shown that ERRα is enough to mediate the action of PGC-1α on mitochondrial biogenesis as in muscle cells induction of mitochondrial biogenesis (Bakshi et al., 2016). Hence, endogenous PGC-1α and ERRα coactivate the nuclear-encoded electron transport chain in neuronal cells through a feed-forward loop (Bakshi et al., 2016). PGC-1α increases the expression of both NRF2 and ERRα, further enhancing ERRα production (Koo et al., 2004). As shown in Fig. 1.16 PGC-1α plays a key regulatory role in controlling mitochondrial biogenesis and function.

PGC-1α is regulated by a range of different protein modifiers, including CREB, SIRT1 and AMPK. CREB activates the PGC-1α promoter and drives PGC-1α expression (Wu et al., 2006). SIRT1 is a member of the sirtuin family of HDACs. Following activation of SIRT1 by an increase in the nicotinamide adenine dinucleotide $(NAD)^+$/NADH ratio (Feige et al., 2008). SIRT1 deacetylates and thereby activates, nuclear PGC-1α and induces mitochondrial biogenesis (Lagouge et al., 2006). Increased NAD^+ biosynthesis and SIRT1 activation have been shown to protect axons

against degeneration (Araki et al., 2004). Thus, SIRT1 is an important neuronal component that modulates dendritic and axonal growth, neuronal plasticity, cognitive function, resistance against stress and other cellular process. SIRT1 has also been suggested to be closely associated with the accumulation of amyloid-β and tau in AD brain, in which SIRT1 has been shown to be reduced (Julien et al., 2009).

Particularly in the peripheral nervous system, PGC-1α function is modulated by AMPK, which is a critical player in mitochondrial bioenergetic processes, particularly during exercise. In muscle, PGC-1α is activated by AMPK through changes in the ratio of AMP/ATP (Hardie et al., 2012). Thus, AMPK is stimulated when ATP reduction is detected either through decreased production, or by increased consumption of ATP. For example, rising cytoplasmic calcium levels typically increase ATP consumption and activate AMPK (Herzig and Shaw, 2018). AMPK may also modulate the function of transcription factors, including FOXO family, that coordinates resistance to oxidative stress and energy metabolism (Greer et al., 2007).

In aging brain, there is an increase in the size of mitochondria that might indicate a compensatory mechanism for age-related decline in mitochondrial function. In neurodegenerative disease, however, it is apparent that there is an increase in abnormal mitochondria (Reddy, 2009). In addition, lysosomal removal of mitochondria through mitophagy is increased in neurodegenerative disease (Hirai et al., 2001). One theory suggests that switching from an enhanced state of mitochondrial biogenesis to a decrease in mitochondrial biogenesis represents a key transition between normal brain aging and neurodegeneration (Reddy, 2006; Onyango et al., 2010). Therefore, this suggests that inducing mitochondrial biogenesis could be a potential pharmacological target for the treatment of neurodegenerative disease. Fig. 1.17 illustrates the potential beneficial effects of compounds and other interventions that could stimulate many of the key players involved in mitochondrial biogenesis.

Fig. 1.17 Mitochondrial biogenesis signalling pathway

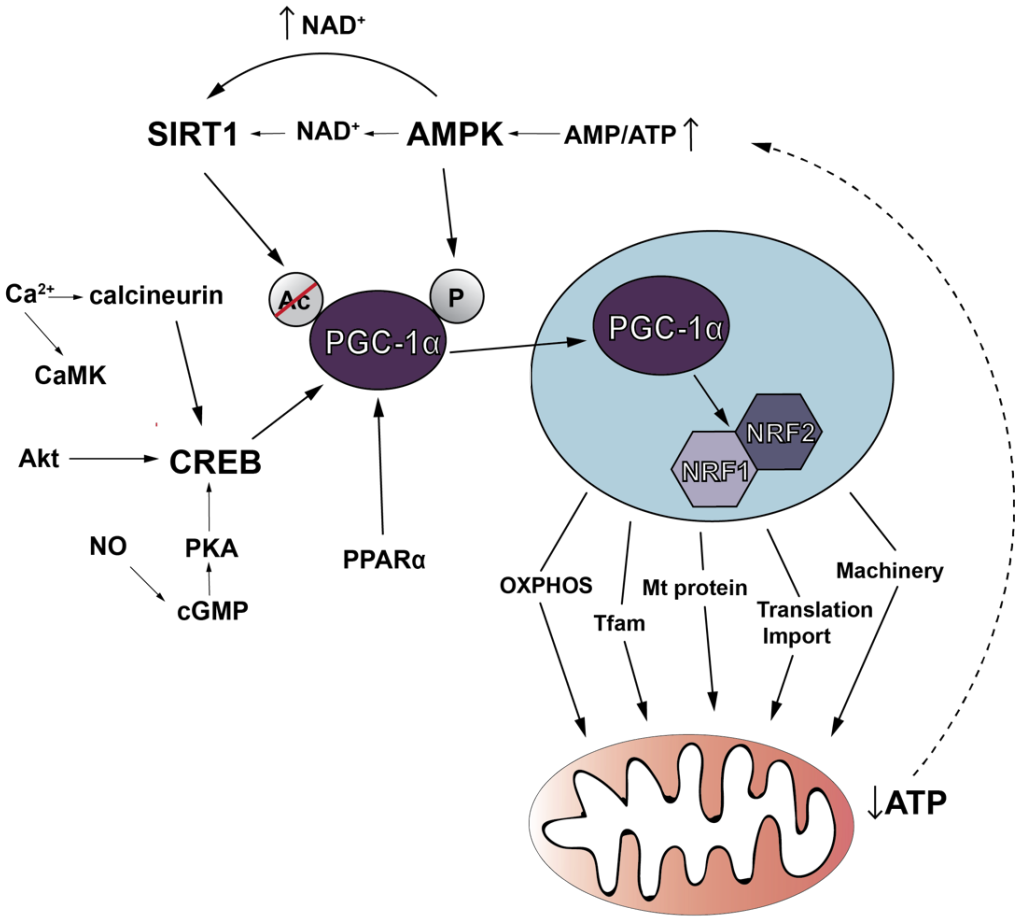

Diagram demonstrates key players in mitochondrial biogenesis pathway. PGC-1α is regulated by AMPK, SIRT1 and CREB. Activation of PGC-1α occurs when the AMP/ATP ratio increases upon reduction of ATP levels in the cells. This further leads to increase of NAD^+ levels that stimulate SIRT1 to activate PGC-1α. CREB gets activated through phosphorylation by kinases such as Akt and PKA. PGC-1α activation leads to a chain of downstream signalling events that are required for

mitochondrial function and biogenesis. These are events like stimulation of OXPHOS, activation of TFAM and other processes needed to facilitate mitochondrial biogenesis.

1.15.4 The relationship between mitochondria and tau

Recent studies have suggested an intrinsic link between tau and mitochondria. Mitochondrial dysfunction has long been demonstrated to have an early pathological role in the development of tauopathy including AD and FTD (Yao et al., 2009). It was found that N-terminally truncated tau (20-22 kDa) (Table 3) is enriched in AD brain and the amount of this tau fragment correlates with pathological synaptic changes (Amadoro et al., 2014). In addition, transgenic mouse models of tauopathy, such as P301L tau knock-in mice, also exhibit mitochondrial dysfunction (Gilley et al., 2012). P301L tau overexpressing mice have been shown to have increased ROS (David et al., 2005). Furthermore, neurons generated from P301L tau knock-in mice demonstrate that expression of this tau mutation significantly reduces the number of mitochondria in axons (Rodríguez-Martín et al., 2016). The findings in P301L tau knock-in brain lysates of increased phosphorylation of endogenous tau, suggest a role for tau and potentially for tau phosphorylation in the regulation of mitochondrial function (Rodríguez-Martín et al., 2016).

Tau may also be involved in mediating cellular apoptosis via effects in mitochondria. Phosphorylated tau can prevent apoptosis through a mechanism involving Bcl2 and caspase-3 in mitochondria (Atlante et al., 2008; Avila et al., 2016). In addition, tau is thought to facilitate mitophagy through the physical insertion of tau into the outer mitochondrial membrane, thereby changing mitochondrial membrane potential (Hu et al., 2016).

It is thought that the interaction between tau and the mitochondrial fission protein DRP1, can be detrimental for the maintenance of mitochondrial function. Interaction between DRP1 and phosphorylated tau increases fragmentation of mitochondria, resulting in mitochondrial deficiency (Manczak and Reddy, 2012). Conversely, reducing DRP1 expression decreases phosphorylated tau and reduces mitochondrial dysfunction in P301L tau over expressing mice (Kandimalla and Reddy, 2016). In AD, there is evidence for both increased fission and decreased fusion of mitochondria, as well as enhanced interaction of Aβ with DRP1, impaired axonal transport of mitochondria, and synaptic degeneration (Manczak and Reddy, 2012). Thus, it is evident that tau is can influence mitochondrial morphology and function.

1.16 The neuromuscular junction and neurodegeneration

The mechanism that leads to loss of motor function in several neurodegenerative diseases is unclear. It is also unknown whether changes in the neuromuscular junction (NMJ) precede or follow the decline of muscle mass and strength in these disorders. Decline in motor function may involve impaired signalling from the CNS, and/or local degeneration and feedback from dysfunctional muscle tissue. The motor unit, which consists of a motor neuron and the myofibres it innervates, undergoes profound changes during the pathogenesis of neurodegenerative disease (Cappello and Francolini, 2017). Irrespective of the cause, when a motor neuron is lost, fibres previously innervated by the neuron are no longer controlled by the nervous system and fail to function as a motor unit. In an attempt to repair the lost connection, denervated orphan fibres express proteins and produce chemotactic signals that stimulate sprouting of new dendrites from the remaining motor neurons (Lain et al., 2009). This process leads to reinnervation by the expansion of existing motor units, which is necessary for returning motor function and this dynamic denervation/reinnervation cycle compensates for neuronal loss. However, in aging

and disease, this compensatory mechanism fails, leading to a progressive decline in muscle mass and strength. The NMJ comprises pre-synaptic (motor nerve terminal), intra-synaptic (synaptic basal lamina) and post-synaptic (muscle fibre and muscle membrane) components (Punga and Ruegg, 2012). The NMJ receives an action potential at the pre-synaptic element, voltage-dependent calcium channels then open, allowing calcium to enter the neuron and trigger the delivery of acetylcholine (ACh) into the synaptic cleft. ACh release triggers nicotinic acetylcholine receptors located in the post-synaptic membrane, to generate an action potential that activates voltage-gated dihydropyridine receptors (Harkins and Fox, 1998). In order to increase the surface area of the NMJ and hence neuromuscular connectivity, the post-synaptic membrane contains multiple folds Fig. 1.18.

It is thought that ACh receptor (AChR) clusters are formed by neurons releasing agrin, that activates muscle specific kinase (MuSK) on the muscle membrane (Fig. 1.18). However, conversely, it has been shown that AChR clusters can be formed in the absence of the neuron, suggesting that MuSK can be activated as the muscle-initiated event (Singhal and Martin, 2011), for example through muscle protein docking protein 7 (Tezuka et al., 2014). NMJs undergo a prolonged maturation process during which the pre- and post-synaptic apparatus are shaped by synaptic activity. In the final stage of NMJ maturation, nerve terminals compete with each other to innervate each muscle fibre and, eventually, in the early postnatal period, this competition evolves into the elimination of supernumerary inputs (Barik et al., 2016). Most of the molecules that play crucial roles in NMJ formation are also essential for NMJ maintenance in adult life. At this stage, NMJ integrity is tightly dependent on the pre-synaptic release of ACh and on clustering of AChRs on the muscle plasma membrane to trigger muscle action potentials.

Fig. 1.18 The motor unit and neuromuscular junctions

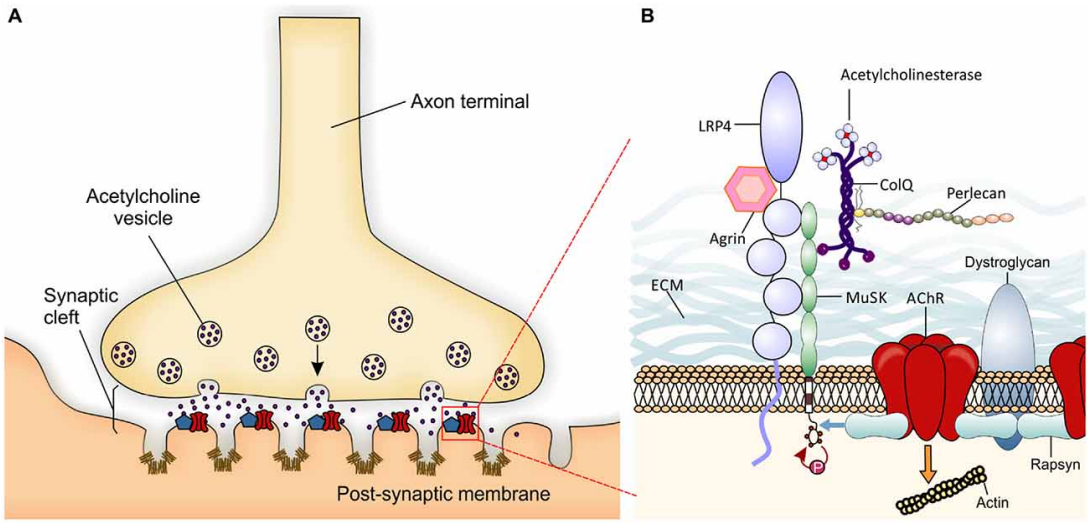

The motor unit consists of the functional component: 1. the cell body of the motor or sensory neuron, 2. the corresponding axons, 3. the neuromuscular junction (the synapse between the motor axon and muscle), and 4. the muscle fibres that are innervated by the motor neuron. **A** Vesicles release ACh neurotransmitter from the presynaptic motor nerve terminal into the synaptic cleft. Postsynaptic skeletal muscle membrane includes several folds of ACh receptors (red) and voltage-gated sodium channels (brown). **B** Neuronal agrin binds to low density lipoprotein receptor-related protein 4 (Lrp4) activating Muscle-specific kinase (MuSK) through phosphorylation. AChE-ColQ complex is essential for the inactivation of ACh. Also, ColQ binds MuSK and perlecan to stabilise the extracellular matrix (ECM). Once activated, MuSK binds rapsyn which in turn links AChRs and dystroglycan (Campanari et al., 2016).

NMJ have been studied mainly in the context of aging and in the motor-neuron disorder, ALS and there has been limited research on the pathological effects on NMJs in the tauopathies. However, tau overexpression has been shown to lead to significant morphological and functional disruption to the NMJ (Chee et al., 2005). Overexpression of human 0N3R tau in *Drosophila* leads to a reduction in the size of NMJs and an increase in the number of NMJs with irregular and abnormal bouton structure (Chee et al., 2005). In addition, analysis of the number and distribution of mitochondria in the pre-synaptic terminal showed that neurons overexpressing tau exhibit a significant reduction in the number of functional mitochondria (Chee et al., 2005). Therefore, it has been shown that tau overexpression leads to synaptic dysfunction, which may be caused by a reduced complement of functional mitochondria and this may be related to defects at the NMJ (Chee et al., 2005).

1.17 Aims and objectives

The aims of the studies reported in this thesis are as follows:

1) To investigate the biochemical and pathological characteristics of central and peripheral nervous system in a novel mouse model of the human brain-derived, 35 kDa tau fragment (Tau35), which leads to a disease phenotype.

2) To morphologically and biochemically characterise primary cortical neurons derived from Tau35 mice to establish it as a cellular model of human tauopathies and as a platform to study new targets for pharmacological intervention.

3) To investigate mitochondrial morphology, dynamics and function to understand the effects of Tau35 on axonal transport and neuronal bioenergetics.

Chapter 2: Materials and Methods

2.1 Materials

All materials were obtained from Sigma-Aldrich unless otherwise indicated. Ultrapure water (Elga Maxima system) was used to prepare all solutions.

2.1.1 Animals and tissue

Mice expressing Tau35 cDNA with an HA-tag and hGHpA under the control of the human tau promoter with targeted insertion into the *Hprt* locus using genOway's 'Quick Knock-in™' technology on a 75% C57BL/6;129Ola background were used in this study. Mice were bred in-house and weaned on day 21. Transgenic animals were identified by genotyping. All the mice used in this project were male Tau35 (hemizygous) or male wild-type (WT), age-matched controls. The animals had access to rodent chow and water at all times. RM1 rodent chow was given to all mice apart from breeders, which received RM3 rodent chow (Special Diet Services). Mice were maintained under a 12-hour light-dark cycle at constant temperature.

2.1.2 Buffer solutions

Phosphate-buffered saline (PBS)	137 mM NaCl
	2.7 mM KCl
	10 mM Na_2HPO_4
	2 mM KH_2PO_4
	pH 7.4
Tris-buffered saline (TBS)	50 mM Tris-HCl
	150 mM NaCl
	pH 7.6

2-(N-morpholino)ethanesulfonic acid (MES) buffer	100 mM 2-(N-morpholino) ethanesulfonic acid (MES), pH 7.4 0.5 mM $MgCl_2$ 1 mM ethylene glycol-bis(β-aminoethyl ether)-N,N,N',N'-tetraacetic acid (EGTA) 1 M NaCl
Extra strong lysis buffer (ESLB)	10 mM Tris-HCl, pH 7.5 75 mM NaCl 0.5% (w/v) sodium dodecyl sulphate (SDS) 20 mM sodium deoxycholate 1% (v/v) Triton X-100 2 mM sodium orthovanadate 1.25 mM NaF 1 mM sodium pyrophosphate 10 mM ethylenediaminetetraacetic acid (EDTA) 1 x cOmplete™ Mini protease inhibitor cocktail tablet (Roche Diagnostics) added to each 10 mL of buffer 1x phosSTOP phosphatase inhibitor tablet (Roche Diagnostics) added to each 10 mL of buffer

2.1.3 Bicinchoninic acid assay (BCA) protein assay

BCA assay kit (Thermo Fisher Scientific)	Pierce BCA protein assay kit BCA Reagent A, 500 mL BCA Reagent B, 25 mL Albumin standard, 2mg/mL

2.1.4 Sodium dodecyl sulphate-polyacrylamide gel electrophoresis (SDS-PAGE)

Laemmli buffer (2x)	65.8 mM Tris-HCl, pH 6.8 2.1% (w/v) SDS 26.3% (w/v) glycerol 0.01% (w/v) bromophenol blue 5% (v/v) β-mercaptoethanol (BME)
Resolving gel	10% (w/v) acrylamide (National Diagnostics) 25% (v/v) resolving buffer, pH 8.8 (National Diagnostics) 0.01% (w/v) ammonium persulphate (APS, National Diagnostics) 0.1% (v/v) N,N,N',N'tetramethylethylendiamine (TEMED, National Diagnostics)

Stacking gel	4% (w/v) acrylamide 25% (v/v) stacking buffer, pH 6.8 (National Diagnostics) 0.075% (w/v) APS 0.15% (v/v) TEMED
Running buffer	25 mM Tris base, pH 6.8 (National Diagnostics) 192 mM glycine 0.1% (w/v) SDS
Electrophoresis molecular weight markers	Precision Plus Protein, All Blue Pre-stained Protein Ladder (Bio-Rad) Chameleon Duo Pre-stained Protein Ladder (Li-Cor Biosciences)
Precast gels	Novex™ 8-16% Tris-glycine mini gels, WedgeWell™ format, 15-well (Thermo Fisher Scientific) Novex™ 8-16% Tris-glycine Plus midi gels 26-well (Thermo Fisher Scientific)
Running buffer for precast gels	Novex™ Tris-glycine SDS running buffer (10X) (Thermo Fisher Scientific)
Sample buffer for precast gels	Novex™ Tris-glycine SDS sample buffer (2X) (Thermo Fisher Scientific)

Reducing reagent for precast gels	NuPAGE™ sample reducing agent (10X) (Thermo Fisher Scientific)

2.1.5 Western blot

Transfer buffer	25 mM Tris base, pH 6.8 (National Diagnostics) 192 mM glycine 20% (v/v) methanol
Blocking solution and antibody diluent	3% (w/v) dried skimmed milk in TBS 4% bovine serum albumin Odyssey® Blocking Buffer (TBS) (Li-Cor Biosciences)
Western blotting membrane	Nitrocellulose membrane 0.45 μm (GE Healthcare)

Table 4 Primary antibodies

Antibody	Epitope/Antigen	Species/Type	Dilution for WB	Dilution for ICC	Source
2H3	Neurofillament medium chain (NF-M)	Mouse monoclonal	N/A	1/50	DSHB*
Aldh1L1	Full-length aldehyde dehydrogenase 1 family, member L1 (aldh1L1)	Mouse monoclonal	1/500	N/A	Antibodies Incorporated
DRP1	Dynamin related protein 1 (DRP1) C-terminus (560-736)	Mouse monoclonal	1/100	N/A	Santa Cruz
Dynactin p150	Total dynactin p150Glued protein	Rabbit monoclonal	1/1,1000	N/A	Cell Signaling
GAPDH (6Ca5)	Glyceraldehyde-3-phosphate dehydrogenase (GAPDH)	Mouse monoclonal	1/1,500	N/A	Santa Cruz Biotech
GFAP	Mammalian glial fibrillary acidic protein (GFAP)	Mouse monoclonal	1/2,000	1/1,1000	Santa Cruz
HA.11 Clone 16B12	Hemagglutinin (HA) tag (YPYDVPDYA)	Mouse monoclonal	1/500	N/A	Covance
HSP60	Heat shock protein 60, clone LK2	Mouse monoclonal	1/2,500	N/A	Sigma Aldrich
Kinesin	Kinesin heavy chain (420-445)	Mouse monoclonal	1/1,000	N/A	Millipore
LC3B	Amino acids 2-15, human LC3B	Rabbit polyclonal	1/2,000	N/A	Sigma Aldrich
NeuN	Neuronal nuclei	Mouse monoclonal	N/A	1/500	Chemicon
OPA1	Optic atrophy type 1 protein (OPA1) (708-830)	Mouse monoclonal	1/1,000	N/A	BD Bioscience
pDRP1	Phospho-DRP1 (S616)	Rabbit polyclonal	1/1,000	N/A	Cell Signaling
pmTOR	Phosphorylated mechanistic target of rapamycin (S2448)	Rabbit monoclonal	1/1,000	N/A	Cell Signaling

pS6	Phosphorylated S6 (S235, S236)	Rabbit polyclonal	1/1,000	N/A	Cell Signaling
S6	Total S6 ribosomal protein	Mouse monoclonal	1/1,000	N/A	Cell Signaling
SOD1	Endogenous superoxide dismutase 1	Mouse monoclonal	1/1,000	N/A	Cell Signaling
SV2	Synaptic vesicle glycoprotein 2A	Mouse monoclonal	N/A	1/100	DSHB
Tom20 (FL-145)	Full length Tom20	Rabbit polyclonal	1/500	N/A	Santa Cruz Biotech
Total tau (K9JA)	Tau residues C-terminal half (243-441)	Rabbit polyclonal	1/1,000	N/A	Dako
TP70	Tau C-terminus (428-441)	Rabbit polyclonal	1/2,000	N/A	Abcam
β-actin	N-terminus of β-actin	Rabbit polyclonal	1/5,000	N/A	Abcam
β-actin	N-terminus of β-actin	Mouse monoclonal	1/5,000	N/A	Sigma Aldrich
Tau1	Tau1, clone PC1C6	Mouse monoclonal	1/1,000	N/A	Millipore
PHF1	Tau phosphorylated at 396/404	Mouse monoclonal	1/1,000	N/A	Prof Peter Davies
Tau5	Tau (210-241)	Mouse monoclonal	1/1,000	N/A	Millipore
SIRT1	Endogenous levels of total SIRT1	Rabbit monoclonal	1/1,000	N/A	Cell Signaling
CREB	Endogenous levels of CREB-1 protein	Rabbit monoclonal	1/1,000	N/A	Cell Signaling
NRF2	NRF2 (550) to the C-terminal	Rabbit polyclonal	1/1,000	N/A	Abcam
pCREB	Phosphorylate CREB (S133)	Rabbit monoclonal	1/1,000	N/A	Cell Signaling
MFN1 (D-10)	Mitofusin 1	Mouse monoclonal	1/100	N/A	Santa Cruz Biotech
GSK3α/β	Full length GSK3α/β (1-420)	Mouse monoclonal	1/1000	N/A	Santa Cruz Biotech

pGSK3α/β	Phosphorylated GSK3α (S21) and phosphorylated GSK3β (S9)	Rabbit polyclonal	1/1000	N/A	Cell Signaling

Table 5 Secondary antibodies for western blots

Antibody	**Dilution**	**Source**
Alexa Fluor 680 goat anti- mouse IgG	1/10,000	Invitrogen
IRDye TM 800 goat anti- rabbit IgG	1/10,000	Invitrogen

Table 6 Secondary antibodies for immunofluorescence

Antibody	**Dilution**	**Source**
Alexa Fluor 488 donkey anti mouse IgG (H+L)	1/1,000	Invitrogen
Alexa Fluor 594 donkey anti rabbit IgG (H+L)	1/1,1000	Invitrogen

***** DSHB- Developmental studies hybridoma bank

Tissues did not require additional pretreatment. The concentration of antibodies was optimised to produce clear signal.

2.1.6 Genotyping

KAPA mouse genotyping kit	10X KAPA express extract buffer 1 U/μL KAPA express extract enzyme 2X KAPA2G fast genotyping mix with dye
REDExtract-N-Amp™ Tissue polymerase chain reaction (PCR) Kit	Extraction solution Tissue preparation solution Neutralisation Solution B REDExtract-N-Amp PCR reaction mix (2X PCR reaction mix containing buffer, salts, dNTPs, Taq polymerase, REDTaq dye, and JumpStart Taq antibody)

Table 7 Primers and sequence used for PCR genotyping

Primer name	**Primer sequence 5' to 3' (number of bases)**
Forward Tau35	CGTATGTGATGGACATGGAGATGGAGG (27)
Reverse Tau35	GCCTCCCTCTTATTAAGGACGCTGAGG (27)
Forward HPRT	TGTCCTTAGAAAACACATATCCAGGGTTTAGG (32)
Reverse HPRT	CTGGCTTAAAGACAACATCTGGAGAAAAA (30)
Forward Sry	TCATGAGACTGCCAACCACAG (21)
Reverse Sry	CATGACCACCACCACCACCAA (21)
Forward Myog 5	TTACGTCCATCGTGGACAGC (20)
Reverse Myog 5	TGGGCTGGGTGTTAGTCTTA (20)

Agarose gel electrophoresis	10 mg/mL ethidium bromide 2% (w/v) agarose Tris-acetate-EDTA (TAE) buffer (Thermo Fisher)

2.1.7 Primary cortical neuronal cell culture

Poly-D-lysine	10 mg/mL poly-D-lysine Poly-D-lysine pre-coated 6-well and 12-well plates (Greiner) Glass-bottomed microwell dishes (MatTek Corporation)
Dissection solution	1 mM 4-(2-hydroxyethyl)-1-piperazineethanesulfonic acid (HEPES, Life Technologies) Ca^{2+}/Mg^{2+}-free Hank's Balanced Salt Solution (HBSS, Life Technologies)
Primary cortical neuronal cell culture medium	Neurobasal medium (Life Technologies) 1% (v/v) penicillin/streptomycin (Life Technologies) 1% (v/v) GlutaMAX (Life Technologies) 2% (v/v) B27 (serum- free supplement)

Cell transfection	Enhanced green fluorescent protein (eGFP) plasmid (Invitrogen) *Discosoma sp.* red fluorescent protein fused with the mitochondrial targeting sequence from subunit VIII of human cytochrome c oxidase (DSRed-Mito) plasmid (Invitrogen) Opti-MEM (Thermo Fisher) Lipofectamine 2000 (Thermo Fisher)
Cell fixation	4% (v/v) paraformaldehyde (PFA) 15% (w/v) sucrose in TBS

2.1.8 Sub-cellular fractionation of mouse brain and muscle

Homogenisation buffer	5 mM HEPES, pH 7.4 1 mM $MgCl_2$ 2 mM EDTA 0.32 M sucrose 1 mM DTT 1 x cOmplete™ Mini protease inhibitor cocktail tablet (Roche Diagnostics) added to each 10 mL of buffer 1x PhosSTOP phosphatase inhibitor tablet (Roche Diagnostics) added to each 10 mL of buffer

Mitochondria buffer	50 mM Tris-HCl pH7.4 1 mM EDTA 0.5% (v/v) Triton X-100
Nuclear buffer	20 mM HEPES pH 7.4 1. 5mM $MgCl_2$ 0.2 mM EDTA 20% (v/v) glycerol 1% (v/v) Triton X-100

2.1.4 Immunohistochemistry (IHC) and immunofluorescence (IF)

TBS-anti freeze	30% (v/v) ethylene glycol 15% (w/v) sucrose 0.05% (w/v) sodium azide in 50 mM TBS
Cryoprotectant	30% (w/v) sucrose in PBS
Optimal cutting temperature compound (OCT)	Cryo-embedding media (Fisher Scientific)
Peroxidase blocking solution	2.5% (v/v) hydrogen peroxide in methanol
Blocking solution	2% (v/v) normal goat serum (NGS, Vector Laboratories) in TBS

Antibody diluent	1% (v/v) NGS in TBS
Avidin-biotin complex (ABC) system (IHC only)	VECTASTAIN ABC kit (VectorLaboratories) TBS
Diaminobenzidine (DAB, IHC only)	DAB substrate kit (Vector Laboratories)
Haematoxylin counterstain (IHC only)	Harris' haematoxylin (Vector Laboratories)
Mounting medium	IHC: DPX (Distyrene, a plasticiser, and xylene) mountant (VWR Chemicals) IF: Fluorescent mounting medium (Dako)
Thioflavin S staining solution	0.1% (v/v) thioflavin S in H_2O

2.1.9 Neuromuscular junction staining

Silicone coating	Sylguard 184 silicone elastomer kit (Dow Corning 01015311)
Fixing solution	4% (w/v) PFA (Electron Microscopy Sciences)
Permeabilisation solution	2% (v/v) Triton X-100 1X PBS, containing 1.37 M NaCl
Antibody diluent solution	1% (v/v) Triton X-100

	4% (w/v) BSA
Blocking solution:	4% (w/v) BSA

2.1.10 Seahorse XF Cell Mito Stress Test

Seahorse calibration solution	Agilent Seahorse XF calibrant
Seahorse XF Agilent Cell Mito Stress Test kit	2μM Oligomycin 1μM FCCP (carbonyl cyanide 4-trifluoromethoxyphenylhydrazone) 0.5μM Rotenone/antimycin A
Seahorse XF Agilent test medium	Agilent Seahorse XF base medium (DMEM) 1mM Pyruvate (Life Technologies) 1 mM Glutamine (Life Technologies) 10mM Glucose (Life Technologies)
Seahorse cell cultures	Agilent Seahorse XF96 cell culture microplates Agilent Seahorse XF96 extracellular flux sensor cartridge

2.2 Methods

2.2.1 Fractionation of human brain

Human frozen post-mortem brain tissue (pre-motor cortex) from two individuals with progressive supranuclear palsy (PSP) and two age-matched controls was obtained from the MRC London Neurodegenerative Diseases Brain Bank (King's College London). Brain tissue was weighed and homogenised in 4 volumes (w/v) MES buffer. The homogenate was centrifuged at 3,000 x g (av) for 20 minutes at 4°C. The supernatant was collected and centrifuged at 100,000 x g (av) for 60 minutes at 4°C. The pellet was then resuspended in Laemmli sample buffer and analysed on western blots.

2.2.2 Mouse tissue collection

Mice were anaesthetised with 200 mg pentobarbital sodium (Euthatal, Merial) via intraperitoneal injection and perfused with PBS. Tissues were collected and either frozen immediately in liquid nitrogen (frontal brain area, hippocampus and associated cortex, amygdala, brain stem and cerebellum regions, spinal cord, sciatic nerve and quadriceps muscle) or post-fixed in 4% (v/v) PFA overnight at 4°C (half brain and sciatic nerve). Samples were frozen immediately in liquid nitrogen and stored at -80°C until use. Fixed brain tissue was transferred to 30% (w/v) sucrose and incubated overnight at 4°C, then frozen in dry cold isopentane. Fixed sciatic nerve was embedded in OCT. To do this, the sciatic nerve was placed flat on a glass slide on top of dry ice. Aluminium foil was used to form a box around the sciatic nerve which was then filled with the OCT compound to create a block. The sample was then stored at -80°C. Mouse hind limbs were collected for neuromuscular dissection (see section 2.2.16).

2.2.3 Mouse brain and muscle homogenisation

Mice were culled by cervical dislocation, and the brains were either kept intact or dissected into four regions (frontal area, hippocampus and associated cortex, amygdala, and brain stem and cerebellum). Tissue was thawed on ice and manually homogenised on ice in 4 volumes (w/v) extra strong lysis buffer (ESLB) using a Dounce homogeniser. The samples were analysed using the protein assay described in section 1.2.5 to determine protein concentration in the homogenates. Homogenates were centrifuged at 13,000 x g (av) for 20 minutes at 4°C. The pellet was retained, and the supernatant was centrifuged at 100,000 x g at 4°C for 60 minutes. The final supernatant and pellet were retained. Pellets were resuspended directly in Laemmli sample buffer and supernatants were mixed with an equal volume of Laemmli sample buffer prior to analysis on western blots.

2.2.4 Protein assay

The protein concentration of mouse brain and muscle homogenate was determined using the bicinchoninic acid protein assay (Pierce BCA protein assay kit), with bovine serum albumin (BSA) as a standard. Samples were centrifuged at 8000 x g (av) for 2 minutes at 4°C and the protein content of the supernatant was measured. In a 96-well plate, a standard curve was created by mixing different amounts of BSA with extra strong lysis buffer (ESLB). Samples were measured in duplicates, where 5 μL of sample was added to 20 μL of ESLB per well. The plate was then incubated in the dark for 30 minutes at 37°C, and the amount of protein present was quantified by measuring the absorbance at 562 nm using a microplate reader. A BSA standard curve was used to determine the protein concentration of each sample.

2.2.5 SDS-PAGE and western blots

Samples in Laemmli sample buffer were heated at 95°C for 10 minutes and centrifuged at 13,000 x g (av) for 2 minutes. Supernatants were loaded onto 10% (w/v) or 12% (w/v) polyacrylamide gels and run at 150 V for 80-100 minutes, or until the blue sample loading dye reached the bottom of the gel. Separated proteins were transferred to 0.45 µm nitrocellulose membranes (GE Healthcare Life Science) at 100 V for 60 minutes on ice, using a wet transfer system (Bio-Rad). This was performed by creating a sandwich assembly with components assembled in the following order: sponge, filter paper (4-6 pieces), gel, nitrocellulose membrane, filter paper (4-6 pieces), and sponge. These components were pre-soaked in cold transfer buffer. The sandwich assembly was then placed into a blotting cassette. Following the transfer, membranes were incubated in blocking solution for 60 minutes to reduce non-specific binding of the antibodies. The blocking solution was selected depending on the antibody specificity: 4% (w/v) BSA in TBS, 3% (w/v) dried skimmed milk in TBS or Odyssey blocking buffer (TBS). The membranes were then incubated in primary antibodies (Table 1.1) diluted in blocking solution overnight at 4°C, with rocking. Blots were then washed in Tween-TBS for 3 x 10 minutes and incubated in appropriate fluorophore-conjugated secondary antibodies (Table 1.2) diluted in blocking solution for 60 minutes at ambient temperature. After two washes in Tween-TBS and final wash in TBS (10 minutes per wash), antigens were visualised using the Odyssey infrared imaging system (Li-Cor Biosciences) and quantified using Image studio lite (Li-Cor). For later western blot experiments, pre-cast gradient (8-16%, w/v) polyacrylamide gels (Invitrogen) were used.

2.2.6 PCR genotyping

Tissue for genotyping, collected by ear notching or tail tipping, was incubated in extraction and tissue preparation solution (KAPA kit or REDExtract-N-Amp) at ambient temperature for 10 minutes, followed by the addition of neutralising solution.

Samples underwent PCR using primers (Table 7) and PCR reaction mix (KAPA kit or REDExtract-N-Amp). DNA samples were loaded onto 2% (w/v) agarose gels containing 10 mg/mL ethidium bromide to visualise DNA. The gels were run at 135 V for 40 minutes and bands were detected using the UVP transilluminator.

PCR program

Initial denaturation	94˚C	3’	
Denaturation	95˚C	15”	35 cycles
Annealing	55˚C	15”	
Extension	72˚C	1’	
Final extension	72˚C	5’	

2.2.7 Immunofluorescence

Immunohistochemistry and immunofluorescence were performed on 30 μm free-floating coronal brain sections from WT and Tau35 mice aged 8 months and 18 months (sections prepared by Marie Bondulich). Sections were washed in TBS (2 x 5 minutes) to remove the TBS-anti-freeze solution and treated with peroxidase blocking solution for 30 minutes to block endogenous peroxidase activity. Sections were washed in TBS (2 x 5 minutes) and blocked in 2% (v/v) normal goat serum (NGS) in TBS for 30-60 minutes, before being incubated in primary antibody (see Table 4) overnight at 4°C, with rocking and then washed in TBS (3 x 15 minutes).

For immunofluorescence analysis, sections were incubated with fluorescently-tagged secondary antibodies (see Table 6) at ambient temperature for 1 hour in the dark, with rocking. Sections were then washed in TBS (3 x 10 minutes), mounted on slides using a paintbrush, and air-dried at ambient temperature overnight. Coverslips were then mounted onto slides using fluorescent mounting media (Dako), and images were captured using a camera on Leica DM5000 B fluorescence microscope.

2.2.8 Preparation and culture of mouse primary cortical neurons

Prior to dissection, glass coverslips were baked for sterilisation at 180°C and placed into a 12-well culture plate. For earlier experiments, all plates (6, 12 and single well) were coated in 1-2 mL poly-D-lysine (PDL, 10 µg/mL) in sterile distilled H_2O, incubating for at least 1 hour at 37°C or overnight at 4°C. Following this, the PDL solution was removed and wells were washed in 1-2 mL sterile distilled H_2O (3 x 5 minutes) and air-dried. For later experiments, PDL pre-coated culture plates were used. Primary cortical neurons were prepared from embryonic (E) day 14-16 (E14-16) mouse embryos. Pregnant mice were culled by cervical dislocation and embryos were removed from the uterus and decapitated. Heads were stored in 1 mM HEPES (Life Technologies) in $Ca^{2+/}Mg^{2+}$-free Hank's balanced salt solution (HBSS, Life Technologies) on ice. Meninges were removed from the cortices, which were isolated from remaining brain structures and placed in HBSS/HEPES solution. The embryonic skulls were retained for subsequent genotyping. Cortical tissue was digested in 0.1% (v/v) trypsin-EDTA (Life Technologies) HBSS for 10 minutes at 37°C. The trypsin was aspirated, and cortices were rinsed in HBSS (3 x 1 minute) to prevent further trypsinisation. Tissue was then homogenised by gentle pipetting using a P1000 automatic pipette (Gilson), and the homogenate was suspended in pre-warmed (37°C) primary cortical neuron cell culture media. Cells were seeded in 6-well or 12-well tissue culture plates (Greiner) at a density of 500,000 cells/well or 250,000 cells/well, respectively. Cells were allowed to attach to the plate during incubation for 2 hours at 37°C in 5% CO_2, after which the medium was replaced with fresh cell culture media.

2.2.9 Preparation of mouse neuronal lysates

Neurons cultured in 6-well and 12-well plates were scraped into ESLB (100 µL and 50 µL, respectively) and placed on ice for 10 minutes. Tubes were vortexed, and the contents were sonicated at 40% amplitude at 4˚C for 3 seconds. The lysed samples were then centrifuged at 12,000 x g (av), for 7 minutes at 4˚C. Neuronal supernatants were collected and stored at -80˚C.

2.2.10 Transfection of primary mouse cortical neurons

DNA plasmids expressing enhanced green fluorescent protein (eGFP) or DSRedMito were prepared using a Plasmid Maxi Kit (Qiagen) or Plasmid Midi Kit (Qiagen). DNA concentration and quality were determined using a Nanodrop 2000 (Thermo Fisher). Cortical neurons cultured on 18 mm^2 round coverslips in 12-well plates or 35 mm glass bottom dishes (MatTek) were transfected with plasmids expressing eGFP and/or DSRedMito at 2, 5, or 7 days *in vitro* (DIV). Transfection mixture was prepared such that 1 µg of DNA, 1 µL of Lipofectamine 2000 and 100 µL of Opti-MEM was added per well. DNA and Lipofectamine 2000 were diluted separately in Opti-MEM and incubated at room temperature for 5 minutes. Both mixtures were then combined and incubated at 37°C for 20 minutes. After the incubation, neurons were transfected by adding 100 µL of transfection mixture directly into the media. Neurons were incubated with transfection complexes for 5 hours, after which half of the medium was replaced with fresh cell culture media. For investigating mouse primary cortical neuronal morphology, cells transfected at 2, 5, and 7 DIV were fixed at 3, 6, and either 9 or 14 DIV, respectively. For live-cell imaging and immunocytochemistry, cells were transfected at 7 DIV and imaged at 9 DIV.

2.2.11 Fixing and mounting of mouse primary cortical neurons

Mouse primary cortical neurons were fixed in freshly prepared, pre-warmed 4% (w/v) PFA in PBS with 15% (w/v) sucrose for 10 minutes at ambient temperature, and then rinsed (3 x 1 minute) in PBS. Coverslips were mounted on glass slides using VECTASHIELD Antifade Mounting Medium with DAPI (Vector Laboratories) and stored in the dark at 4˚C, until ready for imaging.

2.2.12 Fluorescence imaging of mouse primary cortical neurons

Images of the dendritic morphology of mouse cultured cortical neurons were acquired using the GFP channel on an Eclipse T*i* inverted microscope (Nikon Instruments) using NIS Elements Advanced Research software (Nikon Instruments). Images of mouse neurons at 3 and 6 DIV were acquired using a 40X objective, and images from neurons cultured for 9 DIV were captured using a 20X objective. Z-stacks of individual neurons were acquired using a 0.1 µm step size, at each time point (3, 6, 9DIV), in order to capture all projections. 14 DIV neurons were imaged using a 20X objective, using the High Dynamic Range (HDR) module to reduce signal saturation from the soma and to improve resolution of neuronal processes. Images of dendritic spines on neurons at 14 DIV were also acquired using HDR capture, using a 60X objective. Images of multiple dendrites were acquired from the same cell, differing in distance to the soma.

2.2.13 Neuronal morphology and Sholl analysis

Z-stack images acquired from 3, 6, 9 DIV neurons were imported into Fiji image processing software (Schindelin et al., 2012). The Simple Neurite Tracer plugin (Longair et al., 2011) was used for digital reconstruction and to extract morphological information. This plugin enables for semi-automated tracing, data exportation, and Sholl analysis (Sholl, 1953). The 'Segmented Line' and 'Measure' tools in Fiji were used to trace and measure the soma perimeter and area.

The parameters extracted from Simple Neurite Tracer as illustrated in Fig. 2.1:

- Number of end points (tips) per neuron
- Number of branch points per neuron
- Number of primary neurites stemming from the soma
- Number of secondary neurites (stemming from primary neurites)
- Mean neurite length (μm) per neurite
- Radial distance or dendritic extent (μm)

Fig. 2.1 Diagram of morphometric measurements

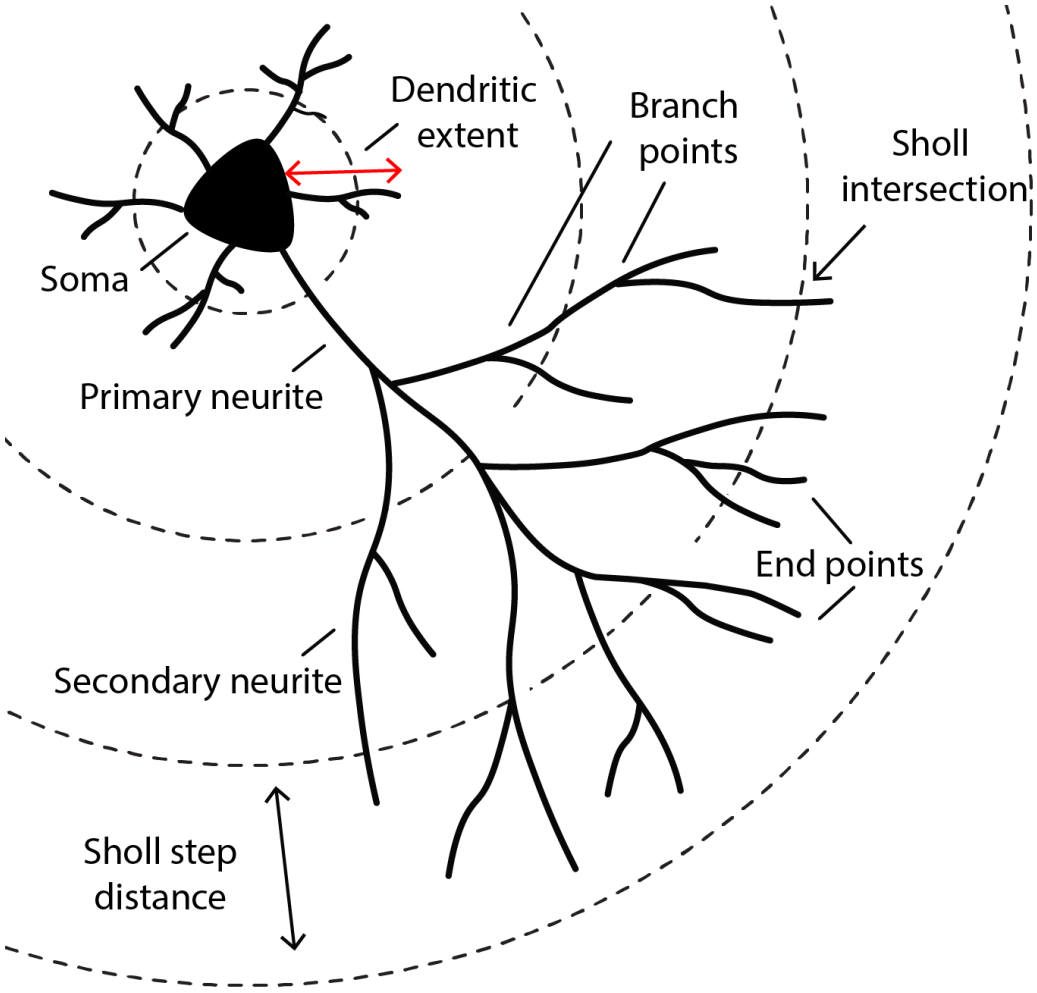

The diagram demonstrates a schematic representation of a neuron. Soma is shown in grey with a dendritic tree originating from it in red. The morphometric measurements are indicated on the diagram (adapted from Rietveld et al., 2015).

Following the construction of traces, Sholl analysis was performed on 3, 6, and 9 DIV neurons. This method analyses dendritic complexity based on the distribution of crossings of concentric circles starting at the focal point of the cell soma (Fig. 2.1). The Sholl step distance was fixed at 10 µm, and the maximal radial distance was set according to the time in culture (3 DIV, 180 µm; 6 DIV, 250 µm; 9 DIV, 330 µm).

The parameters measured were:

- The total sum of intersections of neurites with the concentric circles
- The number of intersections at a given distance from the soma
- The linear profile of intersections as a function of the distance from the soma

2.2.14 Digital reconstruction and quantitative analysis of dendritic spines

TIFF images of 14 DIV neurons from a 60X objective were imported into NeuronStudio (Rodriguez et al., 2006; 2008). This program is designed to semi-manually trace the dendritic arbor as well as detection and classification of dendritic spines. Spine morphology was assigned as follows:

- 'Stubby' spine: width to height ratio > 1
- 'Thin' spine: width to height ratio < 1
- 'Mushroom' spine: width of head to width of neck ratio > 1
- "Other" spine: not attributable to any of the three categories above

Following assignment of spine type analysis, the spine density was calculated and expressed as the number of spines per μm dendrite. The number of spines present on dendrites at different distances (distal and proximal) from the cell soma were compiled to calculate a mean spine density (spines/μm) per neuron. The number of each type of spine ('stubby,' 'thin,' 'mushroom,' or 'other') was recorded as the percentage of the total number of spines analysed, from each individual neuron.

2.2.15 Live imaging of transfected neurons to investigate mitochondrial movement

Neurons transfected at 7 DIV were imaged at 9 DIV in a chamber maintained at 37˚C using a Nikon T*i*-E two camera. Mitochondrial trafficking was observed using a 40X objective and the time-lapse function, collecting images every 3 seconds for up to 5

minutes. In each experiment, images were taken at approximately 50-100 μm from the soma to account for any changes in mitochondrial density and mobility (Niescier et al., 2016). All images were saved in ND2 format and analysed using NIS Elements Viewer (Nikon).

Mitochondrial analysis consisted of mobility and shape analysis, which were performed using ImageJ (Schneider et al., 2012). plugins. For mobility analysis, a neurite was selected using the 'Segmented Line' tool and the image was straightened for all image frames of the acquired time lapse. The straightened neurite time lapse stack was used to create a kymograph. The kymograph is a representation of mitochondrial movement as a function of distance over time and is used to determine the number of mobile and stationary mitochondria as well as their directionality (Fig. 2.2). The "Slope to Velocity" plugin was used to determine the speed of motile mitochondria, including their directionality. For shape analysis, the 'Particle Analysis' ImageJ feature was used. Binary images of mitochondria were used to determine the following morphological parameters of the neuronal mitochondria: surface area, perimeter, major and minor axes, mitochondrial orientation within the neurite (angle).

Fig. 2.2 Graphic representation of a kymograph

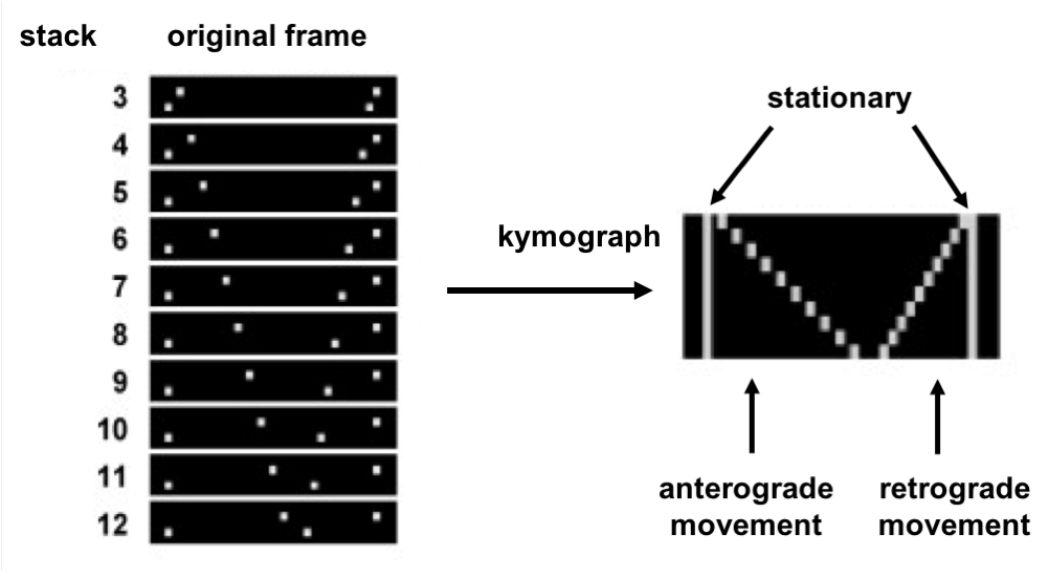

Kymograph represents movement of particles through time across a stack of time lapse image frames. Straight vertical lines represent stationary particles. Diagonal lines from left to right are particles moving anterograde direction and lines going opposite direction show retrograde movement. (adapted from Andrews et al. 2010).

2.2.16 Neuromuscular junction imaging and analysis

The protocol used to dissect the neuromuscular junction (NMJ) and perform immunofluorescent morphological analysis was adapted from Sleigh et al, 2014. The skin was removed from the hind limbs of mice aged 3 or 13 months, within an hour of culling. The dissection was performed on a silicone-covered petri dish in PBS. Using a stereo microscope, the flexor digitorum longus (FDL) muscle tendon was removed and connective tissue was dissected as described in Fig. 2.3 to reveal the lumbrical muscle, which was then collected.

The muscle was fixed for 10 minutes in 4% (w/v) PFA then washed in PBS, and further connective tissue was detached from the muscle. The muscle was transferred to a 96-well plate and permeabilised using 2% (v/v) Triton X-100 in PBS for 30 minutes. Following blocking for 30 minutes in 4% (w/v) BSA in PBS with 1% (v/v) Triton X-100, muscles were incubated overnight at 4°C with primary antibodies recognising neurofilament (2H3, 1/50) and synaptic vesicles (SV2, 1/100) in blocking solution to visualise the axons and pre-synaptic nerve terminals, respectively. Both structures are easily distinguishable morphologically, therefore, the same fluorophores can be used for staining. The following day, the muscles were washed in PBS (3 x 30 minutes) before incubation in AlexaFluor 488 secondary antibody (1/250) and 1.5 µg/ml tetramethylrhodamine –bungarotoxin (-BTX) in PBS for 2 hours in the dark. BTX binds to acetylcholine receptors and therefore labels the endplate of NMJs. Finally, muscles were washed in PBS (3 x 30 minutes) and mounted using Dako fluorescent mounting media.

Fig. 2.3 Hind-limb lumbrical muscle dissection

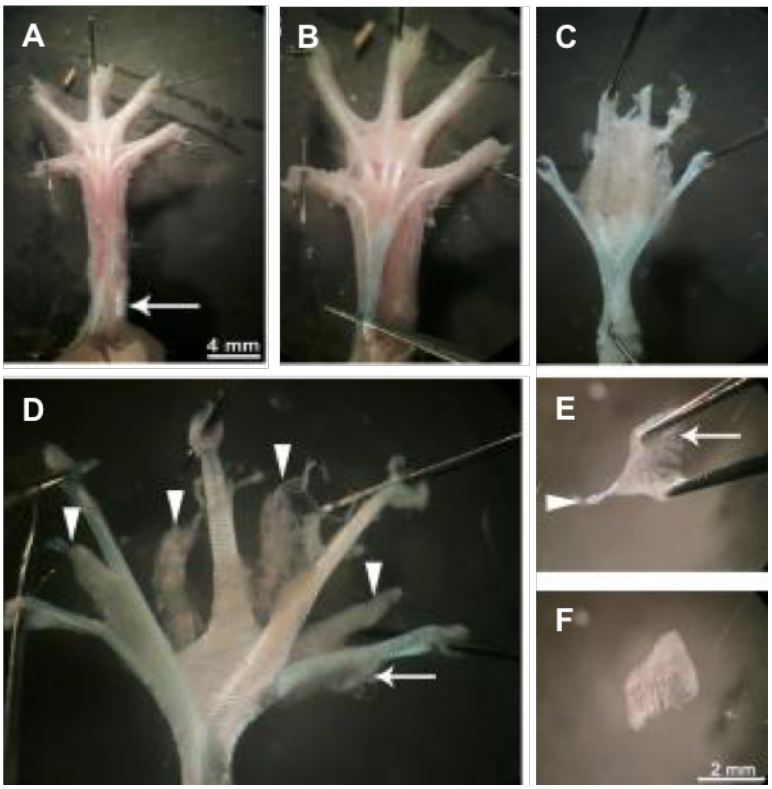

Immediately after culling, the hind-limbs are removed, and overlying skin detached. The leg is then pinned out ventral side up **A**, and the remaining skin dissected away revealing the tendons in the foot. The overlying *flexor digitorum brevis* FDB tendon (arrow) is cut and removed completely by cutting the distal ends. **B,C** The underlying FDL tendon, from which the lumbricals originate, is now dissected. This tendon is also cut proximally and pulled back towards the digits **D** The FDL tendon is then spread and pinned down. The connective tissue is carefully cleared, revealing the underlying lumbricals (arrowheads) between the tendon ends (from medial to lateral, the first to fourth). Excess connective tissue is removed by blunt dissection in the regions between the lumbricals and the tendons before fixation. **E** Lumbrical muscles are excised, and further connective tissue removed. **F** Once cleaned up, the distal FDB tendon (arrowhead) is disconnected, and the muscle is ready for staining. Lumbrical muscles were dissected from a 3 and 13 months-old WT and Tau35 mice (adapted from (Sleigh et al., 2014).

A 60X objective was used to image the degree of innervation and a 20X objective was used to image the NMJ area. Z-stacks were also acquired using a 300 nm interval through the muscle tissue. Before analysis, the images were deconvolved using Richardson-Lucy method on ND2 Nikon software. NMJs were scored on the level of innervation. Binary images were created using ND2 analysis software (Nikon) to distinguish SV2 and BTX labelling at NMJs. If no overlap was present between SV2 and BTX, the NMJ was considered to be denervated. If the denervated NMJ retained a neurofilament-positive axon, the NMJ was rated as partially denervated. If the BTX and SV2 labelling at the NMJ overlapped, this was scored as fully denervated. The size and shape of each NMJ was measured by manual drawing around the perimeter of BTX staining.

2.2.17 Seahorse XF Cell Mito Stress Testing

Mouse primary neurons were seeded at a density of 40,000 cells/well into 96XF 96-well PDL-coated plates (Agilent). At 9 DIV, cell mitochondrial stress testing was performed by following the Seahorse XF cell mito stress test kit protocol (Agilent), according to the manufacturer's instructions (Fig. 2.4).

Fig. 2.4 Preparation process for Seahorse XF Agilent mitochondrial stress test

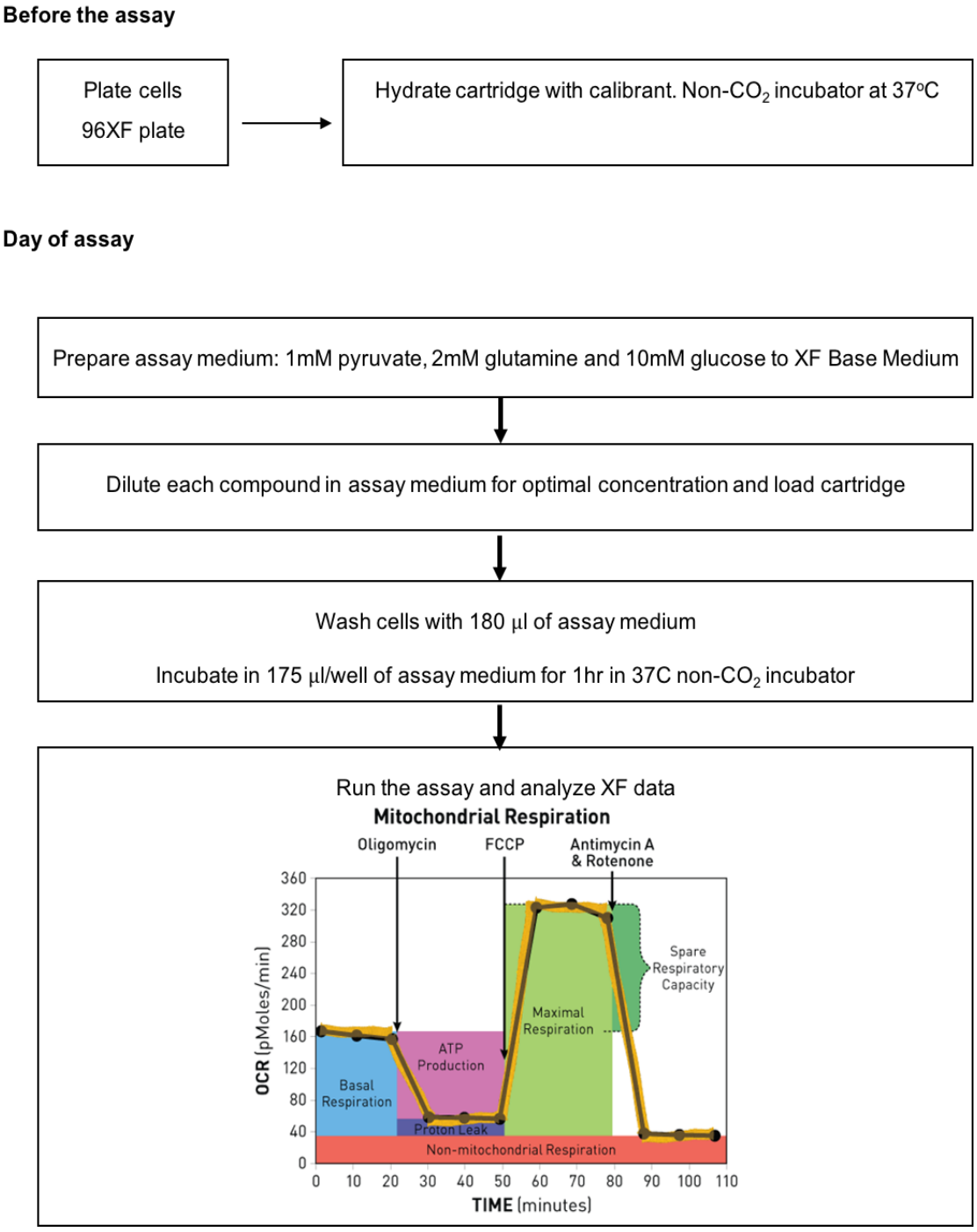

Compounds from the kit were prepared for loading sensor cartridge ports. The concentrations of the compounds were optimised for primary cell cultures.

Table 8 Preparation of compounds for Seahorse XF Agilent mitochondrial stress test

	Final well (μM)	Stock volume (μL)	Media volume (μL)	Add to port (μL)
Port A Oligomycin	2.0	600	2400	20
Port B FCCP	1.0	300	2700	22
Port C Rotenone/ Antimycin A	0.5	300	2700	25

The Wave software was used to run the Seahorse XF machine. The hydrated cartridge was inserted into the machine for calibration. After calibration, the cell culture microplate was inserted, and the reading was completed, generating the Seahorse XF Mito stress test report automatically. The test parameters were then exported from Wave data into Excel and Graphpad Prism.

2.2.18 Statistical analysis and graph representation

All data were checked for normal distribution using the Kolmogorov-Smirnov test (Graphpad Prism, v7). An appropriate statistical test was chosen for each data set. GraphPad Prism software was used for graph generation.

Chapter 3: Biochemical characterisation of Tau35 mice

3.1 Introduction

The tauopathies comprise a broad spectrum of neurodegenerative diseases. In some tauopathies, such as AD, the symptoms mainly manifest as cognitive decline, which progresses to dementia. Other tauopathies, for example PSP and CBD, present predominantly with motor deficits and at later stages often with cognitive decline (Neary et al., 1998; Lee et al., 2001; Goedert and Spillantini, 2011). The causes of tauopathies are not yet fully understood. However, it is likely that a combination of toxic gain-of-function, together with a loss of the normal function of tau protein may be responsible.

In addition, tau protein undergoes proteolysis and such generation of tau fragments might be toxic for the brain (Kolarova et al., 2012). Tau truncation is a pathological modification that can alter the subcellular localisation of tau and lead to the accumulation of truncated tau fragments that cause cellular dysfunction, cell death, neuronal loss and/or increased tau phosphorylation and aggregation in a variety of tauopathies (Wischik et al., 1988; Novák et al., 1993; Arai et al., 2004; Igaz et al., 2008; Quintanilla et al., 2009). However, the precise relationship between tau cleavage, tau phosphorylation, tau aggregation and neuronal loss in the tauopathies remains unknown.

Work from this laboratory showed that a C-terminal tau fragment of 35 kDa (Tau35) is present in PSP and CBD brain (Wray et al., 2008). Using antibody epitope scanning, Tau35 was found to contain four microtubule binding repeats and an intact C-terminus. In addition, Tau35 is phosphorylated at the majority of the sites found in

insoluble tau in AD brain (Hanger et al., 2007; Wray et al., 2008). To evaluate the pathological role of this truncated tau species, a new transgenic mouse line (Tau35 mice) expressing Tau35 under the control of the human tau promoter was generated (Bondulich et al., 2016). In contrast to the majority of tau transgenic mouse overexpression models, transgene expression in Tau35 mice is <10% of the total amount of tau and therefore any potential non-physiological functions of over-expressed tau are avoided (Bondulich et al., 2016). This makes Tau35 mice a good model of tauopathies such as CBD and PSP, which are characterised neuropathologically by the presence of NFT and glial tau pathology that consists primarily of aggregated 4R tau isoforms (Mahapatra et al., 2004).

Behavioural studies in Tau35 mice demonstrated that motor dysfunction was apparent from as early as four months of age, and this manifested before the cognitive deficit. Motor deficits in Tau35 mice included limb clasping, reduced hindlimb grip strength and reduced performance in rotarod testing (Bondulich et al., 2016). The Morris water maze was used to show that cognitive decline in Tau35 mice begins at approximately eight months and progresses with age. In addition, Tau35 mice demonstrated a significant decrease of approximately 10% in median life-span compared to WT mice, as demonstrated by a Kaplan-Meier survival curve (Bondulich et al., 2016). Neurophysiological examination of Tau35 mice identified af minor alteration in electrophysiological activity in dorsal hippocampal neurons of Tau35 mice (Tamagnini et al., 2017) that are thought to be linked to the pathological phenotype, such as GSK3β alterations and synaptic loss, described in (Bondulich et al., 2016). Therefore, the behavioural, biochemical, and neurophysiological studies of Tau35 mice strongly support the disease-relevance of this mouse model.

In this chapter, further biochemical analysis of changes in the central and peripheral nervous system in Tau35 mice is described to further understand the molecular mechanisms underlying the tauopathies and related disorders.

3.2 Results

3.2.1 Tau35 in the cortex of human PSP brain

The tau pattern was investigated on western blots in post-mortem premotor cortical tissue from the brains of two people diagnosed with PSP during life, and two age-matched controls. Brain tissue was homogenised and centrifuged at 100,000g as described in Chapter 2, Section 2.2.1. The 100,000g pellet containing insoluble protein, was assessed on western blots probed with an antibody against the C-terminus of human tau, TP70 (Fig. 3.1). The blot revealed a 35 kDa tau fragment in the insoluble fraction of PSP cortical brain tissue that was absent from control brain. Thus, these results confirm the earlier reported findings from this laboratory of the insoluble Tau35 tau species in PSP brain.

Fig. 3.1 Tau35 is detectable in cortical tissue of human PSP brain

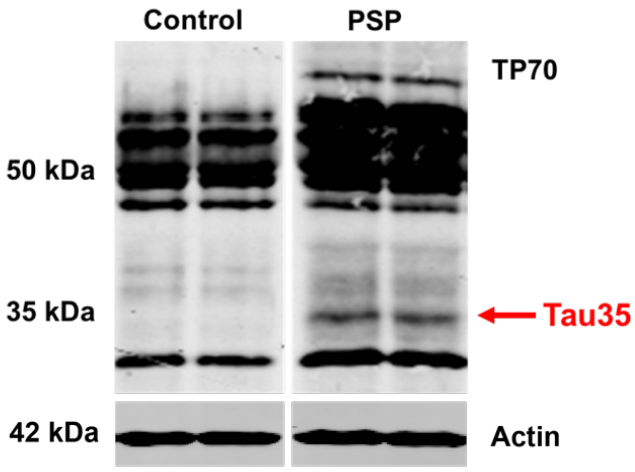

Western blots of human post-mortem premotor cortex 100,000g pellet of controls and PSP brains probed with an antibody against the C-terminus of human tau (TP70). The blot demonstrates the presence of a 35 kDa tau fragment in the PSP pellets. β-actin is shown as loading control. The blots show 2 representative samples for each condition. Molecular weights (kDa) are indicated on the left.

3.2.2 Identification of the HA-tagged Tau35 species in Tau35 mice

Tau35 mice were generated by targeted insertion of the Tau35 fragment into the *Hprt* locus on the X chromosome. In addition, the Tau35 fragment was fused at its C-terminus to a hemagglutinin (HA) tag to distinguish Tau35 from endogenous tau. It is possible that the location of Tau35 on the X chromosome could lead to different expression levels of Tau35, depending on the mouse gender and the degree of silencing of the X chromosome in female mice.

Therefore, Tau35 immunoreactivity in male and female transgenic mice was investigated on western blots probed with antibody against HA. Half brains from male hemizygous (Hemi), female homozygous (Hom), female heterozygous (Het), and female and male WT mice aged one month, were homogenised and probed on blots with HA antibody, including β-actin as a loading control. Fig. 3.2 shows differences in Tau35 expression in male and female transgenic mice, as judged by HA immunoreactivity. Quantitation of the HA signal on blots, relative to β-actin, showed that male (Hemi) mice demonstrate an approximate two-fold increase in Tau35 expression, compared to female (Hom) and female (Het) mice ($P<0.05$ and $P<0.01$, respectively, one-way ANOVA). There was no significant difference in Tau35 protein expression in female (Hom) and female (Het) mice. As expected, no HA signal was detected in the female or male WT mouse brains since HA is generated solely from transgene expression.

Fig. 3.2 Tau35 protein expression in male and female Tau35 transgenic mice

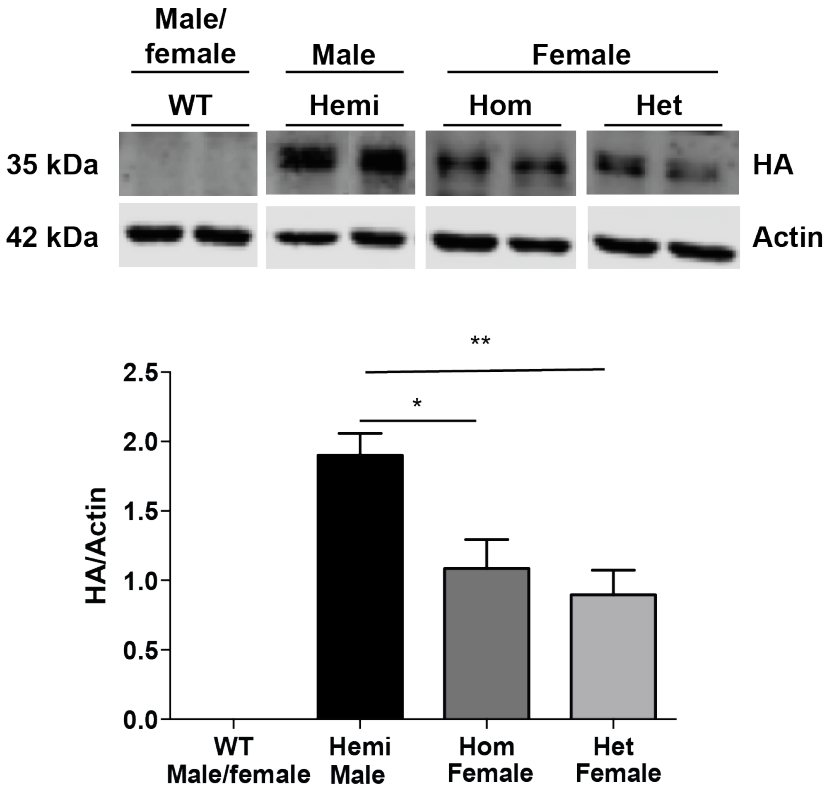

Western blot of brain homogenates from male hemizygous (Hemi), female homozygous (Hom), female heterozygous (Het), and WT (male and female) mice aged one month were probed with HA and β-actin antibodies. The blots show 2 representative samples for each condition. Molecular weights (kDa) indicated on the left correspond to the weight of the proteins of interest. The graph shows the amount of HA relative to β-actin, expressed as mean ± S.E.M., n=4-6 (*P<0.05, **P<0.01, one-way ANOVA).

To investigate the regional expression of Tau35 in mouse brain, tissue from Tau35 male mice (18 months) and WT mice, was crudely dissected into four brain regions: hippocampus and associated cortex; frontal brain; amygdala; and brainstem and cerebellum. Brain tissue was homogenised and probed on western blots with antibodies against HA and β-actin (Fig. 3.3). Quantitation of the blots revealed that the hippocampus and associated cortex expressed significantly more Tau35, relative to β-actin ($P<0.05$), than frontal brain or amygdala (Fig. 3.3). The standardised Tau35 expression in the hippocampus is significantly higher than in frontal brain ($P<0.05$, one-way ANOVA) and amygdala ($P<0.05$, one-way ANOVA). Tau35 in the brainstem and cerebellum was similar to that determined in the hippocampus and cortex ($P>0.05$, one-way ANOVA), and increased relative to the amount in frontal brain ($P<0.05$, one-way ANOVA), although it was not significantly different from the amygdala ($P>0.05$, one-way ANOVA). In addition, levels of endogenous tau are not significantly different between the brain regions ($P>0.05$, ANOVA).

Fig. 3.3 Tau35 protein expression differs across mouse brain regions

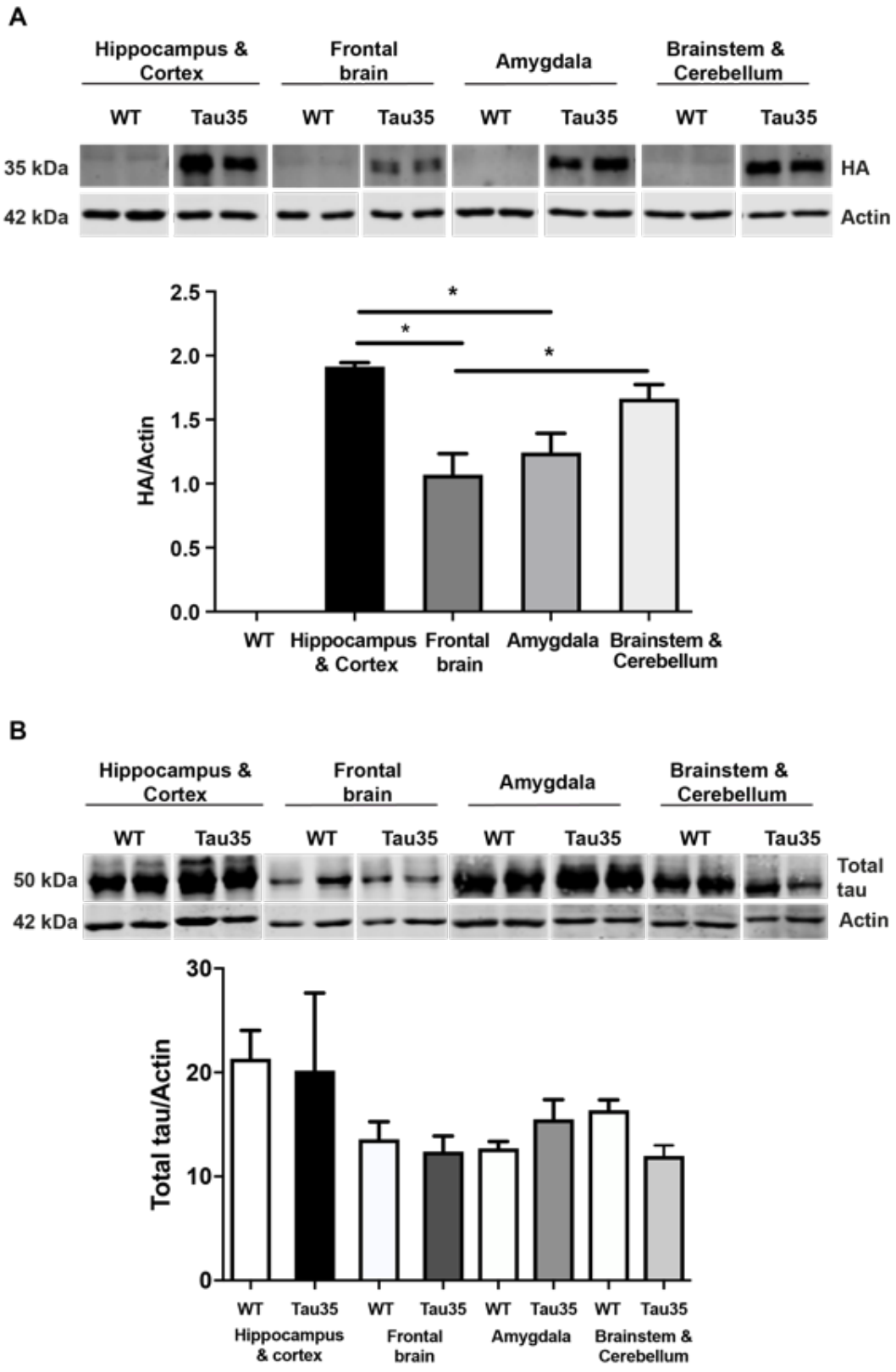

Fig. 3.3 legend

Homogenates of hippocampus and associated cortex, frontal brain, amygdala and associated cortex, and brainstem and cerebellum from WT and Tau35 mice (18 months). Blots are probed with **A** antibodies recognising HA and β-actin and **B** Total tau (K9JA) and β-actin. The blots show 2 representative samples for each condition. Molecular weights (kDa) are indicated on the left. The amount of HA was quantified relative to β-actin and expressed as the mean ± S.E.M., n =3. *P<0.05, one-way ANOVA.

3.2.3 Increased phosphorylation of endogenous tau in the hippocampus and associated cortex of Tau35 mice

To investigate phosphorylation of endogenous tau in Tau35 and WT mice, brain homogenates from mice aged 14 months were investigated on western blots. The phosphorylated serine 422 (pS422) tau epitope has been proposed as a marker of neurofibrillary degeneration and is recognised as a relatively early marker of pre-tangle tau pathology (Guillozet-Bongaarts et al., 2006), such as that observed in Tau35 mice (Bondulich et al., 2016). The amount of pS422, relative to total tau (Tau5 antibody) in Tau35 mouse hippocampus and associated cortex (0.62 ± 0.07, mean ± S.E.M., n=6) demonstrates a 37% (P<0.05, Student's t-test) increase compared to that of WT mice (0.39 ± 0.05, mean ± S.E.M., n=6) (Fig. 3.4A). In contrast to the pS422 tau antibody, the Tau1 antibody recognises tau when it is dephosphorylated at serines 195, 198, 199, and 202. Western blots of the hippocampus and associated cortex probed with Tau1 (Fig. 3.4B) showed a significant reduction of 23% (P<0.05, Student's t-test) in the immunoreactivity of Tau1, relative to total tau (K9JA antibody) in Tau35 mice (0.48 ± 0.03, mean ± S.E.M., n=6) compared to WT mice (0.62 ± 0.04,

mean ± S.E.M., n=6). These results show that expression of Tau35 induces increased phosphorylation of endogenous (WT) mouse tau at both the pS422 tau and Tau1 epitopes in Tau35 mice, indicating elevated phosphorylation at multiple residues, including 195, 198, 199, 202 and 422 on tau.

Fig. 3.4 Increased phosphorylation of endogenous tau in Tau35 mice

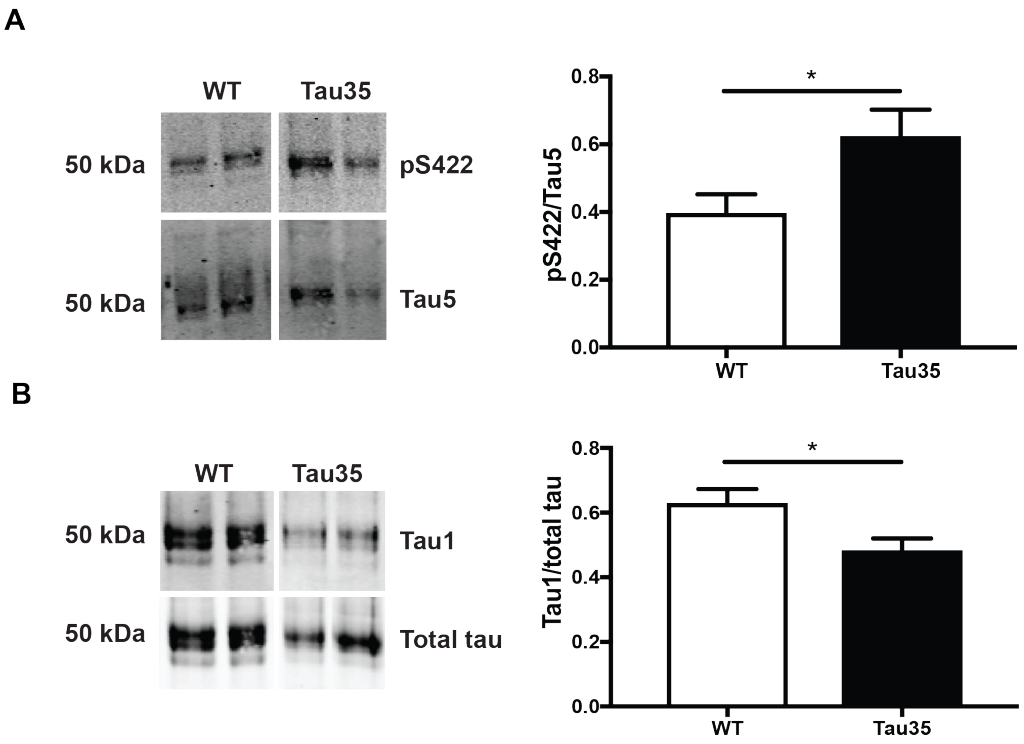

Western blot of 14 months old Tau35 and WT mouse hippocampus and associated cortex probed with antibodies recognising **A** pS422 phosphorylated tau and total tau (Tau5) or **B** Tau1, which recognises a dephosphorylated epitope on tau and total tau (K9JA). The blots show 2 representative samples for each condition. Molecular weights (kDa) are indicated on the left of the blots. Tau phosphorylation was quantified relative to total tau and expressed as mean ± SEM, n=6, *P<0.05, Student's t-test.

3.2.4 Increased insoluble endogenous tau in the hippocampus and associated cortex of Tau35 mice

To investigate pathological tau aggregation in the hippocampus and associated cortex of Tau35 and WT mice aged 14 months, differential centrifugation was used to pellet insoluble tau. Brain homogenates were centrifuged as described in Chapter 2, Section 2.2.3 to generate 100,000g supernatants and pellets, 13,000g pellets and brain homogenates, all of which were assessed on western blots probed with antibodies to total tau (K9JA) and β-actin (Fig. 3.5A). Fig. 3.5B demonstrates the quantitative analysis of the western blots probed with tau, standardised to β-actin. The blots show that different tau species are present in each of the fractions analysed. There was a tau doublet of ~50 kDa visible in the WT 13,000g pellet but in the Tau35 mice, there were multiple tau species, including an additional ladder of higher molecular weight bands of ~75 kDa. Quantification of the amount of tau in the 13,000g pellet revealed a significant two-fold increase in tau, relative to β-actin, in this fraction of Tau35 mouse brain (6.8 ± 1, mean ± S.E.M, n=6) compared to the same fraction from WT mouse brain (3.3 ± 0.33, mean ± S.E.M., n=6). However, the amount of tau in the 100,000g pellet in Tau35 mouse brain (1.66 ± 0.17, mean ± S.E.M., n=6) was similar to WT mice (1.29 ± 0.16, mean ± S.E.M., n=4), as shown in Fig. 3.5D ($P>0.05$, Student's t-test). No significant changes ($P>0.05$, Student's t-test) were detected in the amount of tau present in the 100,000g supernatant of Tau35 (1.68 ± 0.17, mean ± S.E.M., n=6) or WT mice (2.01 ± 0.47, mean ± S.E.M., n=6) (Fig. 3.5E). There was also no difference in the overall amount of tau in the total brain homogenate from WT (5.73 ± 0.35, mean ± S.E.M., n=5) or Tau35 (6.01 ± 0.35, mean ± S.E.M., n=5) mice, confirming that there is no overrepresentation of tau in Tau35 mice (Fig. 3.5 B). Taken together, these findings suggest the presence of highly aggregated tau species in Tau35 brain that were separated by centrifugation at 13,000g, without any significant change in overall tau expression.

Fig. 3.5 Increased amount of endogenous tau in hippocampus and associated cortex in the 13,000g pellet from Tau35 mouse brain

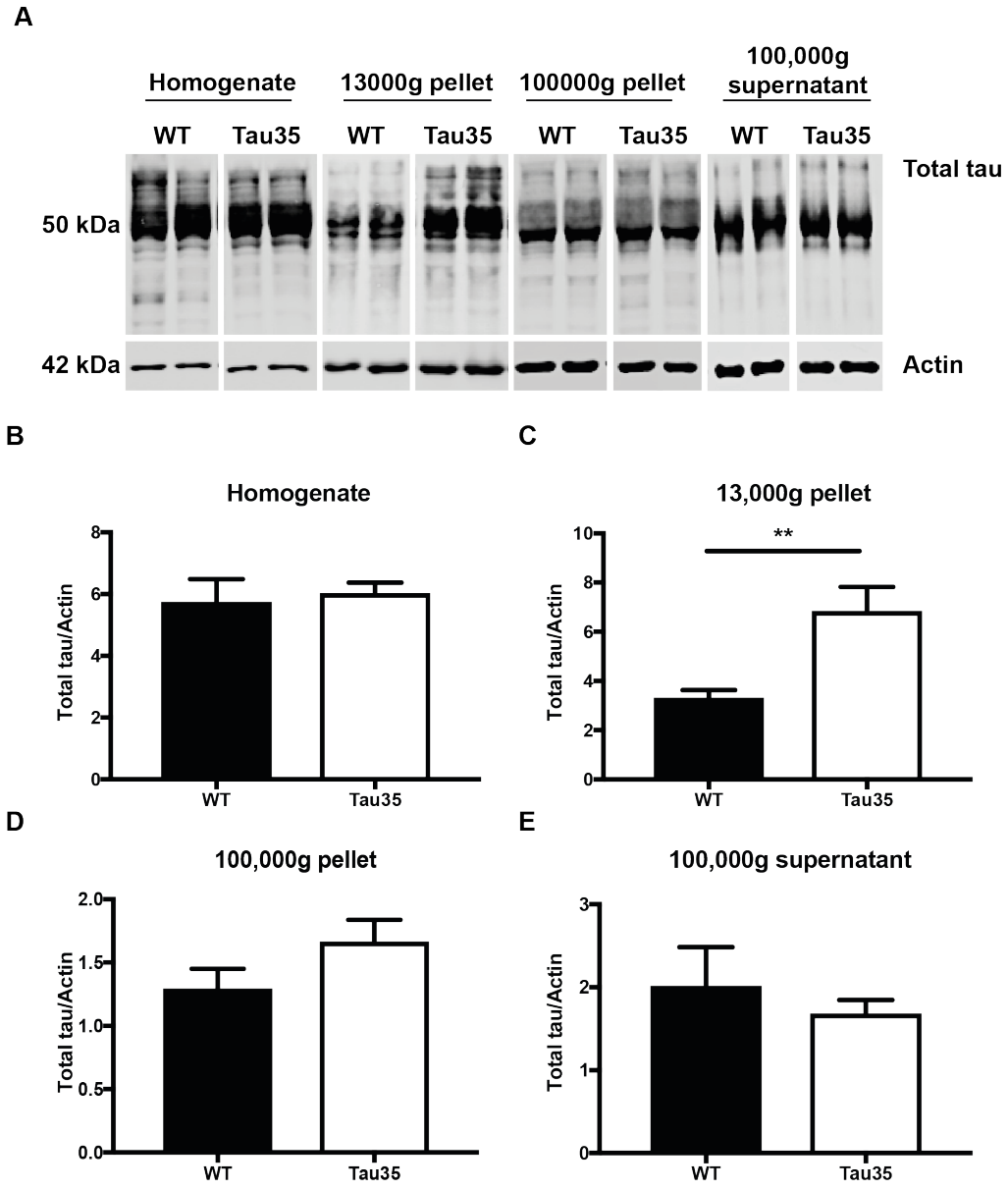

A. Western blots of WT and Tau35 hippocampus and associated cortex (14 months) following differential centrifugation and probing with antibodies to total tau and β-actin. Molecular weight markers (kDa) of proteins of interest are shown on the left. **B-E.** Bar charts show quantitative analysis of total tau normalised to β-actin in **B** brain homogenates, **C** 13,000g pellets, **D** 100,000g pellets, and **E** 100,000g supernatants. The amount of tau on blots was quantified relative to β-actin and expressed as mean ± SEM, n=6, **P<0.01, Student's t-test.

3.2.5 Mitochondrial deficit in the hippocampus and cortex of Tau35 mice

Extensive evidence from animal and clinical studies suggests that mitochondrial abnormalities are involved in age-related neurodegenerative diseases such as AD and PD (DiMauro and Schon, 2008; Reddy, 2009). To investigate the integrity of mitochondria in aged Tau35 mice, homogenates of the four brain regions indicated above, from WT and Tau35 male mice (aged 18 months) were analysed on western blots. The blots were probed with an antibody against a mitochondrial marker (HSP60), which is located on the inner membrane of mitochondria, and with an antibody to β-actin (Fig. 3.6A). This investigation revealed a significant mitochondrial deficit as the HSP60/actin ratio was reduced by 23% ($p<0.01$, Student's t-test) in Tau35 mice in the hippocampus and associated cortex (0.96 ± 0.04, mean ± S.E.M., n=3) compared to WT mice (1.24 ± 0.03, mean ± S.E.M., n=3). Frontal brain demonstrates a 33% reduction in HSP60 in Tau35 mice (0.74 ± 0.08, mean ± S.E.M., n=3)., compared to WT mice (1.11 ± 0.11, mean ± S.E.M., n=3) which was a strong trend but not statistically significant ($P>0.05$, Student's t-test). In addition, the brainstem and cerebellum show a slight tendency towards a mitochondrial deficit however, this was not significant ($P>0.05$, Student's t-test) in Tau35 (0.86 ± 0.02, mean ± S.E.M., n=3) mice compared to WT mice (0.81 ± 0.006, mean ± S.E.M., n=3). There was also no apparent deficit in mitochondria in the amygdala in Tau35 mice (0.56 ± 0.02, mean ± S.E.M., n=3) mice compared to WT mice (0.55 ± 0.05, mean ± S.E.M., n=3). However, the blots probed with TOM20 did not show significant difference between WT and Tau35 brain regions ($P>0.05$, Student's t-test). Overall, these results indicate brain regional variation in the effects of Tau35 expression on mitochondria in transgenic mice.

Fig. 3.6 Mitochondrial deficit in Tau35 hippocampus and cortex

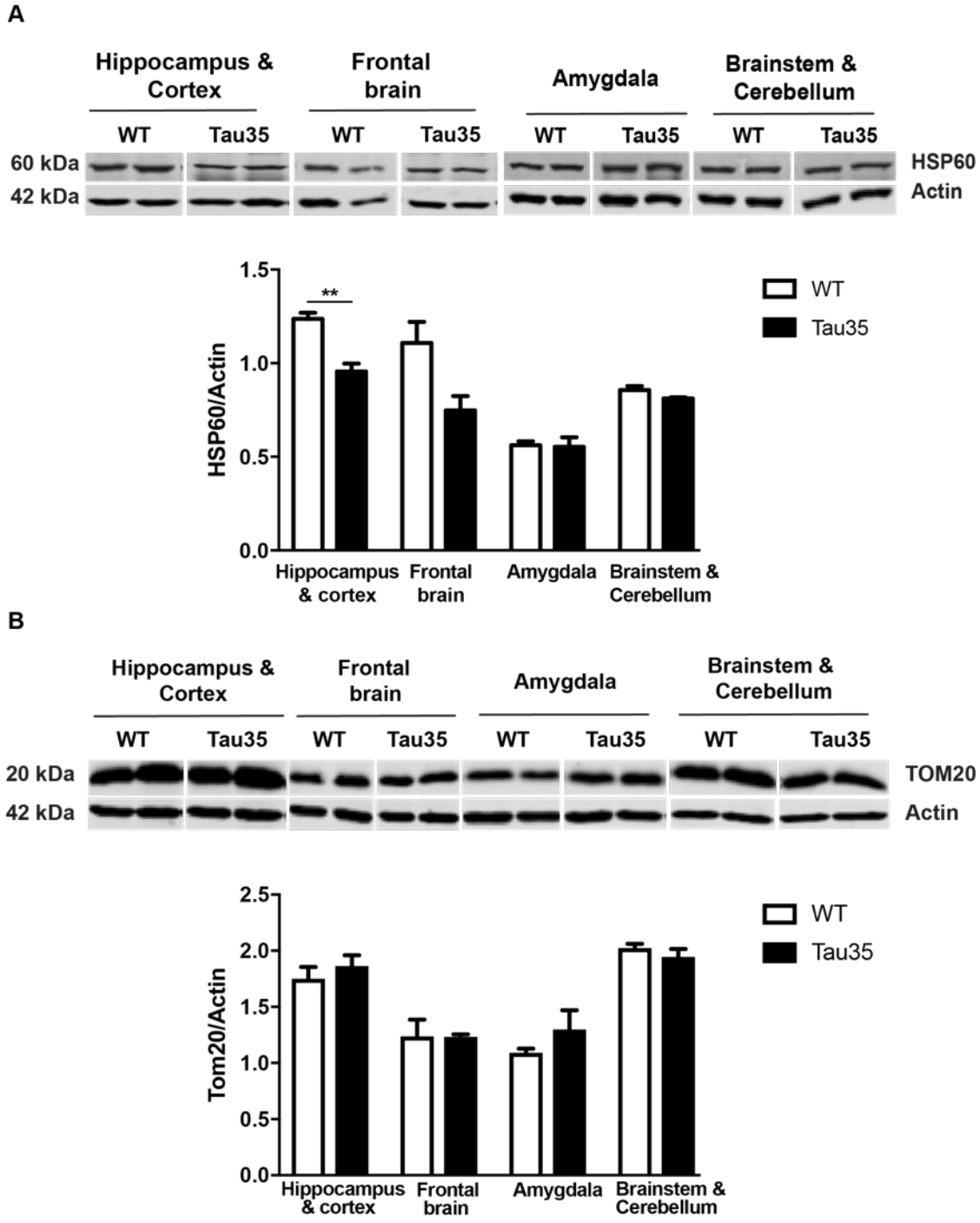

Fig. 3.6 legend

Western blots of homogenates of hippocampal and associated cortex, frontal brain, amygdala and associated cortex, and brainstem and cerebellum from 18-month-old wild-type (WT) and Tau35 mice (n=6). **A** Blots were probed with antibodies recognising the mitochondrial marker HSP60 and β-actin. **B** Blots were probed with antibodies recognising the mitochondrial marker TOM20 and β-actin. Molecular weights (kDa) are indicated on the left. HSP60 was quantified relative to β-actin and expressed as mean ± S.E.M., n=3, **P<0.01, Student's t-test.

3.2.6 Astrocytic activation in aged Tau35 mouse brain

Astrocytic activation is a common hallmark of tauopathies (reviewed in (Leyns and Holtzman, 2017). To investigate whether astrocyte activation is a feature of Tau35 mice, coronal sections of the cortical region of brains from mice aged 18 months (three brains of each genotype), were co-stained using antibodies recognising glial fibrillary acidic protein (GFAP), a marker of astrogliosis, and neuronal nuclei (NeuN) (Fig. 3.7). Notably, a marked increase in GFAP labelling is evident in Tau35 mice compared to WT mice (Fig. 3.7, left panels), particularly in areas with decreased NeuN staining (Fig. 3.7, centre and right panels). These results indicate an increase in gliosis in Tau35 mice, particularly in brain regions in which there may be some neuronal loss.

Fig. 3.7 Astrocytic activation in the cortex of Tau35 mouse models

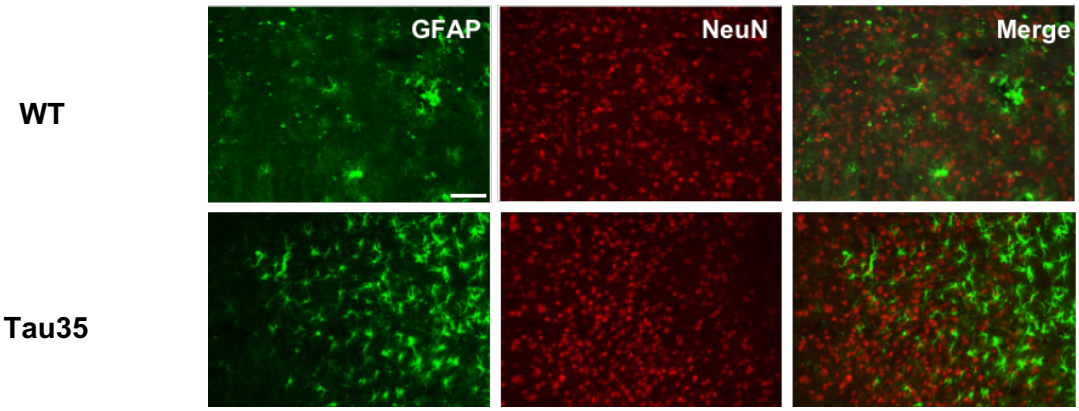

Coronal cortical brain sections from WT and Tau35 mice aged 18 months stained with antibodies recognising glial fibrillary acidic protein (GFAP, green, left panels) and neuronal nuclei (NeuN, red, centre panels). The merged images are shown on the right. Scale bar = 100 μm.

To determine the degree of reactive astrogliosis and to detect any possible changes in other brain regions of Tau35 mice, astrocytic activation was analysed by performing western blots on brain homogenates from Tau35 and WT mice aged 18 months. Brain regions assessed included the hippocampus and associated cortex, the frontal region, the amygdala and associated cortex, and the brainstem and cerebellum (Fig. 3.8A-D, respectively). Blots were probed with antibodies against GFAP, to determine astrocyte activation, aldehyde dehydrogenase 1 family, member L1 (aldh1L1) as a general astrocyte marker (Yang et al., 2012), and β-actin as a loading control. Bands on these blots were detected at the expected sizes of 50 kDa, 100 kDa, and 43 kDa, for GFAP, aldh1L1, and β-actin, respectively (Fig. 3.8).

Fig. 3.8E shows that GFAP expression, normalised to β-actin, was significantly increased in all brain regions of Tau35 mice. There was a 40% increase in GFAP in hippocampus and associated cortex ($P<0.01$, Student's t-test), a 25% increase in the frontal region ($P<0.001$, Student's t-test), a 50% increase in the amygdala and associated cortex ($P<0.01$, Student's t-test), and a 40% increase in brainstem and cerebellum ($P<0.01$, Student's t-test). In contrast, there were no significant differences in expression of aldh1L1, relative to β-actin, in any of the brain regions analysed ($P>0.05$, Student's t-test). These findings thus provide evidence of astrocytic activation in Tau35 aged 18 months, which is not due to an increase in the number of astrocytes in these animals.

Fig. 3.8 Astrocytic activation in Tau35 mouse brain

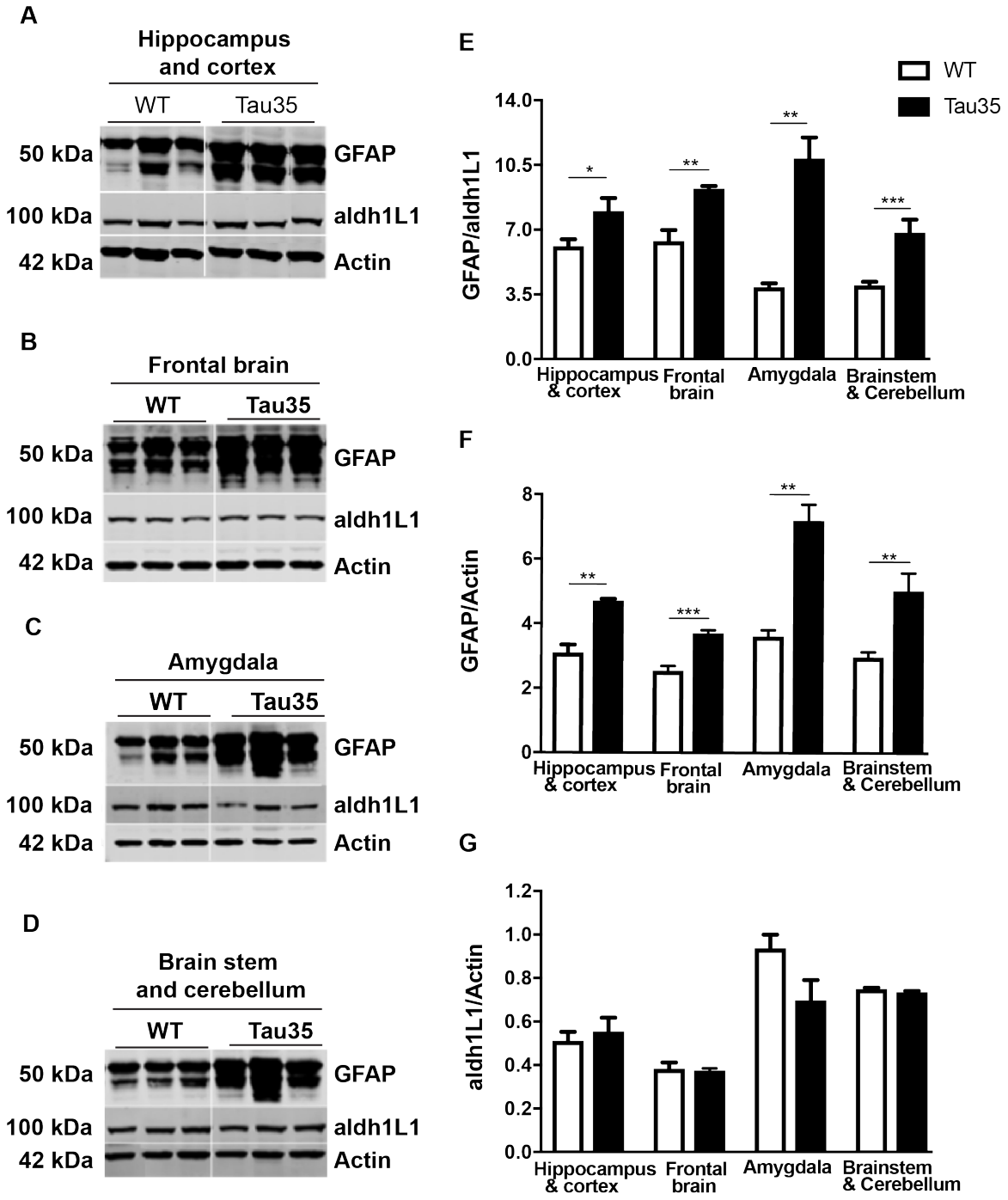

Fig. 3.8 legend

Western blots of homogenates of **A** hippocampal and associated cortex, **B** frontal region, **C** amygdala and associated cortex, and **D** brainstem and cerebellum, from wild-type (WT) and Tau35 mice, aged 18 months. Blots were probed with antibodies recognising glial fibrillary acidic protein (GFAP), aldehyde dehydrogenase 1 family, member L1 (aldh1L1), and β-actin. Molecular weights (kDa) are indicated on the left. Graphs show the amounts of **E** GFAP relative to aldh1L1, and **F** aldh1L1, and **G** GFAP, relative to β-actin. All values are expressed as mean ± S.E.M., n=3-7 *P<0.05, **P<0.01, ***P<0.001, Student's t-test.

3.2.7 Altered autophagy in Tau35 mice

Alterations in lysosomal-mediated degradation and autophagy are features of several human tauopathies (Piras et al., 2016). Therefore, lysosomal degradation in Tau35 mouse hippocampus and associated cortex (18 months) was determined by measuring the amount of microtubule-associated protein 1-light chain 3 (LC3) present. During autophagy, cytosolic LC3-I is conjugated to phosphatidylethanolamine to form LC3-II, which is recruited to the autophagosomal membrane. Lysosomal turnover of LC3-II reflects starvation-induced autophagic activity, and measuring the amount of LC3-II, relative to β-actin, on western blots is considered to be a reliable method for monitoring autophagy (Tanida et al., 2008). In these experiments (Fig. 3.9), LC3-I, relative to β-actin, was found to be significantly decreased (P<0.05, Student's t-test) in the hippocampus of Tau35 mice (2.11 ± 0.11, mean ± S.E.M., n=5) aged 18 months, compared to age-matched WT mice (2.42 ± 0.07, mean ± S.E.M., n=5). However, LC3-II, relative to β-actin, was significantly increased (P<0.05, Student's t-test) in Tau35 mice (1.51 ± 0.10, mean ± S.E.M., n=5)

compared to WT mice (1.21 ± 0.06, mean ± S.E.M., n=5) (Fig. 3.9). These results suggest an increase in number of autophagosomes in the hippocampus and associated cortex of Tau35 mice that could potentially occur either through upregulation of autophagosomal formation or blockage of autophagic degradation (Mizushima and Yoshimori, 2007).

Fig. 3.9 Altered autophagy in the hippocampus and associated cortex of Tau35 mice

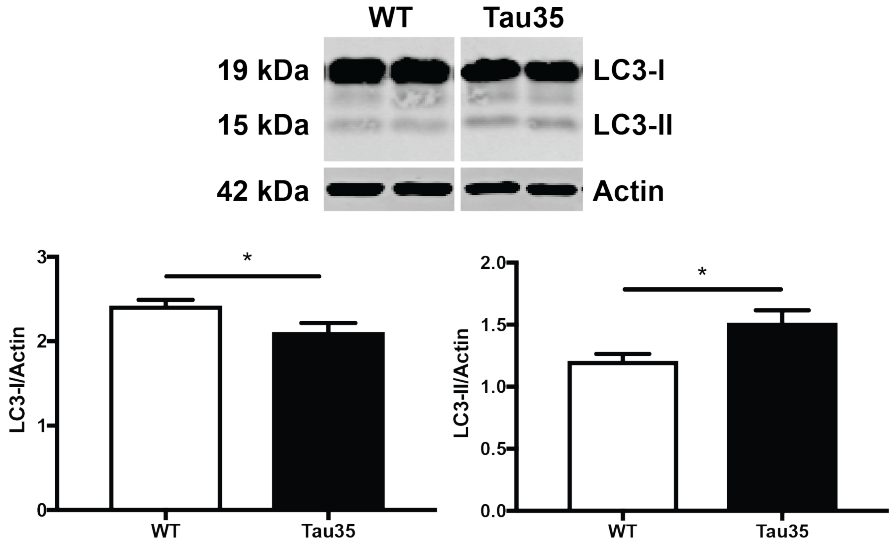

Western blots of hippocampal and associated cortex of WT and Tau35 mice (18 months) probed with an antibody recognising LC3. Molecular weights (kDa) indicated on the left correspond to the weight of the proteins of interest. Graphs show the ratios of LC3-I and LC3-II to β-actin, expressed as mean ± S.E.M., n=5, *P<0.05, Student's t-test.

3.2.8 Progressive deformation of acetylcholine receptors coupled with partial denervation of the neuromuscular junction in Tau35 mice

Tau35 mice show progressive motor dysfunction during behavioural testing such as on the accelerating rotarod, limb clasping, and hindlimb grip strength (Bondulich et al., 2016). To investigate the potential causes of these motor deficits, the neuromuscular junctions (NMJs) in Tau35 mice were investigated. The distal hindlimb lumbricals muscles, involved in the activities required by mice during the behavioural studies indicated above, were dissected from Tau35 and WT mice aged 3 and 13 months and stained as described in Chapter 2, Section 2.2.16. The muscle was immunostained with antibodies against synaptic vesicle glycoprotein 2A (SV2), neurofilament medium polypeptide (NF-M, 2H3), which together label the motor neuron of NMJ, and with α-bungarotoxin (BTX), which labels acetylcholine receptors in the muscle fibre in the NMJ (Fig. 3.10). Notably, neurofilament organisation in Tau35 lumbrical muscle from mice aged 3 months was significantly affected by Tau35 expression and demonstrated a less organised structure compared to the tight bundles of neurofilaments evident in the muscle from WT mice of the same age.

Fig. 3.10 Altered neurofilament organisation in the neuromuscular junction of Tau35 mice

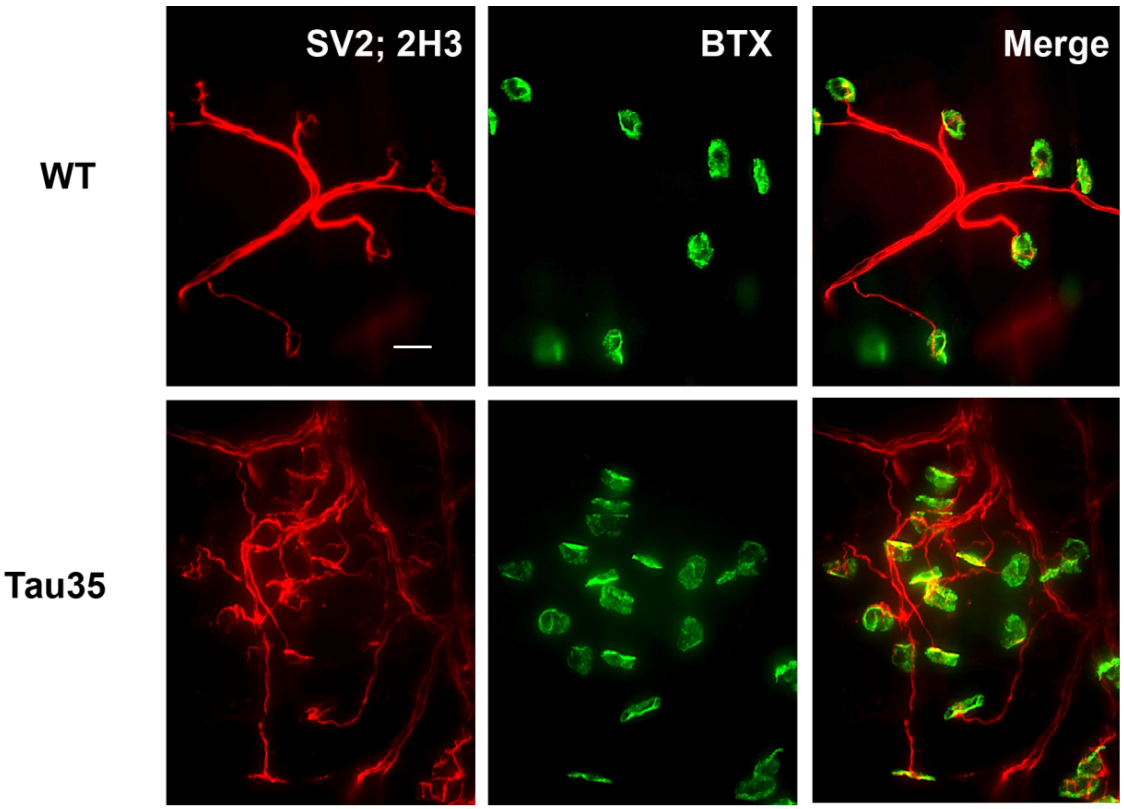

Immunofluorescence of distal hindlimb lumbrical muscle from WT and Tau35 mice aged 3 months. Sections were immunostained with antibodies recognising synaptic vesicles (SV2, red), neurofilament (2H3, red) and α-bungarotoxin (BTX, green). The merged images are shown on the right. Scale bar = 100 μm.

To investigate the abnormalities detected at the NMJ in Tau35 mice (Fig. 3.11), the physical characteristics of NMJs, including their size, shape and degree of innervation, were determined. The size analysis of NMJs from mice aged 3 months demonstrated that the area of Tau35 endplates, assessed as the amount of BTX staining corresponding to acetylcholine receptors, was approximately 700μm^2 (Fig. 3.11A) and this is not altered in Tau35 mice compared to WT mice at 3 months of age. Shape factor describes the shape of the particle, in this case, BTX staining surface, independent of its size, where the value ranges from 0 to 1. The shape factor of NMJs in Tau35 mice (0.67 ± 0.02, mean ± S.E.M., n=21) is significantly reduced by 8% ($P<0.05$, Student's t-test) compared to WT mice (0.73 ± 0.01, mean ± S.E.M., n=22). These results indicate reduced circularity in Tau35 mouse NMJs and potentially suggests that there is a loss of acetylcholine receptors (AChR) and therefore, early signs of AChR instability in Tau35 mice. Innervation of NMJs was determined from scoring their attachment to both neurofilament (2H3) and SV2. SV2 and neurofilament staining can be distinguished morphologically because SV2 staining overlaps with BTX staining, outlining the nerve synaptic site of the NMJ, whereas the thread-like structures of neurofilaments connect to synaptic vesicles labelled by SV2. Partially denervated NMJs are scored as those remaining attached to neurofilament but lacking SV2 staining, indicating a loss of connection between nerve and muscle. Fully denervated NMJs were scored as those that were negative for both neurofilament and SV2. Using this scoring methodology, approximately 38% of NMJs from Tau35 mice aged 3 months were partially denervated, compared to approximately 26% of NMJs in WT mice. However, despite a mean increase of 30% in partially denervated NMJs in the Tau35 mice, this difference was not statistically significant from WT mice, most likely due to the high degree of variation and low number of samples of each genotype (Fig. 3.11C).

Fig. 3.11 Early signs of acetylcholine receptor instability in the neuromuscular junction of young Tau35 mice

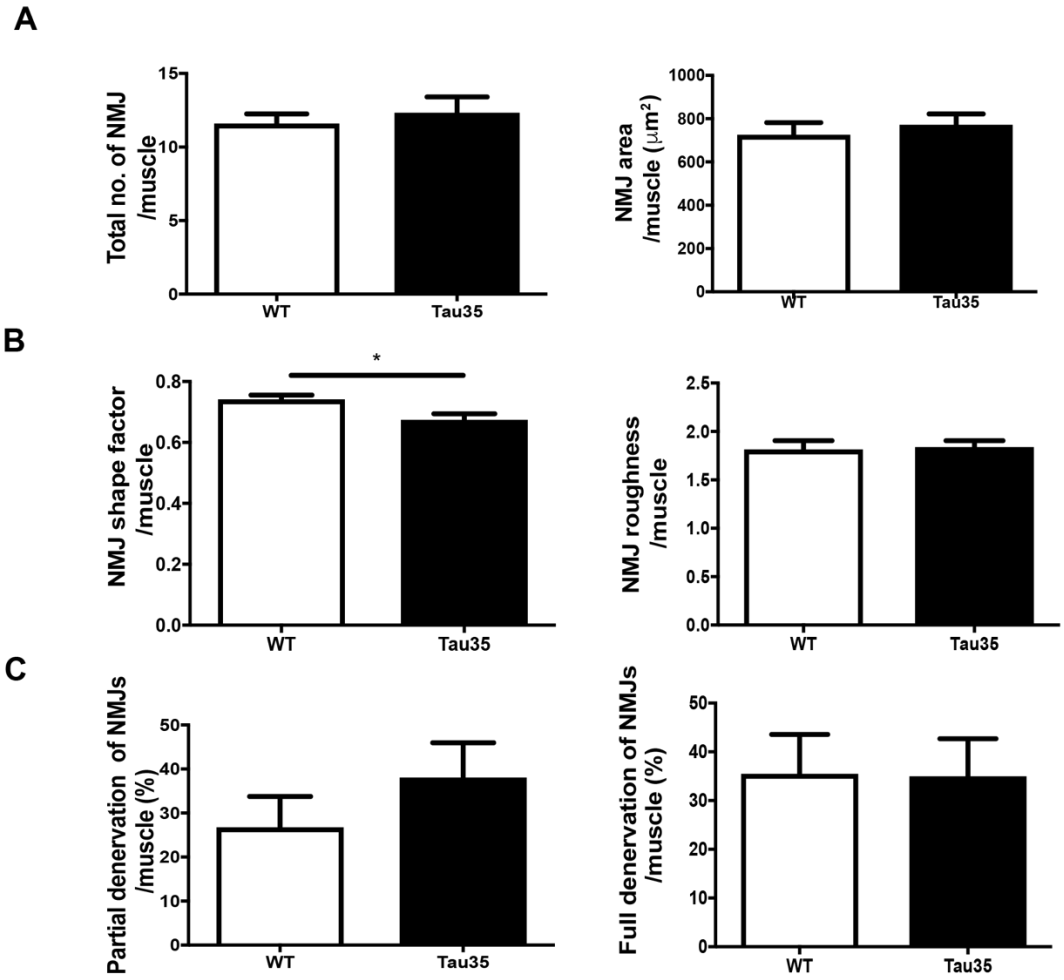

Graphs showing the quantitative analysis of NMJs in the distal hindlimb lumbrical muscle of WT and Tau35 mice aged 3 months. **A** Number and area of NMJs **B** Shape and roughness of NMJs **C** Partial and full denervation of NMJs. Values are show as mean ± S.E.M., n = 3 (*P<0.05, Student t-test).

It is known that in advanced age muscle loses efficiency. Therefore, to study the effects of Tau35 expression on muscle during aging in the transgenic mice, NMJs from mice aged 13 months were investigated. Distal hindlimb lumbrical muscle of WT and Tau35 mice aged 13 months was stained and assessed for the size, shape and degree of innervation at the NMJ (Fig. 3.12). Firstly, the number of NMJs per muscle is not significantly different in Tau35 muscle compered to WT muscle ($p>0.05$, Student's t-test). However, at this age, neurofilament staining in the lumbrical muscle of both WT and Tau35 mice was much weaker and more fragmented than in animals aged 3 months, suggesting the possibility of loss of functional connections between nerve and muscle at the NMJ with age (Fig. 3.12A). It is evident that the surface area of the endplates, determined from BTX staining of the acetylcholine receptors, is significantly decreased by 20% ($P<0.01$, Student's t-test) in the muscle of Tau35 mice (760 ± 25, mean $\pm$ S.E.M., n=11) compared to that of WT mice aged 13 months (950 ± 55, mean $\pm$ S.E.M., n=10). In addition, the shape of Tau35 endplates is altered and this increased roughness is likely due to degeneration of the acetylcholine receptors in Tau35 muscle. There is also a significant increase ($P<0.05$, Student's t-test) in the percentage of partially denervated endplates in Tau35 mouse NMJs (15.5 ± 2.85, mean $\pm$ S.E.M., n=9) compared to WT (7 ± 2.15, mean $\pm$ S.E.M., n=9). However, the percentage of fully denervated endplates was equivalent in Tau35 and WT muscle ($P>0.05$, Studen't t-test). It is also worth noting the swelling of the neurofilament in Tau35 muscle (Fig. 3.12, white arrow) such enlargements have previously been shown to be a precursor to neurofilament degeneration in disease including amyotrophic lateral sclerosis (ALS), Charcot-Marie-Tooth disease (CMT), and spinal muscular atrophy (SMA) (Sleigh et al., 2014).

Fig. 3.12 Progressive deformation of acetylcholine receptors coupled with partial denervation of the neuromuscular junction in lumbrical muscle of aged Tau35 mice

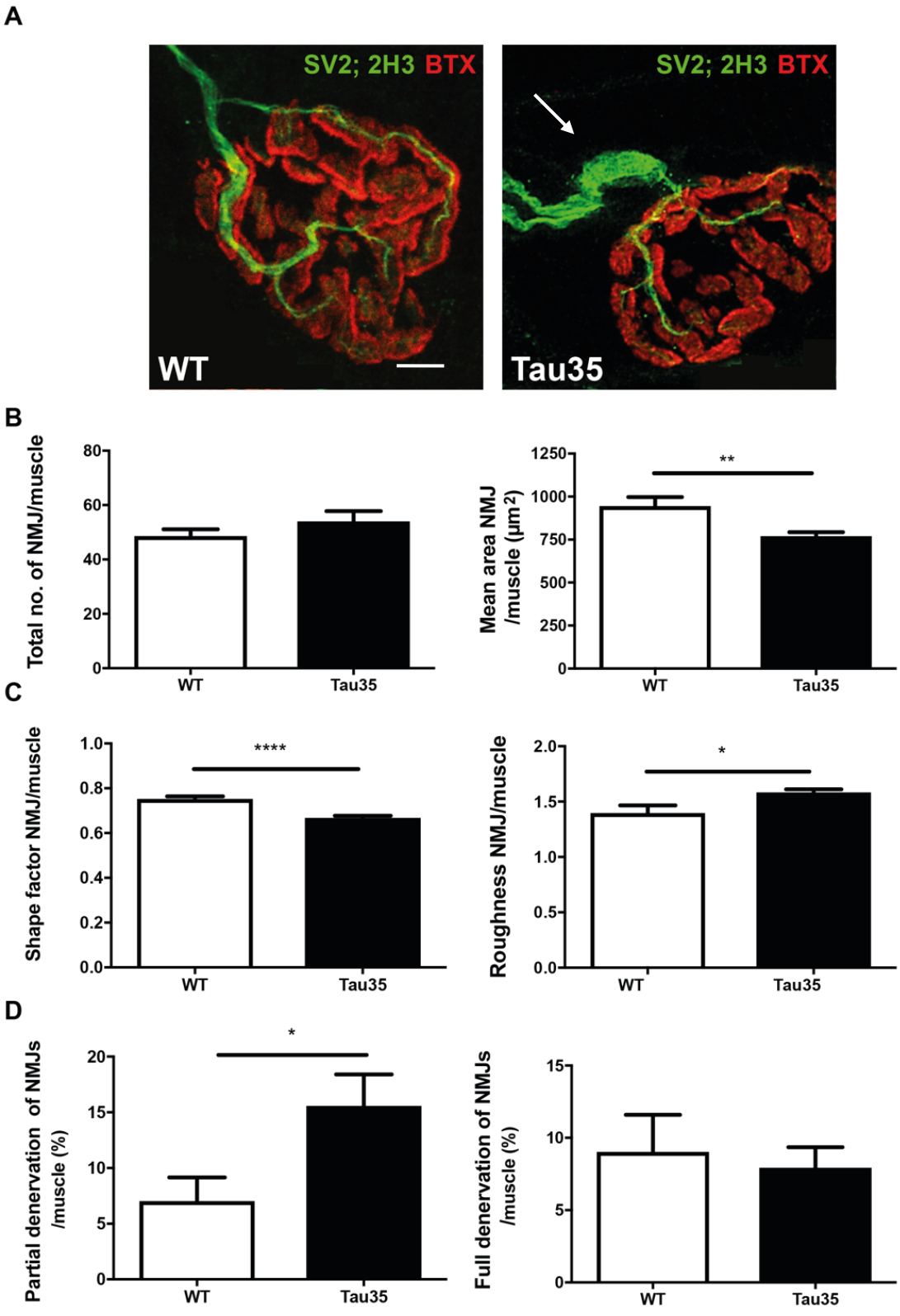

Fig. 3.12 legend

Analysis neuromuscular junctions (NMJs) in distal hindlimb lumbrical muscle from WT and Tau35 mice aged 13 months. **A** NMJs in distal hindlimb lumbrical muscle of WT and Tau35 mice. Sections were immunostained with antibodies recognising synaptic vesicles (SV2), neurofilament (NF-M,2H3) and α-bungarotoxin (BTX). White arrow indicates thickened neurofilament in Tau35 muscle. Scale bar = 10 μm. Bar charts show **B** Number of NMJs per muscle and mean NMJ area (μm^2). **C** Shape and roughness of acetylcholine receptors area. **D** Partial and full denervation in WT and Tau35 NMJs. Values are show as mean $\pm$ S.E.M., n = 4 (*P<0.05, **P<0.01, ****P<0.0001, Student's t-test).

3.2.9 Mitochondria in Tau35 muscle tissue

Since Tau35 expression has a significant detrimental effect at the NMJ, particularly in older mice, and defects in the quadriceps muscle of Tau35 mice have been reported in animals aged 8 and 16 months (Bondulich et al., 2016), the status of mitochondria in muscle from Tau35 mice was investigated. To do this, the amounts of the mitochondrial proteins, TOM20 and superoxide dismutase (SOD) 1, were assessed, relative to GAPDH, on western blots of quadriceps muscle of WT and Tau35 mice aged 8 months. Tau35 mice showed no significant differences in the amounts of TOM20 or SOD1 in the quadriceps muscle compared to WT mice at this age. The amount of TOM20 in Tau35 muscle appeared to be slightly, but not significantly reduced (P>0.05, Student's t-test), possibly due to the amount of variance in the data obtained from the WT mice (Fig. 3.13A). Similar results were obtained with SOD1 (Fig. 3.13B, P>0.05, Student's t-test). Overall, these results indicate the possibility that these may be early signs of alterations in mitochondria in quadriceps muscle in

Tau35 mice, however, an increase in the number of samples and examining older animals might be required in order to assess this more accurately.

Fig. 3.13 Mitochondrial protein levels in Tau35 muscle

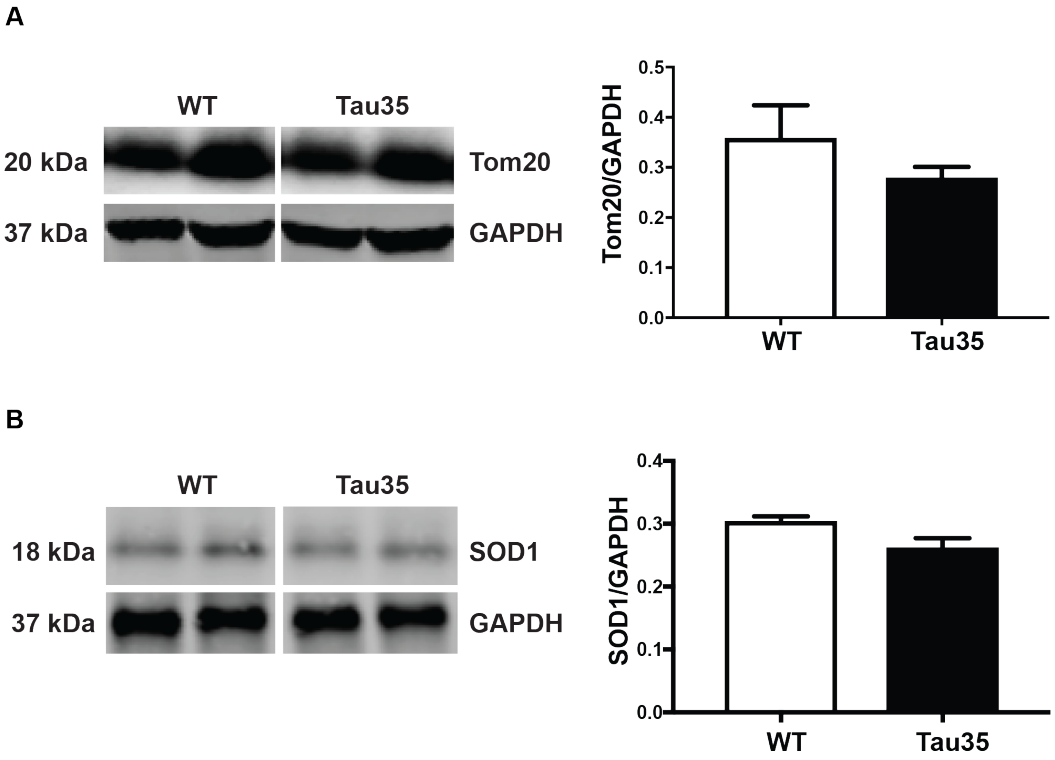

Western blot of WT and Tau35 quadriceps muscle (aged 8 months) probed with antibodies against mitochondrial markers **A** Tom20 and **B** SOD1. Molecular weights (kDa) indicated on the left correspond to the weight of the proteins of interest. The amount of the mitochondrial markers on the blot was quantified relative to glyceraldehyde 3-phosphate dehydrogenase (GAPDH). Values are show as mean ± S.E.M., n = 3 ($P>0.05$, Student's t-test).

3.3 Discussion

This chapter describes the biochemical characterisation of the Tau35 mice, which are a novel mouse model expressing an N-terminally truncated form of WT human tau. The results show that Tau35 expression in mice mimics many of the major hallmarks of tauopathies that lead to the appearance of a disease-related phenotype. The Tau35 mouse is a unique and highly relevant model of human tauopathy that exhibits the following biochemical pathologies:

- Higher expression of Tau35 in male transgenic mice compared to female mice
- Accumulation of endogenous tau in insoluble pellets obtained from the hippocampus and associated cortex of mice aged 14 months
- Increased phosphorylation of endogenous tau in hippocampus and associated cortex of mice aged 14 months
- Signs of increased autophagy in the aged hippocampus and associated cortex region in mice aged 18 months
- Brain region-specific mitochondrial deficit in mice aged 18 months
- Astrocytic activation in all brain regions of mice aged 18 months
- Progressive degeneration and denervation of NMJs in the distal hindlimb lumbrical muscle in mice aged 13 months mice

3.3.1 Variability in levels of Tau35 protein in male and female mice as well as between different brain regions

Almost all existing transgenic mouse models of tauopathy over-express either mutant or WT tau, however, since high tau expression is not a hallmark of the tauopathies, these may not represent ideal models of human disease. Tau35 is a form of truncated tau that is found in PSP and CBD human brain and is free from mutations. Tau35 mice express Tau35 at less than 10% of total tau (Bondulich et al., 2016). Since the

Tau35 transgene was inserted into the *Hprt* locus of the X-chromosome., it was of interest to determine whether the gender of the transgenic mice influenced Tau35 expression. Interestingly, investigation of Tau35 levels in Tau35 mouse models demonstrates a significantly increased amount of Tau35 in male mice compared to that of female mice. This could be due to partial or complete X chromosome inactivation, which is the variable silencing of a single X chromosome in females (Lyon, 1962). Therefore, because of the unpredicted nature of X chromosome silencing, and to eliminate potential variability due to differential expression of Tau35 protein, this study evaluated the effects of Tau35 in male mice only.

In addition to variability between genders in Tau35 mice, differences in the amount of Tau35 were also found in different brain regions of Tau35 male mice. The amount of Tau35 expression is higher in hippocampus and associated cortex, and brainstem and cerebellum, and lower in the frontal region, and amygdala and associated cortex. However, brain region-specific tau transgene expression has not been well studied, perhaps due to the difficulty in discriminating between the transgenic and endogenous mouse proteins in previous studies. However, the HA tag fused to the C-terminus of Tau35 enabled its differentiation from the endogenous tau.

3.3.2 Accumulation of endogenous tau in an insoluble fraction of aged Tau35 brain

Tau accumulation and tau aggregation are defining pathological features of tauopathies and therefore, differential centrifugation was used to assess the amount of tau in pellets obtained from the hippocampal and associated cortex of WT and Tau35 mice aged 14 months. The total amount of tau in brain homogenates from mice of each genotype was similar. However, there was a significant increase in the amount of tau in the insoluble pellet obtained from Tau35 mouse brain, compared to that of WT mice. This indicates that larger aggregates of tau are present in the

insoluble fraction (13,000g pellet) in Tau35 mouse brain, this is supported by the fact that the 100,000g pellet contained similar amounts of tau in Tau35 and WT mice. In addition, sarkosyl-insoluble preparations from hippocampus and associated cortex of WT and Tau35 mice aged 14 months, showed no increase in the amount of aggregated tau present in Tau35 mice (Bondulich et al., 2016). Furthermore, ThioS and silver staining was negative for tau aggregates in Tau35 mouse brain (Bondulich et al., 2016). However, IHC of Tau35 hippocampus and has shown pre-tangle like structures labelled with tau antibodies (Fig. 1.12)

In addition to insoluble protein species, the 13,000g pellet contains cellular organelles, predominantly mitochondria, lysosomes and peroxisomes. It is possible that tau could be associated with these organelles in Tau35 mice. It has been suggested previously that tau accumulation impairs mitochondrial degradation by directly interacting with mitochondria (Hu et al., 2016). It is also believed that the autophagy-lysosome system enables clearance of pathological tau (Rodríguez-Martín et al., 2013). Therefore, the higher levels of tau protein in 13 000g could indicate potential interaction of tau with the organelles that are separated out in this pellet.

3.3.3 Increased phosphorylation of endogenous tau protein in aged Tau35 mice

Tau function is regulated by numerous post-translational modifications, including phosphorylation and proteolytic cleavage (Hanger et al., 2009). Abnormal post-translational modifications alter the normal function of tau and may contribute to the pathology of tauopathies (Mietelska-Porowska et al., 2014). However, tau phosphorylation is an essential part of its physiological function. Furthermore, Tau35 mice show a substantial increase in phosphorylation, and then undergo proteolytic cleavage (Hanger and Wray, 2010), generating a number of tau fragments that can

be transported into different cellular compartments (Paholikova et al., 2015). Both increased tau phosphorylation and tau cleavage, have been suggested to trigger the aggregation of tau in tauopathies (Mietelska-Porowska et al., 2014). Aggregates of highly phosphorylated tau may then cause deterioration of normal cell processes, for example triggering astrocyte activation, as well as leading to dysfunction of cellular organelles such as mitochondria (Schulz et al., 2012; Pekny and Pekna, 2014).

Furthermore, the degree of phosphorylation of endogenous tau depends on the balance of activity between protein kinases and phosphatases, which regulate phosphorylation and dephosphorylation of tau, respectively (Mietelska-Porowska et al., 2014). If this balance is disrupted, either by over-activation of kinases (such as GSK-3) or inhibition of phosphatases (such as PP2A), tau becomes hyperphosphorylated (Hanger et al., 1992; Gong et al., 1994). It has been previously identified that there is an increase in GSK3β activity in Tau35 mouse brain that may make a significant contribution to the observed increase in endogenous tau phosphorylation (Bondulich et al., 2016).

3.3.4 Mitochondrial deficit in Tau35 mouse brain

Tau also interacts with cytoplasmic organelles, such as mitochondria (Hu et al., 2016). In neurons, mitochondria are critical for the production and supply of energy in the form of adenosine triphosphate (ATP), as well as calcium regulation, both of which are essential for controlling neurotransmitter release (Nunnari and Suomalainen, 2012; Beharry et al., 2014). These important functions rely on a dynamic mitochondrial network maintained by membrane fission and fusion (Eckert et al., 2005; DuBoff et al., 2012). The production of ATP occurs via oxidative phosphorylation, which also generates an inner-membrane electrochemical potential that is crucial for mitochondrial protein import (Neupert et al., 2008; Nunnari and Suomalainen, 2012). Growing evidence suggests that mitochondria play a key role in

the execution of neurodegeneration, either due to defects in respiratory function, or by interacting with other organelles such as the endoplasmic reticulum (ER) or the cytoskeleton (Nunnari and Suomalainen, 2012). For example, early deficits in mitochondria are detected in some transgenic mouse models of AD prior to deposition of aggregated amyloid-β and tau (Kopeikina et al., 2011; Amadoro et al., 2014; Rodríguez-Martín et al., 2016). Additionally, a significant reduction in the number of mitochondria has been observed in the axons of cortical neurons cultured from P301L tau knockin mice, which suggests that P301L tau may have a considerable effect on axonal mitochondria (Rodríguez-Martín et al., 2016). Moreover, *in vivo* and *in vitro* models of N-terminally truncated tau have demonstrated that the pathological N-terminal truncation of human tau, which may be involved in the onset and progression of tauopathies, induces defects in mitochondrial fission/fusion dynamics (Garcia-Sierra et al., 2008; Amadoro et al., 2014). Therefore, it has been suggested that mitochondrial dysfunction may precede plaque and tangle formation and that there is a link between mitochondrial deficiency and neurodegeneration (Kopeikina et al., 2011; Rodríguez-Martín et al., 2016). In this study, mitochondrial dysfunction was assessed using antibodies against mitochondrial markers in Tau35 and WT mice. HSP60 is a mitochondrial matrix chaperone which, plays a role in the transportation and folding of imported mitochondrial proteins (Söti et al., 2002; Federico et al., 2012). A decrease in HSP60 in the hippocampus and associated cortex, along with a pronounced trend for a decrease in the frontal region, was observed in Tau35 mice. No changes were observed in the amygdala and associated cortex or the brainstem and cerebellum. These findings suggest that decreased HSP60 could lead to increased protein misfolding and aggregation, which is consistent with the pathological hallmarks of 4R tauopathies. Interestingly, similar changes have also been observed in AD, where HSP60 has been found to be significantly decreased (Yoo et al., 2001). Additionally, (Magen et al., 2008) found that defects in HSP60 can cause neurodegenerative pathologies, such as defective myelination, of varying

severity. Notably, researchers have also found that mild HSP60 deficiencies affect both neurons and glia (Bross et al., 2012), which is in line with the finding of activated astrocytes and areas of neuronal degeneration in Tau35 mice.

3.3.5 Astrocytic activation in Tau35 mouse brain

Reactive astrogliosis, a response of activated astrocytes, is a key factor in the progression of many neurodegenerative diseases (Buffo et al., 2010). The cellular and molecular mechanisms leading to reactive astrogliosis are not completely understood, however reactive astrocytes are a prominent histopathological feature of many neurodegenerative diseases, including AD (Hostenbach et al., 2014; Pekny and Pekna, 2014).

The significant increase in GFAP expression observed in all brain regions of Tau35 mice aged 18 months, is suggestive of astrocyte activation in these animals. Further analysis using immunofluorescence labelling also showed increased GFAP expression in Tau35 mice aged 18 months, as well as morphological changes in astrocytes. Activated astrocytes undergo a variety of morphological changes that affect astrocyte function, including cell hypertrophy, cell proliferation and migration towards affected areas, and increased production of intermediate filament proteins, such as GFAP (Sofroniew and Vinters, 2010). Additionally, an apparent migration of activated astrocytes to areas experiencing neuronal degeneration was detected by immunofluorescence. Taken together, these findings provide evidence for the presence of reactive astrogliosis in aged Tau35 mice. Since Tau35 mice are a model of 4R tauopathies, they closely resemble tauopathies such as PSP and CBD. The findings from this study are consistent with the research on PSP and CBD, in both of which reactive astrocytes have been observed (Song et al., 2009). Interestingly, the biggest differences in GFAP expression between Tau35 mice and WT mice occurred in the frontal brain region as well as the brainstem and cerebellum, which is consistent

with the degenerative profiles of PSP and CBD. In PSP, there is a distinctive form of cortical degeneration confined, at least initially, to pons, premotor and motor cortex (Hauw et al., 1994; Bergeron et al., 1997). The brainstem and cerebellum are particularly affected in PSP, which was once considered to be a 'subcortical dementia' (Buée et al., 2000). Similarly, CBD is characterised by frontoparietal atrophy of the brain (Wakabayashi et al., 1994), and therefore the frontal region experiences increased neuronal death, which could result in migration of activated astrocytes towards that area of the brain.

A preliminary examination of GFAP expression in WT and Tau35 mice aged 14 months did not find any significant differences in GFAP expression (Bondulich et al., 2016), which suggests that reactive astrogliosis may occur as a late event between 14 months and 18 months in Tau35 mice. Indeed, researchers have noted that reactive astrogliosis may only be apparent in the later stages of neurodegenerative conditions and may then become involved in disease progression (Burda and Sofroniew, 2014).

3.3.6 Signs of altered autophagy in hippocampus and associated cortex region in Tau35 mice

Accumulation of autophagic and lysosomal markers have been reported in human tauopathy brains, suggesting that disruption in these processes may be involved in disease pathogenesis (Piras et al., 2016). Tau35 mice demonstrate an increase in the autophagosome marker LC3-II, in the hippocampus and associated cortex region. In addition, the autophagic marker p62/SQSTM1, which binds to LC3-II, is also increased in Tau35 mice (Bondulich et al., 2016). This evidence implies that autophagy is affected in this brain region of Tau35 mice. These findings suggest a potentially detrimental effect of Tau35 on clearance of pathological tau, which could result in tau aggregation.

3.3.7 Degeneration and denervation of neuromuscular junctions in the distal hindlimb lumbrical muscle of Tau35 mice

Bondulich et al (2016) described that Tau35 mice exhibit early motor deficits in behavioural studies. Haematoxylin and eosin staining of quadriceps and latissimus muscle sections in Tau35 mice (aged 16 months) demonstrated occasional split fibres as well as the increased presence of small rounded fibres. In addition, multiple internalised and numerous degenerative muscle fibres were apparent in muscle of Tau35 mice at 8 and 16 months. Interestingly, Tau35 mice show a marked reduction in hindlimb grip strength.

In this study, distal hindlimb lumbrical muscle was investigated from WT and Tau35 mice aged 3 and 13 months. Fluorescence staining of these muscles against acetylcholine receptors, synaptic vesicles and neurofilaments enabled the determination of the size and shape of the endplates, as well as the degree of innervation of NMJs in the mice. At 3 months of age, Tau35 mice showed signs of early alterations of the NMJs and evidence of early signs of deformation of the endplates. Morphologically, a reduction in the number of post-synaptic folds is a result of AChR instability and may lead to functional impairment in the post-synaptic response in NMJs (Arnold et al., 2014). Evidently, ageing has a dramatic effect on the deterioration of neuromuscular connections. There was a dramatic loss of neurofilament staining in mice aged 13 months when compared to the younger cohort aged 3 months that was irrespective of genotype. However, in addition to the significant deterioration caused by aging, at 13 months the Tau35 mice demonstrated a reduction of the surface area of NMJs, as well as morphological deformation of the endplates, compared to WT age-matched animals. In addition, there is a significant increase in partially denervated NMJs in Tau35 mice that could potentially have been caused by the degeneration of the endplates in these animals. Notably, a murine

tauopathy model (Tg30) that overexpressing human 1N4R double-mutant tau (P301S and G272V) also demonstrates NMJ denervation (Audouard et al., 2015a). Tg30 mice exhibit early synaptic vesicle loss in NMJs similar to Tau35 mice. Interestingly, it has been suggested that this denervation event occurs not due to neuronal loss but due to accumulation of Gallyas-positive aggregates, and cathepsin-positive vesicular clusters in axons suggesting that this denervation results from disturbances of axonal transport. (Audouard et al., 2015a). Furthermore, another tau transgenic mouse line Tau 58/4 mice, which over-express P301S tau in neurons, also demonstrates signs of NMJ denervation and muscle atrophy (Yin et al., 2017). Taken together with the results reported herein, these studies suggest a role for tau at the NMJ that is adversely affected by the onset of tauopathy, resulting in the appearance of motor deficits, such as those apparent in PSP and CBD.

Tau35 mice show a strong trend towards a mitochondrial deficit in muscle by the age of 8 months, and also a significant reduction in the brain by18 months of age. It has been previously suggested that one of the signs of unhealthy NMJs is a reduction in the number of mitochondria and increased NMJ morphological alterations (Garcia et al., 2014). Investigating older Tau35 mice could potentially provide more information on the effects of the potential role of mitochondria in NMJ dysfunction. In addition, a recent study has reported that autophagy impairment in muscle has a major impact on neuromuscular synaptic function and muscle strength, ultimately affecting the lifespan of animals, which may parallel some of the changes evident in Tau35 mice (Carnio et al., 2014). The same study also showed that inhibition of autophagy exacerbates mitochondrial dysfunction and oxidative stress at the NMJ (Carnio et al., 2014). Interestingly, Tau35 has been shown to affect autophagy in the brains of Tau35 mice (Bondulich et al., 2016), in addition to that described here, and also in a stable cell of Chinese hamster ovary (CHO) cell expressing Tau35 (personal communication, Dina Dakkak, King's College London).

In conclusion, this work represents an exploratory study to characterise the novel Tau35 mouse model of human tauopathy. The results described here suggest that expression of Tau35, which contains four microtubule binding repeats, causes significant changes in cellular mechanisms in both the central and peripheral nervous systems. These findings position Tau35 mice as a particularly good model of human tauopathies such as PSP and CBD, in both of which 4R tau is overexpressed. However, Tau35 mice are also likely to prove useful in improving our understanding of the molecular and cellular processes that are adversely affected in other tauopathies since they exhibit major biochemical characteristics that are common to disorders including AD. As there are currently no disease-modifying treatments available for the tauopathies, Tau35 mice may represent a good platform in which to test novel therapeutic strategies.

Chapter 4: Establishing Tau35 primary cortical neurons as a cellular model of human tauopathy

4.1 Introduction

Morphological and biochemical neuronal changes are exhibited in many neurodegenerative diseases such as Alzheimer's disease (AD), frontotemporal dementia with parkinsonism linked to chromosome 17 (FTDP-17), Pick's disease, and progressive supranuclear palsy (PSP). In the previous chapter, biochemical investigation of the Tau35 mouse model of the central and peripheral nervous system was demonstrated. Based on the deficits and tau pathology shown in Tau35 mice, it is valuable to study neuronal characteristics to identify changes and the molecular mechanisms underlying the phenotype. To do this, a cell model of primary cortical neuronal cultures, derived from Tau35 and WT mouse embryos was used. This enabled modelling of tauopathy in a controlled and modifiable environment of isolated neurons.

It is well known that maintenance of correct neuronal morphology is essential for the normal function of healthy neurons. Tau protein, as a microtubule binding protein, stabilises microtubules and the cytoskeleton and, therefore, affects neuronal morphology (Avila et al., 2004b). In this chapter, the effect of Tau35 on endogenous tau, neuronal morphology and cellular organisation is demonstrated.

In addition, synaptic loss and dysfunction are common features in tauopathies and in the case of AD, synaptic loss is correlated with disease progression (Hamos et al., 1989; Terry, 2000; Scheff and Price, 2006; Robinson et al., 2014). Indeed, synaptic dysfunction and spine loss demonstrate a stronger correlation with cognitive decline than do neurofibrillary tangles or neuronal loss (Robinson et al., 2014). It has been

suggested that loss of dendritic spines or structural reorganisation of spines and disturbances in synaptic signalling are important for learning and memory and may be one of the first signs of AD (Yuste and Bonhoeffer, 2001; Nimchinsky et al., 2002). In addition, many studies have demonstrated that synaptic or spine loss is a better indicator of cognitive impairment than amyloid pathology (Scheff and Price, 2006; Scheff et al., 2007; Akram et al., 2008), thereby suggesting that changes in spine morphology and distribution may be critical in understanding the synaptic toxicity observed in AD. Therefore, the fact that Tau35 mice demonstrate a decrease in synaptic markers (synapsin 1 and synaptobrevin) without apparent neuronal loss in aged mice, is highly relevant to the investigation of synaptic dysfunction in relation to the tauopathies (Bondulich et al., 2016).

Tau is localised to axons as well as to the somatodendritic compartment, and it plays a key role in microtubule assembly and stabilisation, cellular trafficking, maintenance of neuronal morphology, and the formation of axonal and dendritic processes (reviewed in (Gendron and Petrucelli, 2009)). There is a connection between the accumulation of highly phosphorylated tau in neuronal dendrites and the density and morphology of dendritic spines (Dickstein et al., 2010). This tau phosphorylation could be caused by one of the main kinases implicated in pathological tau phosphorylation, GSK-3 (Hanger et al., 1992; Mandelkow et al., 1992; Cho and Johnson, 2003; Hanger et al., 2009).

Mitochondrial function has previously been shown to be important for the maintenance of synapses (Hollenbeck, 2005). Mitochondria have been found to accumulate in the synapse because synaptic function requires a consistently high supply of ATP to provide energy (Zenisek and Matthews, 2000). In addition, alterations in mitochondrial trafficking, including their speed, directionality of movement and pausing, may affect synaptic activity and the ability of neurons to fire

action potentials (Course and Wang, 2016). Furthermore, the phosphatidylinositol 3-kinase (PI3K), Akt (a serine/threonine kinase), and mammalian target of rapamycin (mTOR) pathway (PI3K-Akt-mTOR) has been identified as a key regulator of energy metabolism in neurons through regulating clearance of damaged mitochondria, known as mitophagy (Agostini et al., 2016).

Therefore, in this chapter, a detailed morphological characterisation of Tau35 primary neurons is presented, including somatic, dendritic and spine morphology. In addition, tau hyperphosphorylation and mitochondrial deficits were evaluated as potential causes of the observed spine loss in Tau35 neurons in culture.

4.2 Results

4.2.1 Tau35 is expressed at all stages of neuronal maturation in Tau35 neurons

Tau35 protein levels in lysates of primary cortical cultures of WT and Tau35 neurons were examined at 8 and 14 DIV on western blots. Following incubation with an antibody to total tau (K9JA), a faint band was visible at approximately 35 kDa in lysates from Tau35 neurons, which was not present in WT neuronal lysates. Western blots probed with an antibody recognising the HA-tag fused to Tau35 were quantified after normalising to β-actin (Fig. 4.1A). A single band corresponding to tau at 35 kDa was observed in both 8 DIV and 14 DIV Tau35 primary cortical neurons, and was absent from WT neurons (Fig. 4.1A). These results show that Tau35 is expressed at both 8 and 14 DIV, but that Tau35 expression does not appear to increase with neuronal maturation in Tau35 neurons ($n=3$, $P>0.05$, 2-way ANOVA).

Fig. 4.1B illustrates the results of immunofluorescence staining of WT and Tau35 primary cortical neurons at 8 DIV. Neurons were labelled with an antibody to the HA tag present on the Tau35 fragment (red) and total tau (green), and nuclei were labelled with DAPI (blue). Tau35, but not WT, neurons stained positively for HA, with a filamentous pattern that was largely coincident with the staining of total tau, as it was localised throughout the neurons but most intense in neurites. These results show that Tau35 co-localises with endogenous mouse tau in 8 DIV cortical neurons.

Fig. 4.1 Tau35 is expressed in primary cortical neurons derived from Tau35 mice

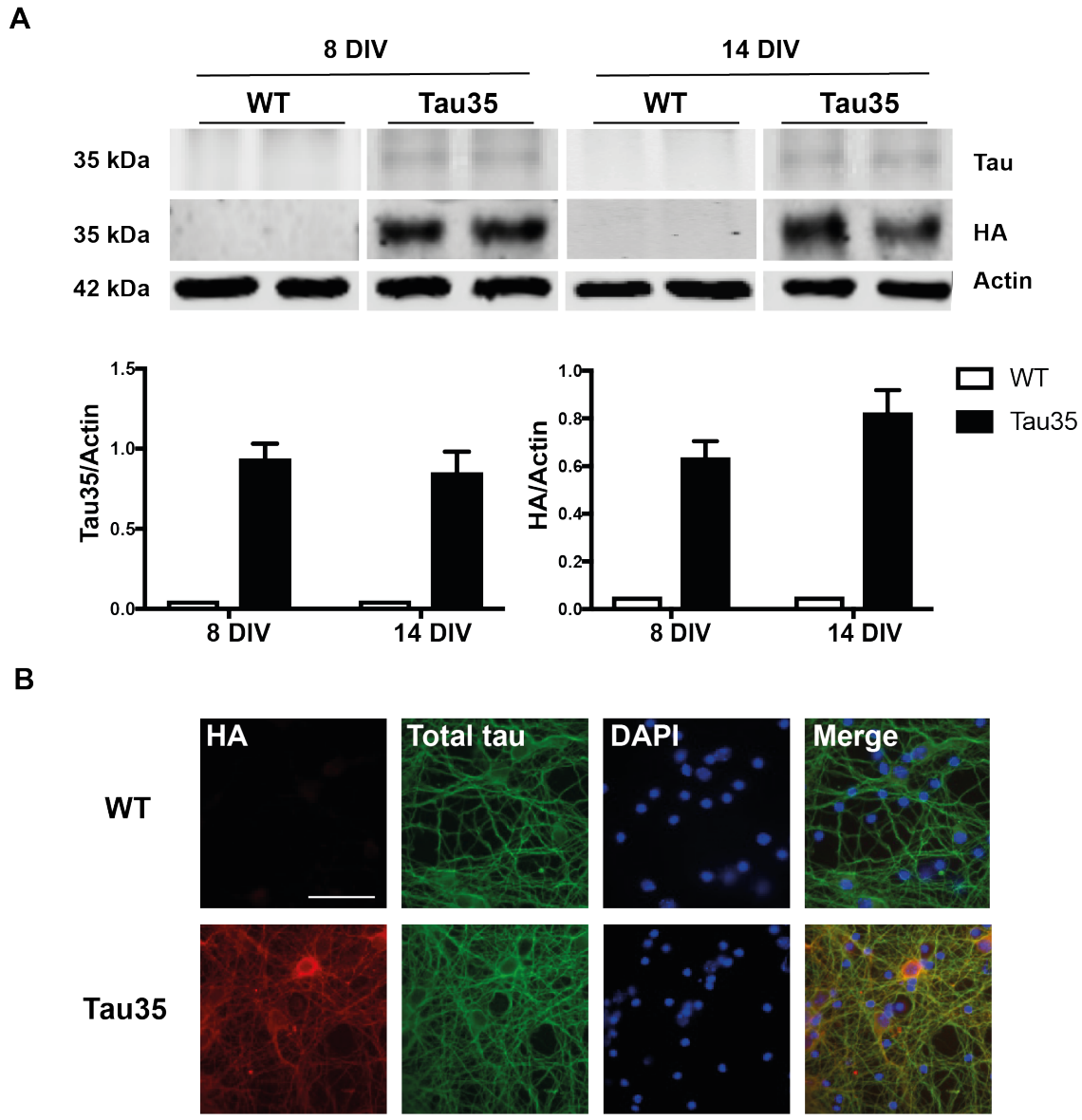

A Western blots of WT and Tau35 primary cortical neurons (8 and 14 DIV) probed with antibodies to HA, total tau (K9JA) and β-actin. Molecular weights (kDa) of proteins of interest are shown on the left (n=3, P>0.05, 2-way ANOVA). **B** Immunofluorescent staining shows WT and Tau35 primary cortical neurons at 8 DIV stained with antibodies recognising HA (red) and total tau (green). Nuclei are labelled with DAPI (blue). The merged image is shown on the right.

4.2.2 Overt neuronal loss is not observed in Tau35 primary cortical cultures

Live/Dead assays were used to analyse the survival of WT and Tau35 primary cortical neurons at different stages of neuronal maturation (3, 6, 9, and 14 DIV). Cells were treated with propidium iodide (PI), which is taken up by dead cells but cannot pass through the plasma membrane of viable cells, followed by labelling with an antibody to β-actin. Neurons were scanned (Odyssey scanner, Li-Cor) to measure the fluorescent signals from PI and β-actin. Fig. 4.2 shows the PI/β-actin ratio, as a measure of the proportion of dead cells in each culture. The graph shows that the proportion of dead cells is not significantly different ($n=3$, $P>0.05$, Student's t-test) between WT and Tau35 neuronal cultures between 3 and 14 DIV. These results suggest that there is no overt neuronal loss of Tau35 neurons, in comparison to WT neurons, when they are maintained in culture for up to 14 days.

Fig. 4.2 Viability of WT and Tau35 primary cortical neurons in culture

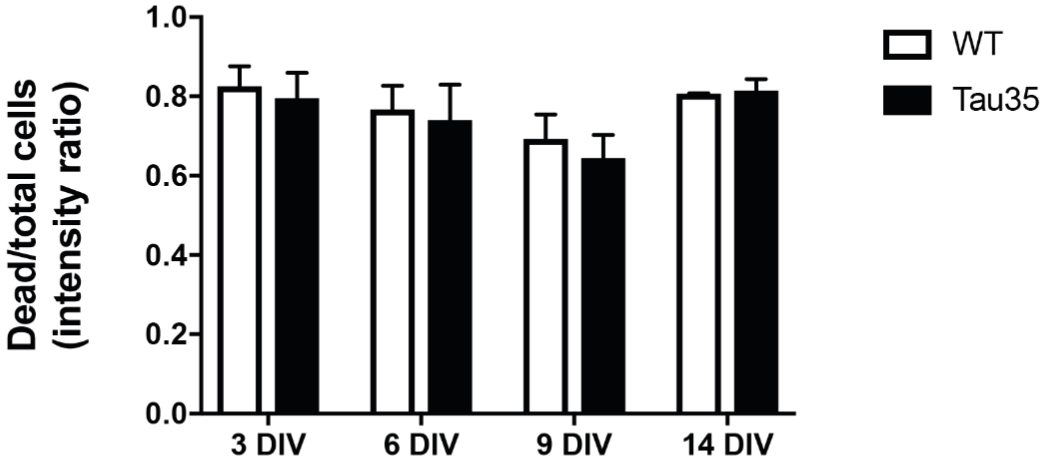

Graph showing the ratio of dead cells (stained with PI) to the total amount of cells (stained with β-actin) in primary cultures of WT and Tau35 cortical neurons maintained for 3, 6, 9, and 14 days *in vitro* (DIV). Values are displayed as mean ± S.E.M. Student's t-test. 12 wells of cells were analysed per genotype at each time point from three independent experiments.

4.2.3 Morphological analysis of WT and Tau35 neurons

To characterise the cultures of WT and Tau35 primary cortical neurons, a morphological analysis was performed following fixing of the cells at different times of neuronal maturation (3, 6, 9 and 14 DIV). Neurites of the primary neurons were traced using the 'Simple Neuron Tracer' plugin in ImageJ. Representative images of 3 (Fig. 4.3A), 6 (Fig. 4.3B) and 9 (Fig. 4.3C) DIV of WT and Tau35 neurons transfected with eGFP are shown on the left in Fig. 4.3. Sholl analysis was used to determine the level of complexity of the neurons as described in Chapter 2, Section 2.2.13. The Sholl analysis of Tau35 neurons at 3 DIV revealed a similar development to that observed in WT neurons at the same stage, with a maximum dendritic radius of 250 μm for both genotypes (Fig. 4.3A). At 6 DIV, the neuronal complexity of Tau35 and WT neurons appeared similar, however, the maximum dendritic radius in Tau35 cells increased by approximately 30%, compared to WT neurons (Fig. 4.3B). By 9 DIV, in comparison to WT neurons, Tau35 neurons showed a statistically significant reduction of approximately 30% in the number of intersections of the dendritic tree with the Sholl analysis grid at distances between 50 μm and 60 μm from the soma (Fig. 4.3C). In Tau35 neurons, the number of intersections also appeared to be slightly increased compared to WT neurons, at extended distances (200-300 μm) from the soma, although this apparent difference was not statistically significant ($P>0.05$, 2-way ANOVA). These results indicate that Tau35 neurons demonstrate morphological alteration compared to WT neurons that occur mainly with neuronal age of 9 DIV. This could suggest that Tau35 neurons undergo healthy development similar to WT neurons, however as the neurons mature, morphological alterations may occur potentially in response to pathological cellular and biochemical changes described below.

Fig. 4.3 Tau35 primary cortical neurons show altered morphology with increased stages of neuronal maturation

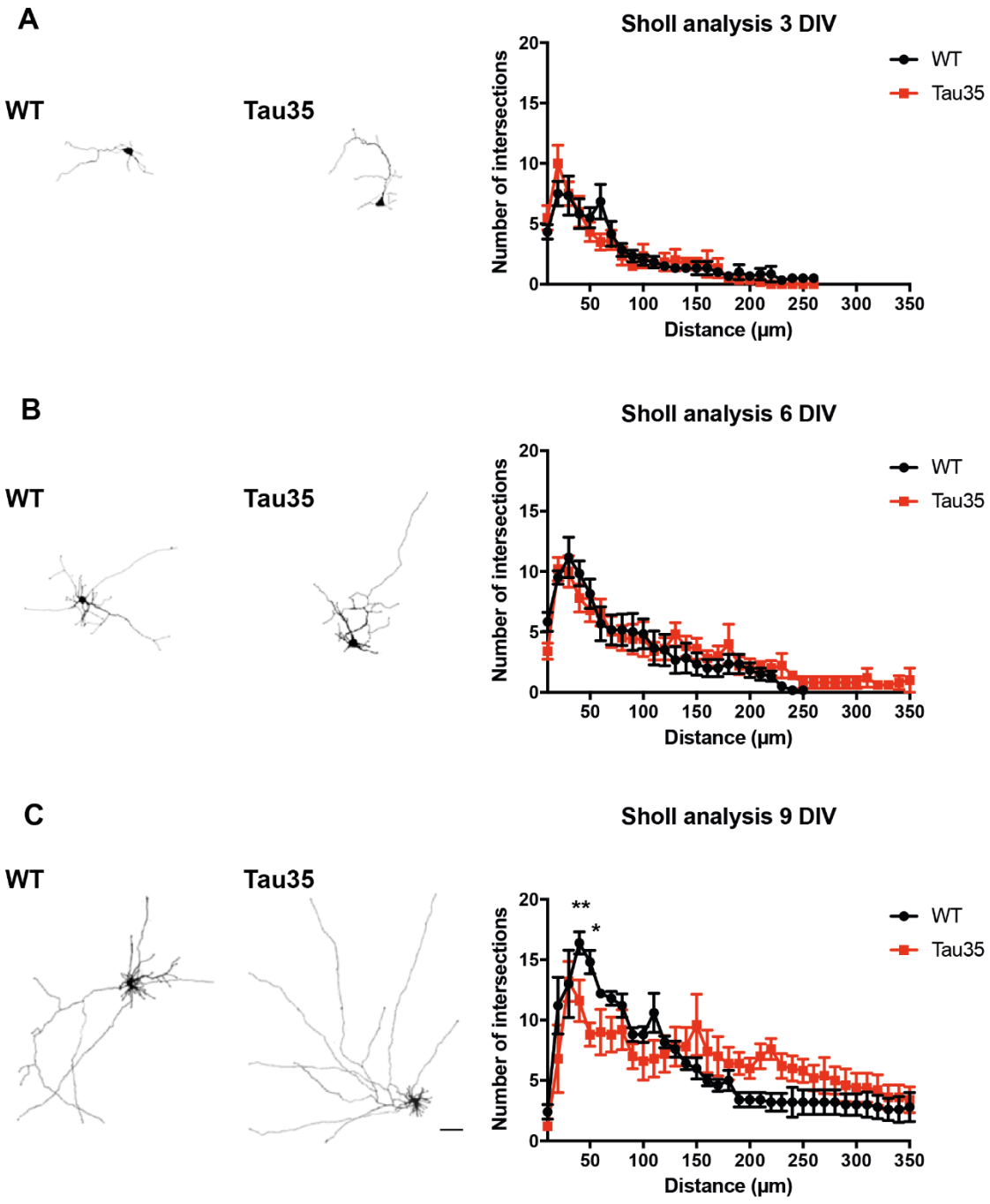

Fig. 4.3 legend

Representative images (left) and Sholl analyses (right) of WT (black) and Tau35 (red) primary cortical neurons. Neurons at **A** 3 DIV, **B** 6 DIV and **C** 9 DIV. Scale bar =100 μm. Values in the graphs are displayed as mean ± S.E.M. 9-12 neurons were analysed per genotype from 2 biological replicates. 2-way ANOVA, *P<0.05, **P<0.005.

A more detailed analysis of eGFP-expressing WT and Tau35 neurons was then performed to determine whether there were any differences in the following parameters: soma perimeter (μm), mean dendritic extent (μm), number of primary neurites, number of secondary neurites, number of dendritic tree end points, and number of branch points of the dendritic tree (Fig. 4.4). It is important to note that this experiment was designed to investigate morphological differences between WT and Tau35 neurons after increasing time in culture. Since this study does not use continuous sampling, the neurons analysed at each time point are from different cultures and therefore each time point was analysed as a separate experiment.

In Tau35 neurons at 3 DIV, the soma perimeter appeared to increase slightly (52 ± 3 μm, mean ± S.E.M., n=12) compared to WT neurons (46 ± 2 μm, mean ± S.E.M., n=12), although this was not significant (P>0.05, Student's t-test) (Fig. 4.4A). At 6 DIV, a slight increase in soma perimeter in Tau35 neurons (78 ± 7 μm, mean ± S.E.M., n=12) compared to WT neurons (62 ± 5 μm, mean ± S.E.M., n=12) was still observed, however it was not a significant difference (P>0.05, Student's t-test). By 9 DIV, the soma perimeter was 15% larger (P<0.05 Student's t-test) in Tau35 neurons (70 ± 1 μm, mean ± S.E.M., n= 8) compared to WT neurons (60 ± 3 μm, mean ± S.E.M., n=10). However, at 14 DIV the mean soma perimeter in Tau35 neurons (97 ± 14 μm, mean ± S.E.M., n=15) was not significantly larger than in WT neurons (81 ± 9 μm,

mean ± S.E.M., n=15) due to the high amount of variability in soma perimeter between neurons (P>0.05, Student's t-test).

The mean dendritic extent of Tau35 neurons at 3 DIV was 98 ± 5 μm (mean ± S.E.M., n=7) and that of WT neurons was 126 ± 7 μm (mean ± S.E.M., n=14). Therefore, Tau35 neurons showed a significant decrease of 22% in their mean dendritic extent compared to WT neurons at 3 DIV (P<0.05, Student's t-test) (Fig. 4.4B). However, at 6 and 9 DIV there were no significant differences in the mean dendritic extent between WT and Tau35 neurons (P>0.05, Student's t-test). At 14 DIV, Tau35 neurons (515 ± 30 μm, mean ± S.E.M., n=15) demonstrated a drastic increase (P<0.005, Student's t-test) in their mean dendritic extent compared to WT neurons (336 ± 11 μm, mean ± S.E.M., n=12).

Primary neurites are identified as those that originate directly from the neuronal soma, with secondary neurites branching from the primary neurites. The number of primary (Fig. 4.4C) and secondary neurites (Fig. 4.4D) in WT and Tau35 neurons was similar, with a mean of 5-8 primary neurites and 5-10 secondary neurites emanating from each neuron. At 3 DIV, WT neurons exhibited 5 ± 0.4 (mean ± S.E.M., n=11) primary neurites and Tau35 neurons had 6 ± 0.6 (mean ± S.E.M., n=12) primary neurites, which were not significantly different. In addition, the number of secondary neurites in WT (5 ± 1, mean ± S.E.M., n=12) and Tau35 neurons (7 ± 1, mean ± S.E.M., n=12) at 3 DIV was not changed (P>0.05, Student's t-test). At 6 DIV, the mean number of primary neurites in WT neurons was 8 ± 0.7 (mean ± S.E.M., n=12), which was not significantly different from the mean number of primary neurites in Tau35 neurons (8.5 ± 0.5, mean ± S.E.M., n=12). Furthermore, the number of secondary neurites in Tau35 neurons (9 ± 1 mean ± S.E.M., n=12) was not significantly different from the number of secondary neurites in WT neurons (10 ± 0.6 mean ± S.E.M., n=12).

Fig. 4.4 Morphological analysis of Tau35 primary cortical neurons

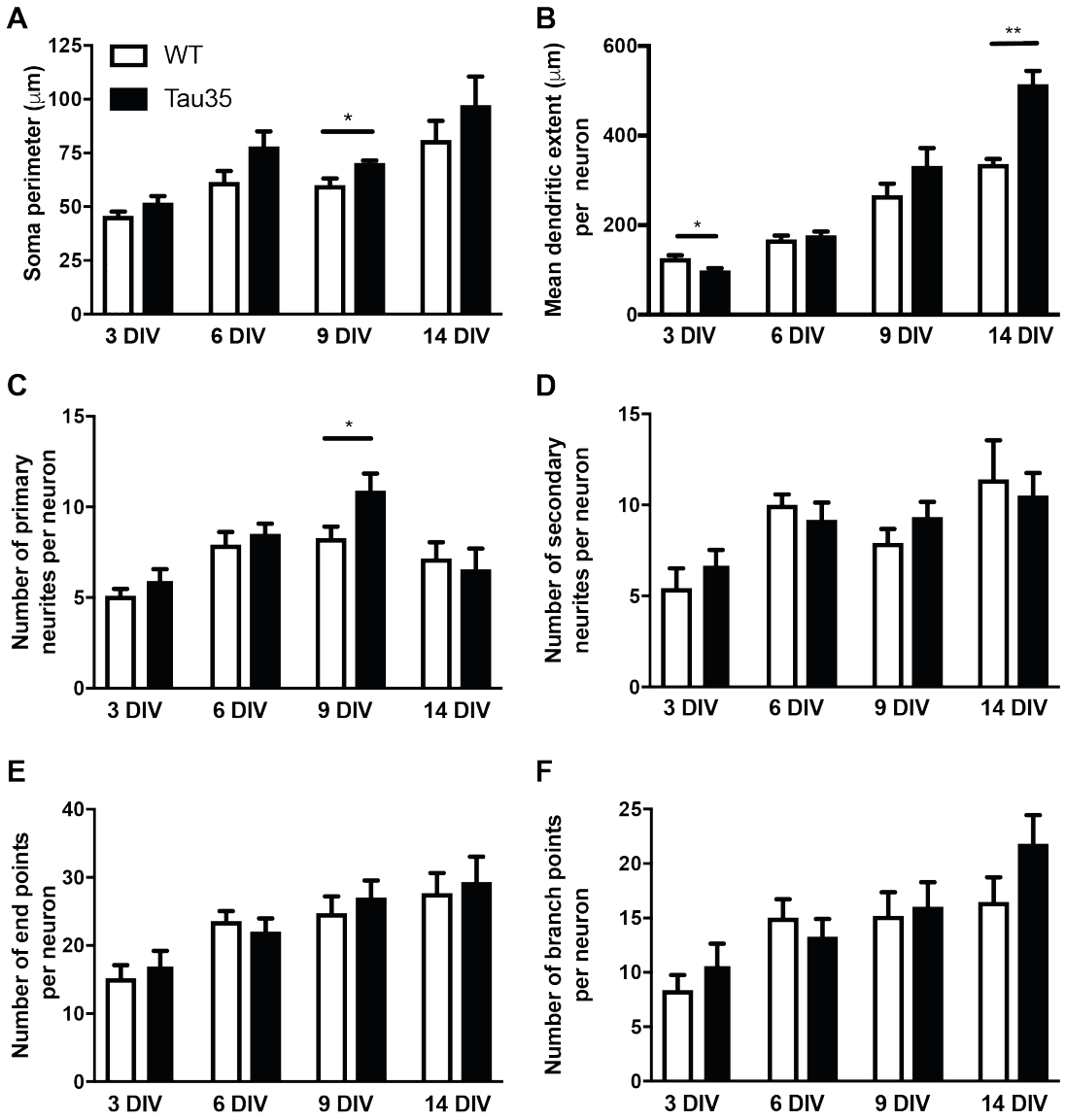

Graphs show the quantitation of the morphological analysis of WT (white) and Tau35 (black) primary cortical neurons at 3, 6, 9, 14 DIV. **A** Soma perimeter (μm), **B** Mean dendritic extent (μm), **C** Number of primary neurites, **D** Number of secondary neurites, **E** Number of end points of neurites per neuron, **F** Number of branch points per neuron. Values are displayed as mean ± S.E.M. n=5-15 neurons per genotype from 2 independent experiments. Student's t-test, *P<0.05, **P<0.005.

However, by 9 DIV, Tau35 neurons exhibited a significant increase in the number of primary neurites (11 ± 1 μm, mean ± S.E.M., n=8) compared to WT neurons (8 ± 0.6 mean ± S.E.M., n=11) ($P<0.05$, Student's t-test). The number of secondary neurites observed at 9 DIV in Tau35 neurons (9 ± 1, mean ± S.E.M., n=9) was similar ($P>0.05$, Student's t-test) to WT neurons (8 ± 1, mean ± S.E.M., n=11). Finally, at 14 DIV, there was no change ($P>0.05$, Student's t-test) in the number of primary neurites in Tau35 neurons (7 ± 1, mean ± S.E.M., n=11) compared to WT neurons (7 ± 1 mean ± S.E.M., n=13). The number of secondary neurites at 14 DIV was also not significantly different ($p>0.05$, Student's t-test) between Tau35 neurons (15 ± 5, mean ± S.E.M., n=5) and WT neurons (11 ± 2, mean ± S.E.M., n=5).

The number of dendritic end points indicate the levels of morphological complexity at the periphery of the neurons. It is also gradually increased with maturation of neurons in culture (Fig. 4.4E). At 3 DIV, Tau35 neurons (17 ± 2, mean ± S.E.M., n=12) exhibited a similar number of end points as WT neurons (15 ± 2, mean ± S.E.M., n=12). At 6 DIV, the number of dendritic end points in Tau35 neurons (22 ± 2 mean ± S.E.M., n=12) was not significantly different from WT neurons (24 ± 2 mean ± S.E.M., n=11). Similarly, there was no change ($P>0.05$, Student's t-test) in the number of dendritic end points in WT (24 ± 2, mean ± S.E.M., n=11) and Tau35 neurons (27 ± 3, mean ± S.E.M., n=9) at 9 DIV. By 14 DIV, the number of termini was 29 ± 4 (mean ± S.E.M., n=11) in Tau35 neurons and 28 ± 3 (mean ± S.E.M., n=13) in WT neurons, representing no significant difference between the genotypes ($P>0.05$, Student's t-test). These results show that, although the number of dendritic termini increases during maturation, the values are similar in both Tau35 and WT neurons.

The number of branch points was increased in both WT and Tau35 neurons as they matured in culture. At 3 DIV, Tau35 neurons had 11 ± 2 (mean ± S.E.M., n=12) branch points, and WT neurons had 8 ± 1 (mean ± S.E.M., n=12) branch points. At 6 DIV

(WT 15 ± 2, mean ± S.E.M., n=11; Tau35 13 ± 2, mean ± S.E.M., n=12) and 9 DIV (WT 15 ± 2 mean ± S.E.M., n=11; Tau35 16 ± 2, mean ± S.E.M., n=9), neurons were not significantly different in the number of branch points present in the dendritic trees of the WT and Tau35 neurons ($P>0.05$, Student's t-test). At 14 DIV, Tau35 neurons showed no significant change ($P>0.05$ Student's t-test) in the number of branch points (22 ± 3, mean ± S.E.M., n=10) compared to WT neurons (16 ± 2, mean ± S.E.M., n=13).

Taken together, this detailed analysis of the morphology of Tau35 and WT neurons in culture shows that as the neurons mature, all of the parameters measured show a progressive increase, with the exception of the number of primary neurites identified at 14 DIV. In this study, the significant differences detected between Tau35 and WT neurons were an increase in soma perimeter and number of primary neurites at 9 DIV, as well as an initial decrease in the mean dendritic extent at 3 DIV, followed by a significant increase at 14 DIV, in Tau35 neurons.

4.2.4 Reduced dendritic spine density in Tau35 neurons

The number of dendritic spines in eGFP-expressing WT and Tau35 cortical neurons was quantified and standardised to dendrite length (μm) to determine the dendritic spine densities in mature neurons cultured for 14 DIV. The density of dendritic spines on WT neurons was 0.24 ± 0.01 spines per μm (mean ± S.E.M., n=12), whereas the spine density of Tau35 neurons was 0.16 ± 0.01 spines per μm (mean ± S.E.M., n=12) (Fig. 4.5A). Therefore, Tau35 neurons exhibit a marked and significant reduction of 33% in their dendritic spine density compared to that of WT neurons at 14 DIV (Student's t-test, $P<0.01$).

The graph in Fig. 3.5B represents the quantitative analysis of spine morphology in WT and Tau35 neurons. The spines are classified as 'mushroom', 'stubby' and 'thin' according to their morphology as described in Chapter 2, Section 2.2.14. A two-way ANOVA analysis of the percentage of each spine type demonstrated that in Tau35 neurons, mushroom spines and stubby spines were not significantly reduced compared to WT neurons ($P>0.05$). However, the percentage of thin spines was significantly decreased in Tau35 neurons ($P<0.005$). A reduction in thin spines in Tau35 neurons suggests that this could be related to the reduced ability to learn and disturbed memory formation reported in Tau35 mice (Bondulich et al., 2016).

Fig. 4.5 Reduced dendritic spine density in Tau35 primary cortical neurons

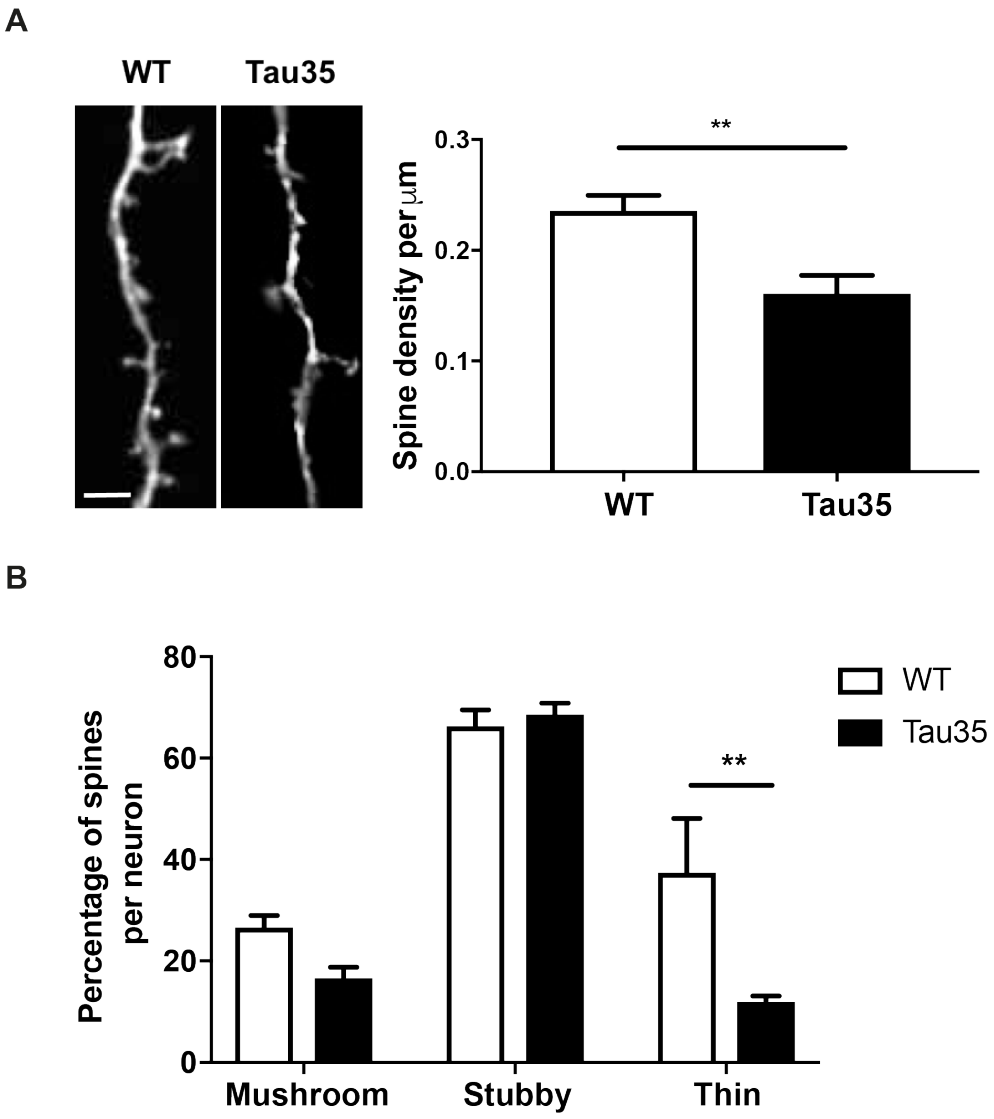

A Fluorescent images of dendrites of wild-type (WT) and Tau35 neurons transiently expressing eGFP at 14 DIV, scale bar=10 μm (left). The graph illustrates the results of the quantitative analysis of the number of dendritic spines per μm dendrite length per neuron in WT and Tau35 neurons., **P<0.01, Student's t-test. **B** The graph represents the quantitative analysis of spine morphology in WT and Tau35 neurons. The spines are classified as 'mushroom', 'stubby' and 'thin'. Values are displayed as mean ± S.E.M., n=12, **P<0.01, two-way ANOVA.

4.2.5 Increased phosphorylation of endogenous tau in Tau35 neurons

Phosphorylation of endogenous tau protein on Ser396/Ser404 was investigated on western blots using lysates of WT and Tau35 neurons cultured for 8 and 14 DIV, and probed with PHF1 or Tau1, combined with total tau (K9JA) (described in Chapter 2, Section 2.2.8 and 2.2.5 respectively) A double band of approximately 50 kDa was recognised by all these tau antibodies in WT and Tau35 neuronal lysates at both 8 and 14 DIV (Fig 4.6A). At 8 DIV, Tau35 neurons showed a 10% increase in tau phosphorylation recognised by PHF1, compared to WT neurons) (Fig. 4.6A) ($P<0.05$, Student's t-test). By 14 DIV, there was a 45% increase in PHF1 immunoreactivity in Tau35 neurons, compared to that in WT neurons ($P<0.01$, Student's t-test).

The immunofluorescence panel in Fig. 4.6A demonstrates representative images of 8 DIV WT and Tau35 neurons stained against PHF1 (red) antibody and total tau (K9JA) (green) with DAPI (blue) as a nuclear marker. In the images, it is observed that there is a higher intensity response to the PHF1 antibody in Tau35 neurons compared to WT neurons.

The Tau1 antibody showed no difference between WT (0.65 ± 0.02, mean ± S.E.M., n=6) and Tau35 neuronal lysates on western blots (0.66 ± 0.01, mean ± S.E.M., n=6). However, at 14 DIV, Tau1 immunoreactivity decreased by 37% in Tau35 neurons (0.35 ± 0.04, mean ± S.E.M., n=3) compared to that in WT neurons (0.56 ± 0.009, mean ± S.E.M., n=3) ($P<0.01$, Student's t-test) (Fig. 4.6B).

These results suggest that there are more phosphorylated and less non-phosphorylated tau epitopes in Tau35 neurons rather than in WT neurons indicating altered tau phosphorylation in Tau35 neurons, particularly in mature 14 DIV neurons.

Fig. 4.6 Increased phosphorylation of endogenous tau in Tau35 primary cortical neurons

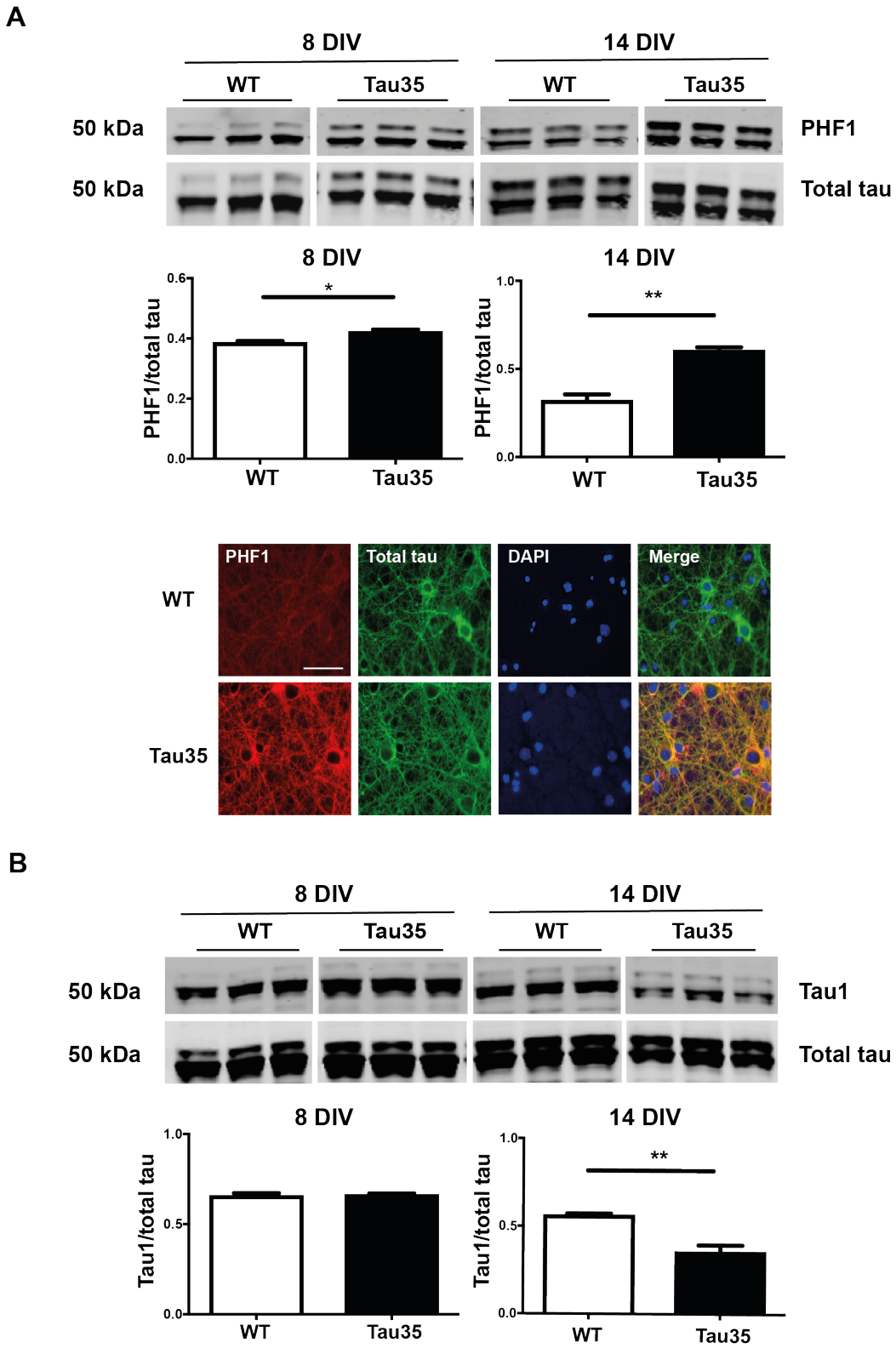

Fig. 4.6 *legend*
A Western blots of WT and Tau35 primary cortical neurons (8 and 14 DIV) probed with antibodies against PHF1 and total tau (K9JA). Graphs demonstrate analysis of PHF1 levels normalised to total tau levels in Tau35 and WT 8 (left) and 14 (right) DIV neurons. Immunofluorescence staining in lower panels shows WT and Tau35 primary cortical neurons at 8 DIV stained with PHF1 (red), total tau (K9JA) antibody (green) and DAPI (blue) to label nuclei. The merged image is shown on the right. **B** Western blot of WT and Tau35 primary cortical neuronal lysates (8 and 14 DIV) probed with antibodies against Tau1 and total tau (K9JA). Values are displayed as mean ± S.E.M., n=3 independent experiments, *P<0.05, **P<0.01, Student's t-test. Molecular weight markers (kDa) shown on the left of the western blot.

To investigate a potential candidate kinase that may be responsible for the increased tau phosphorylation observed in Tau35 neurons, glycogen synthase kinase (GSK)-3α/β and phosphorylated (p)-GSK-3α/β were investigated on western blots. Increased phosphorylation of GSK-3β at the inhibitory Ser9 site indicates decreased GSK-3β activity. Western blots labelled with antibodies to GSK-3α/β and p-GSK-3α/β revealed protein species of 51 kDa and a doublet at 46 kDa, corresponding to GSK-3α and GSK-3β, respectively (Fig. 4.7) The amount of p-GSK-3α, normalised to total GSK3α, was unchanged in WT and Tau35 neurons at both 9 DIV and 14 DIV neurons (P>0.05, Student's t-test). Similarly, p-GSK-3β, normalised to total GSK3β, was also unchanged at 9 DIV (P>0.05, Student's t-test). At 14 DIV, Tau35 neurons exhibited a 20% reduction in the ratio of p-GSK-3β to total GSK-3β in comparison to WT neurons, although this reduction was not statistically significant (P>0.05, Student's t-test). Therefore, these results show no significant activation of GSK-3β in Tau35 primary cortical neurons.

Fig. 4.7 GSK-3β kinase is not activated in Tau35 primary cortical neurons

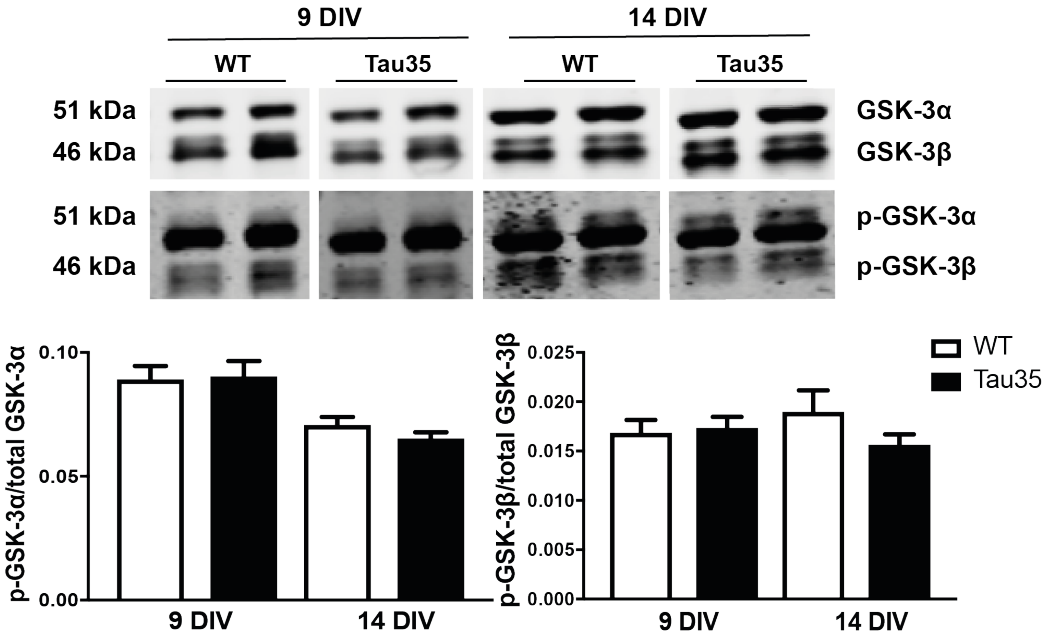

Western blots of WT and Tau35 primary cortical neuronal lysates (9 and 14 DIV) probed with antibodies to total and phosphorylated GSK-3α/β. Molecular weight markers (kDa) indicate the size of the protein of interest. Values are displayed as mean ± S.E.M., n=5 independent experiments.

4.2.6 Mitochondrial deficit in Tau35 neurons

To investigate the mitochondrial content of WT and Tau35 neurons, the protein amounts of the mitochondrial outer membrane markers, translocase of outer membrane receptor (TOM 20) and voltage-dependent anion channel (VDAC), and the inner membrane marker heat shock protein (HSP 60), were measured on western blots using WT and Tau35 neuronal lysates from 14 DIV. Western blots of neuronal lysates probed to TOM20 revealed a single band at 20 kDa, the predicted molecular weight of TOM20 (Fig. 4.8A). Quantification of the western blot showed a significant reduction of 43% ($P<0.05$, Student's t-test) in the amount of TOM20, normalised to β-actin, in Tau35 neuronal lysates (0.74 ± 0.1 mean ± S.E.M., n=6) compared to WT neuronal lysates (1.3 ± 0.18, mean ± S.E.M., n=6). At 32 kDa, a single band of VDAC was observed on the western blot (Fig. 3.9B). The amount of VDAC in Tau35 neurons was 0.52 ± 0.07 (mean ± S.E.M., n=6), showing a 38% reduction ($P<0.05$, Student's t-test) compared to WT neurons (0.84 ± 0.09, mean ± S.E.M., n=6) (Fig. 4.8B). On a western blot the mitochondrial inner membrane marker HSP60 (a single band detected at 60 kDa) displayed a 30% reduction ($P<0.01$, Student's t-test) in Tau35 neurons compared to WT neurons (Fig. 4.8C) These results demonstrate a reduction of mitochondrial markers that could indicate mitochondrial deficit in Tau35 neurons.

Fig. 4.8 Mitochondrial deficit in Tau35 primary cortical neurons

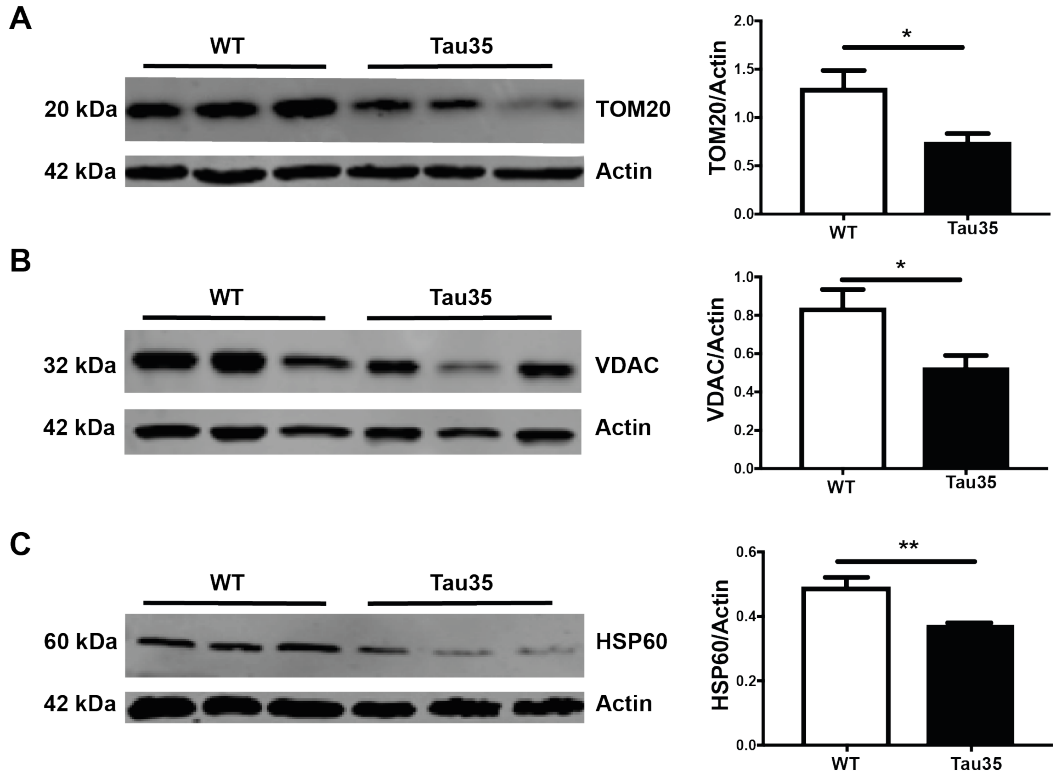

Western blots of WT and Tau35 primary cortical neurons (14 DIV) probed with antibodies against mitochondrial markers **A** TOM20, **B** VDAC, **C** HSP60. Each antibody was normalised to corresponding β-actin as a loading control. Molecular weight markers (kDa) indicate the size of the protein of interest. Values in the graphs are displayed as mean ± S.E.M., n=5 independent experiments, *P<0.05, **P<0.005, Student's t-test.

To investigate potential pathways involved in the apparent loss of mitochondrial capacity, mammalian target of rapamycin (mTOR) signalling, a critical regulator of energy metabolism in neurons was investigated in Tau35 neurons. Rapamycin is a well-established inhibitor of mTOR, which blocks mTOR phosphorylation and thereby initiates autophagy. Western blots of 14 DIV WT and Tau35 neurons treated with 10 nM of rapamycin for 48 h, and vehicle (DMSO) treated neurons, were probed for phosphorylated (p) mTOR and phosphorylated and total ribosomal protein S6 (Fig. 4.9). Rapamycin treatment decreased phosphorylated/total mTOR in both WT and Tau35 neurons by 60% and 40%, respectively. Tau35 neurons demonstrated a reduced susceptibility to rapamycin, although this may be explained by the slight, although not significant, reduction in basal p-mTOR in Tau35 neurons ($P>0.05$, Student's t-test). To confirm that rapamycin inhibited mTOR-mediated pathways in the cultured neurons, WT and Tau35 neurons were probed with antibodies to phosphorylated and total ribosomal S6 protein on western blots. As expected, rapamycin significantly reduced the phosphorylation of S6.

Fig. 4.9 Rapamycin reduces phosphorylation of mTOR and ribosomal S6 protein in Tau35 and WT neurons

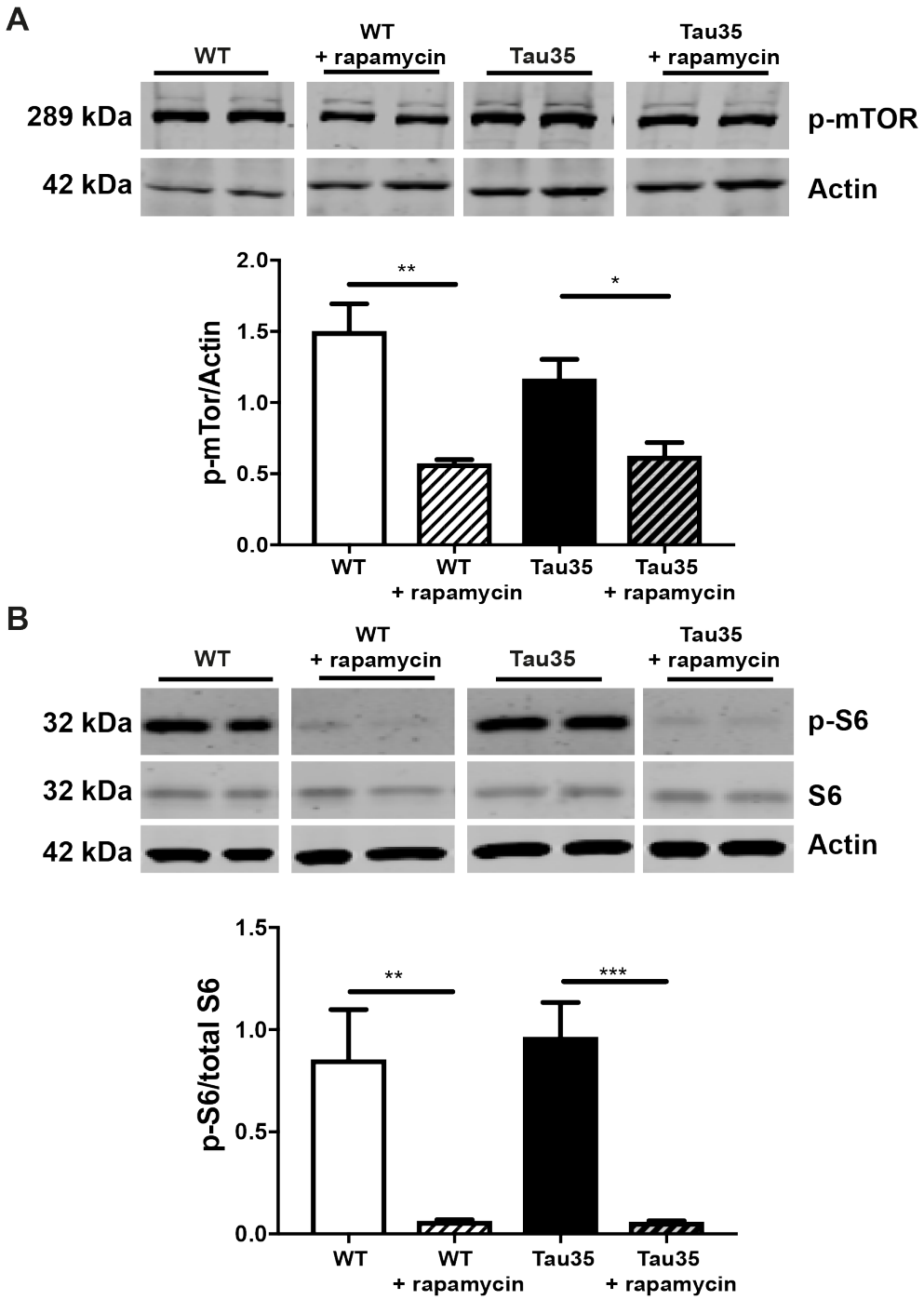

Fig. 4.9 legend

Western blots of WT and Tau35 neurons (14 DIV), either untreated or exposed to 10nM rapamycin for 48h. Western blots were probed with antibodies for **A** phosphorylated (p) -mTOR and normalised to β-actin **B** phosphorylated (p) ribosomal protein S6 and total ribosomal protein S6 normalised to β-actin. Molecular weight markers (kDa) indicate the size of the protein of interest. Graphs show a semi-quantitative analysis of the amounts of proteins of interest in neuronal lysates of treated and non-treated WT and Tau35 neurons. Values are displayed as mean ± S.E.M., n=4 independent experiments. *P<0.05, **P<0.005, ***P<0.001. Student's t-test.

Rapamycin is thought to induce mitophagy to enable the removal of damaged mitochondria via the m-TOR pathway. Therefore, the effect of rapamycin on the mitochondrial marker TOM20 was assessed in WT and Tau35 neurons (Fig. 4.10). However, rapamycin was not found to significantly reduce the ratio of TOM20/Actin in either WT or Tau35 neurons (Fig. 4.10). The previously determined significant reduction (P<0.05) in TOM20 between Tau35 (0.29 ± 0.01, mean ± S.E.M., n=4) and WT (0.19 ± 0.02, mean ± S.E.M., n=4) neurons was maintained after rapamycin treatment.

Fig. 4.10 Rapamycin treatment does not reduce mitochondrial TOM20 in WT or Tau35 neurons

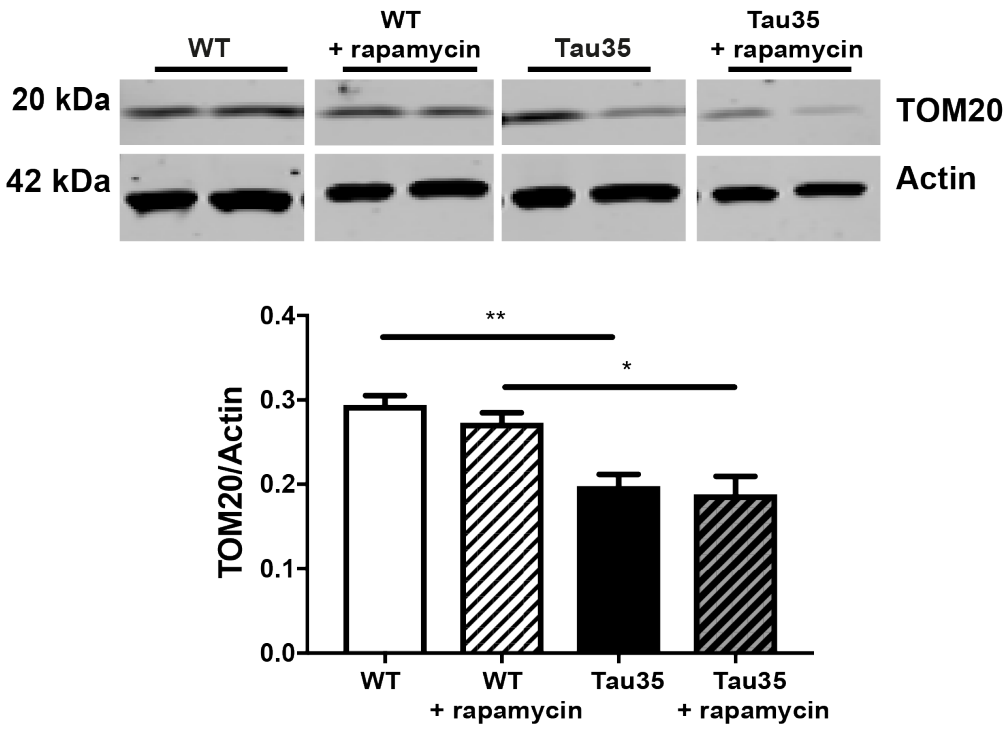

Western blot and analysis of 14 DIV WT and Tau35 neurons, either untreated or exposed to 48h treatment with 10 nM rapamycin, probed with antibodies against a mitochondrial marker TOM20 (normalised to β-actin). Values are displayed as mean ± S.E.M., n=4 independent experiments, *P<0.05, **P<0.005, two-way ANOVA. Molecular weight markers (kDa) indicate the size of the protein of interest.

4.3 Discussion

This chapter describes a detailed characterisation and comparison of WT and Tau35 primary cortical neurons in culture. The results show that expression of the tau fragment, Tau35, causes potentially pathological changes in cultured neurons. In summary, in comparison to WT neurons in culture, Tau35-expressing neurons demonstrate:

- Normal survival in culture, comparable to WT neurons.
- Decreased neuronal complexity, increase in soma perimeter, and increase in dendritic extent.
- Reduced dendritic spine density at 14 DIV.
- Spine morphology alterations showing a decrease in the number of thin spines
- Progressive increase in phosphorylation of endogenous tau throughout neuronal maturation.
- Deficit in mitochondrial markers in 14 DIV neurons, indicating a loss of mitochondria.
- No alterations in mitophagy through mTOR signalling compared to WT neurons, indicating that the observed mitochondrial deficit in Tau35 neurons is not due to increased mitochondrial clearance stimulated by the mTOR pathway.

4.3.1 Morphological changes in Tau35 primary neurons

The structural characteristics of individual neurons are critically important to the maintenance of neuronal health since these features determine neuronal functionality with respect to both synaptic integrity and firing properties. Numerous studies have demonstrated pervasive and significant changes in neuronal morphology in AD and other neurodegenerative diseases (Anderton et al., 1998; Falke et al., 2003; Knobloch and Mansuy, 2008; Tackenberg and Brandt, 2009; Giannakopoulos et al., 2009a).

The Sholl analysis of Tau35 neurons undertaken here demonstrates a decrease in the complexity of those Tau35 neurites that are located in close proximity to the soma. This analysis also revealed an increase in the maximum dendritic length of Tau35 neurons at 9 DIV. The size of the soma in Tau35 neurons showed a tendency to progressively increase at 3 and 6 DIV, and this increase was significant, compared to WT neurons, by 9 DIV. The mean distance of extension of the dendritic tree was also increased in Tau35 neurons. This may represent a compensatory mechanism (Dickstein et al., 2010; Spires and Hyman, 2004) for the dramatic reduction in spine density that is apparent in Tau35 neurons at 14 DIV.

These results obtained from Tau35 mouse neurons are consistent with the results obtained in another mouse model of AD, the Tg2576 mouse, which overexpresses a mutant form of APP (isoform 695) with the Swedish mutation (KM670/671NL) (Hsiao et al., 1996). Tg2576 mice exhibit significantly increased spatial dendritic extents of cortical neurons at 12 months of age (Rocher et al., 2008). However, Tg2576 exhibit no difference in dendritic structure between transgenic and WT animals in young adult animals of 4 months of age. By 12 months of age, Tg2576 mice start to deposit plaques that lead to elongation of dendritic length. However, by 22 months of age, when amyloid plaques are highly abundant in Tg2576 mouse brain, there is a significant reduction in dendritic length when compared with WT animals (Rocher et al., 2008). In addition, overexpression of mutant tau as found in rTg4510 mice, which inducibly express P301L tau, results in destabilisation of the dendritic cytoskeleton and compromised intracellular trafficking (Hall et al., 2000; 2001).

4.3.2 Spine density reduction in Tau35 primary neurons

In many neurodegenerative disorders, altered neuronal function occurs in parallel with spine loss (Halpain et al., 2005). Spine depletion may lead to cognitive decline and is recognised as an early event preceding neuronal loss. Dendritic spine loss is

observed in the hippocampus and throughout the cortex of the brain in AD, the principal areas affected by AD–related pathology (Walsh and Selkoe, 2004). In Tau35 neurons, there is no overt neuronal loss observed, however, there is a dramatic reduction of more than 30% in the spine density. This is similar to the spine density reduction described in other animal models of tauopathies, such as P301L and rTg4510 mice, both of which express mutant P301L tau, that is associated with the development of frontotemporal dementia (Rocher et al., 2008). This suggests that tau pathology, and particularly Tau35 expression, may be directly involved in the loss of dendritic spines.

In addition, spines are divided into three basic morphological subtypes; spines with no necks and a stubby-like appearance (‘stubby spines’), spines with small necks and large, often complex, and irregular heads (‘mushroom spines’), and spines with thin necks and small heads (‘thin spines’). In Tau35 neurons, the reduction in dendritic spines has a trend to occur, but not significantly, in ‘mushroom’ spines, and significantly less in ‘thin’ spines. Literature indicates that ‘mushroom’ spines are responsible for memory formation, whereas ‘thin’ spines are responsible for the ability to learn (Yuste and Bonhoeffer, 2004).

4.3.3 Increased phosphorylation of endogenous tau in Tau35 primary neurons

Phosphorylation is the most commonly described post-translational tau modification and tau contains 85 potential serine, threonine and tyrosine phosphorylation sites, of which more than half have been reported to be phosphorylated in AD brain (Hanger et al., 2009). Increased phosphorylation is a major hallmark of tauopathies that is involved in the self-aggregation of tau. Tau phosphorylation decreases tau binding to microtubules, thereby reducing microtubule stability and allowing the detached tau to undergo self-aggregation (Köpke et al., 1993; Bergen et al., 2000). Tau35 neurons exhibit increased phosphorylation of endogenous tau, as evidenced by elevated

phosphorylation of Ser396/Ser404 and a decrease in dephosphorylated Ser195/Ser198/Ser199/Ser202. Tau phosphorylation is tightly controlled by the balance between protein kinases and phosphatases (Hanger et al., 2009) and many tau phosphorylation sites have been identified as targets of GSK-3 (Hanger et al., 2007). Overactivation of GSK-3β has been reported to contribute to tau phosphorylation in AD brain (Pei et al., 1997). In Tau35 neurons, the amount of phosphorylated GSK-3β shows a tendency to decrease with a concomitant increase in tau phosphorylation throughout neuronal maturation in culture, whereas GSK-3α is unchanged. This finding suggests a selective increase in the activity of GSK-3β in neurons that parallels the elevation of tau phosphorylation in Tau35 neurons.

Elevated tau phosphorylation both detaches tau from microtubules and induces tau missorting from axons into the somatodendritic compartment of neurons (Ittner et al., 2009; Hoover et al., 2010) Such changes in the normal localisation of tau result in compromised axonal microtubule integrity, synaptic dysfunction and potentially spine loss, as is also observed in Tau35 neurons.

4.3.4 Mitochondrial deficit in Tau35 primary neurons

Mitochondrial distribution and trafficking may be key determinants for both the generation and the long-term maintenance of the complex neuronal morphologies essential for brain information processing (MacAskill and Kittler, 2010; Cai et al., 2012). Investigation of mitochondrial dynamics and trafficking in Tau35 and WT neurons is described in Chapter 2.

Tau dysregulation may also lead to mislocalisation of organelles due to disrupted trafficking along microtubules. Indeed, alterations in mitochondrial dynamics compromise synaptic function (MacAskill and Kittler, 2010), and loss of mitochondria or defective mitochondrial trafficking has been associated with the development of

neurodegenerative disease (MacAskill and Kittler, 2010; Cai et al., 2012). Tau35 neurons demonstrated a noticeable decrease in mitochondrial markers located on both the outer and inner membranes of mitochondria. However, rapamycin treatment showed no induction in mitophagy in Tau35 neurons. This might indicate that the remaining mitochondria in Tau35 neurons are not necessarily damaged and therefore they do not require to be cleared from the neurons. Based on this evidence, the reduction in the mitochondrial load in Tau35 neurons appears likely to be due to reduced mitochondrial biogenesis, rather than to increased mitophagy. This is further described in Chapter 5. However, mitochondrial clearance could be performed via an mTOR-independent pathway, and therefore, further investigation of the mitochondrial status of Tau35 neurons is required.

4.3.5 Conclusions

Tau35 neurons demonstrate normal survival rate and no overt neuronal loss, at least up to 14 days in culture. However, Tau35 neuronal morphology undergoes significant alterations throughout maturation and aging of the neurons, including enlarged soma size, increased dendritic length and a dramatic spine loss. These changes could be due to the evident increase in tau phosphorylation that might be facilitated by a disruption to the balance of kinase and phosphatase activities, including a selective increase in GSK3β activity. Elevated tau phosphorylation affects the trafficking of essential cellular organelles such as mitochondria. The mitochondrial deficit apparent in both Tau35 neurons (Chapter 4) and in Tau35 mouse brain (Chapter 3), which would result in a reduced energy supply, could be the primary cause of the spine loss observed in Tau35 neurons. Together, these pathological changes induced by Tau35 expression could therefore lead to the progressive loss of cognitive function and the development of tau pathology found in Tau35 mice (Bondulich et al., 2016).

Chapter 5: Investigating mitochondrial dynamics and function in Tau35 neurons

5.1 Introduction

In previous chapters, mitochondrial deficit was demonstrated in aged Tau35 mouse brain (chapter 3 Section 3.2.5) and in mature 14 DIV Tau35 primary cortical neurons (chapter 4 Section 4.2.6). Past research shows that mitochondrial deficit and dysfunction can have severe consequences on neuronal function and structure. It has been demonstrated that metabolic deficit caused by mitochondrial alterations alone is sufficient to lead to neurological diseases. Further, it has been shown that abnormal mitochondrial dynamics may contribute to mitochondrial dysfunction and neurodegeneration. Impaired axonal transport in particular has been implicated as a prominent early feature of several major neurodegenerative diseases including AD and ALS (De Vos et al., 2008; Vande Velde et al., 2011; Xie et al., 2015). In addition, highly phosphorylated and mutant tau (P301L) disrupts mitochondrial transport in neuronal cells (Rodriguez-Martin et al., 2016; Shahpasand et al., 2012), implicating the involvement of tau in mitochondrial kinetics.

However, the detailed mechanisms underlying abnormal mitochondrial dynamics in AD have not yet been fully determined. It is known that there is a strong interplay between mitochondrial trafficking and mitochondrial fission and fusion allow the exchange of mitochondrial proteins, which is essential for viability of mitochondria in neurons (Wang et al., 2009). Mitochondrial fusion involves outer and inner membranes and is regulated by large GTPase proteins such as mitofusin 1 (MFN1) for mitochondrial outer membrane fusion, and optic atrophy protein (OPA1) for mitochondrial inner membrane fusion (Santel and Fuller, 2001). In turn, a key regulator in the mitochondrial fission process is dynamin-related protein1 (DRP1), a

large GTPase mainly located in the cytosol. Studies that knock down either Opa1 or MFN1 or overexpress DRP1 lead to decreases in spine density, and mitochondrial deficits in hippocampal neurons (Chen et al., 2007; Wang et al., 2009).

In neurons, mitochondrial biogenesis is a dynamic process mainly occurring in the soma, whereby new mitochondria are formed by growth and division of pre-existing mitochondria. Peroxisome proliferated receptor-gamma coactivator-1alpha (PGC-1α) is considered to be a master regulator of mitochondrial biogenesis through its interaction with the key nuclear transcription factors, NRF1 and NRF2. Two major pathways that regulate mitochondrial biogenesis are the AMP-activated kinase (AMPK)-PGC-1α and sirtuin 1 (SIRT1)-PGC-1α signalling pathways. AMPK can either directly phosphorylate PGC-1α or activate SIRT1 by increasing NAD^+ levels. Activated SIRT1 stimulates mitochondrial biogenesis through de-acetylation and, therefore, activation of PGC-1α.

Furthermore, there is constant turnover of mitochondria which is necessary for maintenance of healthy functional neurons (Miller, 2004). Mitochondrial homeostasis is controlled by synchronised fission and fusion machinery, mitochondrial transport and anchoring, mitochondrial biogenesis, and mitophagy. Thus, studying mitochondrial function, transport and dynamics is important to understand disease-causing mechanisms in neurodegenerative disease. This chapter provides a detailed examination of the characteristics of mitochondria in primary cortical neurons derived from embryonic WT and Tau35 mice. The results provide a possible explanation of the dysfunction of several of mitochondrial processes that are associated with neurodegenerative disorders.

5.2 Results

5.2.1 Reduced numbers of mitochondria in neurites of Tau35 primary cortical neurons

Live imaging was used to investigate mitochondrial dynamics in WT and Tau35 neurons in real time. Primary cortical neuronal cultures were selected as a model to study mitochondrial function and dynamics because the cell soma is easily identified, and the neurites adhere closely to the substrate, allowing visualisation in a single plane. This allows distinction of the cell body from the periphery of the neurons, and therefore, the directionality of mitochondrial movement can be readily determined. Moreover, the mitochondria in neurites are separated from the reticulum and exist as separate entities, allowing investigation of mitochondrial shape and dynamics. Primary neurons were co-transfected with DSRedMito and eGFP at 7 DIV to visualise the mitochondria and to identify the neuronal outline, respectively. Neurites of cultured WT and Tau35 neurons were imaged at 9 DIV (Fig. 5.1A). The images of neurites were straightened (Fig. 5.1B) and mitochondrial density (number of mitochondria/20μm neurite length) in Tau35 and WT neurites was determined using ImageJ as described in Chapter 2, Section 2.2.15. WT neurons harboured 2.6 ± 0.19 mitochondria/20 μm neurite length (mean ± S.E.M, n=47). In contrast, the number of mitochondria in Tau35 neurites was 1.7 ± 0.13 mitochondria/20 μm (mean ± S.E.M., n=47), which was significantly reduced ($P<0.001$, Student's t-test) compared to WT neurons (Fig. 5.1C). The frequency distribution of the mitochondria in neurites shows that approximately 42% of Tau35 neurons have only 1 mitochondrion per 20 μm, whereas only 16% of WT neurons have such a low density of mitochondria (Fig. 5.1D). There are also noticeably less (<20%) neurites with 3 or more mitochondria per 20 μm of neurite length in Tau35 neurons compared to WT neurons (~50%; Fig. 5.1D). Thus, expression of Tau35 results in a substantial reduction of 35% in the number of mitochondria present in neurites of cultured neurons.

Fig. 5.1 Reduced mitochondrial number in neurites of Tau35 primary cortical neurons

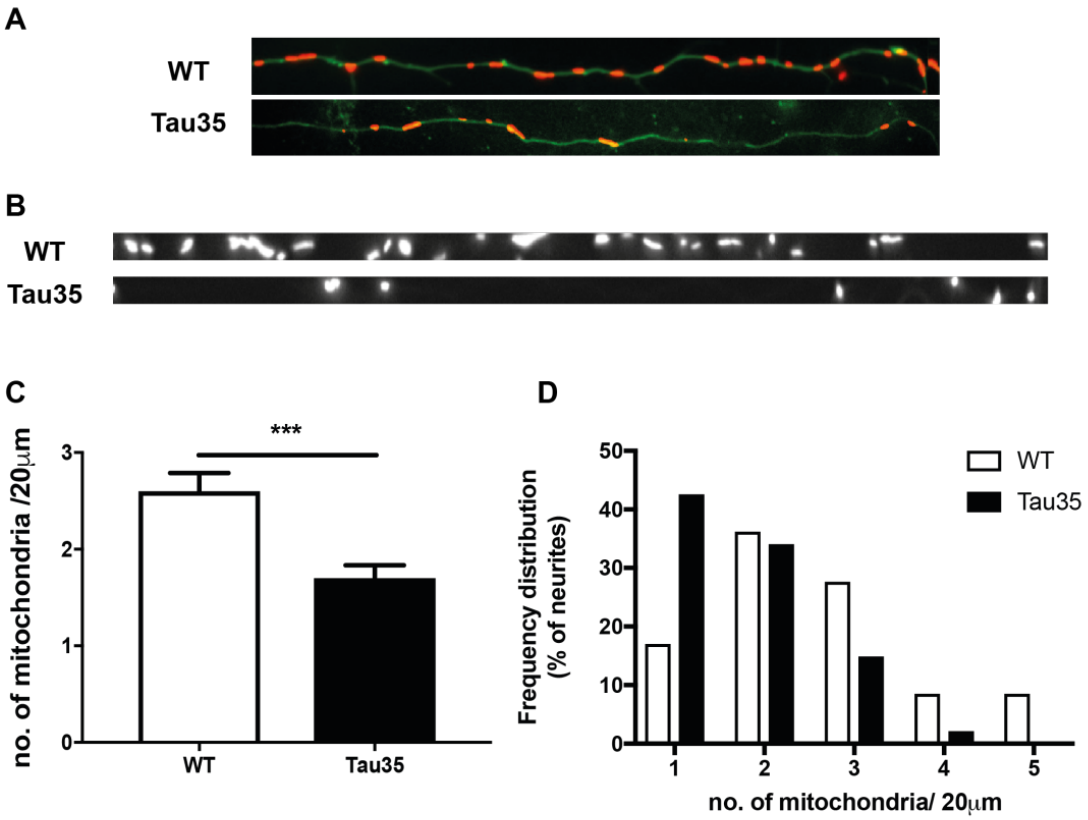

A Representative images of neurites from WT and Tau35 primary cortical neurons imaged at 9 DIV after co-transfection with plasmids expressing DSRedMito (red) and eGFP (green). **B** Straightened images of the neurites. **C** Quantitative analysis confirms a deficit in the number of mitochondria in Tau35 compared to WT neurites. Values are displayed as mean ± S.E.M., ***P<0.001, Student's t-test. **D** Graph shows the frequency distribution of mitochondria in Tau35 compared to WT neurites. 45-57 neurons were analysed per genotype from four biological replicates.

5.2.2 Increased proportion of retrograde mitochondrial movement in Tau35 neurons

The number of motile mitochondria has been shown to progressively reduce with maturation of cultured neurons, partially as a result of presynaptic immobilisation (Lewis et al., 2016). Therefore, 9 DIV was selected as the optimal time in culture to investigate mitochondrial movement. At 9 DIV, in healthy neurons approximately 25% of total mitochondria is mobile at any given time (Lewis et al., 2016). Exogenous expression of DSRedMito and eGFP allows visualisation of mitochondria, as well as identification of cellular compartments to provide information about the directionality of mitochondrial movement. Live images of co-transfected neurons were acquired at 3 s intervals for 5 min. The recordings were then transformed into kymographs as described in chapter 2 Section 2.2.15 to determine the distance moved by individual mitochondria over time (Fig. 5.2A). The kymographs confirmed the original observation of fewer mitochondria in Tau35 neurites and were used to determine the proportion of motile mitochondria in each neuronal type. This analysis revealed that approximately 75% of mitochondria were stationary in the neurites of both WT and Tau35 primary cortical neurons cultured for 9 DIV (Fig. 5.2B), in agreement with a previous report of neuronal mitochondrial motility *in vitro* (Lewis et al., 2016). These results suggest that, although fewer mitochondria were present in neurites of Tau35 neurons, the proportion of moving mitochondria is not affected by Tau35 expression.

Fig. 5.2 The proportion motile mitochondria is unaffected by Tau35 expression in neurons

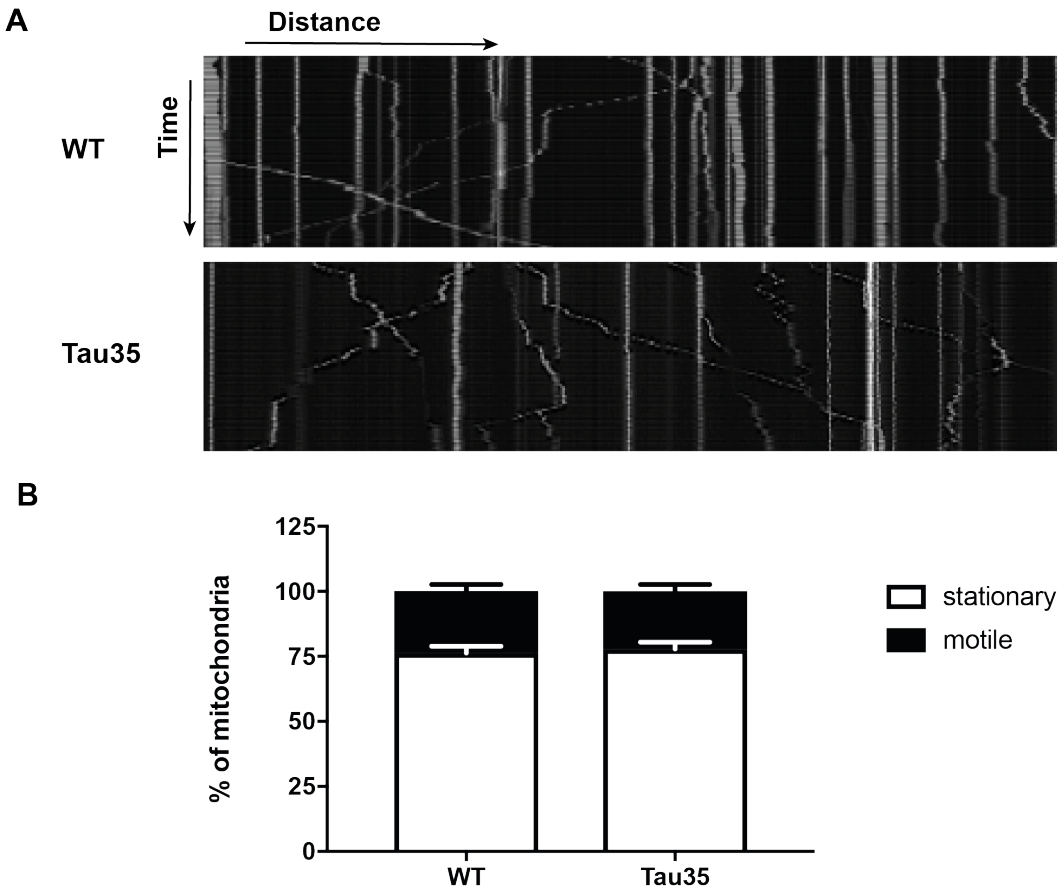

A Representative kymographs demonstrating the movement of mitochondria in WT and Tau35 neurons. **B** Bar chart showing the percentage of motile and stationary mitochondria in WT and Tau35 neurons. Values are displayed as mean ± S.E.M., Mann-Whitney test. 40-54 neurons were analysed per genotype from four biological replicates.

Further analysis of mitochondrial movement on the kymographs, revealed differences in the directionality of mitochondria in neurons of each genotype. Of the motile WT mitochondria, 48 ± 4% (mean ± S.E.M., n=47) were moving in an anterograde direction and 54 ± 4% (mean ± S.E.M., n=54) were moving towards the soma (Fig. 5.3A). In contrast, in Tau35 neurons, 37 ± 5% (mean ± S.E.M., n=40) of mitochondria moved in an anterograde direction and the proportion moving in a retrograde direction increased to 60 ± 4% (mean ± S.E.M., n=49) (Fig. 5.3A). Thus, despite there being equivalent proportions of motile mitochondria neurites of both genotypes, Tau35 expression significantly increased the fraction of mitochondria moving back towards the soma ($P<0.05$, Mann Whitney).

Analysis of the frequency of distribution of mitochondria in the neurites shows that WT neurites with around 50% retrograde-moving mitochondria are most frequent while Tau35 neurons shows a bimodal distribution, with mitochondria moving predominantly either 50% or 100% retrograde (Fig. 5.3B left). In addition, 27% of Tau35 neurites have mitochondria exclusively moving in a retrograde direction, in contrast with only 12% of WT neurites. Further, 30% of Tau35 neurites have no mitochondria moving in an anterograde direction, compared to only 10% of WT neurites.

Fig. 5.3 Mitochondria in Tau35 neurons demonstrate a preference towards retrograde movement

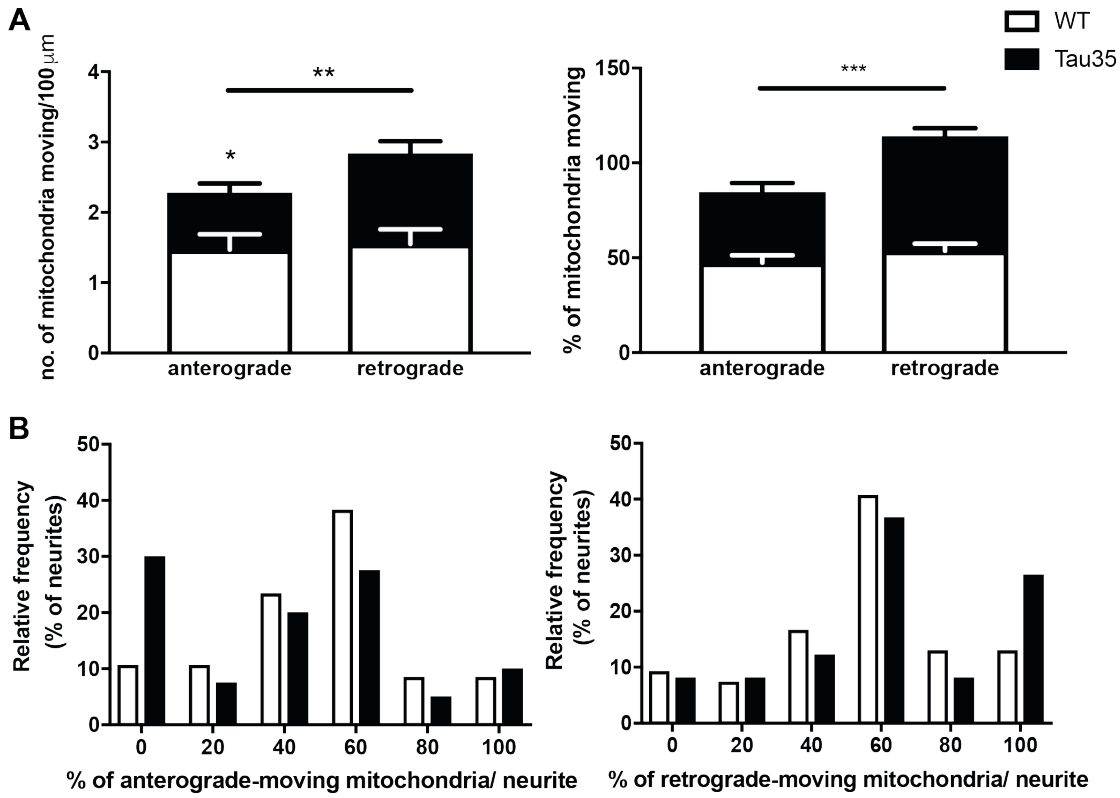

A Bar charts illustrating the numbers (left) and proportions (right) of mitochondrial movement in WT and Tau35 neurites. Graph on the left shows that number of mitochondria moving in the anterograde direction is reduced in Tau35 neurons compared to WT neurons (*P<0.05). Furthermore, number of retrograde moving mitochondria in Tau35 neurons is increased compared to anterograde moving mitochondria in Tau35 neurons (**P<0.005). The graph on the right, shows that higher proportion of mitochondria are moving in the retrograde direction in Tau35 neurons (***P<0.001). **B** Graphs show frequency distributions of mitochondria in Tau35 neurites compared to WT neurites with percentages of mitochondria moving in anterograde (left panel) and retrograde (right panel) directions. 40-54 neurons were analysed per genotype from four biological replicates. Values are displayed as mean ± S.E.M., *P<0.05, **P<0.005, ***P<0.001, Mann-Whitney test.

The kymographs generated in ImageJ were used to investigate the overall and directional velocities and the distances travelled by individual mitochondria in WT and Tau35 neurites. The mean velocity of motile mitochondria in both WT and Tau35 neurons was 0.2 μm/s (Fig. 5.4A). The anterograde velocity of WT mitochondria was 0.3 ± 0.03 μm/s (mean ± S.E.M, n=30), which was similar to that of Tau35 mitochondria (0.28 ± 0.03 μm/s, mean ± S.E.M, n=49). However, the mean velocity of mitochondria moving in the retrograde direction in Tau35 neurons (0.32 ± 0.02 μm/s, mean ± S.E.M, n=44) was significantly increased ($P<0.05$) compared to that of motile WT mitochondria (0.26 ± 0.02 μm/s, mean ± S.E.M, n=74) (Fig. 5.4B). In addition, the distance travelled by individual mitochondria (run length) was assessed in neurons of both genotypes. The mean run length of mitochondria was approximately 40 ± 2.2 μm (mean ± S.E.M, n=121) in WT neurites (Fig. 5.4C), which was not significantly different ($P>0.05$, Student's t-test) from that of Tau35 neurites (39 ± 3.2 μm, mean ± S.E.M, n=69). However, upon classification of directionality, WT mitochondria exhibited anterograde and retrograde run lengths of 48 ± 5.2 μm (mean ± S.E.M, n=48) and 38 ± 2.4 μm (mean ± S.E.M, n=74), respectively, a ratio of 1.26 in favour of the anterograde direction. In contrast, the run lengths of Tau35 mitochondria were 36 ± 5.2 μm (anterograde, mean ± S.E.M, n=29) and 48 ± 5.7 μm (retrograde, mean ± S.E.M, n=74), a ratio of 1.33 in favour of the retrograde direction. This analysis revealed a statistically significant increase ($P<0.05$, Student's t-test) in the run length of retrograde moving mitochondria and a trend towards a decreased run length of anterograde-moving mitochondria in Tau35 neurites ($P>0.05$, Student's t-test).

Fig. 5.4 Retrograde mitochondrial velocity and run length is selectively increased in Tau35 neurites

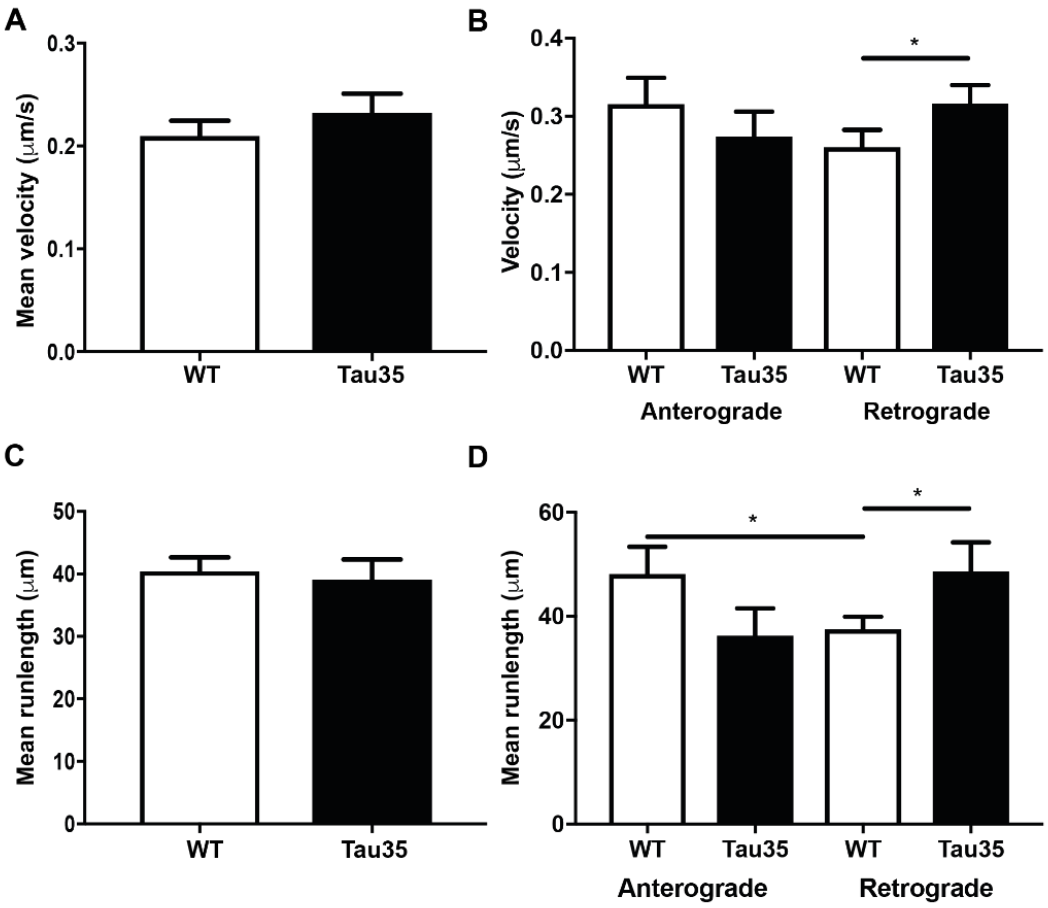

Graphs showing **A** mean overall and **B** directional velocities (μm/s) of motile mitochondria in WT and Tau35 neurites. The mean overall **C** and directional **D** run lengths (μm) of individual mitochondria in WT and Tau35 neurites. Mitochondrial velocities and run lengths were measured at 9 DIV. Values are displayed as mean ±S.E.M., *P<0.05, Mann-Whitney test. 30-74 neurons were analysed per genotype from four biological replicates.

5.2.3 Investigation of motor proteins that facilitate mitochondrial motility

To further investigate mitochondrial motility, dynactin and kinesin 5A, both of which are motor proteins involved in axonal transport of organelles, were assessed on western blots. Dynactin binds to the retrograde motor protein dynein, facilitating retrograde movement. In contrast, kinesin 5A is mitochondrial-associated, exclusively neuronal, motor protein that facilitates anterograde movement. Western blots of 9 DIV Tau35 neuronal lysates indicated similar amounts of dynactin (relative to β-actin), which appeared as a doublet of 150 kDa, in WT and Tau35 neurons. Comparable amounts of kinesin 5A, relative to β-actin, were also present in WT and Tau35 neurons (Fig. 5.5). The lack of effect of Tau35 on proteins involved in mitochondrial movement suggests that the observed increase in retrograde mitochondrial flux in Tau35 neurons is not due to differential interaction with motor proteins.

Fig. 5.5 The amounts of the proteins involved in mitochondrial movement are not affected in Tau35 neurons

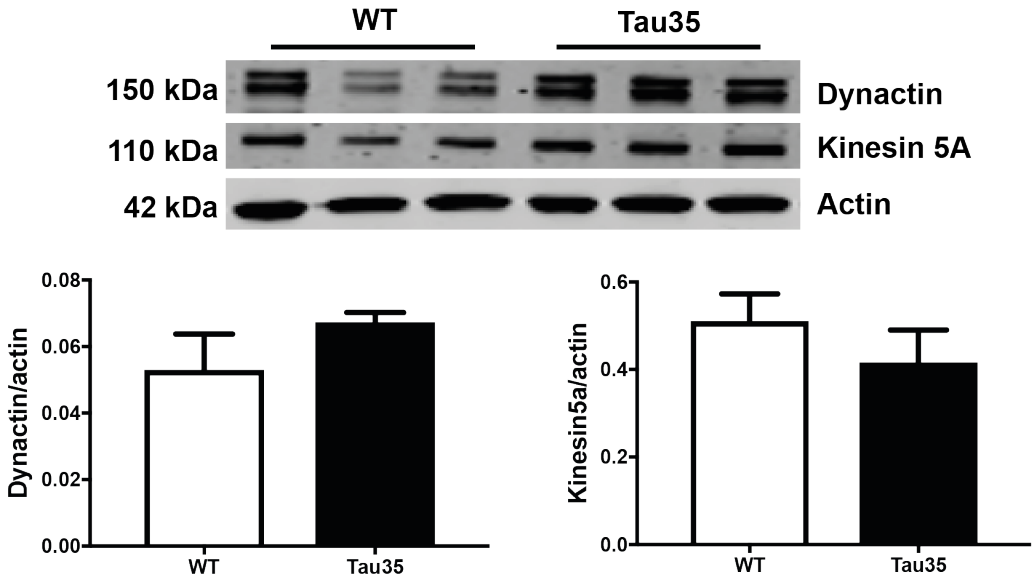

A Western blots of the motor proteins dynactin and kinesin 5A, and β-actin in WT and Tau35 neuronal lysates at 9 DIV. **B** Bar charts quantifying the amounts of dynactin and kinesin 5A, relative to β-actin, in WT and Tau35 neurons. Values are displayed as mean ± S.E.M., Student's t-test n=5 biological replicates. Molecular weight markers (kDa) indicate the size of the protein of interest.

5.2.4 Mitochondrial shape is not altered in Tau35 cortical neurons

Changes in the size or shape of mitochondria could indicate abnormalities in fission and/or fusion, as well as malfunction of mitochondria. The “particle analysis” function of ImageJ (https://imagej.nih.gov/ij/) was used to assess mitochondrial shape in the digitally straightened images of neurites obtained from live recordings of mitochondrial mobility. The area of the mitochondria in WT neurites was 3.3 ± 0.3 μm^2 (mean ±S.E.M. n=55), which was similar to that of Tau35 mitochondria (3.4 ± 0.4 μm^2, mean ± S.E.M, n=53, P>0.05; Students’s t-test)

The measure of circularity indicates if the value is closer to 1, mitochondria are more rounded or less than 1, it is more elongated. Larger, more elongated mitochondria are assumed to be healthier than smaller, more rounded mitochondria, which may be fragmented and destined for degradation. In the case of Tau35 mitochondria, the circularity appears to be equivalent to that of WT mitochondria, indicating that they are not fragmented (Fig. 5.6B). The orientation of mitochondria within neurites, determined by the “angle”, was also similar in WT and Tau35 neurons (Fig. 5.6C). Furthermore, the major and minor axes of the mitochondria were unchanged in Tau35, compared to WT neurons (Fig. 5.6D). These results indicate that the shape and orientation of mitochondria in the neurites is not altered in Tau35 neurons compared to WT neurons.

Fig. 5.6 Mitochondria area, circularity, angle and axes are unaffected in Tau35 neurons

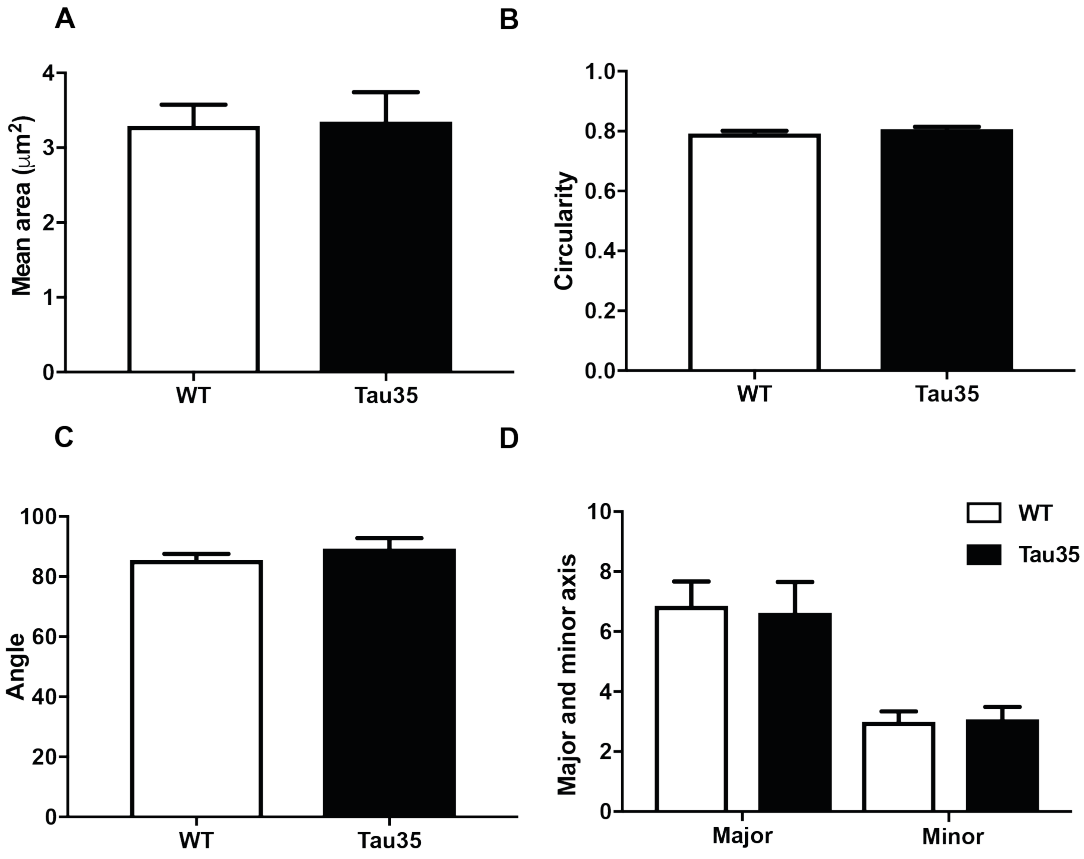

Graphs illustrating the results of the morphological analyses of mitochondria in WT and Tau35 cortical neurons at 9 DIV. **A** Mean area (μm^2) **B** Circularity **C** Angle (orientation within the neurite), and **D** Major and minor axes of the mitochondria remain. Values are displayed as mean ±SEM. Mann-Whitney test. 40-54 neurons were analysed per genotype from four biological replicates.

5.2.5 Mitochondrial fission and fusion is not altered in Tau35 cortical neurons

Mitochondrial shape is strongly dependent on the dynamics of mitochondrial fission and fusion. Thus, increased fission results in larger numbers of small mitochondria and elevated fusion increases mitochondrial length. Mitochondrial fusion is regulated by optic atrophy protein (OPA1) for mitochondria inner membrane fusion and mitofusin 1 (MFN1) for mitochondrial outer membrane fusion (Santel and Fuller, 2001). The key regulator of mitochondrial fission is the cytosolic protein, dynamin-related protein1 (DRP1, (Smirnova et al., 2001). Post-translational modifications to DRP1 such as phosphorylation can alter its activity and affect the rate of fission. Quantitation of the amounts of the fusion-related proteins OPA1 (100 kDa) and MFN1 (86 kDa) on western blots of neuronal lysates demonstrated no significant differences, relative to β-actin (42 kDa), between WT and Tau35 neurons (Fig. 5.7A). Similarly, Fig. 5.7B shows no changes in the amounts of DRP1 (80 kDa), or the pDRP1 (80kDa) to DRP1 ratio, in Tau35 neurons compared to WT neurons at 9 DIV. These results, together with the shape analysis shown in Fig. 5.7, indicate that mitochondrial fission and fusion are not impaired in Tau35 neurons.

Fig. 5.7 Markers of mitochondrial fusion and fission are not affected in Tau35 neurons

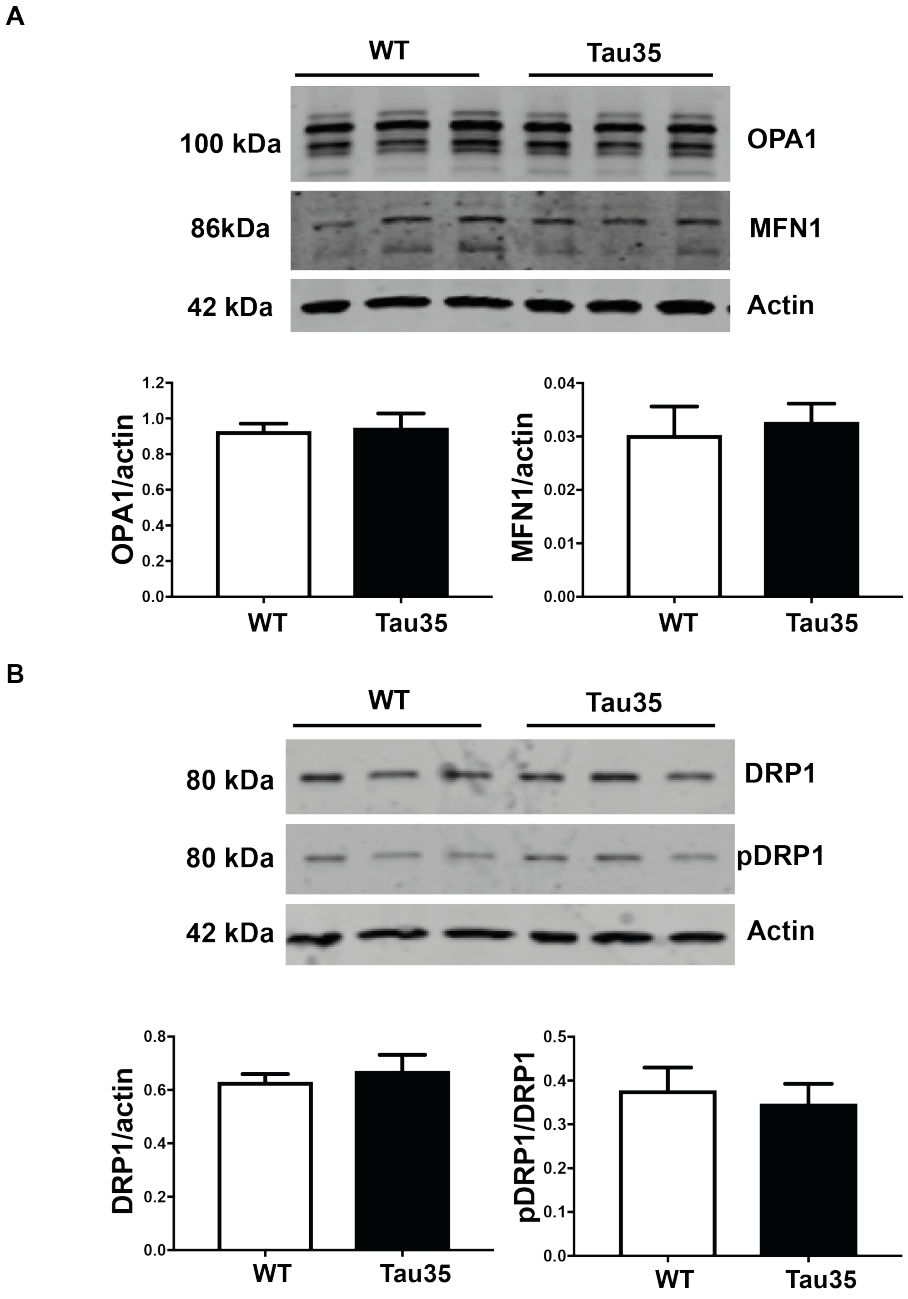

Western blots of 9 DIV WT and Tau35 neuronal lysates probed with antibodies to **A** OPA1, MFN1, and β-actin, and **B** Total DRP1, phosphorylated DRP1, and β-actin. Bar charts show the quantitation of the mitochondrial fusion and fission proteins, relative to β-actin. Values are displayed as mean ±SEM. Student's t-test n=5 biological repeats. Molecular weight markers (kDa) indicate the size of the protein of interest.

5.2.6 Investigation of mitochondrial function in Tau35 cortical neurons

To determine whether the function of mitochondria is affected by expression of Tau35 in cortical neurons, mitochondrial stress was assessed using the Seahorse XF assay of extracellular flux (Agilent). In this assay, the oxygen consumption rate (OCR) of neurons is measured under baseline, inhibited, and maximal conditions, as described in Chapter 2, Section 2.2.17. The effects of the expression of the Tau35 fragment on cellular oxygen consumption rate in 9 DIV cortical neurons are shown in Fig. 5.8. Cells were seeded at 1,250 cells/mm^2. Each well was loaded with 2 µM of oligomycin, 1 µM FCCP and 0.5 µM antimycin A/rotenone in ports A, B and C, respectively.

Tau35 neurons exhibited a baseline OCR that was slightly lower than, but not significantly different from that of WT neurons. Inhibition of ATP synthase using oligomycin resulted in a similar reduction of OCR in both WT and Tau35 mitochondria, indicating that WT and Tau35 neurons are equally capable of generating enough ATP to meet the energetic needs of the cell. There was also no evidence of a potential proton leak, as an indication of mitochondrial damage with oligomycin in Tau35 mitochondria. Maximal OCR, driven by the mitochondrial uncoupler FCCP, showed that Tau35 neurons exhibit a slightly reduced respiratory maximum compared to WT neurons, although this change was not statistically significant (Fig 5.8). Antimycin A/rotenone eliminates mitochondrial respiration, resulting in a measure of non-mitochondrial respiration, which was equivalent in WT and Tau35 neurons (Fig. 5.8). These findings of reduced respiratory function in Tau35 neurons suggests the possibility of impaired mitochondrial function due to expression of Tau35.

Despite a significant decrease (~35%) in mitochondrial numbers in Tau35 neurites (Fig. 5.1), the decrease in respiratory capacity of Tau35 neurons was fairly modest (~15%). This could be due to variability in respiratory capacity in neurons derived from

male and female animals. A study by (Du et al., 2009) demonstrated that male neurons are more vulnerable, where a decrease in mitochondrial respiration was seen to be more profound in males versus females when exposed to stress, such as starvation or disease. In addition, the expression cassette with the Tau35 cDNA is positioned on the X chromosome and protein levels differ between male and female mice, as shown in Chapter 3.

Fig. 5.8 Oxygen consumption rates in Tau35 and WT neurons

-

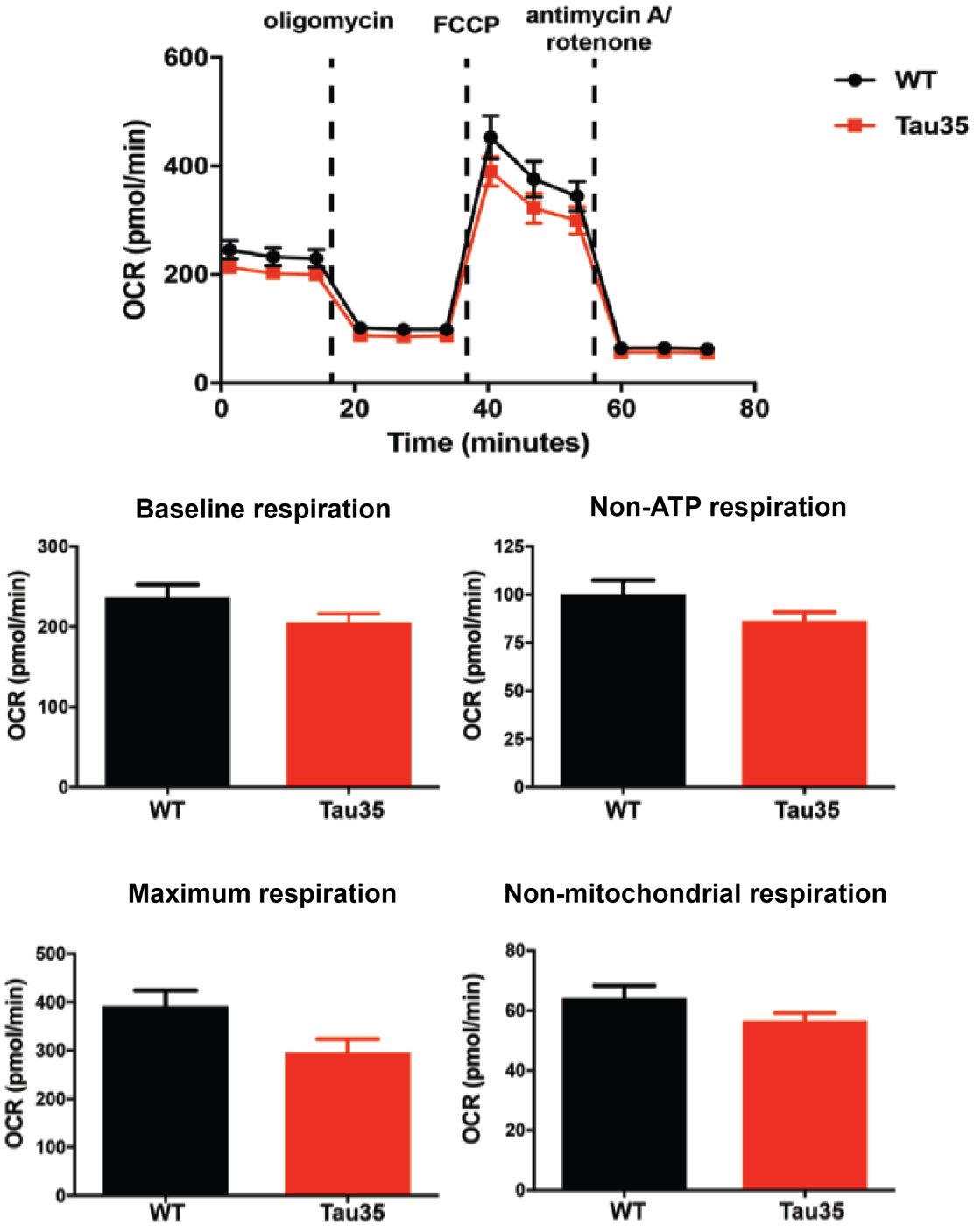

Fig. 5.8 legend

Graph illustrating the oxygen consumption rate (OCR) of WT and Tau35 cortical neurons at 9 DIV, 2way ANOVA. The bar charts below show OCR values upon the addition of the compounds in WT and Tau35 neurons. Basal respiration is slightly reduced, but not significantly, in Tau35 neurons compared to WT ($P>0.05$). Oligomycin is an ATP synthase inhibitor that allows to measure basal respiration that is not coupled to ATP production (WT vs Tau35, $P>0.05$). The uncoupler FCCP, drives the cell to maximum respiratory capacity (WT vs Tau35, $P>0.05$). Non-mitochondrial respiration is measured by addition of antimycin A/rotenone (WT vs Tau35, $P>0.05$) Student's t-test. The values shown are mean $\pm$ S.E.M., WT (black), n=3; Tau35 (red), n=8.

5.2.7 Reduced marker of mitochondrial biogenesis in Tau35 neurons

To investigate whether reduced mitochondrial biogenesis might explain the observed decrease in mitochondria in Tau35 cortical neurons at 9 DIV (Fig. 5.9), components of this pathway were investigated. (Chapter 1, Section 1.14.3) The steady-state amounts of PGC-1α, SIRT1, CREB, pCREB, and NRF2 were assessed on western blots.

Fig. 5.9 illustrates that the amount of PGC-1α, relative to β-actin, is significantly decreased (~25%) in Tau35 neurons ($P<0.05$, Student's t-test).

Fig. 5.9 PGC-1α is reduced in Tau35 neurons

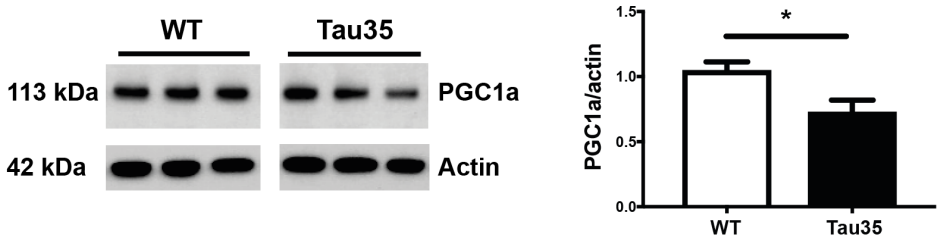

Western blot of WT and Tau35 primary cortical neurons (9 DIV) probed with antibodies to PGC-1α. The values shown are mean ± S.E.M., *P<0.05, n=6 Student's t-test.

PGC-1α activity is regulated by the histone deacetylase sirtuin 1 (SIRT1), which mediates NAD^+-dependent deacetylation of PGC-1α. Therefore, the amount of SIRT1 in WT and Tau35 neurons was assessed on western blots to determine whether the reduction of PGC-1α in Tau35 neurons results from altered expression of SIRT1 (Fig. 5.10). A 33% decrease of SIRT1 relative to β-actin, was observed in Tau35 primary neurons (P<0.05, Student's t-test), possibly explaining the reduction of PGC-1α levels and indicating a potential reduction in PGC-1α activity (Fig. 5.10A, upper panel). PGC-1α also affects expression of NRF2, which regulates electron transport, oxidative phosphorylation and mitochondrial DNA replication (Chapter 1, section1.14.3). Therefore, the amount of NRF2 in WT and Tau35 neurons was determined relative to β-actin, on western blots (Fig 5.10). These results showed that NRF2 was significantly

decreased by 50% in Tau35 neurons ($P<0.05$, Student's t-test), further supporting a potential defect in mitochondrial biogenesis induced by expression of Tau35. In addition, protein levels of total CREB and phosphorylated CREB were measured (Fig. 5.10B). This protein is a key regulator of multiple cellular processes including mitochondrial biogenesis via activation of PGC-1α.

Fig. 5.10 SIRT1 and NRF2 are decreased in Tau35 neurons

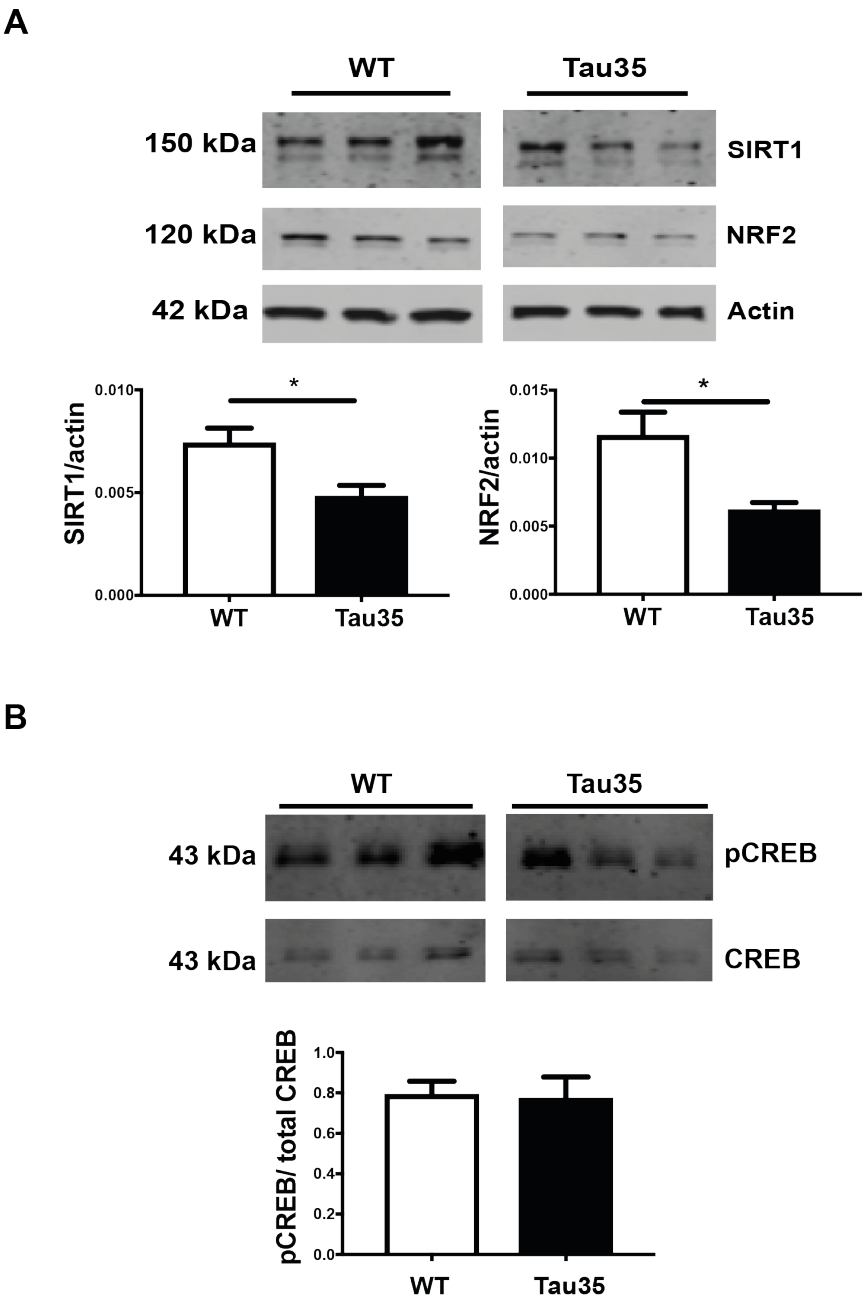

Western blots and analyses of **A** sirtuin 1 (SIRT1) and nuclear factor erythroid 2-related factor 2 (NRF2), and **B** total and phosphorylated cAMP responsive-element binding protein (CREB), relative to actin, in Tau35 and WT cortical neurons. Neurons were assessed at 9 DIV. Values are displayed as mean ±S.E.M., n=6, *P<0.05, Student's t-test.

5.3 Discussion

This chapter describes the results of an investigation into the effects of Tau35 on mitochondrial motility, dynamics, function, and biogenesis in primary cortical neurons cultured for 9 DIV. The results show that expression of the N-terminally truncated WT human tau fragment, Tau35, in mice leads to significant changes in the mitochondria in cultured neurons. These important changes can be summarised as follows:

- Reduction in the number of mitochondria present in neurites.
- Augmented retrograde movement of mitochondria, evidenced by increases in both the velocity and the run length of mitochondria moving towards the neuronal cell soma.
- No overt changes in mitochondrial fission and fusion, suggesting that these processes are unlikely to contribute to altered mitochondrial trafficking.
- Potentially impaired mitochondrial functionality, particularly maximal respiratory capacity.
- Decrease in essential components of the mitochondrial biogenesis pathway.

5.3.1 Mitochondrial deficit in the neurites of Tau35 primary neurons

Tau35 primary cortical neurons demonstrate a decrease in mitochondria in neurites at 9 DIV. These data correlate with the finding of reduced amounts of mitochondrial proteins in Tau35 mouse brain and in primary cortical neurons cultured from Tau35 mice (Chapter 3, Section 3.2.5 and Chapter 4, Section 4.3.4, respectively). Studies in human brain have previously suggested that reduced brain metabolism and/or mitochondrial dysfunction are major hallmarks and prominent early features in the brain in many neurodegenerative diseases including AD, PD and HD (Kopeikina et al., 2011; Lin and Beal, 2006) At first glance, mitochondrial deficits in the neurites of Tau35 neurons are likely to result from an overall reduction in mitochondria due to mitophagy or altered biogenesis. However, deficits in mitochondria present in neurites

in other tau transgenic mice have suggested that such deficits may be due to the mislocalisation of mitochondria and clustering of mitochondria in the perinuclear area of neurons (Kopeikina et al., 2011; Dubey et al., 2008; Mandelkow et al., 2004). For example, rTg4510 and P301L tau transgenic mice, both of which express P301L tau, demonstrate aberrant distribution and/or a decrease in the area occupied by mitochondria in neurites (Kopeikina et al., 2011; Rodriguez-Martin et al., 2016). In rTg4510 mice, the mitochondrial deficit may be caused by soluble tau species as these changes are not dependent on tau aggregation and are fully recovered by suppression of soluble tau. Expression of soluble tau leads to the accumulation of mitochondria around the nucleus due to diminishing the anterograde to retrograde ratio, leading to reduced net anterograde flux (Kopeikina et al., 2011; Stoothoff et al., 2009). Previous studies of the effects of 3R and 4R tau on mitochondrial transport suggest that 4R tau may have a more profound influence on the competition for kinesin-based transport that diminishes the anterograde to retrograde transport ratio (Stoothoff et al., 2009).

5.3.2 Changes in retrograde movement in Tau35 neurons

The net movement of mitochondria is influenced by the balance between their stationary and motile states (Stewart and Chinnery, 2015). In healthy neurons under physiological conditions, approximately half of all motile mitochondria move in a retrograde direction, and half in an anterograde direction (Verburg and Hollenbeck, 2008). It has been surmised that mitochondria moving in an anterograde direction are healthy, while retrograde-moving mitochondria might represent older, damaged organelles that are being transported to the soma for degradation by mitophagy (Miller, 2004; Cai et al., 2012).

Tau35 primary cortical neurons exhibited alterations in mitochondrial transport that correspond to previously reported disease-related tau models such as rTg4510 and

P301L with impaired localisation and trafficking of organelles (Kopeikina et al., 2011; Rodriguez-Martin et al., 2016). The mitochondria in Tau35 neurons displayed a preference for retrograde movement, suggesting that a larger proportion of the mitochondria in Tau35 neurites may be moving towards the soma for degradation. The velocity of mitochondria travelling in a retrograde direction was also increased in Tau35 neurons, as was their mean retrograde run length. A recent report has shown that the mitochondria anchoring protein, syntaphilin, is strongly correlated with stationary mitochondria, and that the deletion of the syntaphilin (*Snph)* gene in mice dramatically increases mitochondrial motility and reduces their density in axons (Lin et al., 2017). These findings suggest that investigation of syntaphilin, including its association with mitochondria in Tau35 neurons, may be warranted.

5.3.3 Mitochondrial fission and fusion are unlikely to contribute to the mitochondrial deficit in Tau35 neurites

It has previously been shown that mitochondrial fission and fusion might contribute to AD progression (Wang et al., 2009). In Tau35 primary cortical neurons, changes in the size and shape of mitochondria were not observed. These findings are consistent with observations made in other mouse models of tauopathy, such as rTg4510 (Kopeikina et al., 2011) and P301L tau mice (David et al., 2005).

The ability of mitochondria to move along neurites is coupled to the degree to which they fuse together and fragment. However, no differences were detected in the amounts of the mitochondrial fission and fusion proteins OPA1, MFN1 and DRP1, in Tau35 neurons, when compared to those in WT neurons. These results suggest that the observed deficits in Tau35 neurons are unlikely to be due to abnormalities in mitochondrial fission or fusion. A recent study from this laboratory has suggested that western blots may not be sufficiently sensitive to detect very subtle changes in

mitochondrial fission and fusion proteins, as only about 30% of mitochondria are motile in neurons at 7 DIV (Rodriguez-Martin et al 2016).

5.3.4 Decreased mitochondrial biogenesis in Tau35 neurons

PGC-1α is reported to be involved in the pathogenesis of AD (Katsouri et al., 2016; Qin et al., 2009; Sweeney and Song, 2016), and PGC-1α knockout mice exhibit neuronal dysfunction and degeneration (Leone et al., 2005; J. Lin et al., 2004). At 9 DIV, Tau35 neurons demonstrate a significant decrease in the amount of PGC-1α protein compared to WT neurons. There are several potential players involved in the activation of PGC-1α, including SIRT1 and CREB.

SIRT1 has been shown to have neuroprotective function in the brain and a decrease in this protein may lead to age-dependent neurodegeneration. SIRT1 deacetylates and activates PGC-1α, which then induces mitochondrial biogenesis (Araki et al., 2004). Increased NAD^+ biosynthesis and SIRT1 activation have been shown to protect axons against degeneration (Araki et al., 2004). Decreased SIRT1 in Tau35 neurons could, therefore, result in an inactivation of PGC-1α and thereby reduce mitochondrial biogenesis. In addition, SIRT1 is reduced in the cortex in AD and it has been suggested that SIRT1 negatively correlates with the number of neurofibrillary tangles in AD brain (Julien et al., 2009). SIRT1 has been shown to acetylate tau and reduction of this protein leads to prevention of degradation of phosphorylated tau in tauopathies (Min et al., 2010; Cohen et al., 2011). Indeed, SIRT1 has the ability to deacetylate tau, and deficiency of SIRT1 results in an enhancement of both acetylated and phosphorylated tau (Min et al., 2010). Interestingly, the SIRT1 gene resides in a locus on chromosome 10 which is associated with familial AD. It would be interesting to investigate whether the effect of SIRT1 on mitochondrial biogenesis or tau acetylation is a primary event that could potentially contribute to the explanation for the disease-related phenotype in the Tau35 mouse model of tauopathy.

PGC-1α levels are also controlled by transcription factor CREB. It activates the PGC-1α promoter and drives PGC-1a expression (Herzig et al., 2001; Wu et al., 2006). PGC-1α transcription is highly reactive to CREB activation, which occurs through phosphorylation of its Ser133 residue. There appears to be no significant difference in CREB and pCREB levels in Tau35 neurons compared to WT neurons, indicating that in Tau35 neurons, it is unlikely to be the cause of the observed decrease in PGC-1α and potential reduction in mitochondrial biogenesis.

NRF2 is a transcription factor that plays an important protective role against oxidative stress (Dinkova-Kostova and Abramov, 2015). Under conditions of stress, activation of NRF2 counteracts the increased reactive oxygen species production in mitochondria via transcriptional upregulation of uncoupling protein 3 and influences mitochondrial biogenesis by maintaining the levels of NRF1 and PGC-1α (Vomund et al., 2017). NRF2 is downstream from PGC-1α and therefore it is possible that the observed reduction in the amounts of both PGC-1α and NRF2 in Tau35 neurons could lead to a deficit of mitochondrial DNA replication.

5.3.5 Conclusions

The complexity of neuronal morphology means that normal cellular function and survival is highly dependent on the energy provided by mitochondria. Defects in mitochondrial dynamics are becoming increasingly recognised as common and early features that may be responsible for disease progression in a range of neurodegenerative disorders. Taken together, the results presented here demonstrate that mitochondrial dysfunction and particularly, defective mitochondrial biogenesis, plays a key role in the development of tauopathy in Tau35 mice. The findings show that mitochondrial dysfunction is a multifactorial event that may have common therapeutic targets to improve mitochondrial and neuronal function and

prevent neurodegeneration. Primary cortical neurons derived from the Tau35 mouse model of human tauopathies demonstrate their potential as an excellent platform in which to study altered mitochondrial dynamics and function as well as to identify new therapeutic targets for human tauopathies.

Chapter 6: Discussion

6.1 Mouse and cellular models of Tau35-mediated degeneration

A truncated form of tau was detected in PSP brain, but not in age-matched control brain (Wray et al., 2008). This fragment was inserted into an *Hprt* locus located on the X-chromosome in mice and driven by the human *MAPT* promoter, generating a unique and novel mouse model of tauopathy (Bondulich et al., 2016). The benefit of using the human tau promoter is that the tau fragment is expressed at low, physiological levels in regions of the CNS that normally express tau. In other animal models of tauopathies, the promoters that were used are typically not the native gene promoters and are designed to drive higher gene expression than would be observed physiologically (Lewis et al., 2001; Billings et al., 2005). This enables the overexpression of tau in order to elicit an accelerated phenotype of tauopathy, which makes these models less accurate representations of human disease. Unlike other existing mouse models, Tau35 mice express a human WT tau fragment, more accurately representing the sporadic tauopathies, which are more common than familial tauopathy (Goedert and Jakes, 2005). Tau35 mice also exhibit behavioural, cognitive and motor characteristics that mimic some of clinical features observed in human tauopathies, such as PSP and CBD (Bondulich et al., 2016). Interestingly, the amount of Tau35 protein expressed in male Tau35 mice was significantly increased compared to female Tau35 mice. However, there is no difference in Tau35 protein expression in heterozygous and homozygous female mice, which may be due to random partial or complete silencing of the second copy of the X chromosome in female mice (Lyon, 1962). The transgenic technique used here has the potential to introduce great variability in expression of Tau35 fragment between male and female mice and hence brain tissue from male mice only was used in this work. Moreover,

Tau35 protein expression is higher in the hippocampus and associated cortex, and the brainstem and cerebellum, and lower in the frontal region, and amygdala and associated cortex demonstrating that Tau35 expression is brain region-specific.

This exploratory study to characterise the novel Tau35 mouse model of human tauopathy showed that expression of Tau35 is capable of causing significant changes in cellular mechanisms in both the central and peripheral nervous systems. Tau35 mice exhibit elevated tau phosphorylation, accumulation of autophagosomes, astrocytic activation, mitochondrial deficits and pathological alteration of the neuromuscular junction. These findings position Tau35 mice as a good model of human tauopathies such as PSP and CBD and that maybe useful to improve our understanding of the molecular and cellular processes that are affected in other tauopathies as the model exhibits common biochemical characteristics that occur in these diseases.

Tau35 cortical neuronal morphology undergoes significant alterations throughout maturation and aging of the neurons, including enlarged soma size, increased dendritic length and dramatic dendritic spine loss. However, there are no significant changes in neuronal survival in cultured cortical neurons from Tau35 mice, suggesting that these events could be early events of disease progression. Biochemical alterations observed in Tau35 neurons, such as increased tau phosphorylation and mitochondrial deficits, are similar to those observed in human tauopathy and in Tau35 mice, establishing this as a relevant cellular model in which to study the mechanisms underlying these early disease changes.

Previously, numerous studies have shown significant changes in neuronal morphology in neurodegenerative diseases (Anderton et al., 1998; Falke et al., 2003; Knobloch and Mansuy, 2008; Tackenberg and Brandt, 2009; Giannakopoulos et al.,

2009b). To study the effect of truncated tau fragment on neuronal morphology, primary neurons from WT and Tau35 cortices were used. Tau35 neurons demonstrate morphological changes starting from 9 DIV. Sholl analysis reveals a decrease in the complexity of Tau35 neurites. However, an increase in maximum dendritic extent of Tau35 neurons at 9 DIV compared to WT neurons at 9 DIV was also observed, suggesting that there is a compensatory mechanism in place (Spires and Hyman, 2004; Dickstein et al., 2010). The size of the soma in Tau35 neurons showed a significant increase at 9 DIV. Similar results were obtained from other mouse models such as Tg2576 mice, a mouse model of AD which overexpresses a mutant form of APP (isoform 695), which also exhibit significantly increased spatial dendritic extents of cortical neurons at 12 months of age (Rocher et al., 2008). In addition, overexpression of mutant P301L tau in rTg4510 mice results in destabilisation of the dendritic cytoskeleton and altered neuronal morphology (Hall et al., 2000; 2001).

Furthermore, the Tau35 fragment alters morphology in another cellular model, Chinese hamster ovary (CHO) cells stably expressing Tau35 fragment. In contrast to normal CHO cells and CHO cells stably expressing full-length tau, CHO-Tau35 demonstrate compromised microtubule organisation and induction of the unfolded protein response. Particulary, disorganised microtubule structures have resulted in changes in cell shape. This could also cause profound effects on other intracellular processes such as recruitment of other microtubule-associated proteins to microtubules and localisation of organelles (personal communication, Tong Guo, King's College London). In the context of neurons, integration of microtubules into the neuronal cytoskeleton is key for normal axonal structure and function, in which they act as rails along which cargoes are moved to different cellular compartments, such as the synapse (Perdiz et al., 2011). Potentially compromised microtubule integrity is considered as being responsible for synapse loss, an early symptom of

neurodegeneration (Scheff and Price, 2006; Shankar and Walsh, 2009). Microtubule instability, caused by the Tau35 fragment, could potentially be the cause for altered axonal transport and spine loss observed in Tau35 primary cortical neurons.

In addition, a dramatic synaptic loss has been observed in Tau35 hippocampus in 14-month-old mice, particularly loss of the pre-synaptic protein Synapsin 1 (Bondulich et al., 2016). In primary Tau35 neurons, a loss of dendritic spines is evident, particularly a decrease in thin spines and a strong trend towards a decrease in the number of mushroom spines. Taken together, this may potentially explain the reduced ability of Tau35 mice in the Morris water maze test, which is a test of hippocampal spatial learning that mirrors the cognitive decline in dementia.

6.2 Tau35 induces biochemical and pathological deficits relevant to 4R tauopathies in mice and in primary neurons

Tau35 mice do not exhibit any apparent neuronal loss, despite the formation of pre-tangle-like, tau-containing structures forming in the brain (Bondulich et al., 2016). This finding is supported by the observation of no difference in neuronal survival in Tau35 cortical neuronal cultures compared to that of WT neurons. However, in both Tau35 mice and Tau35 cortical neurons, it is evident that tau is highly phosphorylated. Increased tau phosphorylation is a major hallmark of tauopathies and is thought to lead to tau accumulation and cell death, resulting in cognitive decline. It is well known that increased tau phosphorylation both detaches tau from microtubules and induces tau missorting from axons into the somatodendritic compartment of neurons (Ittner et al., 2009; Hoover et al., 2010). Indeed, Tau35 mice show increased phosphorylation of tau at numerous epitopes, including Ser422 in the hippocampus and associated cortex. This epitope is thought to represent an early marker of tau aggregation and is associated with pre-tangles (Mufson et al., 2014). These findings together could

suggest that the increased tau phosphorylation that occurs due to expression of Tau35 might also be an early event in disease pathogenesis. In addition, accumulation of endogenous tau in the insoluble 13,000g pellet obtained from the hippocampus and associated cortex is observed. However, this pellet would also have contained cellular organelles; predominantly mitochondria, lysosomes and peroxisomes. It has been previously reported that tau could be associated with various organelles. For example, tau accumulation has been shown to impair mitochondrial degradation by directly interacting with mitochondria (Hu et al., 2016). This could result in compromised axonal microtubule integrity, mitochondrial dysfunction and potentially spine loss.

A possible explanation for tau accumulation could be that the autophagy-lysosome system enables clearance of pathological tau (Min Jae Lee et al., 2013, Rodriguez Martin et al., 2016). In the hippocampus and associated cortex of Tau35 mouse brain, a decrease in LC3-I and increase in LC3-II is observed, suggesting an accumulation of autophagosomes. This could be triggered either through upregulation of autophagosomal formation or blockage of autophagic degradation.

A common feature of neurodegenerative diseases is the presence of reactive astrocytes in the brain. At 14 months of age, WT and Tau35 mice did not show any significant differences in GFAP expression (Bondulich et al., 2016). However, astrocytic activation is observed in all brain regions in Tau35 mice aged 18 months. This suggests that astrogliosis may only be apparent in the later stages of disease (Burda and Sofroniew, 2014). Interestingly, the largest difference in GFAP expression between Tau35 mice and WT mice occurred in the frontal brain region, as well as in the brainstem and cerebellum, which is consistent with the neurodegenerative profiles observed in PSP and CBD (Hauw et al., 1990; Bergeron et al., 1997).

6.3 Tau35-mediated mitochondrial dysfunction

Growing evidence suggests that mitochondria play a key role in the execution of neurodegeneration, either due to defects in respiratory function, or by interacting with other organelles such as the ER or the cytoskeleton (Nunnari and Suomalainen, 2012). Deficit of the mitochondrial marker HSP60 was observed in the hippocampal and cortical region of Tau35 aged mouse brain and in primary cortical neuronal cultures generated from Tau35 mice. Decreased HSP60 could lead to increased protein misfolding and aggregation, which is consistent with the pathological hallmarks of 4R tauopathies. Interestingly, similar changes have also been observed in AD, where HSP60 has been found to be significantly decreased (Yoo et al., 2001). Tau35 and WT primary cortical neurons were used as cellular models to study mitochondrial transport and biogenesis. In addition to an overall decrease in mitochondrial markers in mature neurons, Tau35 primary cortical neurons at 9 DIV demonstrate a decrease in mitochondria, specifically in neurites. However, deficits in mitochondria that present in neurites in other tau transgenic mice are suggested to be due to the mislocalisation of mitochondria and clustering of mitochondria in the perinuclear region of neurons (Mandelkow et al., 2004; Dubey et al., 2008; Kopeikina et al., 2011). For example, tau alterations in rTg4510 and P301L tau transgenic mice demonstrate aberrant distribution and/or a decrease in the area occupied by mitochondria in neurites (Kopeikina et al., 2011; Rodríguez-Martín et al., 2016).

Interestingly, the overall percentage of motile mitochondria is unchanged in Tau35 neurons, compared to the WT neurons. This suggests that mitochondria maintain their ability to be transported along neurites. This is further supported by the lack of any significant alterations in the amounts of the motor proteins, dynein and kinesin, in Tau35 neurons. However, the motile mitochondria in Tau35 neurons displayed a

relative preference for retrograde movement, suggesting that a larger proportion of the mitochondria in Tau35 neurites are moving towards the soma. The velocity of mitochondria travelling in a retrograde direction was also increased in Tau35 neurons, as was the mean retrograde run length of individual mitochondria.

It has been shown that overexpression of tau in cells leads to the accumulation of mitochondria around the nucleus, possibly due to a reduction in the anterograde to retrograde transport ratio, leading to reduced net anterograde flux (Stoothoff et al., 2009; Kopeikina et al., 2011). Previous studies of the effects of 3R and 4R tau isoforms on mitochondrial transport suggest that 4R tau may have a more profound influence on the competition for kinesin-based transport that diminishes the anterograde to retrograde transport ratio (Stoothoff et al., 2009). A recent study has suggested that increased retrograde movement of mitochondria could also be explained by release of the mitochondria anchoring protein, syntaphilin, that could lead to increased mitochondrial retrograde motility and reduced mitochondrial density in axons (Lin et al., 2017). These findings suggest that investigation of syntaphilin, including its association with mitochondria in Tau35 neurons, may be warranted. In addition, it has been surmised that mitochondria moving in an anterograde direction are healthy, while retrograde-moving mitochondria might represent older, damaged organelles that are being transported to the soma for degradation by mitophagy (Miller, 2004; Cai et al., 2012). Therefore, the increased retrograde flux of mitochondria observed in Tau35 cortical neurons could also indicate enhanced mitochondrial degradation.

To investigate the health and functionality of mitochondria, the ability to fuse together and to fragment, as well as mitochondrial morphology was assessed. Interestingly, it has been shown previously that mitochondrial fission and fusion might contribute to neurodegenerative disease progression (Stokin et al., 2005; Wang et al., 2009). In

Tau35 primary cortical neurons, no changes in the size and shape of mitochondria are observed in comparison to those in WT neurons. These findings are consistent with observations made in other mouse models of tauopathy, such as rTg4510 (Kopeikina et al., 2011) and P301L tau mice (David et al., 2005). Furthermore, no differences were detected in the amounts of mitochondrial fission (such as DRP1) and fusion (such as OPA1) proteins in Tau35 neurons. These results suggest that the observed deficits in mitochondria in Tau35 neurons are unlikely to be due to abnormalities in mitochondrial fission or fusion. Furthermore, induction of autophagy with rapamycin did not further reduce the number of mitochondria, indicating no overt effects on mitophagy in Tau35 neurons. This might indicate that the remaining mitochondria in Tau35 neurons are not necessarily damaged and therefore they are not required to be cleared from the neurons. Furthermore, the functionality of mitochondria was investigated by assessing mitochondrial stress. The Seahorse analyser did not show any significant changes in cellular oxygen consumption rate, and the slight decrease that is observed could be accounted for by the reduced number of mitochondria in Tau35 neurites.

Tau35 neurons demonstrate a significant decrease in the amount of the mitochondrial biogenesis master regulator, PGC-1α. In addition, Tau35 neurons exhibit a decrease in SIRT1, which deacetylates and activates PGC-1α (Araki et al., 2004). SIRT1 has been shown to have a neuroprotective function in the brain and a decrease in this protein may lead to age-dependent neurodegeneration (Araki et al., 2004). Decreased SIRT1 in Tau35 neurons could, therefore, result in reduced activation of PGC-1α and thereby reduce mitochondrial biogenesis. In addition, SIRT1 is reduced in the cortex in AD and it has been suggested that SIRT1 negatively correlates with the number of neurofibrillary tangles in AD brain (Julien et al., 2009). Indeed, SIRT1 has the ability to deacetylate tau, and deficiency of SIRT1 results in an enhancement of both acetylated and phosphorylated tau (Min et al., 2010). PGC-1α levels are also

controlled by the transcription factor CREB. However, there was no significant difference in the amount of total and phosphorylated CREB in Tau35 neurons compared to WT neurons. This indicates that in Tau35 neurons, CREB is unlikely to be the cause of the observed decrease in PGC-1α and the resultant reduction in mitochondrial biogenesis. Downstream of PGC-1α, NRF2 is a transcription factor that plays an important protective role against oxidative stress (Ma, 2013). Under conditions of stress, activation of NRF2 counteracts the increased reactive oxygen species production in mitochondria through transcriptional upregulation of uncoupling protein 3, and influences mitochondrial biogenesis by maintaining the levels of NRF1 and PGC-1α (Vomund et al., 2017). The significant reduction of both PGC-1α and NRF2 in Tau35 neurons could be a major factor that could lead to a deficit of mitochondrial DNA replication.

6.4 A proposal for a unified hypothesis to explain the mitochondrial deficit and spine loss in Tau35 neurons

Collectively, the evidence generated in this thesis suggests that the reduction in spine density in Tau35 neurons could be due to increased retrograde axonal transport of mitochondria, with a larger number of mitochondria moving at increased speed and with longer run lengths, towards the soma. If a similar situation also exists in dendrites, this enhanced flux could lead to a net movement of mitochondria away from dendritic spines, preventing mitochondrial anchoring in the region, thereby, depriving spines of energy and resulting in spine loss. There is evidence that tau might lead to peri-nuclear accumulation of mitochondria (Mandelkow et al., 2004). This peri-nuclear accumulation of mitochondria might lead to somatic swelling and enlarged soma size, with reduced complexity of the dendritic tree around the soma. Such a scheme would be compatible with the observations made in Tau35 cortical neurons in culture (Fig. 6.1).

Microtubules are polarised structures. In axons, microtubules are oriented with the plus ends away from the cell body, and in dendrites, microtubules are of a mixed polarity, with both minus and plus ends oriented toward the cell body (Baas, 1989). However, the dynamic plus end of the microtubules enters the dendritic spines to deliver the cargo necessary for spine function. Thus, the plasticity of dendritic spines is dependent on the microtubule dynamic and undoubtedly plays a key role in the proper functioning of the brain, whereas defects in spine plasticity are often associated with disease and neurodegeneration (Sala and Segal, 2014). However, it has been recently shown that mitochondrial transport occurs through a 'hand-off' model of transport into spines. A hand-off occurs between kinesin–microtubule transport to actin-myosin–based transport, resulting in the transport of mitochondria into the dendritic spine (McVicker et al., 2016). As shown in Chapter 5, Section 5.2.2, mitochondria in Tau35 neurites have a preferential motility in the retrograde direction, i.e. towards the minus end of the microtubules. This could potentially prevent the 'hand-off' of mitochondria and transport into the dendritic spine.

Fig. 6.1 Proposed unifying hypothesis that results in dendritic spine loss in Tau35 neurons

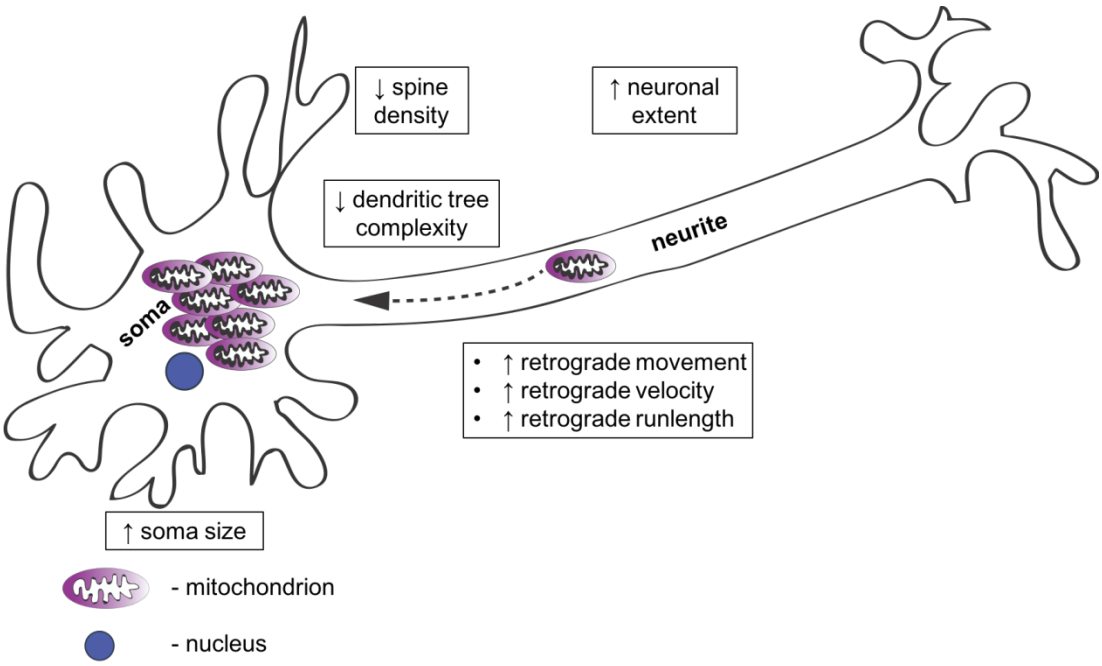

Here it is proposed that in Tau35 neurons, mitochondria in the neurites preferentially move in the retrograde direction. In dendrites, this would result in movement of mitochondria away from dendritic spines, preventing mitochondrial anchoring that is required for spine function. The mitochondria that move to the soma form peri-nuclear clusters that have been previously observed when tau is overexpressed in some cell models. Such an aggregation of mitochondria could lead to an increased soma size, and spine loss may result.

If the accumulation of mitochondria occurs, mitochondrial biogenesis might be reduced due to the overwhelming number of mitochondria in the peri-nuclear region. This could occur due to the altered NAD+/NADH ratio leading to the decrease in SIRT1 that is observed in Tau35 mice, followed by downregulation of PGC-1α and subsequently NRF2 that is summarised in Fig. 6.2.

Fig. 6.2 Proposed mechanism of reduced mitochondrial biogenesis

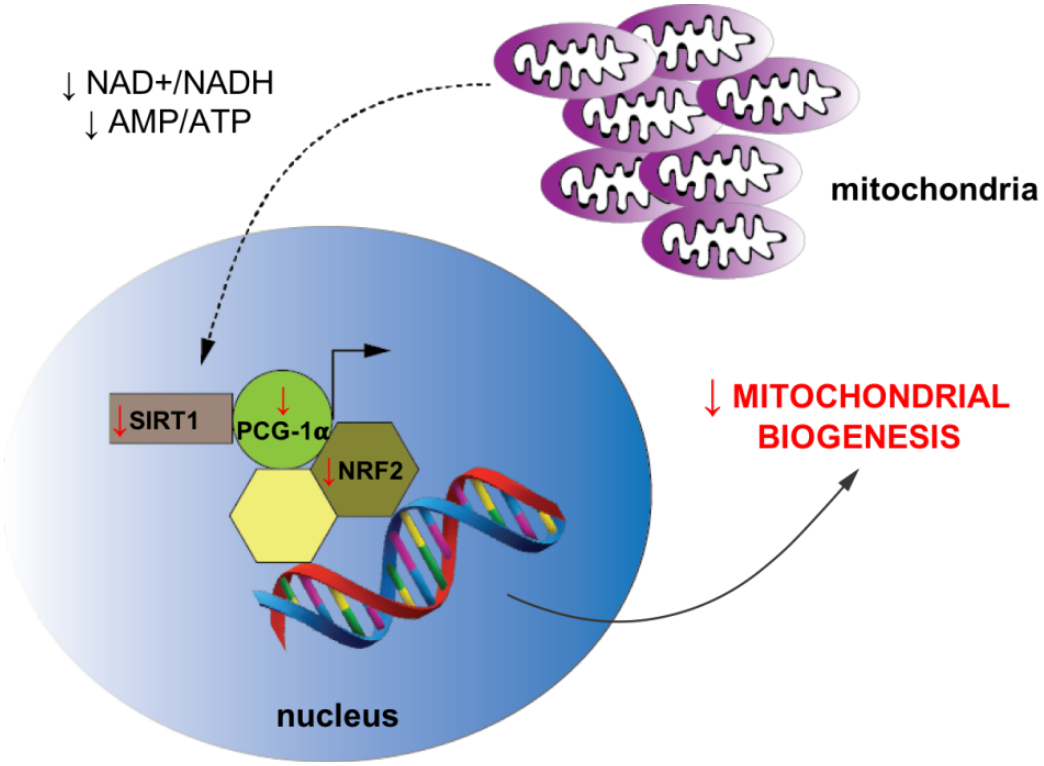

A proposed compensatory mechanism of mitochondrial accumulation in the soma, due to increased retrograde mitochondrial flux, reduces the NAD+/NADH ratio, decreasing SIRT1 and other molecules that initiate transcription of genes regulating mitochondrial biogenesis.

6.5 Pathological effects of Tau35 on the peripheral nervous system

Tau35 mice demonstrate reduced grip strength of the hindlimbs and they also exhibit motor deficits from an early age, prior to cognitive decline (Bondulich et al., 2016). Here, data is presented showing altered NMJ morphology in hindlimb muscles, with evidence of early signs of NMJ deformation apparent as early as 3 months in Tau35 mice. Morphologically, alterations of the folds that consist of acetylcholine receptors may lead to functional impairment in the post-synaptic response in NMJs (Kurokawa et al, 1990). In addition, progressive changes in NMJs were observed with increasing age in Tau35 mice. At 13 months, NMJs in Tau35 mice exhibited morphological deformation and reduced surface area. Furthermore, a significant increase in partially denervated NMJs in Tau35 mice was observed, potentially due to degeneration of the NMJ endplates. As there are several tauopathies that present with both cognitive and motor deficits, it is thought that alterations in the tau protein may lead to pathological motor symptoms (Pratt et al., 2015). Findings in Tau35 mice are consistent with previous work on other models of tauopathies such as the Tg30 mouse line, that expresses mutant 1N4R double-mutant tau (P301S and G272V) human tau (Audouard et al., 2015). Tg30 mice show a severe motor deficit, with tau aggregates in the brain and spinal cord. Interestingly, progressive and severe muscle denervation was observed that is thought to result from disturbance of axonal transport rather than loss of motor neurons (Audouard et al., 2015).

6.6 Therapeutic prospective

Increasing work has been done in the past years to investigate potential therapeutic targets that may lead to finding a cure for human tauopathies. Multiple neuroprotective strategies have been aimed at targeting tau pathology (summarised in Fig. 6.3).

Inhibiting tau phosphorylation has been proposed as a possible route to prevent tau toxicity, proteolysis, and tau aggregation (Panza et al., 2016). Other suggestions have included promotion of both intracellular and extracellular tau clearance and/or increasing microtubule stabilisation (Šimić et al., 2017).

Fig. 6.3 Potential neuroprotective strategies to reduce tau pathology

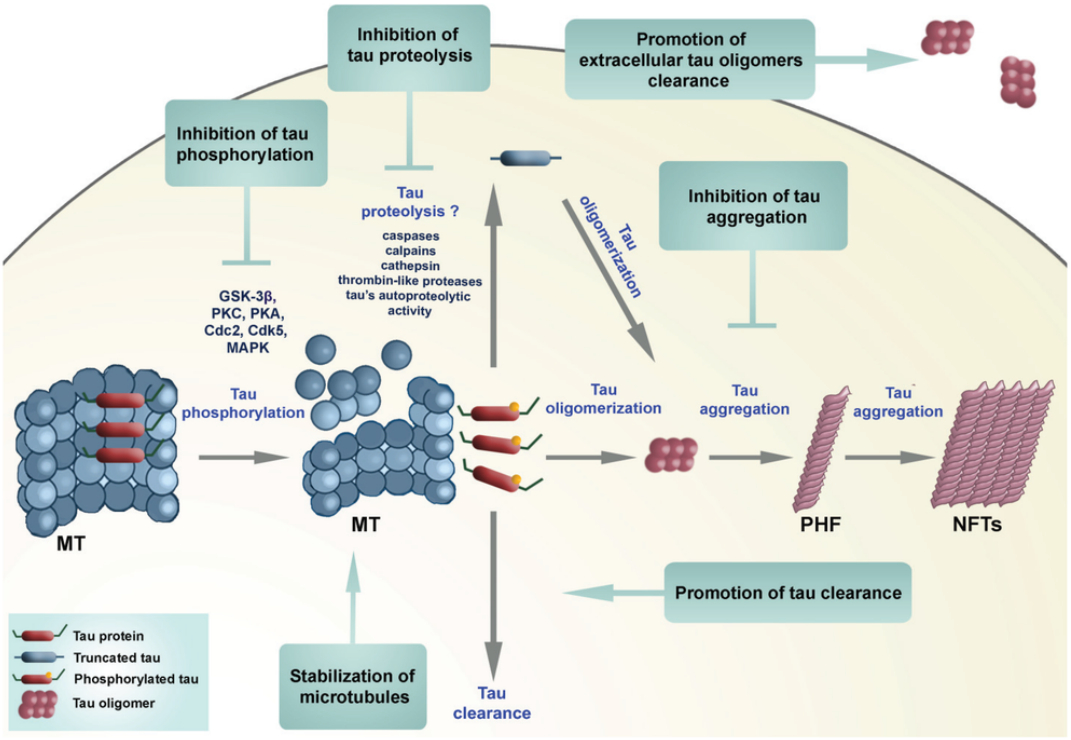

Potential therapeutic strategies that have been proposed to target tau pathology in human tauopathy. These include, inhibition of tau phosphorylation, proteolysis and clearance. Furthermore, promotionof tau and tau oligomers clearance (Šimić et al., 2017).

In this project, various mitochondrial alterations have been described, such as changes in mitochondrial number and transport. The pathological mechanism suggested in this chapter in that decreased mitochondrial biogenesis affects spine density loss that could further cause cognitive and motor deficits. An overview of mitochondrial biogenesis pathway is presented in Section 1.14.3.

Activation of PGC-1α could be targeted directly or via molecules that influence its activation such as SIRT1, AMPK and CREB. PGC-1α expression can be increased directly by pharmacological compound, bezafibrate, which further leads to an increased expression level of NRF1 and NRF2, enhancing mitochondrial biogenesis (Uittenbogaard et. al., 2014). The retrograde signalling pathway is under control of AMP/ATP ratio that is increased when there is a decrease in ATP. This is a signal for AMPK to activate PGC-1α expression via phosphorylation that in turn activates mitochondrial biogenesis. AMPK activity is stimulated by a number of pharmacological compounds, such as AICAR, resveratrol and metformin (Uittenbogaard et. al., 2014). Finally, SIRT1 is activated through phosphorylation either by AMPK or by increase of NAD^+/NADH ratio. Pharmacologically, Isoflavones and SRT1720 activate SIRT1 that deacetylates PGC-1α driving mitochondrial biogenesis (Uittenbogaard et. al., 2014). Interestingly, activation of SIRT1 has previously been shown to increase life-span (Mitchell et al., 2014).

6.7 Conclusions and future work

Deficits in the numbers of mitochondrial and dendritic spines are observed in the neurons of Tau35 mice. Sub-cellular fractions of mitochondria and synaptosomes could offer a more sensitive method with which to investigate the changes in synaptic mitochondria and synaptic proteins in Tau35 neurons (Lores-Arnaiz et al., 2016).

Mitochondrial fusion and fission were investigated by analysing the mitochondrial shape and levels of fusion and fission proteins using western blots. However, mitochondrial fusion and fission occur predominantly in motile mitochondria, which comprise only ~20% of the total mitochondria in the cultured cortical neurons. Therefore, more sensitive methods, such as imaging live neurons transfected with fission/fusion protein markers, may be required to detect any subtle changes in mitochondrial dynamics in Tau35 neurons.

Mitophagy has been previously implicated in cases of neuronal mitochondrial deficits (Martinez-Vicente, 2017). It is common to test mitophagy by inducing it using the mitochondrial uncoupler, carbonyl cyanide m-chlorophenylhydrazone (CCCP). However, in this study mitophagy was not directly studied due to the time restrictions and hence this may warrant further investigation.

Table 9 Summary of changes induced by Tau35 expression in mouse brain and in primary cortical neurons

Disease-causing pathological effects of Tau35 fragment
In the hippocampus and associated cortex of Tau35 mouse model: • ↑Tau35 compared to other brain regions • ↑Tau phosphorylation • ↓Tau dephosphorylation • ↓Number of mitochondria • ↑Astrocytic activation • ↑Number of autophagosomes
In Tau35 primary cortical neurons: • ↑Tau phosphorylation • ↓Tau dephosphorylation • ↓Number of mitochondria • ↑Mitochondrial retrograde transport (direction, velocity, runlength) • ↓Mitochondrial biogenesis • ↓Spine density • ↑Dendritic extent • ↑Soma size • ↓Neuronal complexity

In conclusion, this thesis describes a novel mouse model of human tauopathy. The Tau35 mouse and Tau35 primary neurons exhibit numerous pathological changes that are summarised above (Table 9). These results add new information and increase our understanding of the mechanisms underlying the pathogenesis of tau-mediated neurodegeneration. The work described here provides evidence that this novel model of disease can be used to explore the role of tau truncation in tauopathy and could provide a useful tool for the screening, assessment and potential development of novel therapeutics.

References

Agostini M, Romeo F, Inoue S, Niklison-Chirou MV, Elia AJ, Dinsdale D, Morone N, Knight RA, Mak TW, Melino G (2016) Metabolic reprogramming during neuronal differentiation. Cell Death Differ 23:1502–1514.

Akram A, Christoffel D, Rocher AB, Bouras C, Kövari E, Perl DP, Morrison JH, Herrmann FR, Haroutunian V, Giannakopoulos P, Hof PR (2008) Stereologic estimates of total spinophilin-immunoreactive spine number in area 9 and the CA1 field: relationship with the progression of Alzheimer's disease. Neurobiol Aging 29:1296–1307.

Alafuzoff I, Arzberger T, Al-Sarraj S, Bodi I, Bogdanovic N, Braak H, et al. Staging of Neurofibrillary Pathology in Alzheimer's Disease: A Study of the BrainNet Europe Consortium. Brain Pathology. 2008 Mar 27;0(0):080509082911413

Altmann K, Frank M, Neumann D, Jakobs S, Westermann B (2008) The class V myosin motor protein, Myo2, plays a major role in mitochondrial motility in Saccharomyces cerevisiae. J Cell Biol 181:119–130.

Amadoro G, Corsetti V, Florenzano F, Atlante A, Ciotti MT, Mongiardi MP, Bussani R, Nicolin V, Nori SL, Campanella M, Calissano P (2014) AD-linked, toxic NH_2human tau affects the quality control of mitochondria in neurons. Neurobiol Dis 62:489–507.

Anderson DW, Bradbury KA, Schneider JS (2006) Neuroprotection in Parkinson models varies with toxin administration protocol. Eur J Neurosci 24:3174–3182.

Anderson S, Bankier At, Barrell Bg, Debruijn M, Coulson Ar, Drouin J, Eperon Ic, Nierlich Dp, Roe Ba, Sanger F, Schreier Ph, Smith A, Staden R, Young Ig (1981) Sequence and Organization of the Human Mitochondrial Genome. Nature 290:457–465.

Anderton BH, Callahan L, Coleman P, Davies P, Flood D, Jicha GA, Ohm T, Weaver C (1998) Dendritic changes in Alzheimer's disease and factors that may underlie these changes. Prog Neurobiol 55:595–609.

Andreadis A (2006) Misregulation of tau alternative splicing in neurodegeneration and dementia. Prog Mol Subcell Biol 44:89–107.

Angelova PR, Abramov AY (2018) Role of mitochondrial ROS in the brain: from physiology to neurodegeneration. Bateman JM, Just W, FEBS Lett 592:692–702.

Arai T, Guo J-P, McGeer PL (2005) Proteolysis of non-phosphorylated and phosphorylated tau by thrombin. J Biol Chem 280:5145–5153.

Arai T, Ikeda K, Akiyama H, Nonaka T, Hasegawa M, Ishiguro K, Iritani S, Tsuchiya K, Iseki E, Yagishita S, Oda T, Mochizuki A (2004) Identification of amino-terminally cleaved tau fragments that distinguish progressive supranuclear palsy from corticobasal degeneration. Ann Neurol 55:72–79.

Araki T, Sasaki Y, Milbrandt J (2004) Increased nuclear NAD biosynthesis and SIRT1 activation prevent axonal degeneration. Science 305:1010–1013.

Arendt KL, Royo M, Fernández-Monreal M, Knafo S, Petrok CN, Martens JR, Esteban JA (2010) PIP3 controls synaptic function by maintaining AMPA receptor clustering at the postsynaptic membrane. Nat Neurosci 13:36–44.

Armstrong MJ et al. (2013) Criteria for the diagnosis of corticobasal degeneration. Neurology 80:496–503.

Arnold A-S, Gill J, Christe M, Ruiz R, McGuirk S, St-Pierre J, Tabares L, Handschin C (2014) Morphological and functional remodelling of the neuromuscular junction by skeletal muscle PGC-1α. Nat Commun 5:3569.

Arnold SE, Lee VM, Gur RE, Trojanowski JQ (1991) Abnormal expression of two microtubule-associated proteins (MAP2 and MAP5) in specific subfields of the hippocampal formation in schizophrenia. Proc Natl Acad Sci USA 88:10850–10854.

Ashe KH, Zahs KR (2010) Probing the biology of Alzheimer's disease in mice. Neuron 66:631–645.

Atlante A, Amadoro G, Bobba A, de Bari L, Corsetti V, Pappalardo G, Marra E, Calissano P, Passarella S (2008) A peptide containing residues 26-44 of tau protein impairs mitochondrial oxidative phosphorylation acting at the level of the adenine nucleotide translocator. Biochim Biophys Acta 1777:1289–1300.

Attwell D, Laughlin SB (2001) An energy budget for signaling in the grey matter of the brain. J Cereb Blood Flow Metab 21:1133–1145.

Audouard E, Van Hees L, Suain V, Yilmaz Z, Poncelet L, Leroy K, Brion J-P (2015a) Motor deficit in a tauopathy model is induced by disturbances of axonal transport leading to dying-back degeneration and denervation of neuromuscular junctions. Am J Pathol 185:2685–2697.

Avila J, Jiménez JS, Sayas CL, Bolós M, Zabala JC, Rivas G, Hernández F (2016) Tau Structures. Front Aging Neurosci 8:262.

Avila J, Lucas JJ, Pérez M, Hernández F (2004a) Role of Tau Protein in Both Physiological and Pathological Conditions. Physiol Rev 84:361–384.

Avila J, Pérez M, Lucas JJ, Gómez-Ramos A, Santa María I, Moreno F, Smith M, Perry G, Hernández F (2004b) Assembly in vitro of tau protein and its implications in Alzheimer's disease. Curr Alzheimer Res 1:97–101.

Baas PW (1989) Changes in microtubule polarity orientation during the development of hippocampal neurons in culture. J Cell Biol 109:3085–3094.

Baker M, Litvan I, Houlden H, Adamson J, Dickson D, Perez-Tur J, Hardy J, Lynch T, Bigio E, Hutton M (1999) Association of an extended haplotype in the tau gene with progressive supranuclear palsy. Hum Mol Genet 8:711–715.

Bakshi R, Mittal S, Liao Z, Scherzer CR (2016) A feed-forward circuit of endogenous PGC-1α and estrogen related receptor α regulates the neuronal electron transport chain. Parkinsons Dis 2016:2405176–2405179.

Ballatore C, Hyde E, Deiches RF, Lee VM-Y, Trojanowski JQ, Huryn D, Smith AB (2007) Paclitaxel C-10 carbamates: potential candidates for the treatment of neurodegenerative tauopathies. Bioorg Med Chem Lett 17:3642–3646.

Barghorn S, Mandelkow E (2002) Toward a unified scheme for the aggregation of tau into Alzheimer paired helical filaments. Biochemistry 41:14885–14896.

Barik A, Li L, Sathyamurthy A, Xiong W-C, Mei L (2016) Schwann Cells in Neuromuscular Junction Formation and Maintenance. J Neurosci 36:9770–9781.

Beharry C, Cohen LS, Di J, Ibrahim K, Briffa-Mirabella S, Alonso ADC (2014) Tau-induced neurodegeneration: mechanisms and targets. Neurosci Bull 30:346–358.

Benard G, Faustin B, Galinier A, Rocher C, Bellance N, Smolkova K, Casteilla L, Rossignol R, Letellier T (2008) Functional dynamic compartmentalization of respiratory chain intermediate substrates: implications for the control of energy production and mitochondrial diseases. Int J Biochem Cell Biol 40:1543–1554.

Bergen von M, Friedhoff P, Biernat J, Heberle J, Mandelkow EM, Mandelkow E (2000) Assembly of tau protein into Alzheimer paired helical filaments depends on a local sequence motif ((306)VQIVYK(311)) forming beta structure. Proc Natl Acad Sci USA 97:5129–5134.

Bergeron C, Pollanen MS, Neuropathology LWO, 1997 Cortical degeneration in progressive supranuclear palsy. A comparison with cortical-basal ganglionic degeneration.

Bhaskar K, Hobbs GA, Yen SH, Lee G (2010) Tyrosine phosphorylation of tau accompanies disease progression in transgenic mouse models of tauopathy. Neuropathol Appl Neurobiol 36:462–477.

Billings LM, Oddo S, Green KN, McGaugh JL, LaFerla FM (2005) Intraneuronal Abeta causes the onset of early Alzheimer's disease-related cognitive deficits in transgenic mice. Neuron 45:675–688.

Bjørkøy G, Lamark T, Johansen T (2006) p62/SQSTM1: a missing link between protein aggregates and the autophagy machinery. Autophagy 2:138–139.

Black MM, Slaughter T, Moshiach S, Obrocka M, Fischer I (1996) Tau is enriched on dynamic microtubules in the distal region of growing axons. J Neurosci 16:3601–3619.

Bodea L-G, Eckert A, Ittner LM, Piguet O, Götz J (2016) Tau Physiology and Pathomechanisms in Frontotemporal Lobar Degeneration. Wiley/Blackwell

Boeve BF, Maraganore DM, Parisi JE, Ahlskog JE, Graff-Radford N, Caselli RJ, Dickson DW, Kokmen E, Petersen RC (1999) Pathologic heterogeneity in clinically diagnosed corticobasal degeneration. Neurology 53:795–800.

Boland B, Kumar A, Lee S, Platt FM, Wegiel J, Yu WH, Nixon RA (2008) Autophagy induction and autophagosome clearance in neurons: relationship to autophagic pathology in Alzheimer's disease. J Neurosci 28:6926–6937.

Boldogh IR, Yang HC, Pon LA (2001) Mitochondrial inheritance in budding yeast. Traffic 2:368–374.

Bondareff W, Wischik CM, Novák M, Amos WB, Klug A, Roth M (1990) Molecular analysis of neurofibrillary degeneration in Alzheimer's disease. An immunohistochemical study. Am J Pathol 137:711–723.

Bondolfi L, Calhoun M, Ermini F, Kuhn HG, Wiederhold K-H, Walker L, Staufenbiel M, Jucker M (2002) Amyloid-associated neuron loss and gliogenesis in the neocortex of amyloid precursor protein transgenic mice. J Neurosci 22:515–522.

Bondulich MK, Guo T, Meehan C, Manion J, Rodríguez-Martín T, Mitchell JC, Hortobagyi T, Yankova N, Stygelbout V, Brion J-P, Noble W, Hanger DP (2016) Tauopathy induced by low level expression of a human brain-derived tau fragment in mice is rescued by phenylbutyrate. Brain 139:2290–2306.

Braak H, Braak E (1991) Demonstration of amyloid deposits and neurofibrillary changes in whole brain sections. Brain Pathol 1:213–216.

Braithwaite SP, Stock JB, Lombroso PJ, Nairn AC (2012) Protein phosphatases and Alzheimer's Disease. in: protein phosphorylation in health and disease, pp 343–379 Progress in Molecular Biology and Translational Science. Elsevier.

Brandt R, Hundelt M, Shahani N (2005) Tau alteration and neuronal degeneration in tauopathies: mechanisms and models. Biochim Biophys Acta 1739:331–354.

Bretteville A, Planel E (2008) Tau aggregates: toxic, inert, or protective species? Journal of Alzheimer's Disease 14:431–436.

Brookmeyer R, Johnson E, Ziegler-Graham K, Arrighi HM (2007) Forecasting the global burden of Alzheimer's disease. Alzheimers Dement 3:186–191.

Bross P, Magnoni R, Bie AS (2012) Molecular chaperone disorders: defective Hsp60 in neurodegeneration. Curr Top Med Chem 12:2491–2503.

Brown JWP, Buell AK, Michaels TCT, Meisl G, Carozza J, Flagmeier P, et al. β-Synuclein suppresses both the initiation and amplification steps of α-synuclein aggregation via competitive binding to surfaces. Sci Rep. Nature Publishing Group; 2016 Nov 3;6(1):36010.

Buée L, Bussière T, Buée-Scherrer V, Delacourte A, Hof PR (2000) Tau protein isoforms, phosphorylation and role in neurodegenerative disorders. Brain Res Brain Res Rev 33:95–130.

Buffo A, Rolando C, Ceruti S (2010) Astrocytes in the damaged brain: molecular and cellular insights into their reactive response and healing potential. Biochem Pharmacol 79:77–89.

Bulic B, Pickhardt M, Mandelkow E-M, Mandelkow E (2010) Tau protein and tau aggregation inhibitors. Neuropharmacology 59:276–289.

Bulinski JC (2007) Microtubule modification: acetylation speeds anterograde traffic flow. Curr Biol 17:R18–R20.

Burda JE, Sofroniew MV (2014) Reactive Gliosis and the Multicellular Response to CNS Damage and Disease. Neuron 81:229–248.

Burté F, Carelli V, Chinnery PF, Yu-Wai-Man P (2015) Disturbed mitochondrial dynamics and neurodegenerative disorders. Nat Rev Neurol 11:11–24.

Cagalinec M, Safiulina D, Liiv M, Liiv J, Choubey V, Wareski P, Veksler V, Kaasik A (2013) Principles of the mitochondrial fusion and fission cycle in neurons. J Cell Sci 126:2187–2197.

Cai Q, Zakaria HM, Sheng Z-H (2012) Long time-lapse imaging reveals unique features of PARK2/Parkin-mediated mitophagy in mature cortical neurons. Autophagy 8:976–978.

Campanari M-L, García-Ayllón M-S, Ciura S, Sáez-Valero J, Kabashi E (2016) Neuromuscular Junction Impairment in Amyotrophic Lateral Sclerosis: Reassessing the Role of Acetylcholinesterase. Front Mol Neurosci 9:160.

Cappello V, Francolini M (2017) Neuromuscular Junction Dismantling in Amyotrophic Lateral Sclerosis. International Journal of Molecular Sciences 18:2092.

Carnio S, LoVerso F, Baraibar MA, Longa E, Khan MM, Maffei M, Reischl M, Canepari M, Loefler S, Kern H, Blaauw B, Friguet B, Bottinelli R, Rudolf R, Sandri M (2014) Autophagy impairment in muscle induces neuromuscular junction degeneration and precocious aging. Cell Rep 8:1509–1521.

Chan DC (2006a) Mitochondrial fusion and fission in mammals. Annu Rev Cell Dev Biol 22:79–99.

Chan DC (2006b) Mitochondria: dynamic organelles in disease, aging, and development. Cell 125:1241–1252.

Chapman PF, White GL, Jones MW, Cooper-Blacketer D, Marshall VJ, Irizarry M, Younkin L, Good MA, Bliss TV, Hyman BT, Younkin SG, Hsiao KK (1999) Impaired synaptic plasticity and learning in aged amyloid precursor protein transgenic mice. Nat Neurosci 2:271–276.

Chee FC, Mudher A, Cuttle MF, Newman TA, MacKay D, Lovestone S, Shepherd D (2005) Over-expression of tau results in defective synaptic transmission in Drosophila neuromuscular junctions. Neurobiol Dis 20:918–928.

Chen H, McCaffery JM, Chan DC (2007) Mitochondrial fusion protects against neurodegeneration in the cerebellum. Cell 130:548–562.

Chen J, Kanai Y, Cowan NJ, Hirokawa N (1992) Projection domains of MAP2 and tau determine spacings between microtubules in dendrites and axons. Nature 360:674–677.

Chen M, Chen Z, Wang Y, Tan Z, Zhu C, Li Y, Han Z, Chen L, Gao R, Liu L, Chen Q (2016) Mitophagy receptor FUNDC1 regulates mitochondrial dynamics and mitophagy. Autophagy 12:689–702.

Chesser AS, Pritchard SM, Johnson GVW (2013) Tau clearance mechanisms and their possible role in the pathogenesis of Alzheimer disease. Front Neurol 4:122.

Chklovskii DB, Schikorski T, Stevens CF (2002) Wiring Optimization in Cortical Circuits. Neuron 34:341–347.

Cho J-H, Johnson GVW (2003) Glycogen synthase kinase 3beta phosphorylates tau at both primed and unprimed sites. Differential impact on microtubule binding. J Biol Chem 278:187–193.

Clavaguera F, Akatsu H, Fraser G, Crowther RA, Frank S, Hench J, Probst A, Winkler DT, Reichwald J, Staufenbiel M, Ghetti B, Goedert M, Tolnay M (2013) Brain homogenates from human tauopathies induce tau inclusions in mouse brain. Proc Natl Acad Sci USA 110:9535–9540.

Cohen TJ, Friedmann D, Hwang AW, Marmorstein R, Lee VM-Y (2013) The microtubule-associated tau protein has intrinsic acetyltransferase activity. Nat Struct Mol Biol 20:756–762.

Cohen TJ, Guo JL, Hurtado DE, Kwong LK, Mills IP, Trojanowski JQ, Lee VM-Y (2011) The acetylation of tau inhibits its function and promotes pathological tau aggregation. Nat Commun 2:252.

Cohen-Kfir E, Artsi H, Levin A, Abramowitz E, 2011. Sirt1 Is a Regulator of Bone Mass and a Repressor of Sost Encoding for Sclerostin, a Bone Formation Inhibitor.

Colangelo AM, Alberghina L, Papa M (2014) Astrogliosis as a therapeutic target for neurodegenerative diseases. Neurosci Lett 565:59–64.

Conrad C, Andreadis A, Trojanowski JQ, Dickson DW, Kang D, Chen XH, Wiederholt W, Hansen L, Masliah E, Thal LJ, Katzman R, Xia Y, Saitoh T (1997) Genetic evidence for the involvement of tau in progressive supranuclear palsy. Ann Neurol 41:277–281.

Conrad C, Zhu J, Conrad C, Schoenfeld D, Fang Z, Ingelsson M, Stamm S, Church G, Hyman BT (2007) Single molecule profiling of tau gene expression in Alzheimer’s disease. J Neurochem 103:1228–1236.

Cook C, Carlomagno Y, Gendron TF, Dunmore J, Scheffel K, Stetler C, Davis M, Dickson D, Jarpe M, DeTure M, Petrucelli L (2014) Acetylation of the KXGS motifs in tau is a critical determinant in modulation of tau aggregation and clearance. Hum Mol Genet 23:104–116.

Coskun PE, Wyrembak J, Derbereva O, Melkonian G, Doran E, Lott IT, Head E, Cotman CW, Wallace DC (2010) Systemic mitochondrial dysfunction and the etiology of Alzheimer's disease and down syndrome dementia. Zhu X, Beal MF, Wang X, Perry G, Smith MA, eds. J Alzheimers Dis 20 Suppl 2:S293–S310.

Course MM, Wang X (2016) Transporting mitochondria in neurons. F1000Res 5:1735.

Crimins JL, Rocher AB, Peters A, Shultz P, Lewis J, Luebke JI (2011) Homeostatic responses by surviving cortical pyramidal cells in neurodegenerative tauopathy. Acta Neuropathol 122:551–564.

Cuchillo-Ibáñez I, Seereeram A, Byers HL, Leung K-Y, Ward MA, Anderton BH, Hanger DP (2008) Phosphorylation of tau regulates its axonal transport by controlling its binding to kinesin. FASEB J 22:3186–3195.

Cuervo AM (2004) Autophagy: in sickness and in health. Trends Cell Biol 14:70–77.

David DC, Hauptmann S, Scherping I, Schuessel K, Keil U, Rizzu P, Ravid R, Dröse S, Brandt U, Müller WE, Eckert A, Götz J (2005) Proteomic and functional analyses reveal a mitochondrial dysfunction in P301L tau transgenic mice. J Biol Chem 280:23802–23814.

Dawson HN, Ferreira A, Eyster MV, Ghoshal N, Binder LI, Vitek MP (2001) Inhibition of neuronal maturation in primary hippocampal neurons from tau deficient mice. J Cell Sci 114:1179–1187.

de Calignon A, Fox LM, Pitstick R, Carlson GA, Bacskai BJ, Spires-Jones TL, Hyman BT (2010) Caspase activation precedes and leads to tangles. Nature 464:1201–1204.

De Vos KJ, Grierson AJ, Ackerley S, Miller CCJ (2008) Role of axonal transport in neurodegenerative diseases. Annu Rev Neurosci 31:151–173.

Decker JM, Krüger L, Sydow A, Zhao S, Frotscher M, Mandelkow E, Mandelkow E-M (2015) Pro-aggregant Tau impairs mossy fiber plasticity due to structural changes and Ca(++) dysregulation. Acta Neuropathol Commun 3:23.

DeKosky ST, Scheff SW (1990) Synapse loss in frontal cortex biopsies in Alzheimer's disease: correlation with cognitive severity. Ann Neurol 27:457–464.

Denk F, Wade-Martins R (2009) Knock-out and transgenic mouse models of tauopathies. Neurobiol Aging 30:1–13.

Derisbourg M, Leghay C, Chiappetta G, Fernandez-Gomez F-J, Laurent C, Demeyer D, Carrier S, Buée-Scherrer V, Blum D, Vinh J, Sergeant N, Verdier Y, Buée L, Hamdane M (2015) Role of the Tau N-terminal region in microtubule stabilization revealed by new endogenous truncated forms. Sci Rep 5:9659.

Detmer SA, Chan DC (2007) Functions and dysfunctions of mitochondrial dynamics. Nat Rev Mol Cell Biol 8:870–879.

Dickson DW (2001) Neuropathology of Pick's disease. Neurology 56:S16–S20.

Dickson DW, Kouri N, Murray ME, Josephs KA (2011) Neuropathology of frontotemporal lobar degeneration-tau (FTLD-tau). J Mol Neurosci 45:384–389.

Dickstein DL, Brautigam H, Stockton SD, Schmeidler J, Hof PR (2010) Changes in dendritic complexity and spine morphology in transgenic mice expressing human wild-type tau. Brain Struct Funct 214:161–179.

DiMauro S, Schon EA (2008) Mitochondrial disorders in the nervous system. Annu Rev Neurosci 31:91–123.

Dinkova-Kostova AT, Abramov AY (2015) The emerging role of Nrf2 in mitochondrial function. Free Radic Biol Med 88:179–188.

Dixit R, Ross JL, Goldman YE, Holzbaur ELF (2008) Differential regulation of dynein and kinesin motor proteins by tau. Science 319:1086–1089.

Doble A (1996) The pharmacology and mechanism of action of riluzole. Neurology 47.

Dompierre JP, Godin JD, Charrin BC, Cordelières FP, King SJ, Humbert S, Saudou F (2007) Histone deacetylase 6 inhibition compensates for the transport deficit in Huntington's disease by increasing tubulin acetylation. J Neurosci 27:3571–3583.

Drewes G, Trinczek B, Illenberger S, Biernat J, Schmitt-Ulms G, Meyer HE, Mandelkow EM, Mandelkow E (1995) Microtubule-associated protein/microtubule affinity-regulating kinase (p110mark). A novel protein kinase that regulates tau-microtubule interactions and dynamic instability by phosphorylation at the Alzheimer-specific site serine 262. J Biol Chem 270:7679–7688.

Drubin DG, Caput D, Kirschner MW (1984) Studies on the expression of the microtubule-associated protein, tau, during mouse brain development, with newly isolated complementary DNA probes. J Cell Biol 98:1090–1097.

Du L, Hickey RW, Bayir H, Watkins SC, Tyurin VA, Guo F, Kochanek PM, Jenkins LW, Ren J, Gibson G, Chu CT, Kagan VE, Clark RSB (2009) Starving neurons show sex difference in autophagy. J Biol Chem 284:2383–2396.

Dubey M, Chaudhury P, Kabiru H, Shea TB (2008) Tau inhibits anterograde axonal transport and perturbs stability in growing axonal neurites in part by displacing kinesin cargo: neurofilaments attenuate tau-mediated neurite instability. Cell Motil Cytoskeleton 65:89–99.

DuBoff B, Goetz J, Feany MB (2012) Tau Promotes Neurodegeneration via DRP1 Mislocalization In Vivo. Neuron 75:618–632.

Ebneth A, Godemann R, Stamer K, Illenberger S, Trinczek B, Mandelkow E (1998) Overexpression of tau protein inhibits kinesin-dependent trafficking of vesicles, mitochondria, and endoplasmic reticulum: implications for Alzheimer's disease. J Cell Biol 143:777–794.

Eckert A, Keil U, Scherping I, Hauptmann S, Muller WE (2005) Stabilization of mitochondrial membrane potential and improvement of neuronal energy metabolism by Ginkgo biloba extract EGb 761. Ann N Y Acad Sci 1056:474–485.

Eidenmüller J, Fath T, Maas T, Pool M, Sontag E, Brandt R (2001) Phosphorylation-mimicking glutamate clusters in the proline-rich region are sufficient to simulate the functional deficiencies of hyperphosphorylated tau protein. Biochem J 357:759–767.

Eng Lf, Ghirnikar Rs (1994) Gfap and Astrogliosis. Brain Pathol 4:229–237.

Falke E, Nissanov J, Mitchell TW, Bennett DA, Trojanowski JQ, Arnold SE (2003) Subicular dendritic arborization in Alzheimer's disease correlates with neurofibrillary tangle density. Am J Pathol 163:1615–1621.

Fan M, Rhee J, St-Pierre J, Handschin C, Puigserver P, Lin J, Jäeger S, Erdjument-Bromage H, Tempst P, Spiegelman BM (2004) Suppression of mitochondrial respiration through recruitment of p160 myb binding protein to PGC-1alpha: modulation by p38 MAPK. Genes Dev 18:278–289.

Feany MB, Dickson DW (1996) Neurodegenerative disorders with extensive tau pathology: A comparative study and review. Ann Neurol 40:139–148.

Federico A, Cardaioli E, Da Pozzo P, Formichi P, Gallus GN, Radi E (2012) Mitochondria, oxidative stress and neurodegeneration. J Neurol Sci 322:254–262.

Feige JN, Lagouge M, Canto C, Strehle A, Houten SM, Milne JC, Lambert PD, Mataki C, Elliott PJ, Auwerx J (2008) Specific SIRT1 activation mimics low energy levels and protects against diet-induced metabolic disorders by enhancing fat oxidation. Cell Metab 8:347–358.

Filipcik P, Novak P, Mravec B, Ondicova K, Krajciova G, Novak M, Kvetnansky R (2012) Tau protein phosphorylation in diverse brain areas of normal and CRH deficient mice: up-regulation by stress. Cell Mol Neurobiol 32:837–845.

Fink BD, Herlein JA, Guo DF, Kulkarni C, Weidemann BJ, Yu L, Grobe JL, Rahmouni K, Kerns RJ, Sivitz WI (2014) A mitochondrial-targeted coenzyme q analog prevents weight gain and ameliorates hepatic dysfunction in high-fat-fed mice. J Pharmacol Exp Ther 351:699–708.

Frieden M, James D, Castelbou C, Danckaert A, Martinou J-C, Demaurex N (2004) Ca(2+) homeostasis during mitochondrial fragmentation and perinuclear clustering induced by hFis1. J Biol Chem 279:22704–22714.

Friedman JR, Lackner LL, West M, DiBenedetto JR, Nunnari J, Voeltz GK (2011) ER tubules mark sites of mitochondrial division. Science 334:358–362.

Frohman MA (2015) Role of mitochondrial lipids in guiding fission and fusion. J Mol Med 93:263–269.

Fulga TA, Elson-Schwab I, Khurana V, Steinhilb ML, Spires TL, Hyman BT, Feany MB (2007) Abnormal bundling and accumulation of F-actin mediates tau-induced neuronal degeneration in vivo. Nat Cell Biol 9:139–148.

Fuster-Matanzo A, Llorens-Martin M, Jurado-Arjona J, Avila J, Hernández F (2012) Tau protein and adult hippocampal neurogenesis. Front Neurosci 6:104.

Gafni J, Ellerby LM (2002) Calpain activation in Huntington's disease. J Neurosci 22:4842–4849.

Gafni J, Hermel E, Young JE, Wellington CL, Hayden MR, Ellerby LM (2004) Inhibition of calpain cleavage of huntingtin reduces toxicity: accumulation of calpain/caspase fragments in the nucleus. J Biol Chem 279:20211–20220.

Gamblin TC, Chen F, Zambrano A, Abraha A, Lagalwar S, Guillozet AL, Lu M, Fu Y, Garcia-Sierra F, LaPointe N, Miller R, Berry RW, Binder LI, Cryns VL (2003) Caspase cleavage of tau: linking amyloid and neurofibrillary tangles in Alzheimer's disease. Proc Natl Acad Sci USA 100:10032–10037.

Gao F, Chen D, Si J, Hu Q, Qin Z, Fang M, Wang G (2015) The mitochondrial protein BNIP3L is the substrate of PARK2 and mediates mitophagy in PINK1/PARK2 pathway. Hum Mol Genet 24:2528–2538.

Gao J, Wang L, Liu J, Xie F, Su B, Wang X (2017) Abnormalities of Mitochondrial Dynamics in Neurodegenerative Diseases. Antioxidants (Basel) 6:25.

Garcia N, Priego M, Hurtado E, Obis T, Santafe MM, Tomàs M, Lanuza MA, Tomàs J (2014) Adenosine A2B and A3 receptor location at the mouse neuromuscular junction. Journal of Anatomy 225:109–117.

Garcia-Sierra F, Mondragón-Rodríguez S, Basurto-Islas G (2008) Truncation of tau protein and its pathological significance in Alzheimer's disease. Journal of Alzheimer's Disease 14:401–409.

Garg S, Timm T, Mandelkow E-M, Mandelkow E, Wang Y (2011) Cleavage of Tau by calpain in Alzheimer's disease: the quest for the toxic 17 kD fragment. Neurobiol Aging 32:1–14.

Gauthier-Kemper A, Weissmann C, Golovyashkina N, Sebö-Lemke Z, Drewes G, Gerke V, Heinisch JJ, Brandt R (2011) The frontotemporal dementia mutation R406W blocks tau's interaction with the membrane in an annexin A2-dependent manner. J Cell Biol 192:647–661.

Gendron TF, Petrucelli L (2009) The role of tau in neurodegeneration. Mol Neurodegener 4:13.

Giannakopoulos P, Kövari E, Gold G, Gunten von A, Hof PR, Bouras C (2009a) Pathological substrates of cognitive decline in Alzheimer's disease. Front Neurol Neurosci 24:20–29.

Giannakopoulos P, Kövari E, Herrmann FR, Hof PR, Bouras C (2009b) Interhemispheric distribution of Alzheimer disease and vascular pathology in brain aging. Stroke 40:983–986.

Gibson DG, Smith HO, Hutchison CA, Venter JC, Merryman C (2010) Chemical synthesis of the mouse mitochondrial genome. Nat Methods 7:901–903.

Gilley J, Seereeram A, Ando K, Mosely S, Andrews S, Kerschensteiner M, Misgeld T, Brion J-P, Anderton B, Hanger DP, Coleman MP (2012) Age-dependent axonal transport and locomotor changes and tau hypophosphorylation in a “P301L” tau knockin mouse. Neurobiol Aging 33:621.e1–621.e15.

Ginsberg SD, Che S, Counts SE, Mufson EJ (2006) Shift in the ratio of three-repeat tau and four-repeat tau mRNAs in individual cholinergic basal forebrain neurons in mild cognitive impairment and Alzheimer's disease. J Neurochem 96:1401–1408.

Glater EE, Megeath LJ, Stowers RS, Schwarz TL (2006) Axonal transport of mitochondria requires milton to recruit kinesin heavy chain and is light chain independent. J Cell Biol 173:545–557.

Goedert M. Alzheimer’s and Parkinson’s diseases: The prion concept in relation to assembled Aβ, tau, and α-synuclein. Science. American Association for the Advancement of Science; 2015 Aug 7;349(6248):1255555–5.

Goedert M, Jakes R (1990) Expression of separate isoforms of human tau protein: correlation with the tau pattern in brain and effects on tubulin polymerization. EMBO J 9:4225–4230.

Goedert M, Jakes R (2005) Mutations causing neurodegenerative tauopathies. Biochim Biophys Acta 1739:240–250.

Goedert M, Jakes R, Spillantini MG, Hasegawa M, Smith MJ, Crowther RA (1996) Assembly of microtubule-associated protein tau into Alzheimer-like filaments induced by sulphated glycosaminoglycans. Nature 383:550–553.

Goedert M, Spillantini MG (2011) Pathogenesis of the tauopathies. J Mol Neurosci 45:425–431.

Goedert M, Spillantini MG, Jakes R, Rutherford D, Crowther RA (1989) Multiple isoforms of human microtubule-associated protein tau: sequences and localization in neurofibrillary tangles of Alzheimer's disease. Neuron 3:519–526.

Goedert M, Wischik CM, Crowther RA, Walker JE, Klug A (1988) Cloning and sequencing of the cDNA encoding a core protein of the paired helical filament of Alzheimer disease: identification as the microtubule-associated protein tau. Proc Natl Acad Sci USA 85:4051–4055.

Gold M, Lorenzl S, Stewart AJ, Morimoto BH, Williams DR, Gozes I (2012) Critical appraisal of the role of davunetide in the treatment of progressive supranuclear palsy. Neuropsychiatr Dis Treat 8:85–93.

Gong CX, Singh TJ, Grundke-Iqbal I, Iqbal K (1994) Alzheimer's disease abnormally phosphorylated tau is dephosphorylated by protein phosphatase-2B (calcineurin). J Neurochem 62:803–806.

Gómez-Ramos A, Díaz-Hernández M, Rubio A, Díaz-Hernández JI, Miras-Portugal MT, Avila J (2009) Characteristics and consequences of muscarinic receptor activation by tau protein. Eur Neuropsychopharmacol 19:708–717.

Greer EL, Oskoui PR, Banko MR, Maniar JM, Gygi MP, Gygi SP, Brunet A (2007) The energy sensor AMP-activated protein kinase directly regulates the mammalian FOXO3 transcription factor. J Biol Chem 282:30107–30119.

Grinberg LT, Wang X, Wang C, Sohn PD, Theofilas P, Sidhu M, Arevalo JB, Heinsen H, Huang EJ, Rosen H, Miller BL, Gan L, Seeley WW (2013) Argyrophilic grain disease differs from other tauopathies by lacking tau acetylation. Acta Neuropathol 125:581–593.

Guillozet-Bongaarts AL, Cahill ME, Cryns VL, Reynolds MR, Berry RW, Binder LI (2006) Pseudophosphorylation of tau at serine 422 inhibits caspase cleavage: in vitro evidence and implications for tangle formation in vivo. J Neurochem 97:1005–1014.

Guillozet-Bongaarts AL, Glajch KE, Libson EG, Cahill ME, Bigio E, Berry RW, Binder LI (2007) Phosphorylation and cleavage of tau in non-AD tauopathies. Acta Neuropathol 113:513–520.

Guo H, Albrecht S, Bourdeau M, Petzke T, Bergeron C, LeBlanc AC (2004) Active caspase-6 and caspase-6-cleaved tau in neuropil threads, neuritic plaques, and neurofibrillary tangles of Alzheimer's disease. Am J Pathol 165:523–531.

Guo T, Noble W, Hanger DP (2017) Roles of tau protein in health and disease. Acta Neuropathol 133:665–704.

Gureviciene I, Ikonen S, Gurevicius K, Sarkaki A, van Groen T, Pussinen R, Ylinen A, Tanila H (2004) Normal induction but accelerated decay of LTP in APP + PS1 transgenic mice. Neurobiol Dis 15:188–195.

Hall GF, Chu B, Lee G, Yao J (2000) Human tau filaments induce microtubule and synapse loss in an in vivo model of neurofibrillary degenerative disease. J Cell Sci 113 (Pt 8):1373–1387.

Hall GF, Lee VM, Lee G, Yao J (2001) Staging of neurofibrillary degeneration caused by human tau overexpression in a unique cellular model of human tauopathy. Am J Pathol 158:235–246.

Halpain S, Spencer K, Graber S (2005) Dynamics and pathology of dendritic spines. Prog Brain Res 147:29–37.

Hamos JE, DeGennaro LJ, Drachman DA (1989) Synaptic loss in Alzheimer's disease and other dementias. Neurology 39:355–361.

Handschin C, Spiegelman BM (2006) Peroxisome proliferator-activated receptor gamma coactivator 1 coactivators, energy homeostasis, and metabolism. Endocr Rev 27:728–735.

Hanger DP, Byers HL, Wray S, Leung K-Y, Saxton MJ, Seereeram A, Reynolds CH, Ward MA, Anderton BH (2007) Novel phosphorylation sites in tau from Alzheimer brain support a role for casein kinase 1 in disease pathogenesis. J Biol Chem 282:23645–23654.

Hanger DP, Hughes K, Woodgett JR, Brion JP, Anderton BH (1992) Glycogen synthase kinase-3 induces Alzheimer's disease-like phosphorylation of tau: generation of paired helical filament epitopes and neuronal localisation of the kinase. Neurosci Lett 147:58–62.

Hanger DP, Seereeram A, Noble W (2009) Mediators of tau phosphorylation in the pathogenesis of Alzheimer's disease. Expert Rev Neurother 9:1647–1666.

Hanger DP, Wray S (2010) Tau cleavage and tau aggregation in neurodegenerative disease. Biochem Soc Trans 38:1016–1020.

Harada A, Oguchi K, Okabe S, Kuno J, Terada S, Ohshima T, et al. Altered microtubule organization in small-calibre axons of mice lacking tau protein. Nature. Nature Publishing Group; 1994 Jun 1;369(6480):488–91.

Hardie DG, Ross FA, Hawley SA (2012) AMPK: a nutrient and energy sensor that maintains energy homeostasis. Nat Rev Mol Cell Biol 13:251–262.

Harkins AB, Fox AP (1998) Activation of nicotinic acetylcholine receptors augments calcium channel-mediated exocytosis in rat pheochromocytoma (PC12) cells. J Gen Physiol 111:257–269.

Harris JA, Koyama A, Maeda S, Ho K, Devidze N, Dubal DB, Yu G-Q, Masliah E, Mucke L (2012) Human P301L-mutant tau expression in mouse entorhinal-hippocampal network causes tau aggregation and presynaptic pathology but no cognitive deficits. Ikezu T, ed. PLoS ONE 7:e45881.

Hassan A, Whitwell JL, Josephs KA (2014) The corticobasal syndrome–Alzheimer's disease conundrum. Expert Rev Neurother 11:1569–1578.

Hatch AL, Gurel PS, Higgs HN (2014) Novel roles for actin in mitochondrial fission. J Cell Sci 127:4549–4560.

Hauw JJ, Daniel SE, Dickson D, Horoupian DS, Jellinger K, Lantos PL, McKee A, Tabaton M, Litvan I (1994) Preliminary NINDS neuropathologic criteria for Steele-Richardson-Olszewski syndrome (progressive supranuclear palsy). Neurology 44:2015–2019.

Hayakawa K, Esposito E, Wang X, Terasaki Y, Liu Y, Xing C, Ji X, Lo EH (2016) Transfer of mitochondria from astrocytes to neurons after stroke. Nature 535:551–555.

He C, Klionsky DJ (2009) Regulation Mechanisms and Signaling Pathways of Autophagy. Annual Review of Genetics 43:67–93.

He Z (2009) Fluorogold induces persistent neurological deficits and circling behavior in mice over-expressing human mutant tau. Curr Neurovasc Res 6:54–61.

Herzig S, Long F, Jhala US, Hedrick S, Quinn R, Bauer A, Rudolph D, Schutz G, Yoon C, Puigserver P, Spiegelman B, Montminy M (2001) CREB regulates hepatic gluconeogenesis through the coactivator PGC-1. Nature 413:179–183.

Herzig S, Shaw RJ (2018) AMPK: Guardian of metabolism and mitochondrial homeostasis. Nat Rev Mol Cell Biol 19:121–135.

Hirai K, Aliev G, Nunomura A, Fujioka H, Russell RL, Atwood CS, Johnson AB, Kress Y, Vinters HV, Tabaton M, Shimohama S, Cash AD, Siedlak SL, Harris PL, Jones PK, Petersen RB, Perry G, Smith MA (2001) Mitochondrial abnormalities in Alzheimer's disease. J Neurosci 21:3017–3023.

Hoffmann NA, Dorostkar MM, Blumenstock S, Goedert M, Herms J (2013) Impaired plasticity of cortical dendritic spines in P301S tau transgenic mice. Acta Neuropathol Commun 1:82.

Hollenbeck PJ (1993) Products of endocytosis and autophagy are retrieved from axons by regulated retrograde organelle transport. J Cell Biol 121:305–315.

Hollenbeck PJ (2005) Mitochondria and neurotransmission: evacuating the synapse. Neuron 47:331–333.

Hoover BR, Reed MN, Su J, Penrod RD, Kotilinek LA, Grant MK, Pitstick R, Carlson GA, Lanier LM, Yuan L-L, Ashe KH, Liao D (2010) Tau mislocalization to dendritic spines mediates synaptic dysfunction independently of neurodegeneration. Neuron 68:1067–1081.

Horowitz PM, Patterson KR, Guillozet-Bongaarts AL, Reynolds MR, Carroll CA, Weintraub ST, Bennett DA, Cryns VL, Berry RW, Binder LI (2004) Early N-terminal changes and caspase-6 cleavage of tau in Alzheimer's disease. J Neurosci 24:7895–7902.

Hostenbach S, Cambron M, D'haeseleer M, Kooijman R, De Keyser J (2014) Astrocyte loss and astrogliosis in neuroinflammatory disorders. Neurosci Lett 565:39–41.

Houlden H et al. (2001) Corticobasal degeneration and progressive supranuclear palsy share a common tau haplotype. Neurology 56:1702–1706.

Houten SM, Auwerx J (2004) PGC-1alpha: turbocharging mitochondria. Cell 119:5–7.

Hsiao K, Chapman P, Nilsen S, Eckman C, Harigaya Y, Younkin S, Yang F, Cole G (1996) Correlative memory deficits, Abeta elevation, and amyloid plaques in transgenic mice. Science 274:99–102.

Hu Y, Li X-C, Wang Z-H, Luo Y, Zhang X, Liu X-P, Feng Q, Wang Q, Yue Z, Chen Z, Ye K, Wang J-Z, Liu G-P (2016) Tau accumulation impairs mitophagy via increasing mitochondrial membrane potential and reducing mitochondrial Parkin. Oncotarget 7:17356–17368.

Hutton M et al. (1998) Association of missense and 5'-splice-site mutations in tau with the inherited dementia FTDP-17. Nature 393:702–705.

Hyman BT, Van Hoesen GW, Damasio AR, Barnes CL (1984) Alzheimer's disease: cell-specific pathology isolates the hippocampal formation. Science 225:1168–1170.

Ichimura Y, Kominami E, Tanaka K, Komatsu M (2008) Selective turnover of p62/A170/SQSTM1 by autophagy. Autophagy 4:1063–1066.

Igaz LM, Kwong LK, Chen-Plotkin A, Winton MJ, Unger TL, Xu Y, Neumann M, Trojanowski JQ, Lee VM-Y (2009) Expression of TDP-43 C-terminal Fragments in Vitro Recapitulates Pathological Features of TDP-43 Proteinopathies. J Biol Chem 284:8516–8524.

Igaz LM, Kwong LK, Xu Y, Truax AC, Uryu K, Neumann M, Clark CM, Elman LB, Miller BL, Grossman M, McCluskey LF, Trojanowski JQ, Lee VM-Y (2008) Enrichment of C-terminal fragments in TAR DNA-binding protein-43 cytoplasmic inclusions in brain but not in spinal cord of frontotemporal lobar degeneration and amyotrophic lateral sclerosis. Am J Pathol 173:182–194.

Ikeda K, Haga C, Akiyama H, Kase K, Iritani S (1992) Coexistence of paired helical filaments and glial filaments in astrocytic processes within ghost tangles. Neurosci Lett 148:126–128.

Irwin DJ, Cairns NJ, Grossman M, McMillan CT, Lee EB, Van Deerlin VM, Lee VM-Y, Trojanowski JQ (2015) Frontotemporal lobar degeneration: defining phenotypic diversity through personalized medicine. Acta Neuropathol 129:469–491.

Irwin DJ, Cohen TJ, Grossman M, Arnold SE, McCarty-Wood E, Van Deerlin VM, Lee VM-Y, Trojanowski JQ (2013) Acetylated tau neuropathology in sporadic and hereditary tauopathies. Am J Pathol 183:344–351.

Irwin DJ, Cohen TJ, Grossman M, Arnold SE, Xie SX, Lee VM-Y, Trojanowski JQ (2012) Acetylated tau, a novel pathological signature in Alzheimer's disease and other tauopathies. Brain 135:807–818.

Ishihara N, Eura Y, Mihara K (2004) Mitofusin 1 and 2 play distinct roles in mitochondrial fusion reactions via GTPase activity. J Cell Sci 117:6535–6546.

Itoh K, Tamura Y, Iijima M, Sesaki H (2013) Effects of Fcj1-Mos1 and mitochondrial division on aggregation of mitochondrial DNA nucleoids and organelle morphology. Mol Biol Cell 24:1842–1851.

Ittner LM, Götz J (2011) Amyloid-β and tau--a toxic pas de deux in Alzheimer's disease. Nat Rev Neurosci 12:65–72.

Ittner LM, Ke YD, Delerue F, Bi M, Gladbach A, van Eersel J, Wölfing H, Chieng BC, Christie MJ, Napier IA, Eckert A, Staufenbiel M, Hardeman E, Götz J (2010) Dendritic function of tau mediates amyloid-beta toxicity in Alzheimer's disease mouse models. Cell 142:387–397.

Ittner LM, Ke YD, Götz J (2009) Phosphorylated Tau interacts with c-Jun N-terminal kinase-interacting protein 1 (JIP1) in Alzheimer disease. J Biol Chem 284:20909–20916.

Jeganathan S, Bergen von M, Brutlach H, Steinhoff H-J, Mandelkow E (2006) Global hairpin folding of tau in solution. Biochemistry 45:2283–2293.

Jeganathan S, Hascher A, Chinnathambi S, Biernat J, Mandelkow E-M, Mandelkow E (2008) Proline-directed pseudo-phosphorylation at AT8 and PHF1 epitopes induces a compaction of the paperclip folding of Tau and generates a pathological (MC-1) conformation. J Biol Chem 283:32066–32076.

Jensen PH, Li J-Y, Dahlström A, Dotti CG (2008) Axonal transport of synucleins is mediated by all rate components. European Journal of Neuroscience 11:3369–3376.

Johansen T, Lamark T (2011) Selective autophagy mediated by autophagic adapter proteins. Autophagy 7:279–296.

Julien C, Tremblay C, Émond V, Lebbadi M, Salem N Jr., Bennett DA, Calon F (2009) Sirtuin 1 Reduction parallels the accumulation of tau in Alzheimer disease. J Neuropathol Exp Neurol 68:48–58.

Kabeya Y, Mizushima N, Ueno T, Yamamoto A, Kirisako T, Noda T, Kominami E, Ohsumi Y, Yoshimori T (2000) LC3, a mammalian homologue of yeast Apg8p, is localized in autophagosome membranes after processing. EMBO J 19:5720–5728.

Kamah A, Huvent I, Cantrelle F-X, Qi H, Lippens G, Landrieu I, Smet-Nocca C (2014) Nuclear magnetic resonance analysis of the acetylation pattern of the neuronal Tau protein. Biochemistry 53:3020–3032.

Kanaan NM, Morfini GA, LaPointe NE, Pigino GF, Patterson KR, Song Y, Andreadis A, Fu Y, Brady ST, Binder LI (2011) Pathogenic forms of tau inhibit kinesin-dependent axonal transport through a mechanism involving activation of axonal phosphotransferases. J Neurosci 31:9858–9868.

Kandimalla R, Reddy PH (2016) Multiple faces of dynamin-related protein 1 and its role in Alzheimer's disease pathogenesis. Biochim Biophys Acta 1862:814–828.

Kang MJ, Kim C, Jeong H, Cho B-K, Ryou AL, Hwang D, Mook-Jung I, Yi EC (2013) Synapsin-1 and tau reciprocal O-GlcNAcylation and phosphorylation sites in mouse brain synaptosomes. Exp Mol Med 45:e29–e29.

Kann O, Kovács R (2007) Mitochondria and neuronal activity. Am J Physiol, Cell Physiol 292:C641–C657.

Katsouri L, Lim YM, Blondrath K, Eleftheriadou I, Lombardero L, Birch AM, et al. PPARγ-coactivator-1α gene transfer reduces neuronal loss and amyloid-β generation by reducing β-secretase in an Alzheimer's disease model. PNAS. National Academy of Sciences; 2016 Oct 25;113(43):12292–7.

Kempf M, Clement A, Faissner A, Lee G, Brandt R (1996) Tau binds to the distal axon early in development of polarity in a microtubule- and microfilament-dependent manner. J Neurosci 16:5583–5592.

Kerr JS, Adriaanse BA, Greig NH, Mattson MP, Cader MZ, Bohr VA, Fang EF (2017) Mitophagy and Alzheimer's disease: cellular and molecular mechanisms. Trends Neurosci 40:151–166.

Kimura T, Ishiguro K, Hisanaga S-I (2014a) Physiological and pathological phosphorylation of tau by Cdk5. Front Mol Neurosci 7:65.

Kimura T, Whitcomb DJ, Jo J, Regan P, Piers T, Heo S, Brown C, Hashikawa T, Murayama M, Seok H, Sotiropoulos I, Kim E, Collingridge GL, Takashima A, Cho K (2014b) Microtubule-associated protein tau is essential for long-term depression in the hippocampus. Philos Trans R Soc Lond, B, Biol Sci 369:20130144–20130144.

Kins S, Crameri A, Evans DR, Hemmings BA, Nitsch RM, Gotz J (2001) Reduced protein phosphatase 2A activity induces hyperphosphorylation and altered compartmentalization of tau in transgenic mice. J Biol Chem 276:38193–38200.

Knobloch M, Mansuy IM (2008) Dendritic spine loss and synaptic alterations in Alzheimer's disease. Mol Neurobiol 37:73–82.

Knutti D, Kralli A (2001) PGC-1, a versatile coactivator. Trends Endocrinol Metab 12:360–365.

Kolarova M, Garcia-Sierra F, Bartos A, Ricny J, Ripova D (2012) Structure and pathology of tau protein in Alzheimer disease. Int J Alzheimers Dis 2012:731526–13.

Kompoliti K, Goetz CG, Boeve BF, Maraganore DM, Ahlskog JE, Marsden CD, Bhatia KP, Greene PE, Przedborski S, Seal EC, Burns RS, Hauser RA, Gauger LL, Factor SA, Molho ES, Riley DE (1998) Clinical presentation and pharmacological therapy in corticobasal degeneration. Arch Neurol 55:957–961.

Koo S-H, Satoh H, Herzig S, Lee C-H, Hedrick S, Kulkarni R, Evans RM, Olefsky J, Montminy M (2004) PGC-1 promotes insulin resistance in liver through PPAR-alpha-dependent induction of TRB-3. Nat Med 10:530–534.

Kopeikina KJ, Carlson GA, Pitstick R, Ludvigson AE, Peters A, Luebke JI, Koffie RM, Frosch MP, Hyman BT, Spires-Jones TL (2011) Tau accumulation causes mitochondrial distribution deficits in neurons in a mouse model of tauopathy and in human Alzheimer's disease brain. Am J Pathol 179:2071–2082.

Kopeikina KJ, Polydoro M, Tai H-C, Yaeger E, Carlson GA, Pitstick R, Hyman BT, Spires-Jones TL (2013) Synaptic alterations in the rTg4510 mouse model of tauopathy. J Comp Neurol 521:1334–1353.

Korobova F, Ramabhadran V, Higgs HN (2013) An actin-dependent step in mitochondrial fission mediated by the ER-associated formin INF2. Science 339:464–467.

Kotani S, Nishida E, Kumagai H, Sakai H (1985) Calmodulin inhibits interaction of actin with MAP2 and Tau, two major microtubule-associated proteins. J Biol Chem 260:10779–10783.

Köpke E, Tung YC, Shaikh S, Alonso AC, Iqbal K, Grundke-Iqbal I (1993) Microtubule-associated protein tau. Abnormal phosphorylation of a non-paired helical filament pool in Alzheimer disease. J Biol Chem 268:24374–24384.

Kretzschmar H (2009) Brain banking: opportunities, challenges and meaning for the future. Nat Rev Neurosci 10:70–78.

Lackner LL, Nunnari JM (2009) The molecular mechanism and cellular functions of mitochondrial division. Biochim Biophys Acta 1792:1138–1144.

Lagouge M, Argmann C, Gerhart-Hines Z, Meziane H, Lerin C, Daussin F, Messadeq N, Milne J, Lambert P, Elliott P, Geny B, Laakso M, Puigserver P, Auwerx J (2006) Resveratrol improves mitochondrial function and protects against metabolic disease by activating SIRT1 and PGC-1alpha. Cell 127:1109–1122.

Lain E, Carnejac S, Escher P, Wilson MC, Lømo T, Gajendran N, Brenner HR (2009) A novel role for embigin to promote sprouting of motor nerve terminals at the neuromuscular junction. J Biol Chem 284:8930–8939.

Lalonde R, Strazielle C (2011) Genetic models of cerebellar dysfunction. in: animal models of movement disorders, pp 241–262 Neuromethods. Totowa, NJ: Humana Press.

Lang AE, Miyasaki J, Olanow CW, Stoessl AJ, Suchowersky O (2005) Progress in clinical neurosciences: a forum on the early management of Parkinson's disease. Can J Neurol Sci 32:277–286.

Lasagna-Reeves CA, Kayed R (2011) Astrocytes contain amyloid-β annular protofibrils in Alzheimer's disease brains. FEBS Lett 585:3052–3057.

Laws N, Hoey A (2004) Progression of kyphosis in mdxmice. Journal of Applied Physiology 97:1970–1977.

Lazarou M, Sliter DA, Kane LA, Sarraf SA, Wang C, Burman JL, Sideris DP, Fogel AI, Youle RJ (2015) The ubiquitin kinase PINK1 recruits autophagy receptors to induce mitophagy. Nature 524:309–314.

Leclair-Visonneau L, Rouaud T, Debilly B, Durif F, Houeto J-L, Kreisler A, Defebvre L, Lamy E, Volteau C, Nguyen J-M, Dily SL, Damier P, Boutoleau-Bretonnière C, Lejeune P, Derkinderen P (2016) Randomized placebo-controlled trial of sodium valproate in progressive supranuclear palsy. Clin Neurol Neurosurg 146:35–39.

Lee VM, Goedert M, Trojanowski JQ (2001) Neurodegenerative tauopathies. Annu Rev Neurosci 24:1121–1159.

Leone TC, Lehman JJ, Finck BN, Schaeffer PJ, Wende AR, Boudina S, et al. PGC-1α Deficiency Causes Multi-System Energy Metabolic Derangements: Muscle Dysfunction, Abnormal Weight Control and Hepatic Steatosis. Vidal-Puig A, editor. PLoS Biol. Public Library of Science; 2005 Mar 15;3(4):e101.

Levin J, Giese A, Boetzel K, Israel L, Högen T, Nübling G, Kretzschmar H, Lorenzl S (2009) Increased alpha-synuclein aggregation following limited cleavage by certain matrix metalloproteinases. Exp Neurol 215:201–208.

Lewis J, Dickson DW, Lin WL, Chisholm L, Corral A, Jones G, Yen SH, Sahara N, Skipper L, Yager D, Eckman C, Hardy J, Hutton M, McGowan E (2001) Enhanced neurofibrillary degeneration in transgenic mice expressing mutant tau and APP. Science 293:1487–1491.

Lewis J, McGowan E, Rockwood J, Melrose H, Nacharaju P, Van Slegtenhorst M, Gwinn-Hardy K, Paul Murphy M, Baker M, Yu X, Duff K, Hardy J, Corral A, Lin WL, Yen SH, Dickson DW, Davies P, Hutton M (2000) Neurofibrillary tangles, amyotrophy and progressive motor disturbance in mice expressing mutant (P301L) tau protein. Nat Genet 25:402–405.

Lewis TL, Turi GF, Kwon S-K, Losonczy A, Polleux F (2016) Progressive decrease of mitochondrial motility during maturation of cortical axons in vitro and in vivo. Curr Biol 26:2602–2608.

Leyns CEG, Holtzman DM (2017) Glial contributions to neurodegeneration in tauopathies. Mol Neurodegener 12.

Li PA, Hou X, Hao S (2017) Mitochondrial biogenesis in neurodegeneration. J Neurosci Res 95:2025–2029.

Li Z, Okamoto K-I, Hayashi Y, Sheng M (2004) The importance of dendritic mitochondria in the morphogenesis and plasticity of spines and synapses. Cell 119:873–887.

Liang WS, Reiman EM, Valla J, Dunckley T, Beach TG, Grover A, Niedzielko TL, Schneider LE, Mastroeni D, Caselli R, Kukull W, Morris JC, Hulette CM, Schmechel D, Rogers J, Stephan DA (2008) Alzheimer's disease is associated with reduced expression of energy metabolism genes in posterior cingulate neurons. Proc Natl Acad Sci USA 105:4441–4446.

Lin M-Y, Cheng X-T, Tammineni P, Xie Y, Zhou B, Cai Q, Sheng Z-H (2017) Releasing Syntaphilin Removes Stressed Mitochondria from Axons Independent of Mitophagy under Pathophysiological Conditions. Neuron 94:595–610.e596.

Lin MT, Beal MF (2006) Mitochondrial dysfunction and oxidative stress in neurodegenerative diseases. Nature 443:787–795.

Lin J, Wu P-H, Tarr PT, Lindenberg KS, St-Pierre J, Zhang C-Y, et al. Defects in Adaptive Energy Metabolism with CNS-Linked Hyperactivity in PGC-1α Null Mice. Cell. Cell Press; 2004 Oct 1;119(1):121–35.

Lindsay J, Laurin D, Verreault R, Hébert R, Helliwell B, Hill GB, McDowell I (2002) Risk factors for Alzheimer's disease: a prospective analysis from the Canadian Study of Health and Aging. Am J Epidemiol 156:445–453.

Litvan I, Agid Y, Goetz C, Jankovic J, Wenning GK, Brandel JP, Lai EC, Verny M, Ray-Chaudhuri K, McKee A, Jellinger K, Pearce RK, Bartko JJ (1997) Accuracy

of the clinical diagnosis of corticobasal degeneration: a clinicopathologic study. Neurology 48:119–125.

Liu C, Götz J (2013) Profiling murine tau with 0N, 1N and 2N isoform-specific antibodies in brain and peripheral organs reveals distinct subcellular localization, with the 1N isoform being enriched in the nucleus. Gong C-X, ed. PLoS ONE 8:e84849.

Liu C-C, Kanekiyo T, Xu H, Bu G. Apolipoprotein E and Alzheimer disease: risk, mechanisms and therapy. Nature Reviews Neurology 2013 9:2. Nature Publishing Group; 2013 Feb 1;9(2):106–18.

Liu C, Song X, Nisbet R, Götz J (2016) Co-immunoprecipitation with tau isoform-specific antibodies reveals distinct protein interactions and highlights a putative role for 2N tau in disease. J Biol Chem 291:8173–8188.

Liu F, Li B, Tung E-J, Grundke-Iqbal I, Iqbal K, Gong C-X (2007) Site-specific effects of tau phosphorylation on its microtubule assembly activity and self-aggregation. Eur J Neurosci 26:3429–3436.

Llorens-Martin M, Teixeira CM, Fuster-Matanzo A, Jurado-Arjona J, Borrell V, Soriano E, Avila J, Hernández F (2012) Tau isoform with three microtubule binding domains is a marker of new axons generated from the subgranular zone in the hippocampal dentate gyrus: implications for Alzheimer's Disease. Journal of Alzheimer's Disease 29:921–930.

LoPresti P, Szuchet S, Papasozomenos SC, Zinkowski RP, Binder LI (1995) Functional implications for the microtubule-associated protein tau: localization in oligodendrocytes. Proc Natl Acad Sci USA 92:10369–10373.

Lores-Arnaiz S, Lombardi P, Karadayian AG, Orgambide F, Cicerchia D, Bustamante J (2016) Brain cortex mitochondrial bioenergetics in synaptosomes and non-synaptic mitochondria during aging. Neurochem Res 41:353–363.

Losón OC, Song Z, Chen H, Chan DC (2013) Fis1, Mff, MiD49, and MiD51 mediate Drp1 recruitment in mitochondrial fission. Mol Biol Cell 24:659–667.

Lovestone S, Reynolds CH, Latimer D, Davis DR, Anderton BH, Gallo J-M, et al. Alzheimer's disease-like phosphorylation of the microtubule-associated protein tau by glycogen synthase kinase-3 in transfected mammalian cells. Current Biology. Cell Press; 1994 Dec 1;4(12):1077–86.

Ludolph AC et al. (2009) Tauopathies with parkinsonism: clinical spectrum, neuropathologic basis, biological markers, and treatment options. Eur J Neurol 16:297–309.

Lyon MF (1962) Sex chromatin and gene action in the mammalian X-chromosome. American Journal of Human Genetics 14:135–148.

Ma Q (2013) Role of nrf2 in oxidative stress and toxicity. Annu Rev Pharmacol Toxicol 53:401–426.

MacAskill AF, Kittler JT (2010) Control of mitochondrial transport and localization in neurons. Trends Cell Biol 20:102–112.

Magen D, Georgopoulos C, Bross P, Ang D, Segev Y, Goldsher D, Nemirovski A, Shahar E, Ravid S, Luder A, Heno B, Gershoni-Baruch R, Skorecki K, Mandel H (2008) Mitochondrial hsp60 chaperonopathy causes an autosomal-recessive neurodegenerative disorder linked to brain hypomyelination and leukodystrophy. American Journal of Human Genetics 83:30–42.

Magnani E, Fan J, Gasparini L, Golding M, Williams M, Schiavo G, Goedert M, Amos LA, Spillantini MG (2007) Interaction of tau protein with the dynactin complex. EMBO J 26:4546–4554.

Maina MB, Al-Hilaly Y, Serpell L. Nuclear Tau and Its Potential Role in Alzheimer's Disease. Biomolecules 2016, Vol 6, Page 9. Multidisciplinary Digital Publishing Institute; 2016 Jan 7;6(1):9.

Mahapatra RK, Edwards MJ, Schott JM, Bhatia KP (2004) Corticobasal degeneration. Lancet Neurol 3:736–743.

Malenka RC, Bear MF (2004) LTP and LTD: an embarrassment of riches. Neuron 44:5–21.

Manczak M, Reddy PH (2012) Abnormal interaction between the mitochondrial fission protein Drp1 and hyperphosphorylated tau in Alzheimer's disease neurons: implications for mitochondrial dysfunction and neuronal damage. Hum Mol Genet 21:2538–2547.

Mandelkow E-M, Thies E, Trinczek B, Biernat J, Mandelkow E (2004) MARK/PAR1 kinase is a regulator of microtubule-dependent transport in axons. J Cell Biol 167:99–110.

Mandelkow EM, Drewes G, Biernat J, Gustke N, Van Lint J, Vandenheede JR, Mandelkow E (1992) Glycogen synthase kinase-3 and the Alzheimer-like state of microtubule-associated protein tau. FEBS Lett 314:315–321.

Mandelkow EM, Schweers O, Drewes G, Biernat J, Gustke N, Trinczek B, Mandelkow E (1996) Structure, microtubule interactions, and phosphorylation of tau protein. Ann N Y Acad Sci 777:96–106.

Mandell JW, Banker GA (1996) A spatial gradient of tau protein phosphorylation in nascent axons. J Neurosci 16:5727–5740.

Mann SS, Hammarback JA (1994) Molecular characterization of light chain 3. A microtubule binding subunit of MAP1A and MAP1B. J Biol Chem 269:11492–11497.

Martinez-Vicente M (2017) Neuronal Mitophagy in Neurodegenerative Diseases. Front Mol Neurosci 10:64.

Marttinen M, Kurkinen KM, Soininen H, Haapasalo A, Hiltunen M (2015) Synaptic dysfunction and septin protein family members in neurodegenerative diseases. Mol Neurodegener 10:16.

Masliah E, Terry RD, DeTeresa RM, Hansen LA (1989) Immunohistochemical quantification of the synapse-related protein synaptophysin in Alzheimer disease. Neurosci Lett 103:234–239.

Matsumoto S-E, Motoi Y, Ishiguro K, Tabira T, Kametani F, Hasegawa M, Hattori N (2015) The twenty-four KDa C-terminal tau fragment increases with aging in tauopathy mice: implications of prion-like properties. Hum Mol Genet 24:6403–6416.

McKhann GM, Albert MS, Grossman M, Miller B, Dickson D, Trojanowski JQ, Work Group on Frontotemporal Dementia and Pick's Disease (2001) Clinical and pathological diagnosis of frontotemporal dementia: report of the Work Group on Frontotemporal Dementia and Pick's Disease. Arch Neurol 58:1803–1809.

McVicker DP, Awe AM, Richters KE, Wilson RL, Cowdrey DA, Hu X, Chapman ER, Dent EW (2016) Transport of a kinesin-cargo pair along microtubules into dendritic spines undergoing synaptic plasticity. Nat Commun 7:12741.

Menzies FM, Fleming A, Rubinsztein DC (2015) Compromised autophagy and neurodegenerative diseases. Nat Rev Neurosci 16:345–357.

Mietelska-Porowska A, Wasik U, Goras M, Filipek A, Niewiadomska G (2014) Tau protein modifications and interactions: their role in function and dysfunction. International Journal of Molecular Sciences 15:4671–4713.

Millecamps S, Julien J-P (2013) Axonal transport deficits and neurodegenerative diseases. Nat Rev Neurosci 14:161–176.

Miller KE (2004) Axonal mitochondrial transport and potential are correlated. J Cell Sci 117:2791–2804.

Miller M (1981) Maturation of rat visual cortex. I. A quantitative study of Golgi-impregnated pyramidal neurons. J Neurocytol 10:859–878.

Min S-W et al. (2015) Critical role of acetylation in tau-mediated neurodegeneration and cognitive deficits. Nat Med 21:1154–1162.

Min S-W, Cho S-H, Zhou Y, Schroeder S, Haroutunian V, Seeley WW, Huang EJ, Shen Y, Masliah E, Mukherjee C, Meyers D, Cole PA, Ott M, Gan L (2010) Acetylation of tau inhibits its degradation and contributes to tauopathy. Neuron 67:953–966.

Mirra SS (1999) Apolipoprotein E and the neuropathology of Alzheimer's disease. Human Pathology 30:1125–1127.

Mitchell SJ, Martin-Montalvo A, Mercken EM, Palacios HH, Ward TM, Abulwerdi G, Minor RK, Vlasuk GP, Ellis JL, Sinclair DA, Dawson J, Allison DB, Zhang Y, Becker KG, Bernier M, de Cabo R (2014) The SIRT1 activator SRT1720 extends lifespan and improves health of mice fed a standard diet. Cell Rep 6:836–843.

Mocanu M-M, Nissen A, Eckermann K, Khlistunova I, Biernat J, Drexler D, Petrova O, Schönig K, Bujard H, Mandelkow E, Zhou L, Rune G, Mandelkow E-M (2008) The potential for beta-structure in the repeat domain of tau protein determines aggregation, synaptic decay, neuronal loss, and coassembly with endogenous Tau in inducible mouse models of tauopathy. J Neurosci 28:737–748.

Montine TJ, Phelps CH, Beach TG, Bigio EH, Cairns NJ, Dickson DW, et al. National Institute on Aging–Alzheimer’s Association guidelines for the neuropathologic

assessment of Alzheimer's disease: a practical approach. Acta Neuropathol. 2011 Nov 20;123(1):1–11.

Morel M, Héraud C, Nicaise C, Suain V, Brion J-P (2012) Levels of kinesin light chain and dynein intermediate chain are reduced in the frontal cortex in Alzheimer's disease: implications for axoplasmic transport. Acta Neuropathol 123:71–84.

Morris M, Knudsen GM, Maeda S, Trinidad JC, Ioanoviciu A, Burlingame AL, Mucke L (2015) Tau post-translational modifications in wild-type and human amyloid precursor protein transgenic mice. Nat Neurosci 18:1183–1189.

Morris M, Koyama A, Masliah E, Mucke L (2011) Tau reduction does not prevent motor deficits in two mouse models of Parkinson's disease. Feany MB, ed. PLoS ONE 6:e29257.

Mosconi L, Mistur R, Switalski R, Tsui WH, Glodzik L, Li Y, Pirraglia E, De Santi S, Reisberg B, Wisniewski T, de Leon MJ (2009) FDG-PET changes in brain glucose metabolism from normal cognition to pathologically verified Alzheimer's disease. Eur J Nucl Med Mol Imaging 36:811–822.

Mufson EJ, Ward S, Binder L (2014) Prefibrillar Tau Oligomers in Mild Cognitive Impairment and Alzheimer's Disease. NDD 13:151–153.

Mukrasch MD, Bibow S, Korukottu J, Jeganathan S, Biernat J, Griesinger C, Mandelkow E, Zweckstetter M (2009) Structural polymorphism of 441-residue tau at single residue resolution. Petsko GA, ed. PLoS Biol 7:e34.

Mukrasch MD, Markwick P, Biernat J, Bergen MV, Bernadó P, Griesinger C, Mandelkow E, Zweckstetter M, Blackledge M (2007) Highly populated turn conformations in natively unfolded tau protein identified from residual dipolar couplings and molecular simulation. J Am Chem Soc 129:5235–5243.

Navarro X, Vivó M, Valero-Cabré A (2007) Neural plasticity after peripheral nerve injury and regeneration. Prog Neurobiol 82:163–201.

Neary D, Snowden JS, Gustafson L, Passant U, Stuss D, Black S, Freedman M, Kertesz A, Robert PH, Albert M, Boone K, Miller BL, Cummings J, Benson DF (1998) Frontotemporal lobar degeneration: a consensus on clinical diagnostic criteria. In, pp 1546–1554.

Neupert W, Brunner M, Hell K (2008) Proteins Import into Mitochondria. Weinheim, Germany: Wiley-VCH Verlag GmbH & Co. KGaA.

Neve RL, Harris P, Kosik KS, Kurnit DM, Donlon TA (1986) Identification of cDNA clones for the human microtubule-associated protein tau and chromosomal localization of the genes for tau and microtubule-associated protein 2. Molecular Brain Research 1:271–280.

Nie CL, Wei Y, Chen X, Liu YY, Dui W, Liu Y, Davies MC, Tendler SJB, He RG (2007) Formaldehyde at low concentration induces protein tau into globular amyloid-like aggregates in vitro and in vivo. Herman C, ed. PLoS ONE 2:e629.

Nieto A, Correas I, López-Otín C, Avila J (1991) Tau-related protein present in paired helical filaments has a decreased tubulin binding capacity as compared with microtubule-associated protein tau. Biochim Biophys Acta 1096:197–204.

Nimchinsky EA, Sabatini BL, Svoboda K (2002) Structure and function of dendritic spines. Annu Rev Physiol 64:313–353.

Nixon RA, Wegiel J, Kumar A, Yu WH, Peterhoff C, Cataldo A, Cuervo AM (2005) Extensive involvement of autophagy in Alzheimer disease: an immuno-electron microscopy study. J Neuropathol Exp Neurol 64:113–122.

Noble W, Hanger DP, Gallo J-M (2010) Transgenic mouse models of tauopathy in drug discovery. CNS Neurol Disord Drug Targets 9:403–428.

Noble W, Hanger DP, Miller CCJ, Lovestone S (2013) The importance of tau phosphorylation for neurodegenerative diseases. Front Neurol 4:83.

Novák M, Kabat J, Wischik CM (1993) Molecular characterization of the minimal protease resistant tau unit of the Alzheimer's disease paired helical filament. EMBO J 12:365–370.

Nunnari J, Suomalainen A (2012) Mitochondria: In Sickness and in Health. Cell 148:1145–1159.

Onyango IG, Lu J, Rodova M, Lezi E, Crafter AB, Swerdlow RH (2010) Regulation of neuron mitochondrial biogenesis and relevance to brain health. Biochim Biophys Acta 1802:228–234.

Osborn LM, Kamphuis W, Wadman WJ, Hol EM (2016) Astrogliosis: An integral player in the pathogenesis of Alzheimer's disease. Prog Neurobiol 144:121–141.

Otera H, Wang C, Cleland MM, Setoguchi K, Yokota S, Youle RJ, Mihara K (2010) Mff is an essential factor for mitochondrial recruitment of Drp1 during mitochondrial fission in mammalian cells. J Cell Biol 191:1141–1158.

Paholikova K, Salingova B, Opattova A, Skrabana R, Majerova P, Zilka N, Kovacech B, Zilkova M, Barath P, Novak M (2015) N-terminal Truncation of Microtubule Associated Protein Tau Dysregulates its Cellular Localization. Journal of Alzheimer's Disease 43:915–926.

Palmer CS, Osellame LD, Stojanovski D, Ryan MT (2011) The regulation of mitochondrial morphology: intricate mechanisms and dynamic machinery. Cell Signal 23:1534–1545.

Panza F, Solfrizzi V, Seripa D, Imbimbo BP, Lozupone M, Santamato A, Zecca C, Barulli MR, Bellomo A, Pilotto A, Daniele A, Greco A, Logroscino G (2016) Tau-Centric Targets and Drugs in Clinical Development for the Treatment of Alzheimer's Disease. Biomed Res Int 2016:3245935–15.

Papasozomenos SC, Binder LI (1987) Phosphorylation determines two distinct species of Tau in the central nervous system. Cell Motil Cytoskeleton 8:210–226.

Parisi MA, Clayton DA (1991) Similarity of human mitochondrial transcription factor 1 to high mobility group proteins. Science 252:965–969.

Parkes JD, Vollum D, Marsden CD, Branfoot AC (1972) Café-au-lait spots and vitiligo in Parkinson's disease. Lancet 2:1373.

Pei JJ, Tanaka T, Tung YC, Braak E, Iqbal K, Grundke-Iqbal I (1997) Distribution, levels, and activity of glycogen synthase kinase-3 in the Alzheimer disease brain. J Neuropathol Exp Neurol 56:70–78.

Pekny M, Pekna M (2014) Astrocyte reactivity and reactive astrogliosis: costs and benefits. Physiol Rev 94:1077–1098.

Pérez M, Valpuesta JM, Medina M, Montejo de Garcini E, Avila J (1996) Polymerization of tau into filaments in the presence of heparin: the minimal sequence required for tau-tau interaction. J Neurochem 67:1183–1190.

Piras A, Collin L, Grüninger F, Graff C, Rönnbäck A (2016) Autophagic and lysosomal defects in human tauopathies: analysis of post-mortem brain from patients with familial Alzheimer disease, corticobasal degeneration and progressive supranuclear palsy. Acta Neuropathol Commun 4:22.

Polydoro M, de Calignon A, Suárez-Calvet M, Sanchez L, Kay KR, Nicholls SB, Roe AD, Pitstick R, Carlson GA, Gómez-Isla T, Spires-Jones TL, Hyman BT (2013) Reversal of neurofibrillary tangles and tau-associated phenotype in the rTgTauEC model of early Alzheimer's disease. J Neurosci 33:13300–13311.

Pooler AM, Noble W, Hanger DP (2014) A role for tau at the synapse in Alzheimer's disease pathogenesis. Neuropharmacology 76 Pt A:1–8.

Pratt SJP, Valencia AP, Le GK, Shah SB, Lovering RM (2015) Pre- and postsynaptic changes in the neuromuscular junction in dystrophic mice. Front Physiol 6:252.

Puigserver P, Rhee J, Lin J, Wu Z, Yoon JC, Zhang CY, Krauss S, Mootha VK, Lowell BB, Spiegelman BM (2001) Cytokine stimulation of energy expenditure through p38 MAP kinase activation of PPARgamma coactivator-1. Mol Cell 8:971–982.

Punga AR, Ruegg MA (2012) Signaling and aging at the neuromuscular synapse: lessons learnt from neuromuscular diseases. Curr Opin Pharmacol 12:340–346.

Qin W, Haroutunian V, Katsel P, Cardozo CP, Ho L, Buxbaum JD, et al. PGC-1α Expression Decreases in the Alzheimer Disease Brain as a Function of Dementia. Arch Neurol. American Medical Association; 2009 Mar 1;66(3):352–61.

Quintanilla RA, Matthews-Roberson TA, Dolan PJ, Johnson GVW (2009) Caspase-Cleaved Tau Expression Induces Mitochondrial Dysfunction In Immortalized Cortical Neurons Implications For The Pathogenesis Of Alzheimer Disease. J Biol Chem 284:18754–18766.

Ramachandran A, Basu U, Sultana S, Nandakumar D, Patel SS (2017) Human mitochondrial transcription factors TFAM and TFB2M work synergistically in promoter melting during transcription initiation. Nucleic Acids Res 45:861–874.

Rankin CA, Sun Q, Gamblin TC (2007) Tau phosphorylation by GSK-3beta promotes tangle-like filament morphology. Mol Neurodegener 2:12.

Reddy PH (2006) Mitochondrial oxidative damage in aging and Alzheimer's disease: implications for mitochondrially targeted antioxidant therapeutics. J Biomed Biotechnol 2006:31372–13.

Reddy PH (2009) Role of mitochondria in neurodegenerative diseases: mitochondria as a therapeutic target in Alzheimer's disease. CNS Spectr 14:8–13

Reynolds CH, Garwood CJ, Wray S, Price C, Kellie S, Perera T, Zvelebil M, Yang A, Sheppard PW, Varndell IM, Hanger DP, Anderton BH (2008) Phosphorylation regulates tau interactions with Src homology 3 domains of phosphatidylinositol 3-kinase, phospholipase Cgamma1, Grb2, and Src family kinases. J Biol Chem 283:18177–18186.

Ridet JL, Malhotra SK, Privat A, Gage FH (1997) Reactive astrocytes: cellular and molecular cues to biological function. Trends Neurosci 20:570–577.

Rietveld L, Stuss DP, McPhee D, Delaney KR (2015) Genotype-specific effects of Mecp2 loss-of-function on morphology of Layer V pyramidal neurons in heterozygous female Rett syndrome model mice. Front Cell Neurosci 9:145.

Rissman RA, Poon WW, Blurton-Jones M, Oddo S, Torp R, Vitek MP, LaFerla FM, Rohn TT, Cotman CW (2004) Caspase-cleavage of tau is an early event in Alzheimer disease tangle pathology. J Clin Invest 114:121–130.

Robert M, Mathuranath PS (2007) Tau and Tauopathies. Neurology India 55:11.

Robinson JL, Molina-Porcel L, Corrada MM, Raible K, Lee EB, Lee VM-Y, Kawas CH, Trojanowski JQ (2014) Perforant path synaptic loss correlates with cognitive impairment and Alzheimer's disease in the oldest-old. Brain 137:2578–2587.

Rocher AB, Crimins JL, Amatrudo JM, Kinson MS, Todd-Brown MA, Lewis J, Luebke JI (2010) Structural and functional changes in tau mutant mice neurons are not linked to the presence of NFTs. Exp Neurol 223:385–393.

Rocher AB, Kinson MS, Luebke JI (2008) Significant structural but not physiological changes in cortical neurons of 12-month-old Tg2576 mice. Neurobiol Dis 32:309–318.

Rodríguez-Martín T, Cuchillo-Ibáñez I, Noble W, Nyenya F, Anderton BH, Hanger DP (2013) Tau phosphorylation affects its axonal transport and degradation. Neurobiol Aging 34:2146–2157.

Rodríguez-Martín T, Pooler AM, Lau DHW, Mórotz GM, De Vos KJ, Gilley J, Coleman MP, Hanger DP (2016) Reduced number of axonal mitochondria and tau hypophosphorylation in mouse P301L tau knockin neurons. Neurobiol Dis 85:1–10.

Rolfe DF, Brown GC (1997) Cellular energy utilization and molecular origin of standard metabolic rate in mammals. Physiol Rev 77:731–758.

Rowland KC, Irby NK, Spirou GA (2000) Specialized synapse-associated structures within the calyx of Held. J Neurosci 20:9135–9144.

Rupp A, Morrison I, Barrie JA, Halstead SK, Townson KH, Greenshields KN, Willison HJ (2012) Motor nerve terminal destruction and regeneration following anti-ganglioside antibody and complement-mediated injury: an in and ex vivo imaging study in the mouse. Exp Neurol 233:836–848.

Sandoval H, Yao C-K, Chen K, Jaiswal M, Donti T, Lin YQ, Bayat V, Xiong B, Zhang K, David G, Charng W-L, Yamamoto S, Duraine L, Graham BH, Bellen HJ (2014) Mitochondrial fusion but not fission regulates larval growth and synaptic development through steroid hormone production. Elife 3:211.

Santacruz K, Lewis J, Spires T, Paulson J, Kotilinek L, Ingelsson M, Guimaraes A, DeTure M, Ramsden M, McGowan E, Forster C, Yue M, Orne J, Janus C, Mariash A, Kuskowski M, Hyman B, Hutton M, Ashe KH (2005) Tau suppression in a neurodegenerative mouse model improves memory function. Science 309:476–481.

Santel A, Fuller MT (2001) Control of mitochondrial morphology by a human mitofusin. J Cell Sci 114:867–874.

Scaravilli T, Tolosa E, Ferrer I (2005) Progressive supranuclear palsy and corticobasal degeneration: lumping versus splitting. Mov Disord 20 Suppl 12:S21–S28.

Scarpulla RC (2002) Nuclear activators and coactivators in mammalian mitochondrial biogenesis. Biochim Biophys Acta 1576:1–14.

Scarpulla RC (2008) Nuclear control of respiratory chain expression by nuclear respiratory factors and PGC-1-related coactivator. Ann N Y Acad Sci 1147:321–334.

Schaeffer V, Lavenir I, Ozcelik S, Tolnay M, Winkler DT, Goedert M (2012) Stimulation of autophagy reduces neurodegeneration in a mouse model of human tauopathy. Brain 135:2169–2177.

Schafer KN, Cisek K, Huseby CJ, Chang E, Kuret J (2013) Structural determinants of Tau aggregation inhibitor potency. J Biol Chem 288:32599–32611.

Scheff SW, Price DA (2006) Alzheimer's disease-related alterations in synaptic density: neocortex and hippocampus. Journal of Alzheimer's Disease 9:101–115.

Scheff SW, Price DA, Schmitt FA, DeKosky ST, Mufson EJ (2007) Synaptic alterations in CA1 in mild Alzheimer disease and mild cognitive impairment. Neurology 68:1501–1508.

Schindelin J, Arganda-Carreras I, Frise E, Kaynig V, Longair M, Pietzsch T, Preibisch S, Rueden C, Saalfeld S, Schmid B, Tinevez J-Y, White DJ, Hartenstein V, Eliceiri K, Tomancak P, Cardona A (2012) Fiji: an open-source platform for biological-image analysis. Nat Methods 9:676–682.

Schneider CA, Rasband WS, Eliceiri KW (2012) NIH Image to ImageJ: 25 years of image analysis. Nat Methods 9:671–675.

Schrag A, Ben-Shlomo Y, Quinn NP (1999) Prevalence of progressive supranuclear palsy and multiple system atrophy: a cross-sectional study. Lancet 354:1771–1775.

Schulz KL, Eckert A, Rhein V, Mai S, Haase W, Reichert AS, Jendrach M, Müller WE, Leuner K (2012) A new link to mitochondrial impairment in tauopathies. Mol Neurobiol 46:205–216.

Seitz A, Kojima H, Oiwa K, Mandelkow E-M, Song Y-H, Mandelkow E (2002) Single-molecule investigation of the interference between kinesin, tau and MAP2c. EMBO J 21:4896–4905.

Serenó L, Coma M, Rodríguez M, Sánchez-Ferrer P, Sánchez MB, Gich I, et al. A novel GSK-3beta inhibitor reduces Alzheimer's pathology and rescues neuronal loss in vivo. Neurobiol Dis. 2009 Sep;35(3):359–67.

Serrano-Pozo A, Frosch MP, Masliah E, Hyman BT (2011) Neuropathological alterations in Alzheimer disease. Cold Spring Harb Perspect Med 1:a006189–a006189.

Shahpasand K, Uemura I, Saito T, Asano T, Hata K, Shibata K, et al. Regulation of Mitochondrial Transport and Inter-Microtubule Spacing by Tau Phosphorylation at the Sites Hyperphosphorylated in Alzheimer's Disease. J Neurosci. Society for Neuroscience; 2012 Feb 15;32(7):2430–41.

Shankar GM, Walsh DM (2009) Alzheimer's disease: synaptic dysfunction and Abeta. Mol Neurodegener 4:48.

Shehata HS, Shalaby NM, Esmail EH, Fahmy E (2015) Corticobasal degeneration: clinical characteristics and multidisciplinary therapeutic approach in 26 patients. Neurol Sci 36:1651–1657.

Sheng B, Wang X, Su B, Lee H-G, Casadesus G, Perry G, Zhu X (2012) Impaired mitochondrial biogenesis contributes to mitochondrial dysfunction in Alzheimer's disease. J Neurochem 120:419–429.

Sheng Z-H (2014) Mitochondrial trafficking and anchoring in neurons: New insight and implications. J Cell Biol 204:1087–1098.

Singhal N, Martin PT. Role of extracellular matrix proteins and their receptors in the development of the vertebrate neuromuscular junction. Prokop A, Reichardt LF, editors. Developmental Neurobiology. Wiley-Blackwell; 2011 Nov 1;71(11):982–1005.

Sjöberg MK, Shestakova E, Mansuroglu Z, Maccioni RB, Bonnefoy E (2006) Tau protein binds to pericentromeric DNA: a putative role for nuclear tau in nucleolar organization. J Cell Sci 119:2025–2034.

Sleigh JN, Burgess RW, Gillingwater TH, Cader MZ (2014) Morphological analysis of neuromuscular junction development and degeneration in rodent lumbrical muscles. J Neurosci Methods 227:159–165.

Slot RER, Van Harten AC, Kester MI, Jongbloed W, Bouwman FH, Teunissen CE, et al. Apolipoprotein A1 in Cerebrospinal Fluid and Plasma and Progression to Alzheimer’s Disease in Non-Demented Elderly. Darreh-Shori T, editor. Journal of Alzheimer's Disease. IOS Press; 2017 Jan 1;56(2):687–97.

Smirnova E, Griparic L, Shurland DL, van der Bliek AM (2001) Dynamin-related protein Drp1 is required for mitochondrial division in mammalian cells. Mol Biol Cell 12:2245–2256.

Sofroniew MV, Vinters HV (2010) Astrocytes: Biology and pathology. Acta Neuropathol 119:7–35.

Soininen H, Lehtovirta M, Helisalmi S, Linnaranta K, Heinonen O, Riekkinen P (1995) Increased acetylcholinesterase activity in the CSF of Alzheimer patients carrying apolipoprotein epsilon4 allele. Neuroreport 6:2518–2520.

Sokolow S, Henkins KM, Bilousova T, Gonzalez B, Vinters HV, Miller CA, Cornwell L, Poon WW, Gylys KH (2015) Pre-synaptic C-terminal truncated tau is released from cortical synapses in Alzheimer's disease. J Neurochem 133:368–379.

Song YJC, Halliday GM, Holton JL, Lashley T, O'Sullivan SS, McCann H, Lees AJ, Ozawa T, Williams DR, Lockhart PJ, Revesz TR (2009) Degeneration in different parkinsonian syndromes relates to astrocyte type and astrocyte protein expression. J Neuropathol Exp Neurol 68:1073–1083.

Söti C, Rácz A, Csermely P (2002) A nucleotide-dependent molecular switch controls atp binding at the C-terminal domain of HSP90 N-terminal nucleotide binding unmasks a C-terminal binding pocket. J Biol Chem 277:7066–7075.

Spillantini MG, Goedert M (2013) Tau pathology and neurodegeneration. Lancet Neurol 12:609–622.

Spires TL, Hyman BT (2004) Neuronal Structure is Altered by Amyloid Plaques. Reviews in the Neurosciences 15:267–278.

Spires TL, Orne JD, SantaCruz K, Pitstick R, Carlson GA, Ashe KH, Hyman BT (2006) Region-specific dissociation of neuronal loss and neurofibrillary pathology in a mouse model of tauopathy. Am J Pathol 168:1598–1607.

Spires-Jones TL, Kay K, Matsouka R, Rozkalne A, Betensky RA, Hyman BT (2011) Calcineurin inhibition with systemic FK506 treatment increases dendritic branching and dendritic spine density in healthy adult mouse brain. Neurosci Lett 487:260–263.

Sriwimol W, Limprasert P. Significant Changes in Plasma Alpha-Synuclein and Beta-Synuclein Levels in Male Children with Autism Spectrum Disorder. BioMed Research International. Hindawi; 2018 Apr 8;2018(1):1–7.

Stewart JB, Chinnery PF (2015) The dynamics of mitochondrial DNA heteroplasmy: implications for human health and disease. Nature Reviews Genetics 2015 16:9 16:530–542.

Stokin GB, Lillo C, Falzone TL, Brusch RG, Rockenstein E, Mount SL, Raman R, Davies P, Masliah E, Williams DS, Goldstein LSB (2005) Axonopathy and Transport Deficits Early in the Pathogenesis of Alzheimer's Disease. Science 307:1282–1288.

Stoothoff W, Jones PB, Spires-Jones TL, Joyner D, Chhabra E, Bercury K, Fan Z, Xie H, Bacskai B, Edd J, Irimia D, Hyman BT (2009) Differential effect of three-repeat and four-repeat tau on mitochondrial axonal transport. J Neurochem 111:417–427.

Suen D-F, Norris KL, Youle RJ (2008) Mitochondrial dynamics and apoptosis. Genes Dev 22:1577–1590.

Sugioka R, Shimizu S, Tsujimoto Y (2004) Fzo1, a protein involved in mitochondrial fusion, inhibits apoptosis. J Biol Chem 279:52726–52734.

Sultan A, Nesslany F, Violet M, Bégard S, Loyens A, Talahari S, Mansuroglu Z, Marzin D, Sergeant N, Humez S, Colin M, Bonnefoy E, Buée L, Galas M-C (2011) Nuclear tau, a key player in neuronal DNA protection. J Biol Chem 286:4566–4575.

Sweeney G, Song J. The association between PGC-1α and Alzheimer's disease. Anat Cell Biol. 2016 Mar;49(1):1–6.

Swerdlow RH, Khan SM (2004) A “mitochondrial cascade hypothesis” for sporadic Alzheimer's disease. Medical Hypotheses 63:8–20.

Szabadkai G, Simoni AM, Chami M, Wieckowski MR, Youle RJ, Rizzuto R (2004) Drp-1-dependent division of the mitochondrial network blocks intraorganellar Ca2+ waves and protects against Ca2+-mediated apoptosis. Mol Cell 16:59–68.

Šimić G, Babić Leko M, Wray S, Harrington CR, Delalle I, Jovanov-Milošević N, Bažadona D, Buée L, de Silva R, Di Giovanni G, Wischik CM, Hof PR (2017) Monoaminergic neuropathology in Alzheimer's disease. Prog Neurobiol 151:101–138.

Tackenberg C, Brandt R (2009) Divergent pathways mediate spine alterations and cell death induced by amyloid-beta, wild-type tau, and R406W tau. J Neurosci 29:14439–14450.

Takeda T, Sato T, Ito T, Sumi Y, Kobayashi T, Kitagawa M, Hirokawa K, Uchihara T (2013) Four-repeat tau-selective deposition in subthalamic nucleus and motor cortex in Alzheimer disease. Clin Neurol Neurosurg 115:641–643.

Takei Y, Teng J, Harada A, Hirokawa N (2000) Defects in axonal elongation and neuronal migration in mice with disrupted tau and map1b genes. J Cell Biol 150:989–1000.

Takuma H, Arawaka S, Mori H (2003) Isoforms changes of tau protein during development in various species. Brain Res Dev Brain Res 142:121–127.

Tamagnini F, Walsh DA, Brown JT, Bondulich MK, Hanger DP, Randall AD (2017) Hippocampal neurophysiology is modified by a disease-associated C-terminal fragment of tau protein. Neurobiol Aging 60:44–56.

Tanida I, Minematsu-Ikeguchi N, Ueno T, Kominami E (2005) Lysosomal turnover, but not a cellular level, of endogenous LC3 is a marker for autophagy. Autophagy 1:84–91.

Tanida I, Ueno T, Kominami E (2008) LC3 and Autophagy. Methods Mol Biol 445:77–88.

Tawana K, Ramsden DB (2001) Progressive supranuclear palsy. MP, Mol Pathol 54:427–434.

Terry RD (2000) Cell death or synaptic loss in Alzheimer disease. J Neuropathol Exp Neurol 59:1118–1119.

Tezuka T, Inoue A, Hoshi T, Weatherbee SD, Burgess RW, Ueta R, Yamanashi Y (2014) The MuSK activator agrin has a separate role essential for postnatal maintenance of neuromuscular synapses. Proc Natl Acad Sci USA 111:16556–16561.

Togo T, Dickson DW (2002) Ballooned neurons in progressive supranuclear palsy are usually due to concurrent argyrophilic grain disease. Acta Neuropathol 104:53–56.

Tortosa E, Montenegro-Venegas C, Benoist M, Härtel S, González-Billault C, Esteban JA, Avila J (2011) Microtubule-associated protein 1B (MAP1B) is required for dendritic spine development and synaptic maturation. J Biol Chem 286:40638–40648.

Trzeciakiewicz H, Tseng J-H, Wander CM, Madden V, Tripathy A, Yuan C-X, Cohen TJ (2017) A Dual Pathogenic Mechanism Links Tau Acetylation to Sporadic Tauopathy. Sci Rep 7:44102.

Twig G, Elorza A, Molina AJA, Mohamed H, Wikstrom JD, Walzer G, Stiles L, Haigh SE, Katz S, Las G, Alroy J, Wu M, Py BF, Yuan J, Deeney JT, Corkey BE, Shirihai OS (2008) Fission and selective fusion govern mitochondrial segregation and elimination by autophagy. EMBO J 27:433–446.

Uittenbogaard, M., & Chiaramello, A. (2014). Mitochondrial biogenesis: a therapeutic target for neurodevelopmental disorders and neurodegenerative diseases. Curr Pharm Des*, 20*(35), 5574-5593.

Vande Velde C, McDonald KK, Boukhedimi Y, McAlonis-Downes M, Lobsiger CS, Bel Hadj S, Zandona A, Julien J-P, Shah SB, Cleveland DW (2011) Misfolded SOD1 associated with motor neuron mitochondria alters mitochondrial shape and distribution prior to clinical onset. Dawson TM, ed. PLoS ONE 6:e22031.

Vega RB, Horton JL, Kelly DP (2015) Maintaining ancient organelles: mitochondrial biogenesis and maturation. Circulation Research 116:1820–1834.

Verburg J, Hollenbeck PJ (2008) Mitochondrial membrane potential in axons increases with local nerve growth factor or semaphorin signaling. J Neurosci 28:8306–8315.

Vomund S, Schäfer A, Parnham MJ, Brüne B, Knethen von A (2017) Nrf2, the Master Regulator of Anti-Oxidative Responses. International Journal of Molecular Sciences 18:2772.

Wadia PM, Lang AE (2007) The many faces of corticobasal degeneration. Parkinsonism Relat Disord 13 Suppl 3:S336–S340.

Wagner J et al. (2015) Reducing tau aggregates with anle138b delays disease progression in a mouse model of tauopathies. Acta Neuropathol 130:619–631.

Wakabayashi K, Oyanagi K, Makifuchi T, Ikuta F, Homma A, Homma Y, Horikawa Y, Tokiguchi S (1994) Corticobasal degeneration: etiopathological significance of the cytoskeletal alterations. Acta Neuropathol 87:545–553.

Wallace DC, Brown MD, Lott MT (1999) Mitochondrial DNA variation in human evolution and disease. Gene 238:211–230.

Walsh DM, Selkoe DJ (2004) Deciphering the molecular basis of memory failure in Alzheimer's disease. Neuron 44:181–193.

Wang X, Su B, Lee H-G, Li X, Perry G, Smith MA, Zhu X (2009) Impaired balance of mitochondrial fission and fusion in Alzheimer's disease. J Neurosci 29:9090–9103.

Wang Y, Garg S, Mandelkow E-M, Mandelkow E (2010) Proteolytic processing of tau. Biochem Soc Trans 38:955–961.

Wang Y, Mandelkow E (2012) Degradation of tau protein by autophagy and proteasomal pathways. Biochem Soc Trans 40:644–652.

Wang Y, Mandelkow E (2016) Tau in physiology and pathology. Nat Rev Neurosci 17:5–21.

Wang Y-P, Biernat J, Pickhardt M, Mandelkow E, Mandelkow EM (2007) Stepwise proteolysis liberates tau fragments that nucleate the Alzheimer-like aggregation of full-length tau in a neuronal cell model. Proc Natl Acad Sci USA 104:10252–10257.

Wang Y-P, Wang X-C, Tian Q, Yang Y, Zhang Q, Zhang J-Y, Zhang Y-C, Wang Z-F, Wang Q, Li H, Wang J-Z (2006) Endogenous overproduction of beta-amyloid induces tau hyperphosphorylation and decreases the solubility of tau in N2a cells. J Neural Transm (Vienna) 113:1723–1732.

Weingarten MD, Lockwood AH, Hwo SY, Kirschner MW (1975) A protein factor essential for microtubule assembly. Proc Natl Acad Sci USA 72:1858–1862.

Westrate LM, Drocco JA, Martin KR, Hlavacek WS, MacKeigan JP (2014) Mitochondrial morphological features are associated with fission and fusion events. Shirihai OS, ed. PLoS ONE 9:e95265.

Williams DR, Lees AJ (2009) Progressive supranuclear palsy: clinicopathological concepts and diagnostic challenges. Lancet Neurol 8:270–279.

Wimo A, Religa D, Spångberg K, Edlund A-K, Winblad B, Eriksdotter M (2013) Costs of diagnosing dementia: results from SveDem, the Swedish Dementia Registry. Int J Geriatr Psychiatry 28:1039–1044.

Wischik CM, Harrington CR, Storey JMD (2014) Tau-aggregation inhibitor therapy for Alzheimer's disease. Biochem Pharmacol 88:529–539.

Wischik CM, Novák M, Edwards PC, Klug A, Tichelaar W, Crowther RA (1988) Structural characterization of the core of the paired helical filament of Alzheimer disease. Proc Natl Acad Sci USA 85:4884–4888.

Wittmann CW, Wszolek MF, Shulman JM, Salvaterra PM, Lewis J, Hutton M, Feany MB (2001) Tauopathy in Drosophila: neurodegeneration without neurofibrillary tangles. Science 293:711–714.

Wray S, Saxton M, Anderton BH, Hanger DP (2008) Direct analysis of tau from PSP brain identifies new phosphorylation sites and a major fragment of N-terminally cleaved tau containing four microtubule-binding repeats. J Neurochem 105:2343–2352.

Wu G, Sankaranarayanan S, Wong J, Tugusheva K, Michener MS, Shi X, Cook JJ, Simon AJ, Savage MJ (2012) Characterization of plasma β-secretase (BACE1)

activity and soluble amyloid precursor proteins as potential biomarkers for Alzheimer's disease. J Neurosci Res 90:2247–2258.

Wu Z, Huang X, Feng Y, Handschin C, Feng Y, Gullicksen PS, Bare O, Labow M, Spiegelman B, Stevenson SC (2006) Transducer of regulated CREB-binding proteins (TORCs) induce PGC-1alpha transcription and mitochondrial biogenesis in muscle cells. Proc Natl Acad Sci USA 103:14379–14384.

Xie Y, Zhou B, Lin M-Y, Wang S, Foust KD, Sheng Z-H (2015) Endolysosomal deficits augment mitochondria pathology in spinal motor neurons of asymptomatic fals mice. Neuron 87:355–370.

Xie Z, Klionsky DJ (2007) Autophagosome formation: core machinery and adaptations. Nat Cell Biol 9:1102–1109.

Xie Z, Yang D, Stephenson D, Morton D, Hicks C, Brown T, Bocan T (2010) Characterizing the regional structural difference of the brain between tau transgenic (rTg4510) and wild-type mice using MRI. Med Image Comput Comput Assist Interv 13:308–315.

Yamada K (2017) Extracellular Tau and Its Potential Role in the Propagation of Tau Pathology. Front Neurosci 11:667.

Yao J, Irwin RW, Zhao L, Nilsen J, Hamilton RT, Brinton RD (2009) Mitochondrial bioenergetic deficit precedes Alzheimer“s pathology in female mouse model of Alzheimer”s disease. Proc Natl Acad Sci USA 106:14670–14675.

Yin Z, Valkenburg F, Hornix BE, Mantingh-Otter I, Zhou X, Mari M, Reggiori F, Van Dam D, Eggen BJL, De Deyn PP, Boddeke E (2017) Progressive motor deficit is mediated by the denervation of neuromuscular junctions and axonal degeneration in transgenic mice expressing mutant (p301s) tau protein. J Alzheimers Dis 60:S41–S57.

Yoo BC, Fountoulakis M, Cairns N, Lubec G (2001) Changes of voltage-dependent anion-selective channel proteins VDAC1 and VDAC2 brain levels in patients with Alzheimer's disease and Down syndrome. Electrophoresis 22:172–179.

Yoshiyama Y, Higuchi M, Zhang B, Huang S-M, Iwata N, Saido TC, Maeda J, Suhara T, Trojanowski JQ, Lee VM-Y (2007) Synapse loss and microglial activation precede tangles in a p301s tauopathy mouse model. Neuron 54:343–344.

Yu T, Robotham JL, Yoon Y (2006) Increased production of reactive oxygen species in hyperglycemic conditions requires dynamic change of mitochondrial morphology. Proc Natl Acad Sci USA 103:2653–2658.

Yu WH, Kumar A, Peterhoff C, Shapiro Kulnane L, Uchiyama Y, Lamb BT, Cuervo AM, Nixon RA (2004) Autophagic vacuoles are enriched in amyloid precursor protein-secretase activities: implications for beta-amyloid peptide over-production and localization in Alzheimer's disease. Int J Biochem Cell Biol 36:2531–2540.

Yuste R, Bonhoeffer T (2001) Morphological changes in dendritic spines associated with long-term synaptic plasticity. Annu Rev Neurosci 24:1071–1089.

Yuste R, Bonhoeffer T (2004) Genesis of dendritic spines: insights from ultrastructural and imaging studies. Nat Rev Neurosci 5:24–34.

Zaffagnini G, Savova A, Danieli A, Romanov J, Tremel S, Ebner M, Peterbauer T, Sztacho M, Trapannone R, Tarafder AK, Sachse C, Martens S (2018) p62 filaments capture and present ubiquitinated cargos for autophagy. EMBO J 37:e98308.

Zenisek D, Matthews G (2000) The role of mitochondria in presynaptic calcium handling at a ribbon synapse. Neuron 25:229–237.

Zilka N, Filipcik P, Koson P, Fialova L, Skrabana R, Zilkova M, Rolkova G, Kontsekova E, Novak M (2006) Truncated tau from sporadic Alzheimer's disease suffices to drive neurofibrillary degeneration in vivo. FEBS Lett 580:3582–3588.

Zilka N, Korenova M, Novak M (2009) Misfolded tau protein and disease modifying pathways in transgenic rodent models of human tauopathies. Acta Neuropathol 118:71–86.

Zunino R, Braschi E, Xu L, McBride HM (2009) Translocation of SenP5 from the nucleoli to the mitochondria modulates DRP1-dependent fission during mitosis. J Biol Chem 284:17783–17795.

Züchner S et al. (2004) Mutations in the mitochondrial GTPase mitofusin 2 cause Charcot-Marie-Tooth neuropathy type 2A. Nat Genet 36:449–451.